UNIVERSITY
OF TASMANIA

Organolanthanide Chemistry
of Modified Porphyrinogens

By

Jun Wang, M. Sc.

A thesis submitted in fulfillment
of the requirements for the degree of

Doctor of Philosophy

School of Chemistry, University of Tasmania, June 2003

This thesis contains no material which has been accepted for the award of any other degree or diploma in any University, and contains no copy or paraphrase of material previously presented by another person, except where due reference is made in the text.

This thesis may be made available for loan and limited copying in accordance with the Copyright Act, 1968.

Jun Wang

June 2003

ACKNOWLEDGEMENTS

ABSTRACT

This thesis describes studies into the synthesis, characterisation and reactivity of samarium(II) and (III) halide, alkyl and amide complexes derived from the modified porphyrinogens *meso*-octaethyl-*trans*-dioxaporphyrinogen, $Et_8O_2N_2H_2$, and *trans*-*N,N'*-dimethyl-*meso*-octaethylporphyrinogen, $Et_8N_4Me_2H_2$. The macrocycles themselves and various Group 1 metal derivatives that are accessed in the preparation of the target lanthanide complexes are also described in relation to their synthesis, characterisation and reactivity.

Chapter 2 is concerned with the synthesis of the modified porphyrinogens $Et_8O_2N_2H_2$ and $Et_8N_4Me_2H_2$. The new dioxaporphyrinogen $Et_8O_2N_2H_2$ was prepared in a '3+1' approach from the condensation of 2,5-bis{(2'-pyrrolyl)diethylmethyl}furan and 2,5-bis(hydroxydiethylmethyl)furan in toluene in the presence of trifluoroacetic acid. The *trans*-*N,N'*-dimethylated porphyrinogen $Et_8N_4Me_2H_2$ was prepared from the selective *N*-methylation of the parent porphyrinogen through metallation with sodium hydride in the presence of 18-crown-6 followed by reaction with methyl iodide. Other byproducts such as *N,N',N''*-trimethyl-*meso*-octaethylporphyrinogen, $Et_8N_4Me_3H$, and *N,N',N'',N'''*-tetramethyl-*meso*-octaethylporphyrinogen, $Et_8N_4Me_4$, were also isolated.

Chapter 3 details the synthesis of Group 1 metal complexes of both the modified porphyrinogens $Et_8O_2N_2H_2$ and $Et_8N_4Me_2H_2$ by direct metallation of the macrocycles. Complexes $[(Et_8O_2N_2)M_2L_n]$ and $[(Et_8N_4Me_2)M_2L_n]$, M = Li, Na, K, L = THF, TMEDA, n = 1, 2 or 4, were obtained as THF or TMEDA adducts from reactions with *n*-butyllithium, sodium hydride and potassium metal, respectively. The complexes display both monomeric and polymeric forms in the solid state, as determined by X-ray crystallography in some cases. Variable temperature ^1H NMR spectroscopic studies were undertaken to explore the conformational variation of the complexes in solution.

Chapter 4 describes samarium(II) complexes of both the modified porphyrinogens $Et_8O_2N_2H_2$ and $Et_8N_4Me_2H_2$. The complexes were prepared from the metathetical exchange reactions of the dipotassium complexes of the metallated modified porphyrinogens with samarium(II) diiodide in THF. The dimeric $[\{(THF)_2K(Et_8N_2O_2)Sm(\mu-I)\}_2]$ and monomeric $[(Et_8N_4Me_2)Sm(THF)_2]$ complexes were isolated and their crystal structures determined. Variable temperature ^1H NMR

spectroscopic studies of [(Et$_8$N$_4$Me$_2$)Sm(THF)$_2$] were performed and the paramagnetic properties shown to obey the Curie-Weiss law.

Chapter 5 details samarium(III) halide, alkyl and amide complexes of the modified porphyrinogens Et$_8$O$_2$N$_2$H$_2$ and Et$_8$N$_4$Me$_2$H$_2$. The samarium(III) iodide and chloride complexes [(Et$_8$O$_2$N$_2$)SmI] and [(Et$_8$N$_4$Me$_2$)SmCl]$_n$ (n = 1, 2) were prepared through oxidation of the samarium(II) precursors through iodine or *tert*-butyl chloride in THF, respectively. The alkyl complexes, [(Et$_8$N$_4$Me$_2$)SmR] (R = Me, CH$_2$SiMe$_3$), and amide complexes [(Et$_8$O$_2$N$_2$)SmN(SiMe$_3$)$_2$] and [(Et$_8$N$_4$Me$_2$)SmN(SiMe$_3$)$_2$], were synthesised through metathetical exchange reactions of the samarium(III) halides and alkyl lithium reagents or sodium bis(trimethylsilyl)amide in THF. The γ-methyl deprotonation of [(Et$_8$O$_2$N$_2$)SmN(SiMe$_3$)$_2$] was serendipitously found to be a rapid reaction, with the product, [(toluene)Na(Et$_8$O$_2$N$_2$)SmN(SiMe$_3$)SiMe$_2$CH$_2$], having been identified and fully characterised. Variable temperature ^{1}H NMR spectroscopic studies of [(Et$_8$N$_4$Me$_2$)SmN(SiMe$_3$)$_2$] were conducted, and compliance with the Curie-Weiss law was shown.

Chapter 6 mainly describes the initial exploration of the chemistry of 2,5-bis{(3'-indolyl)diethylmethyl}furan, H$_2$(IOI), and its Group 1 metal complexes formed through direct dimetallation using *n*-butyllithium, sodium hydride and potassium metal. The synthesis and characterisation of a lithiated derivative of *N,N',N''*-trimethyl-*meso*-octaethylporphyrinogen is also described.

CONTENTS

CHAPTER 1
INTRODUCTION

CHAPTER 2
SYNTHESES OF MODIFIED PORPHYRINOGENS

CHAPTER 3
GROUP 1 METAL COMPLEXES
OF MODIFIED PORPHYRINOGENS

CHAPTER 4
SAMARIUM(II) COMPLEXES
OF MODIFIED PORPHYRINOGENS

CHAPTER 5
SAMARIUM(III) COMPLEXES
OF MODIFIED PORPHYRINOGENS

CHAPTER 6
INDOLIDE AND PYRROLIDE RELATED CHEMISTRY

CHAPTER 7
CONCLUSION

ABBREVIATIONS

Å	Ångström, 10^{-10} m
Anal.	microanalysis
b	broad
Bu^n	normalbutyl
Bu^t	*tert*-butyl
Bz	benzyl
Calcd.	calculated
Cbz	benzyloxycarbonyl
18-crown-6	1,4,7,10,13,16-hexaoxacyclooctadecane
d	doublet
DADMB	2,2'-bis{*tert*-butyldimethylsilyl)amido}-6,6'-dimethylbiphenyl
diglyme	di(2-methoxyethyl) ether
DME	1,2-dimethoxyethane
EI	electron ionisation
Et	ethyl
$Et_8N_4H_4$	*meso*-octaethylporphyrinogen
$Et_8N_4MeH_3$	*N*-methyl-*meso*-octaethylporphyrinogen
$Et_8N_4Me_2H_2$	*trans*-*N,N′*-dimethyl-*meso*-octaethylporphyrinogen
$Et_8N_4Me_3H$	*N,N′,N″*-trimethyl-*meso*-octaethylporphyrinogen
$Et_8N_4Me_4$	*N,N′,N″,N‴*-tetramethyl-*meso*-octaethylporphyrinogen
Et_2O	diethyl ether
$Et_8O_2N_2H_2$	*meso*-octaethyl-*trans*-dioxaporphyrinogen
GC/MS	gas chromatography/mass spectrometry
gCOSY	gradient correlation spectroscopy
gHMBC	gradient heteronuclear multiple bond correlation
gHMQC	gradient heteronuclear multiple quantum correlation
gNOESY	gradient nuclear overhauser effect spectroscopy
$H_2(IOI)$	2,5-bis{(3'-indolyl)diethylmethyl}furan
IR	infra-red
L	ligand
Ln	lanthanide
M	metal
M^+	parent molecular ion peak
m	multiplet (NMR), medium (IR)
Me	methyl

m/e	mass to charge ratio
m.p.	melting point
MS	mass spectrum
NMR	nuclear magnetic resonance
Ph	phenyl
pin	2-phenylindole
PMDETA	N,N,N',N'',N''-pentamethyldiethylenetriamine
ppm	parts per million
q	quartet
R	alkyl, aryl
$R_8N_4H_4$	*meso*-octaalkylporphyrinogen
s	singlet (NMR), strong (IR)
t	triplet
THF	tetrahydrofuran
TMEDA	N,N,N',N'-tetramethylethylenediamine
$Tp^{t\text{-}Bu,Me}$	hydrotris(3-*tert*-butyl, 5-methyl-pyrazolyl)borate
w	weak
X	halide
υ	frequency
δ	chemical shift

CHAPTER 1

INTRODUCTION

1.1 GENERAL CONSIDERATIONS

'Lanthanides' or 'lanthanoids' with a general element symbol 'Ln', are the fifteen elements lanthanum (La), cerium (Ce), praseodymium (Pr), neodymium (Nd), promethium (Pm), samarium (Sm), europium (Eu), gadolinium (Gd), terbium (Tb), dysprosium (Dy), holmium (Ho), erbium (Er), thulium (Tm), ytterbium (Yb) and lutetium (Lu), which bear the electronic configuration ($[Xe]4f^{0-14}5d^{1-2}6s^2$). Since the 4f electrons have little involvement in bonding, the highly electropositive lanthanides usually form trivalent compounds. Some lanthanides, such as samarium, europium and ytterbium can also form organometallic complexes in the +2 oxidation state but are prone to oxidisation to trivalent species. These metals, together with scandium (Sc) and yttrium (Y) display many common reactivity patterns, and thus in general organolanthanide chemistry refers to the organometallic chemistry of the seventeen elements as an expanded set of the fourteen rare earth metals.

In 1954 Birmingham and Wilkinson reported tris(cyclopentadienyl)lanthanide complexes, [Ln(Cp)$_3$] (Ln = Sc, Y, La, Ce, Pr, Nd, Sm and Gd), which marked the birth of organolanthanide chemistry[1]. However, the following two decades witnessed little development owing to the intrinsic instability of organolanthanide compounds towards air and moisture. This position changed slowly in the late 1970s and the early 1980s when more effective preparative and analytical techniques become available, especially single crystal X-ray diffraction. From that time, the chemistry has developed enormously. In particular, it was found that metallocene derivatives of the lanthanides exhibit unique chemical, structural and physical properties and often display unusually high catalytic activity. Lanthanide chemistry with the cyclopentadienyl ligand systems still plays a dominant role and a number of review articles have been devoted to cyclopentadienyl based organolanthanide chemistry[2]. However, a tremendous effort has recently been devoted to searching for alternatives to cyclopentadienyl ligand systems which can further expand the range of applications. The organolanthanide chemistry of non-cyclopentadienyl ligands have been reviewed recently in several articles[3].

The introduction in this Chapter emphasises synthetic organolanthanide chemistry with strategically designed ligand systems. The coordination chemistry of pyrrolide based ligands, which show potential as alternative to cyclopentadienyl based ligand systems is also reviewed.

1.2 ORGANOLANTHANIDE CHEMISTRY OF STRATEGICALLY DESIGNED LIGAND SYSTEMS

Ligand design plays an important role in organolanthanide chemistry. The nature of the ligand, including its size, basicity and functionalisation, affects features of complexes such as bonding modes, nuclearity, reactivity and so on. The stabilisation of complexes is a basic prerequisite for organolanthanide chemistry and mononuclearity is considered a general positive sign for both solubility and reactivity. Several strategies for ligand design have been employed to achieve these goals including utilising, (i) bulky ligands and/or donor atom functionalisation, (ii) non-aromatic π-delocalised ligands, (iii) aromatic π-delocalised ligands, and, (iv) macrocyclic/cage ligands. Each of these approaches is detailed below.

(i) Bulky ligands and/or donor atom functionalised ligands

Sterically demanding groups are essential for the generation of mononuclear lanthanide complexes with improved solubility and preparative yield. The bulky bis(trimethylsilyl)amide or (trimethylsilyl)methyl ligands are very commonly used examples in organolanthanide chemistry. The bulky aryl ligand 2,6-dimesitylphenyl, (I), is an example which has two bulky groups employed neighbouring the coordinating carbon centre[4].

(I)   (II)   (III)

Me₂ Si

Bu'O   NBu'
            ⊖

(IV)

Me₂   Me₂
Si   Si
      N
      ⊖
PPr'₂   Pr'₂P

(V)

O

N⊖   ⊖N
R   R

(VI)
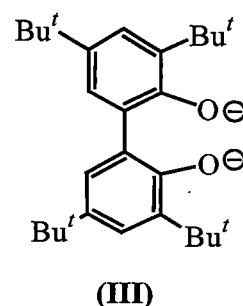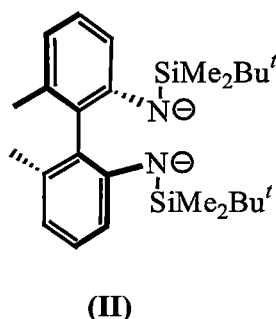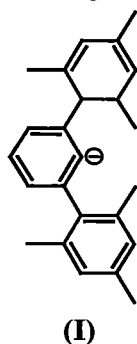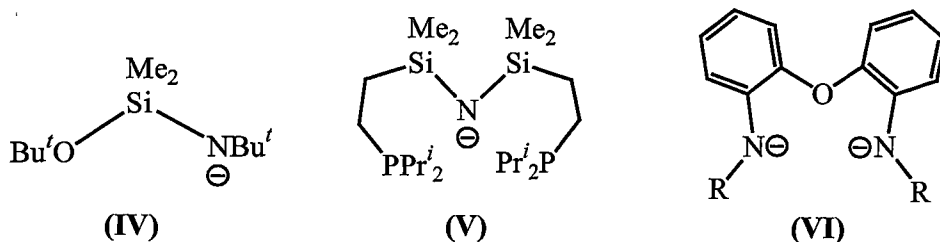
The bulky chelating amide ligand 2,2'-bis{*tert*-butyldimethylsilyl)amido}-6,6'-dimethylbiphenyl (DADMB), **(II)**, was reported to have a strong tendency to form monomeric lanthanide complexes[5]. The yttrium(III) chloride complex [DADMB)YCl(THF)₂], **(VII)**, was obtained in 92% from the reaction of Li₂(DADMB) with YCl₃(THF)₃. The reaction of **(VII)** with methyl lithium led to the methyl complex [(DADMB)YMe(THF)₂] **(VIII)** which reacts with phenylsilane or hydrogen forming a dimeric yttrium(III) hydride complex [{(DADMB)Y(μ-H)(THF)}₂]·C₆H₆, **(IX)**. The hydride complex **(IX)** proved to be catalytically active in alkene hydrosilylation. The related chelating aryloxide ligand system 3,3',5,5'-tetra-*tert*-butylbiphenyl-2,2'-diolate, **(III)**, with bulky substituents also stabilises monomeric alkyllanthanide(III) alkoxides[6].

SiMe₂Bu'
N   THF
N   Y—Cl
SiMe₂Bu'   THF

(VII)

SiMe₂Bu'
N   THF
N   Y—Me
SiMe₂Bu'   THF

(VIII)
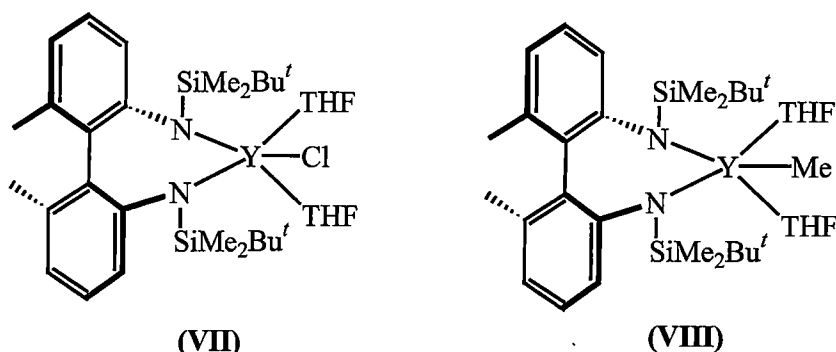
Donor atom functionalisation by the incorporation of potentially coordinating Lewis basic groups is a popular approach in organolanthanide chemistry. Due to the large size and high coordination number requirements of lanthanide metals, such pendant coordinating centres are needed to occupy coordination sites on the metals to preclude the coordination of other neutral ligands or oligmerisation from occurring.

Donor atom functionalisation (*e.g.,* **(IV)** and **(V)**, **(VI)**) has been applied in lanthanide alkyl, amide[7] and alkoxide[8] chemistry. Even though hard Lewis basic donor atom functional groups (such as -NR₂, -OR) are dominate, softer Lewis basic functionalisation, such as -PR₂, is also used (*e.g.,* **(V)**).

The alkylyttrium(III) complex (XI) of the bidentate, anionic N,O-bis(*tert*-butyl)(alkoxydimethylsilyl)amide ligand system, (IV), prepared from the precursor chloroyttrium complex (X) displays C-H activation towards substituted pyridines forming novel organoyttrium species (*e.g.*, XII)[9].

Me₂Si——OBu*t*

Bu*t*N*''''*... THF
Y
Bu*t*N Cl

Me₂Si——OBu*t*

(X)

Me₂Si——OBu*t*

Bu*t*N*''''*...
Y—CH(SiMe₃)₂
Bu*t*N

Me₂Si——OBu*t*

(XI)

Me₂Si——OBu*t*

Bu*t*N*''''*...
Y—N
Bu*t*N

Me₂Si——OBu*t*

(XII)
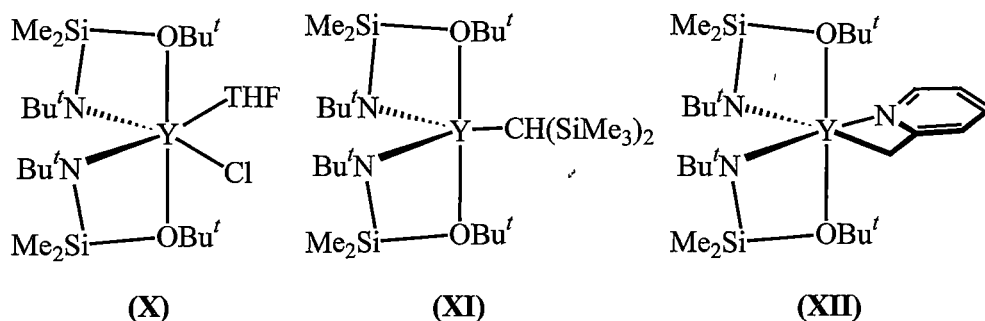
(ii) non-aromatic π-delocalised ligands

Several pure hydrocarbyl or heteroatom substituted π-delocalised anions have shown potential as substitutes for pentamethylcyclopentadienyl ligands in stabilising lanthanide complexes. These anionic ligands feature either two η^1-bonding interactions forming a bidentate chelate or η^3-bonding modes. Examples of these systems are allyl ligands, (XIII)[10], substituted benzamidinates, (XIV)[11], 1-azaallyl ligands, (XV)[12] and β-diketiminates, (XVI)[13].

H_2C ⊖ CH_2
C
H
(XIII)

Me_3Si—N ⊖ N—$SiMe_3$
Ph
(XIV)

Me_3Si—N ⊖ CH—$SiMe_3$
Bu*t*
(XV)

N ⊖ N
C
H
(XVI)
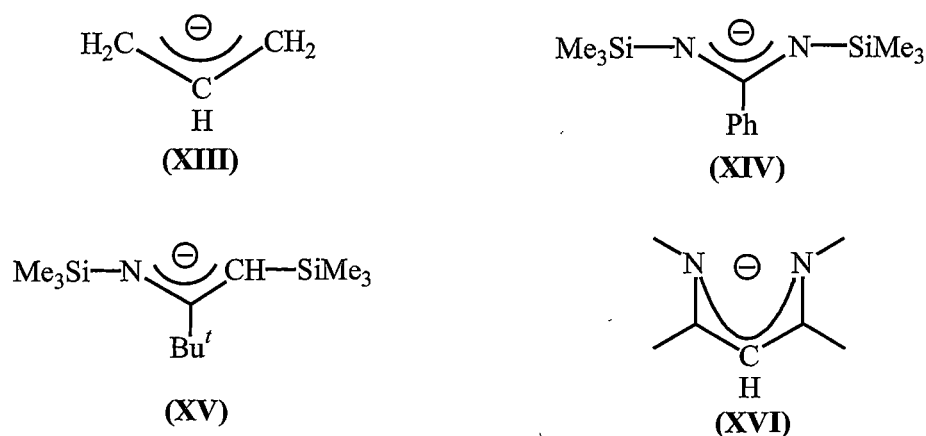
The monomeric disubstituted benzamidinate scandium(III) alkyl and aryl complexes [{PhC(NSiMe₃)₂}ScMe(THF)], (XVII), and [{PhC(NSiMe₃)₂}ScCH₂SiMe₃], (XVIII), were prepared by the initial metathetical exchange reaction between scandium trichloride and two equivalents of the sodium benzamidinate Na[PhC(NSiMe₃)₂] in THF[11f]. The reaction led to a chloroscandium(III) benzamidinate complex [{PhC(NSiMe₃)₂}ScCl(THF)], which

was transformed to the methylscandium(III) benzamidinate complex **(XVII)** as a THF adduct *via* the reaction with methyllithium. When the reaction was performed with trimethylsilylmethyllithium, an unsolvated alkyl complex **(XVIII)** was formed. Complex **(XVIII)** reacts readily with hydrogen to form the dimeric hydride complex [{[PhC(NSiMe$_3$)$_2$]Sc(μ-H)}$_2$].
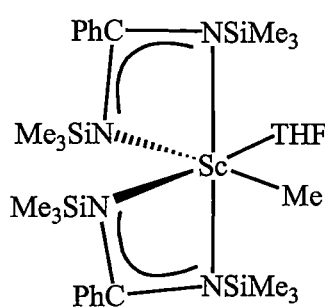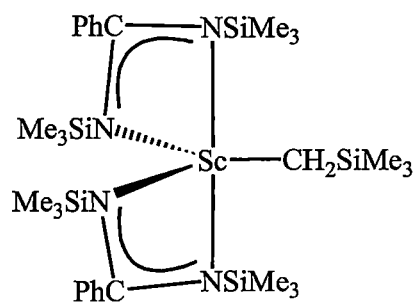
(XVII)

(XVIII)

The 1,3-bis(trimethylsilyl)-1-azaallyl system, **(XV)**, has been reported to have stabilised divalent lanthanide complexes[12]. 1,3-Bis(trimethylsilyl)-1-azaallyl lithium or sodium reacted with ytterbium diiodide affording the ytterbium(II) complex [{Me$_3$SiNC(Bu^t)CHSiMe$_3$}$_2$Yb], **(XIX)**, which is a monomer in the solid state. H-Agostic interactions exist between the ytterbium centre and a methyl of one *N*-trimethylsilyl group of each ligand. Trivalent lanthanide complexes can be obtained from the oxidation of the corresponding lanthanide(II) complexes, *e.g.*, [{Me$_3$SiNC(Bu^t)CHSiMe$_3$}$_2$SmCl(THF)], **(XX)**.
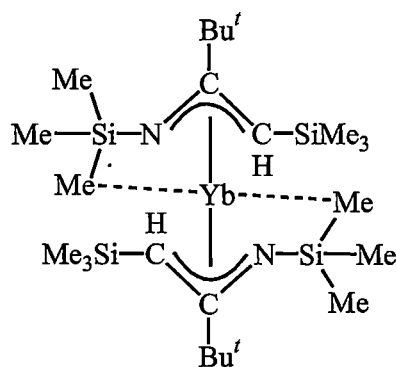
(XIX)

(XX)
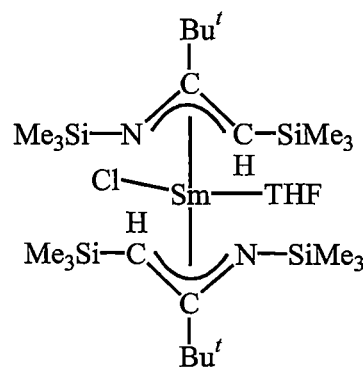
(iii) aromatic π-delocalised ligands

Cyclopentadienyl derivatives, (XXI), and related systems such as indenyls and fluorenyls have played a dominant role in organolanthanide chemistry research, especially in the earlier stages. Lanthanide complexes of this ligand system display the ubiquitous bent metallocene structural feature. Most significantly, some complexes display highly efficient homogeneous catalytic activities.

(XXI)   (XXII)   (XXIII)

(XXIV)   (XXV)   (XXVI)
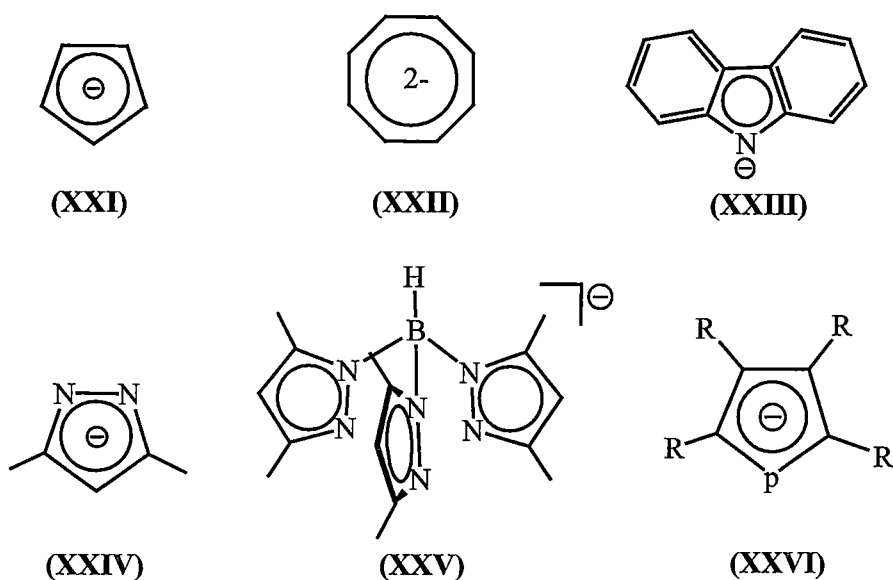
The large, flat cyclooctatetraendiyl ligands (XXII) are considered a valuable alternative to cylopentadienyl ligands. η^8-Bonding modes have mainly been established for its lanthanide complexes, e.g., the lanthanide(II) complexes (XXVII) and the chlorolanthanide(III) complexes (XXVIII)[14].

(XXVII)

(XXVIII)
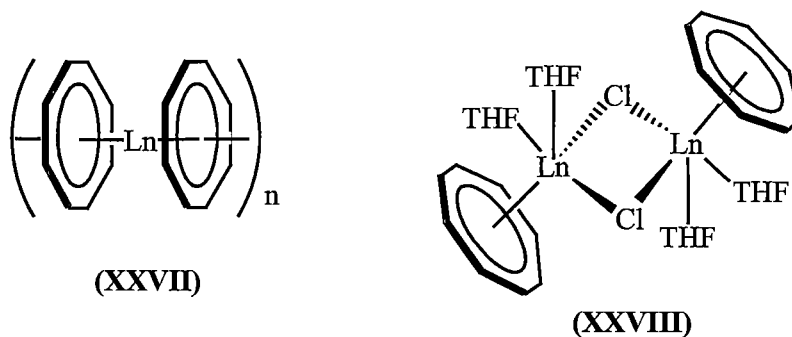
Organolanthanide chemistry featuring various heterocyclic ligands has drawn much attention recently. The heterocycles studied include mainly nitrogen and phosphorus based systems.

Pyrrolide complexes are known that contain various binding modes ranging from η^1- to η^5-interactions and the retention of alkali metal cations occurs for the majority of complexes, which will be discussed in detail in the next Section. Indolide and carbazolide, (XXIII)[15], anionic ligands have rarely been explored and the examples available so far have shown them to adopt only η^1-bonding modes in coordination with lanthanide metals.

Metal complexes of the 1,2-dinitrogen containing anion heterocyclic pyrazolide, (XXIV)[16], and hydrotrispyrazolylborate, (XXV)[17], have been studied extensively. Pyrazolides can adopt, (a) η^2-, (b) μ:η^2-, and, (c) μ:η^1-bonding modes, as shown in Figure 1.

(a)   (b)   (c)
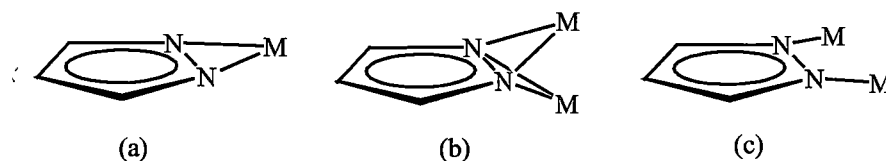
Figure 1: Common binding modes of pyrazolides.

There are quite a few examples of pyrazolide complexes additionally featuring cyclopentadienyl ligands, both solvated and solvent free. However, alkyl and amide derivatives have not been prepared. The more bulky hydrotrispyrazolylborate ligands (XXV) show a stronger ability to stabilise lanthanide complexes[17]. The sterically demanding ligands are especially suitable for divalent lanthanides since only five of the six pyrazolyl arms of the two potentially tridentate trispyrazolylborate ligands of [Ln(Tp$^{t\text{-Bu,Me}}$)$_2$] units are coordinated with lanthanide centres in some complexes. A series of divalent lanthanide halide, alkyl, aryloxide and hydride complexes have been synthesised, as shown in Scheme 1. The divalent lanthanide hydride, [{(Tp$^{t\text{-Bu,Me}}$)Yb(μ-H)}$_2$] was reported to have insertion reactivity with Lewis bases and Brønstead acids such as perfluoroaryl boranes, ketones, alkynes, amides, alcohols, *etc*.

$$[(Tp^{t\text{-}Bu,Me})YbI(THF)] \xrightarrow{\begin{array}{c} KOMes \\ \hline -KI \end{array}} [(Tp^{t\text{-}Bu,Me})Yb(OMes)(THF)]$$

$$\xrightarrow{\begin{array}{c} KN(SiMe_3)_2 \\ \hline -KI \end{array}} [(Tp^{t\text{-}Bu,Me})Yb\{N(SiMe_3)_2\}]$$

$$\xrightarrow{\begin{array}{c} KCH(SiMe_3)_2 \\ \hline -KI \end{array}} [(Tp^{t\text{-}Bu,Me})Yb\{CH(SiMe_3)_2\}]$$

$$\xrightarrow{\begin{array}{c} H_2, pentane \\ \hline -HI \end{array}} [\{(Tp^{t\text{-}Bu,Me})Yb(\mu\text{-}H)\}_2]$$
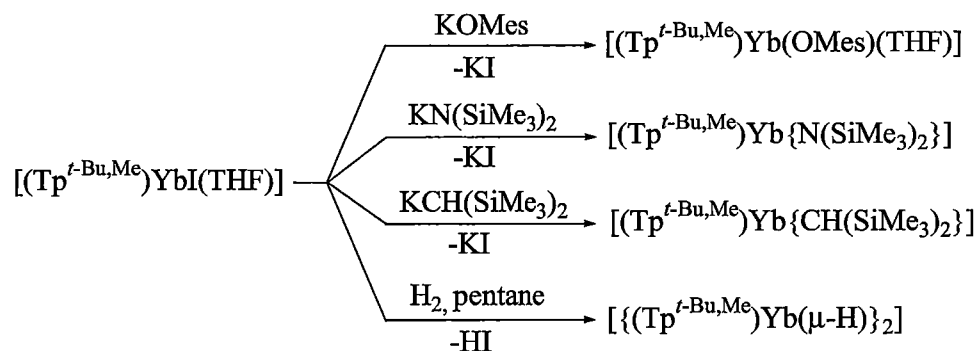
Scheme 1

Heterocyles of the softer donor atom phosphorus in the phospholide (**XXVI**)[18] adopt η^5-bonding modes more readily than the corresponding pyrrolide ligands. The ytterbium(II) complex (**XXVII**) with a bent metallocene structure was obtained by either the metathesis reaction of the potassium phospholide with YbI$_2$(THF)$_2$, or insertion of metallic ytterbium into the P-P bond of a 1,1'-biphospholyl. The polymeric samarium(III) complex [{(η^5-C$_4$Me$_4$P)Sm(μ:η^5,η^1-C$_4$Me$_4$P)$_2$(μ-Cl)K(η^6-toluene)}$_n$] featuring the 2,3,4,5,-tetramethylphospholide (**XXVI**) was prepared from the reaction of three equivalents of the potassium phospholide with SmCl$_3$ in toluene. The analogous reaction using the less bulky 3,4-dimethylphospholide led to [{(η^5-3,4-C$_4$Me$_2$H$_2$P)$_2$(μ:η^5,η^1-3,4-C$_4$Me$_2$H$_2$P)Sm}$_2$], (**XXVIII**), which adopts a dimeric form with absence of any alkali metal cation retention.

(**XXVII**)   (**XXVIII**)
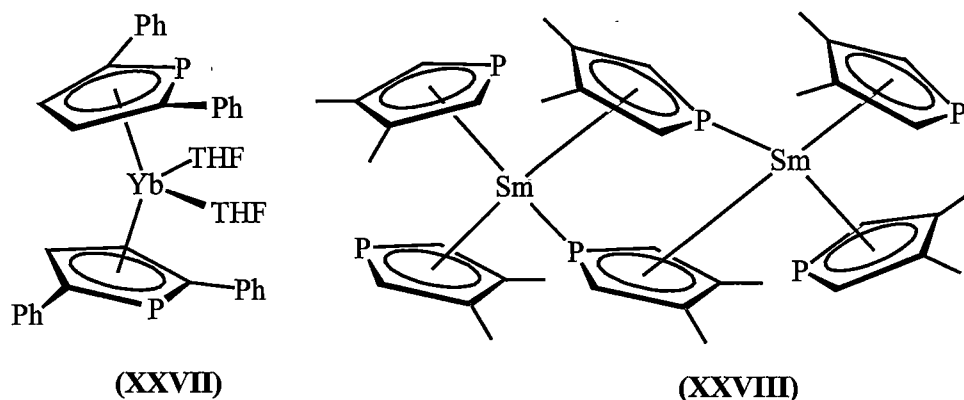
The coordination of other heterocycles such as 1,2,4-di-*tert*-butyltriphospholide, (**XXIX**)[19], and 1,4,2-di-*tert*-butylstibadiphospholide, (**XXX**)[20], resembles that of both the phospholide (**XXVI**) and pyrazolide (**XXIV**) heterocycles in certain respects.
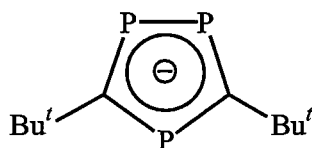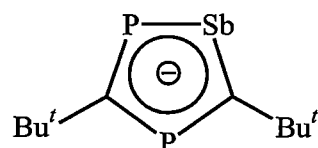
(XXIX)   (XXX)

(iv) Macrocyclic and cage ligand

Some macrocyclic ligands are able to control the coordination of lanthanide metals in similar ways to both bulky and donor atom functionalised ligands. Mononuclear lanthanide complexes of the macrocycle (XXXI)[21] and related ligands have been reported. Carbon-boron cage ligand systems[22] (e.g., (XXXII)) have also shown good ability to stabilise lanthanide metals. The lanthanide coordination chemistry of other pyrrolide based macrocycles such as porphyrinogens, is reviewed in detail in the following Section.
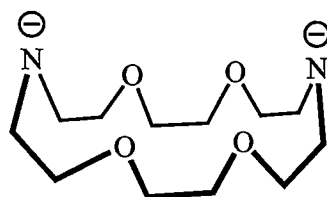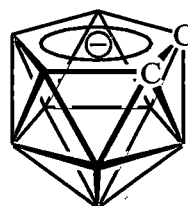
(XXXI)   (XXXII) (nido-$C_2B_9H_{12}$)

1.3 METAL PYRROLIDE CHEMISTRY

Pyrroles are five membered aromatic heterocycles which include a nitrogen and four carbon atoms. The nitrogen centre bears a relatively acidic proton (pK_a = 23.3)[23] which is amenable to abstraction by various bases (e.g., Na, NaH, Bu^nLi, K) to form the pyrrolide anion, (XXXIII). Due to the more ready availability of the lone pair of electrons occupying a sp^2 hybridised atomic orbital of the nitrogen centre, the pyrrolide anion should, in general, prefer to form σ-binding modes when coordinating to metals. This contrasts with the cyclopentadienyl anion, (XXI), which commonly forms η^5-bound metal complexes due to the absence of lone pair sp^2 orbitals on the carbon centres. Pyrrolide anions only tend to adopt π bonding modes when coordinating to metals under some specific conditions, for example, when bulky 2,5-disubstitution shields the nitrogen centred electron pair responsibly for forming σ-interactions and when a favourable electronic structure for the metal arises

as a result, *e.g.*, the 18 valence electron azaferrocenes. The π electron density of pyrrolide is unevenly distributed among the five atoms of the ring, with more electronic density on the nitrogen centre due to its high electronegativity. As a result, there are further reasons for π-bonding modes to vary from η^5-, η^3- or η^2- forms. The diversity of bonding modes is probably an important reason why this research area has found little application until the 1990s. Researchers are only now beginning to see this feature as a potential benefit in certain applications.
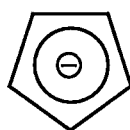
(**XXI**) Cyclopentadienyl anion   (**XXXIII**) Pyrrolide anion
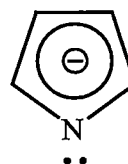
The coordination chemistry of pyrrolide anions is partly reviewed in two parts in this Chapter, (i) non-macrocyclic pyrrolide coordination chemistry, and, (ii) macrocyclic pyrrolide coordination chemistry. The coordination chemistry of alkali metal and lanthanide pyrrolides will be discussed mainly in Sections 3.1, 4.1 and 5.1.

1.3.1. Non-macrocyclic pyrrolide coordination chemistry

The σ-bound pyrrolide complexes $[(\eta^5\text{-}C_5H_5)_2M(\eta^1\text{-}NC_4H_4)_2]$, (**XXXIV**), (M = Zr, Ti), were reported to be prepared from the reaction of $[(\eta^5\text{-}C_5H_5)_2MCl_2]$ with sodium pyrrolide in THF at room temperature. Complexes (**XXXIV**) display two σ-bound pyrrolide rings and two η^5-bound cyclopentadienyl rings resulting in a bent metalllocene structure. For M = Zr, at reflux temperature, the cyclopentadienyl ligands are lost and the hexapyrrolylzirconate anion $[Na(THF)_6]_2[Zr(\eta^1\text{-}NC_4H_4)_6]$, is formed[24] even though the reaction stoichiometry favours the formation of (**XXXIV**).
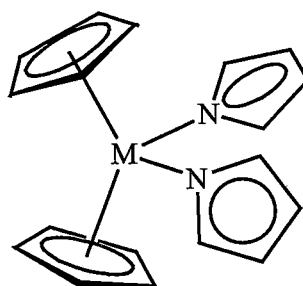
(**XXXIV**) (M = Zr, Ti)

Even though pyrrolide ligands are considered to favour σ-coordination modes, especially unsubstituted pyrrolide itself, π-coordination chemistry with late transition metals was established as early as the 1960s. Azaferrocene [(η^5-C_5H_5)Fe(η^5-NC_4H_4)], (**XXXVI**), contains a π-bound pyrrolide ligand[25]. The reaction of potassium pyrrolide with bromodicarbonylcyclopentadienyliron forms a σ-bound pyrrolide complex, [(η^5-C_5H_5)Fe(CO)_2(η^1-NC_4H_4)], (**XXXV**), which transforms to azaferrocene, (**XXXVI**), under very mild conditions by the loss of both carbonyl ligands, as shown in Equation 1. This observation is analogous ferrocene reactivity, with the electronic requirements of the metal centre driving the binding mode of the pyrrolide anion.
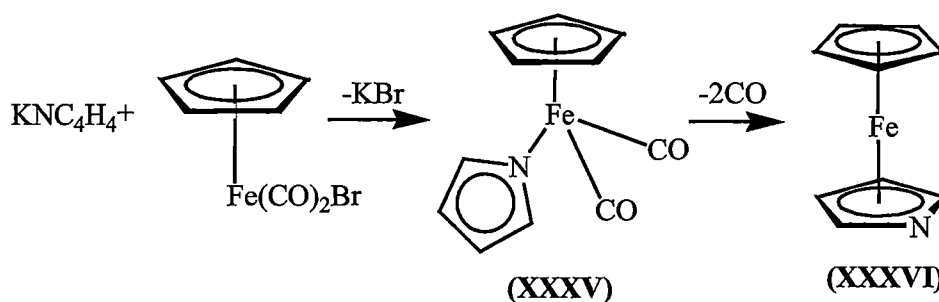
Equation 1

[(η^5-NC_4H_4)Mn(CO)_3], (**XXXVII**), can be prepared in a similar manner to the iron complex (**XXXVI**) from the reaction of the pyrrolide anion with bromopentacarbonyl manganese[26], but no σ-bound pyrrolide intermediate analogous to (**XXXV**) was observable in the process. Complex (**XXXVII**) can also be synthesised through the direct reaction between pyrrole and [Mn_2(CO)_{10}], as shown in Equation 2.
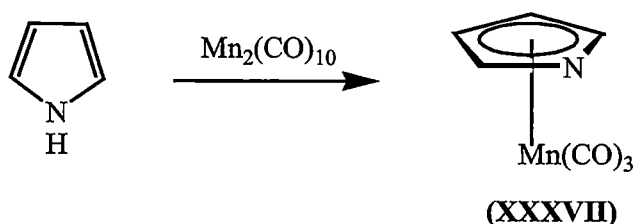
(XXXVII)

Equation 2

The reaction of *N*-methylpyrrole with a manganese(I) iodide precursor in the presence of a Lewis acid resulted in the formation of the cationic complex (**XXXVIII**)[27], as shown in Equation 3. Cationic complexes of *N*-methylpyrrole have also been prepared through the direct methylation of pyrrolide complexes, including azaferrocene (**XXXVI**).
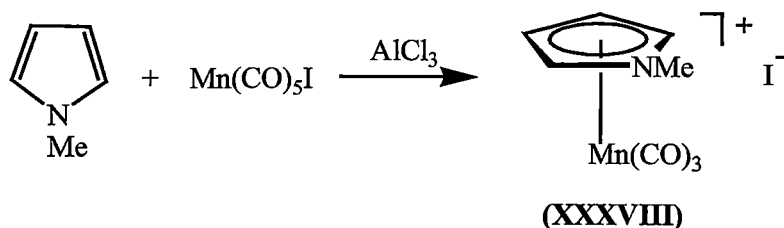
(XXXVIII)

Equation 3

The acylation of tricarbonylpyrrolylmanganese, **(XXXVII)**, leads to a dinuclear species **(XXXIX)**[28], as shown in Equation 4. The acylation occurs at the α-position and the binding mode of the pyrolide ring is changed to a σ-interaction to the metal with the ketone functionality also acting as a ligand. Further coordination of the manganese centre results through a σ-coordinated molecule of **(XXXVII)**, *via* the nitrogen centre of the pyrrolide unit.

(XXXVII)

(XXXIX)
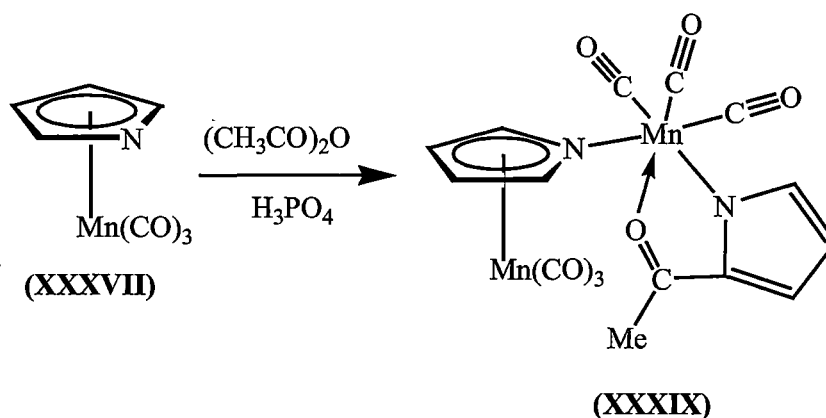
Equation 4

A series of homoleptic di-1,1'-azametallocenes have been prepared from the 2,5-di(*tert*-butyl)substituted pyrrolide anion which is disfavoured from forming σ-bonding interactions with metals by virtue of its steric bulk. Diazametallocene complexes have been synthesised not only with transition metals[29], such as iron **(XL)** and cobalt **(XLI)**, but also for main group metals[30], including lead **(XLII)** and tin **(XLIII)**. However, σ-bound examples are also known for this bulky anion, setting precedence for the possibility of either σ- or π-bonding in 2,5-di(*tert*-alkyl)pyrrolide systems, of which the metallated *meso*-octaalkylporphyrinogens featuring in this thesis can be classified.

Bu^t ⟨N⟩ Bu^t — Fe — Bu^t ⟨N⟩ Bu^t

(XL)

Bu^t ⟨N⟩ Bu^t — Co — Bu^t ⟨N⟩ Bu^t

(XLI)

Bu^t ⟨N⟩ Bu^t — Sn — Bu^t ⟨N⟩ Bu^t

(XLIII)
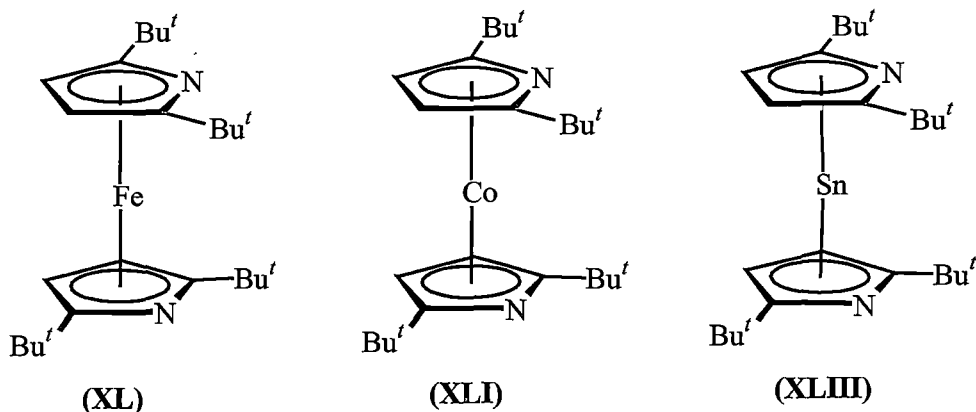
η^5-Bound pyrrolide complexes have shown application in the synthesis of substituted pyrroles. For example, rhenium complexes $[(\eta^5\text{-}NC_4H_4)Re(PR_3)_2(H)I]$, **(XLIV)**, partake in nucleophilic substitution reactions at the 2-position of the pyrrolide ring, forming $[(\eta^5\text{-}NC_4H_3\text{-}2\text{-}R)Re(PR_3)_2(H)_2]$, **(XLV)**, as shown in Scheme 2. Further substitution at the 5-position of the pyrrolide unit forms $[(\eta^5\text{-}NC_4H_2\text{-}2,5\text{-}R_2)Re(PR_3)_2(H)_2]$, **(XLVI)**[31]. The reactions involve hydrogen transfer from the pyrrolide ring to the metal centre.

R$_3$P—Re—I / R$_3$P H
(XLIV)

$\xrightarrow[\text{-LiI}]{\text{RLi}}$

R$_3$P—Re—H / R$_3$P H ⟨N⟩—R
(XLV)

$\xrightarrow[\text{-LiI}]{\text{i) } I_2\text{-}CO_3^{2-}\text{ ii) RLi}}$

R—⟨N⟩—R R$_3$P—Re—H / R$_3$P H
(XLVI)
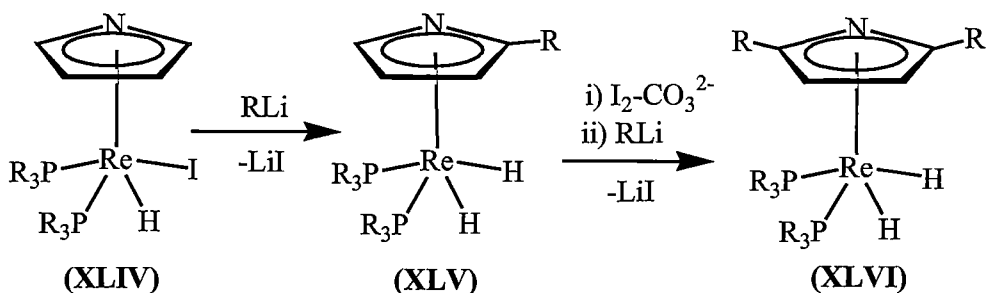
Scheme 2

The coordination chemistry of dimetallated di(2'-pyrrolyl)methanes, **(XLVII)**, has been mainly focused on lanthanide metals. A diverse range of structural types have been reported, establishing a high degree of unpredictability in this chemistry. Some complexes feature the retention of alkali metal cations arising from the metathetical exchange reactions employed and simultaneous σ- and π-bonding modes of the dipyrrolides, resulting in extensive metal bridging capabilities. The structure of **(XLVIII)**[32] is representative (see also Section 4.1).

$R^1 = R^2 = Ph,$

(XLVII) $R^1 = Ph, R^2 = Me$

$R^1 = R^2 = (-CH_2-)_5$

$[\{(THF)_2Na[Ph_2C(C_4H_3N)_2]Yb\}_2]$, (XLVIII)
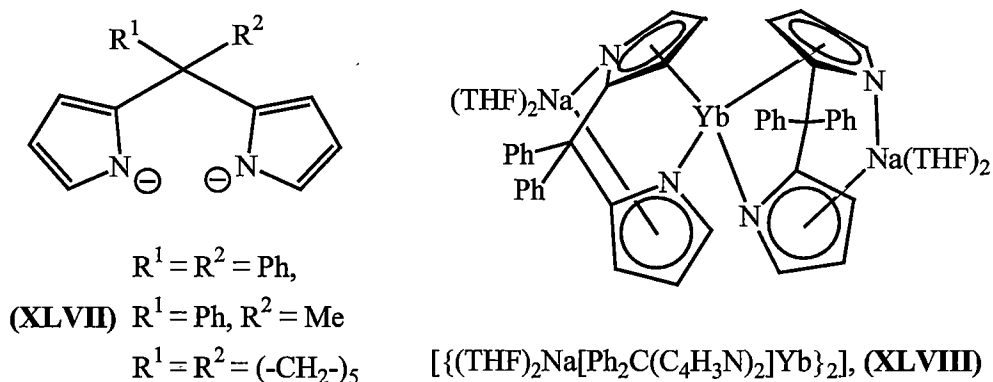
Complexes featuring trimetallated tri(2'-pyrrolyl)methane, (XLIX), are rare and only complexes of niobium have been reported so far. $[\{Nb[(NC_4H_3)_3CH](THF)\}_2]$, (L), adopts a dimeric form displaying both π- and σ-bonding modes in its structure[33], as shown in Figure 2.

(XLIX)
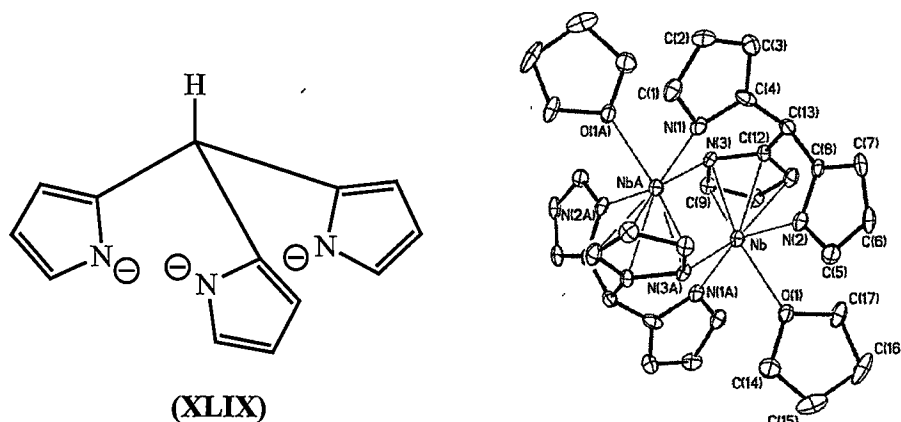
Figure 2: Crystal structure of complex (L)[33]

1.3.2. Macrocyclic pyrrolide coordination chemistry

Macrocyclic based pyrrolide coordination chemistry has been concentrated on the porphyrin and porphyrinogen tetracyclic classes of macrocycles, stemming from the macrocyclic cavities that these macrocycles possess and the assessibility of the simplest examples of the macrocycles. An extraordinary coordination chemistry of these macrocyclic systems has been established in a range of fields.

Invariably porphyrin complexes feature σ-bonding with metal cations which reside in the plane of the near-planar macrocycle, for small metals, or on the vector directly above or below the near-planar macrocycle, for larger metals. The completely delocalised π-system of the macrocycle is not directly involved in

bonding with metals, instead each pyrrolide ring uses the lone pair electrons of the nitrogen centres to σ-bind to metal centres. To satisfy the coordination number requirements of many metals, a second porphyrin can coordinate to the metal with the same σ-bonding mode, forming 'decker' complexes. In most complexes, the π-electrons have no participation in coordination to metals. However, some complexes can make use of the π-electrons of individual pyrrolide units to π-bind with additional metal centres. For example, the zinc and nickel complexes **(LI)** and **(LII)** bind Ru and Ir cations through π-interactions of a single pyrrolide ring in addition to binding the nickel and zinc centres through nitrogen centres[34].

(LI)   **(LII)**
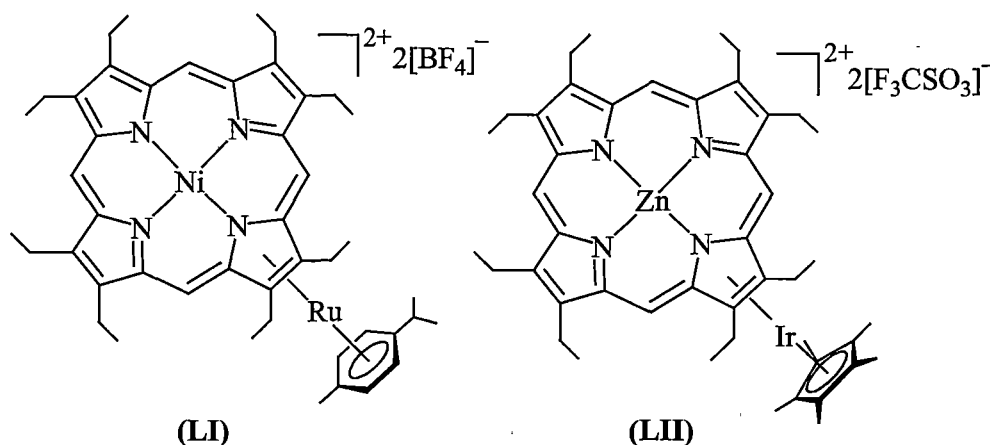
Compared to porphyrins, porphyrinogens, **(LIII)**, feature the constituent pyrrole units as individual aromatic rings linked by sp^3 hybridised *meso*-carbon linkers. This results in major structural and reactivity differences compared with porphyrins, which have completely delocalised π-systems through sp^2 hybridised *meso*-carbon linkers. The porphyrinogens are thus non-planar and possess a deep cavity surrounded by pyrrolyl rings which are capable of adjusting their "tilt" angle with respect to the plane of the macrocycle in response to the size of the metal to be hosted in their metallated complexes. The individual pyrrolide rings of metallated porphyrinogens have shown the ability to bind metals through η^1-, η^2-, η^3- and η^5-bonding modes.
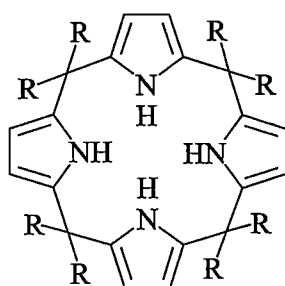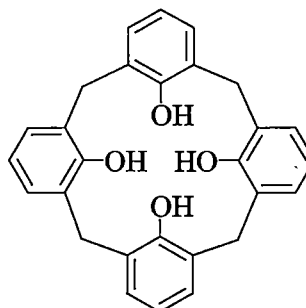
(LIII)   (LIV)

For convenience, porphyrinogens are represented throughout this thesis with the general formula $R_8N_4H_4$. 'R' represents the *meso*-substituents, 'N' the pyrrole ring and 'H' corresponds to the acidic protons of the each of the pyrrole units. For its tetrametallated porphyrinogens, the formula $(R_8N_4)^{4-}$ has been adopted. $Et_8N_4H_4$ and $(Et_8N_4)^{4-}$ thus represent *meso*-octaethylporphyrinogen and its tetraanion formed on metallation, which have been employed in this research due to the convenient synthesis, derivatisation and ease of product identification through spectroscopic means. For clarity, the *meso*-groups of porphyrinogens are often not shown in the figures throughout this thesis.

Bearing eight alkyl groups in the *meso*-positions, porphyrinogens are not susceptible to oxidation. Thus *meso*-octaalkylporphyrinogens are not *bona fide* precursors of porphyrins. Moreover, the macrocyclic conformations of porphyrinogens give rise to the shape of the macrocyclic cavity being similar to calix[4]arenes, (LIV). Some authors have suggested that the term 'calixpyrrole' should be more suitable to describe the macrocycle[35]. Calix[4]pyrrole more correctly defines the tetrapyrrolic macrocycle, while expanded systems are similarly defined, such as the known calix[6]pyrroles. The term porphyrinogen is used throughout this thesis.

Due to the sp^3 hybridised *meso*-carbons, porphyrinogens can adopt various conformations akind to those of calix[4]arenes. The terms used to describe calix[4]arene conformations are also adopted for porphyrinogens and metallated porphyrinogen complexes throughout this thesis, as shown in Figure 3[36].

1,3-alternate   1,2-alternate   partial cone

full cone   flattened   partially flattened
                                                    double cone
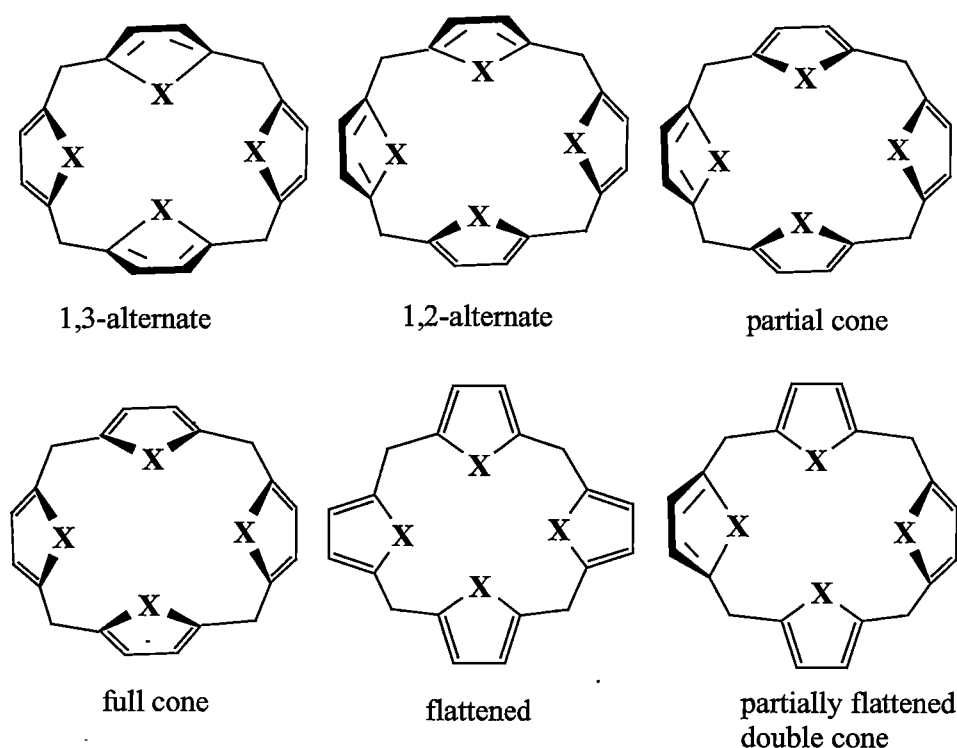
Figure 3: Typical conformations of porphyrinogens

In the absence of effects arising from outside factors such as cavity-bound anions, neutral molecules or metals, porphyrinogens typically adopt 1,3-alternate conformations with only a few exceptions. The 1,3-alternate conformation is usually energetically advantageous compared to other conformations except in a limited number of examples with certain β- or *meso*-substituents.

Hosting small anions or neutral molecules often alters the conformation of porphyrinogens in response to the formation of hydrogen bonds to the *N*-H pyrrolic protons or nonconventional hydrogen bonds with the π-electrons of the pyrrole units. Various types of conformations such as 1,2-alternate and full cone conformations have been reported for such supramolecular complexes of porphyrinogens.

Various conformations have been found for metallated complexes of porphyrinogens. The 1,3-alternate conformation is still the most common conformation for complexes. However, this is influenced not only by macrocyclic substituents but also the metal itself and other metal bound ligands.

The chemistry of metallated porphyrinogens has been studied extensively in the last decade. The research groups of Floriani and Gambarotta have been the sole

contributors to the research achievements in this area, which includes s-, p- and d-
and f-block metals. Some pertinent s-, p-, and d-block chemistry is reviewed in the
following Sections. s-Block metal chemistry is also discussed in Chapter 3 and f-
block chemistry is reviewed in Chapters 4-5. The chemistry reviewed highlights that
porphyrinogens can be involved non-innocently in various manners, with redox and
rearrangement chemistry being the most prominent means.

i) Coordination of s-block metals

Alkali metal complexes of deprotonated porphyrinogens are generally made
from the reaction of the porphyrinogen with reagents including *n*-butyllithium or
tert-butyllithium for lithium complexes, while for potassium, rubidium and cesium
the corresponding complexes are prepared from the metal itself in the presence of
naphthalene as an electron transfer reagent. The tetraanionic porphyrinogens are
capable of coordinating all four alkali metal cations in their complexes. The
complexes of small alkali metals feature dominant η^1- and η^2- bonding modes with
the macrocycles adopting flattened or 'chaise longue' conformations rather than the
1,3-alternate conformation of the macrocycle itself[37]. Larger alkali metals choose
both η^1- and η^5- bonding modes and the macrocycles often adopt 1,3-alternate or,
occasionally, full cone conformations. For example, [Et$_8$N$_4$Cs$_4$(digly)$_2$]$_n$, **(LV)**, has
two *endo*-cavity-bound cesium cations η^1:η^1:η^1:η^1- and η^5:η^5:η^5:η^5- bound to
pyrrolide rings, as shown in Figure 4. The complex is polymeric with the *exo*-cavity-
bound cations bridging each macrocyclic unit through η^5-interactions to pyrrolide
rings forming a two-dimensional array[38].

Figure 4: Crystal structure of **(LV)**[38] (diglyme solvent molecules have not been
shown).
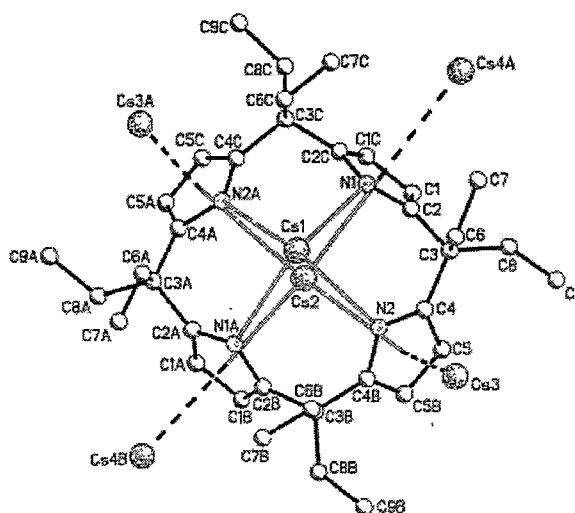
In alkali earth metal complexes, the divalent cations both reside in the tetraanionic macrocyclic cavity, giving rise to monomeric structures. η^1:η^3:η^1:η^3-Interactions are observed for the relatively small calcium dication in [(Et$_8$N$_4$)Ca$_2$(THF)$_4$], **(LVI)**, Figure 5[39]. With the partial replacement of lithium cations, as shown in Figure 6 for [(Et$_8$N$_4$)CaLi$_2$(THF)$_3$], **(LVII)**[39], the calcium centre is η^5:η^1:η^5:η^1-bound to the macrocyclic unit and lithium cations are bound to adjacent pyrrolide rings with η^1- and η^3-bonding modes. Complexes of larger alkali earth metals feature two *endo*-bound metal cations which are η^5:η^1:η^5:η^1-bound to the porphyrinogens[38].
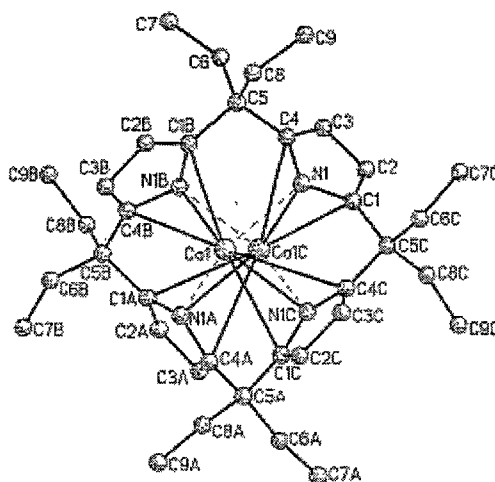
Figure 5: Crystal structure of **(LVI)** (THF solvent molecules have not been shown)[39].
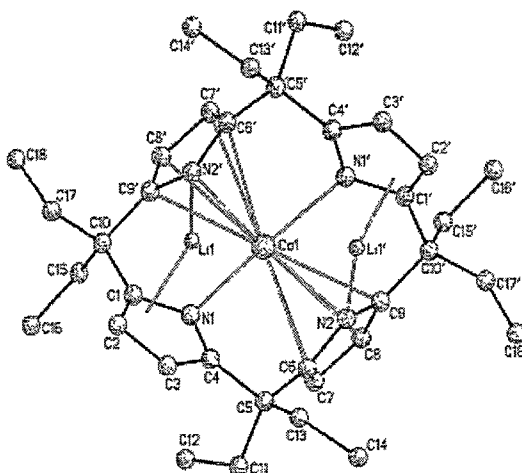
Figure 6: Crystal structure of **(LVII)** (THF solvent molecules have not been shown)[39].

ii) Coordination of p-block metals

The tin complex **(LVIII)** featuring $\eta^1{:}\eta^1{:}\eta^1{:}\eta^1$-bonding displays unique redox properties[40]. Complex **(LVIII)** was prepared from the reaction of the tetralithium salt of *meso*-octaethylporphyrinogen reacting with tetrachlorotin. Complex **(LVIII)** can be oxidised to the corresponding tin complexes of porphomethene or porphodimethene by reaction with excess of the tetrachlorotin reagent. The tin complexes perform reductive demetallations using lithium metal resulting in trilithium complexes of the porphomethene or dilithium complexes of porphodimethene. Hydrolysis of these lithium complexes yield new porphomethenes or porphodimethenes, as shown in Scheme 3.
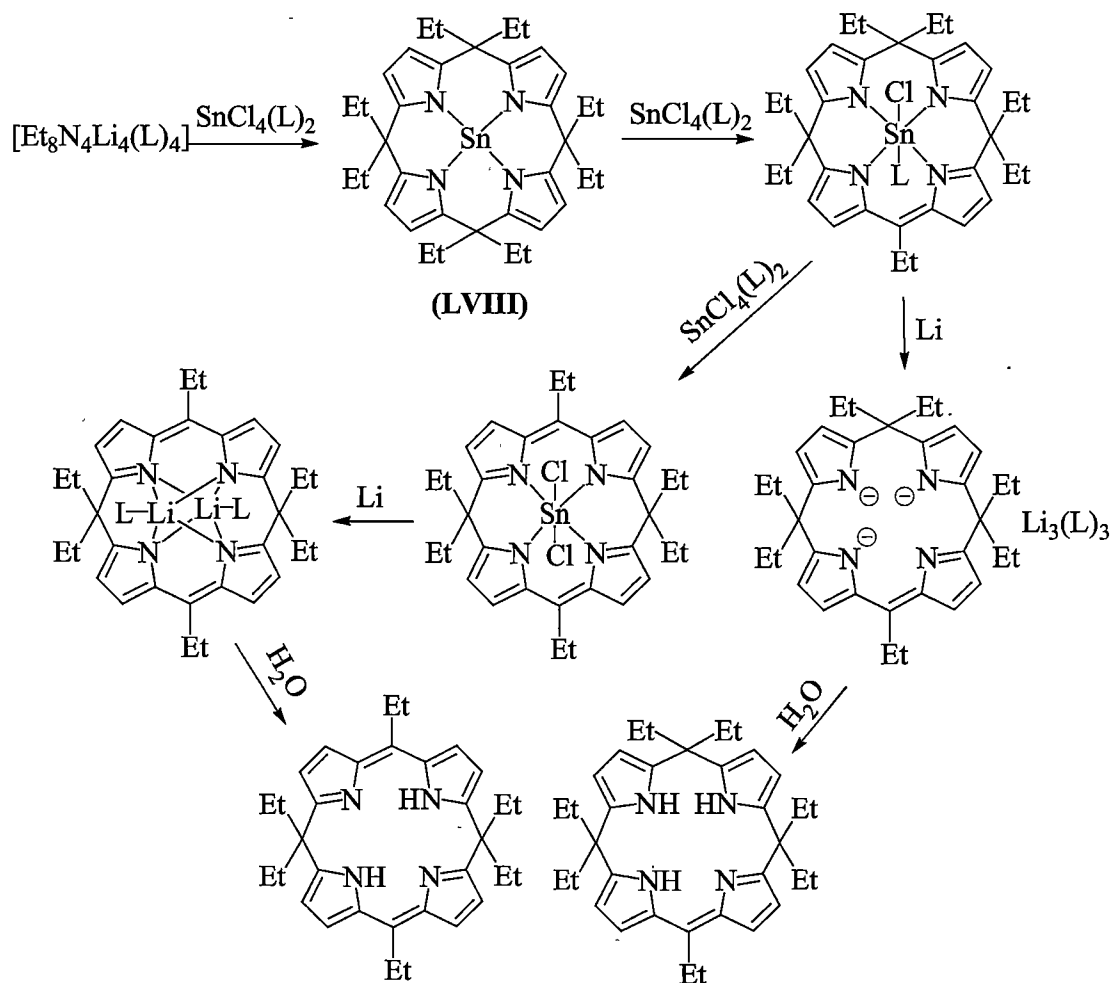
Scheme 3 (L = THF).

iii) Coordination of early transition metals

Complexes of both Group 4 and 5 metals have been synthesised from metathetical exchange reactions between alkali metal complexes of porphyrinogens with metal halide reagents. Because of the high oxidation state of the d-block metals (+4 and +5), the complexes tend not to retain residual alkali metal cations in their structures. The structure of the titanium complex **(LIX)** features $\eta^1:\eta^1:\eta^1:\eta^1$-bonding between the small sized metal cation and the porphyrinogen[41]. The macrocycle in **(LIX)** features a flattened 1,3-alternate conformation with an additional two THF molecules interacting with the titanium centre giving a distorted octahedral coordination geometry. In the zirconium complex **(LX)**[42], the larger sized metal centre adopts $\eta^5:\eta^1:\eta^5:\eta^1$-bonding to the macrocycle, while niobium chooses a $\eta^5:\eta^1:\eta^1:\eta^1$-bonding mode in complex **(LXI)**[43].

(LIX)   **(LX)**   **(LXI)**
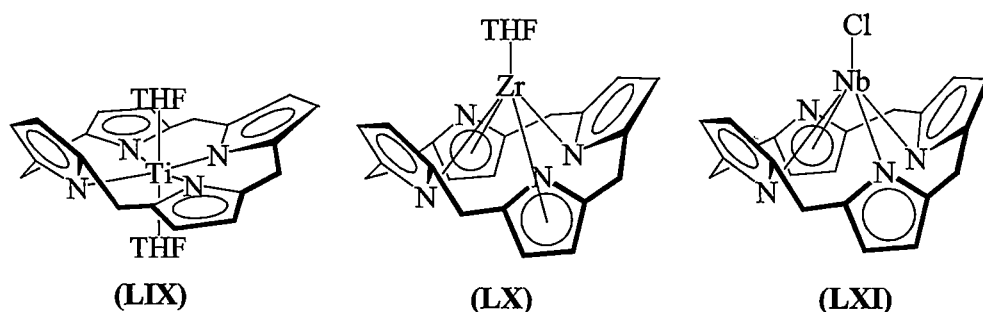
Alkylation of the niobium complex **(LXI)** with methyllithium gave a quite stable methyl complex **(LXII)** without retention of lithium cations. The subsequent reaction of **(LXII)** with two equivalents of *tert*-butylisocyanide gave the iminoacyl complex **(LXIV)** as a result of a migratory insertion of the isocyanide, as shown in Scheme 4.

(LXI)   **(LXII)**

$\xrightarrow{\text{Bu}^t\text{NC}}$ (Et$_8$N$_4$)NbMe(CNBu^t) $\xrightarrow{\text{Bu}^t\text{NC}}$ (Et$_8$N$_4$)Nb—C≡N—Bu^t

(LXIII)   **(LXIV)**
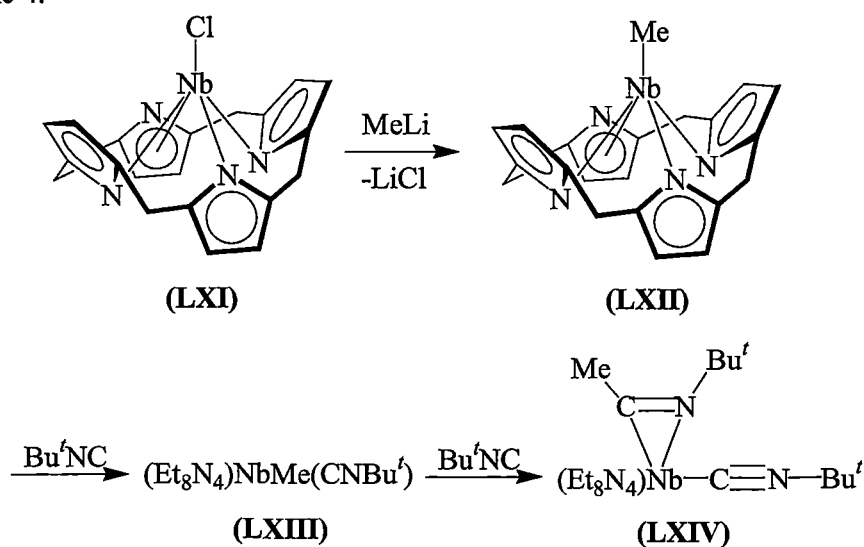
Scheme 4

Unlike the niobium(V) complex **(LXI)**, the titanium and zirconium complexes **(LIX)** and **(LX)** lack anionic ligands bound to the metal centres and thus cannot be reacted further through normal ligand substitution by metathetical exchange reactions. However, the complexes are still reactive towards many reagents, as a result of being bifunctional compounds which have two complementary reactive sites. The reactive sites being the Lewis acidic metal centre and the electron rich pyrrolide units that can act as carriers for various reagents such as alkali metal alkyls and hydrides, *etc*.

The addition of MH (M = K, Na) to complex **(LX)** leads to complex **(LXV)**. Complex **(LXV)** undergoes insertion reactions with alkenes giving the alkyl derivatives **(LXVI)**, and *tert*-butylisocyanide forming an iminoformyl complex **(LXVII)**, as shown in Scheme 5[42, 44].
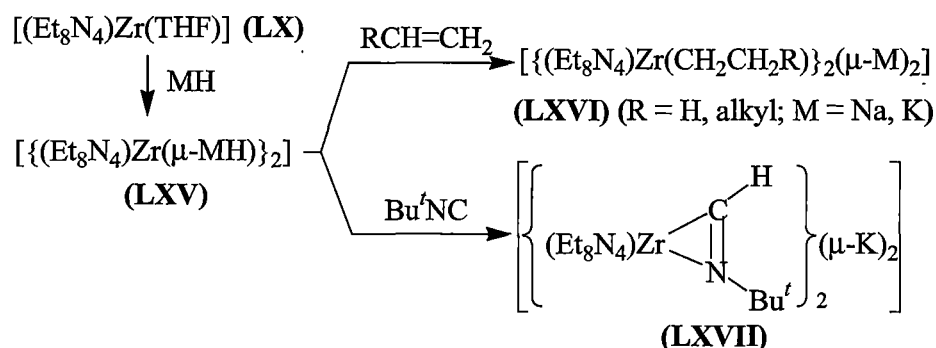
Scheme 5

Group 4 metal porphyrinogen complexes can be involved in pyrrolide ring expansions, as shown in Scheme 6. The reaction of the zirconium complex **(LX)** with carbon monoxide, followed by hydrolysis led to a new macrocycle **(LXVIII)** in 40-60% yield. Further similar treatment of **(LXVIII)** involving a hafnium derivative led to the dipyridine containing macrocycle **(LXIX)**[45].

$[(Et_8N_4)Zr(THF)]$ **(LX)** → (A) → **(LXVIII)** → (B) → **(LXIX)**
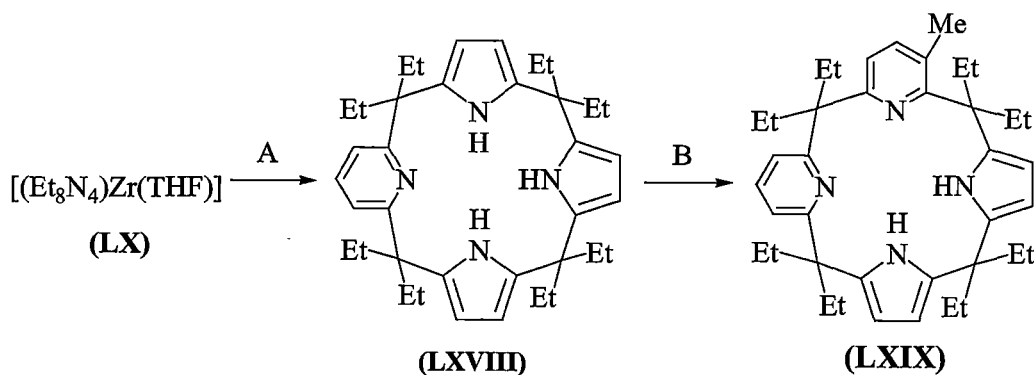
A: i) KH or NaH; ii) CO; iii) hydrolysis

B: i) Bu^nLi; ii) $HfCl_4$; iii) MeLi; iv) CO; v) hydrolysis

Scheme 6

The alkali metal hydride containing zirconium complex **(LXV)** performs an intramolecular C-H activation with the metathesis of Zr-C and Zr-H bonds, giving complex **(LXX)**. The complex **(LXX)** containing potassium hydride performs further metallation on a *meso*-substituent giving complex **(LXXI)**, while the analogous LiH reactions stop at the stage of the singly metallated product **(LXX)**. The deprotonation of complex **(LXV)** occurs predominantly at the methyl groups, leading to complexes **(LXX)** or **(LXXI)**, while lower yields of products **(LXXII)** and **(LXXIII)** derived from methylene metallation are also observed. Along with all these transformations, the complexes witness variations in bonding modes between the zirconium centres and the macrocycles ranging from $\eta^5:\eta^1:\eta^5:\eta^1$- (for **(LX)**) to $\eta^5:\eta^1:\eta^1:\eta^1$- (for **(LXX)** and **(LXXII)**)) and $\eta^1:\eta^1:\eta^1:\eta^1$-bonding modes (for **(LXXI)** and **(LXXIII)**)[44a, 46].
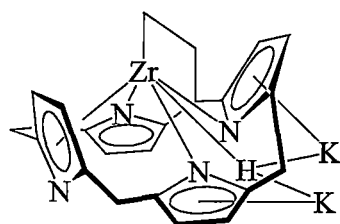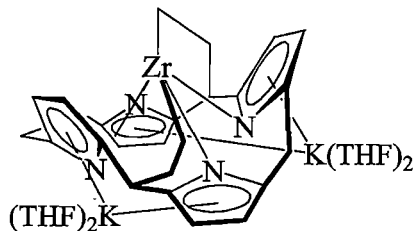
(LXX) (M = K)   **(LXXI)**
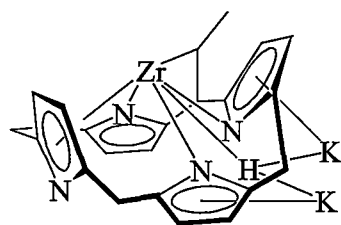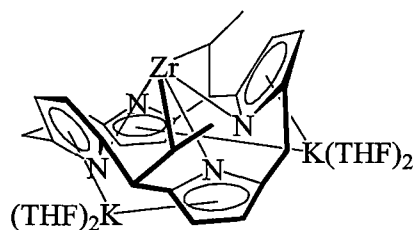
(LXXII)   **(LXXIII)**

The metallated complex **(LXX)** can be employed to modify the *meso-*
substituent of the porphyrinogen and an adjacent pyrrolide ring through sequential
insertion and migratory insertion reactions. The reaction of **(LXX)** (M = Li) with
carbon monoxide results in conversion of one pyrrolide unit to a pyridine unit with
an additional five membered ring tethering the *meso*-carbon to the β-position of the
pyridine forming complex **(LXXIV)**. Complex **(LXX)** (M = Li) also reacts with *tert*-
butylisocyanide followed by reduction leading to the new porphyrinogen **(LXXV)**
with *meso*-functionalisation, as shown in Scheme 7[44a].

(LXX) (M = Li)

(LXXIV)

(LXXV)
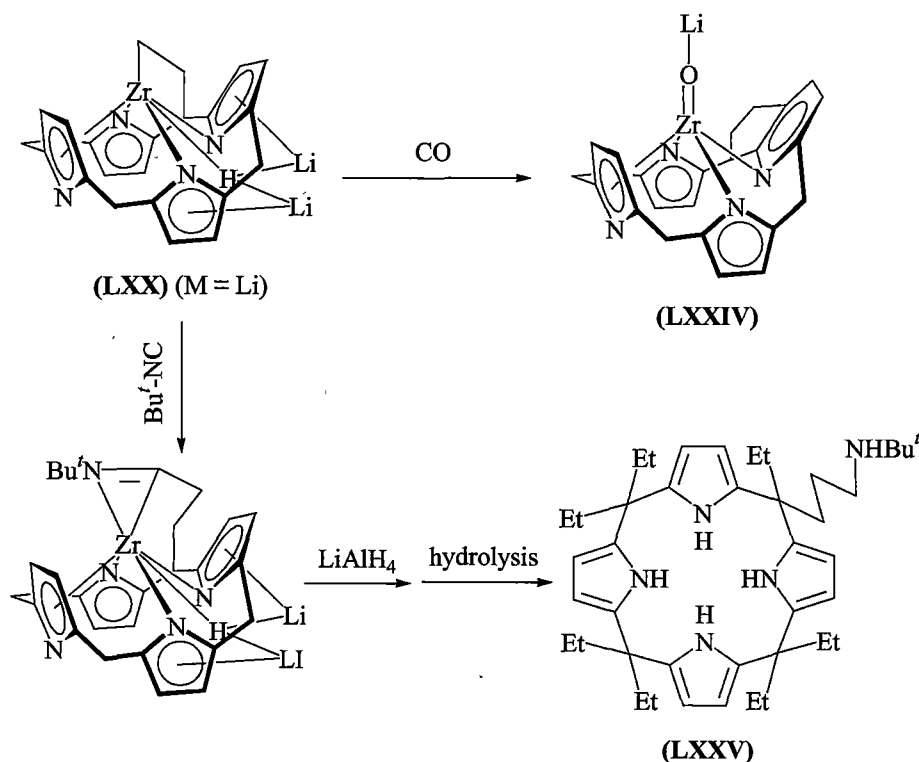
Scheme 7

iv) Coordination of late transition metals

Late transition metal complexes feature consistently η^1:η^1:η^1:η^1-bonding modes between the metals and the tetrametallated porphyrinogens which adopt flattened conformations[47]. The σ-bonding interactions affect the reactivity of the pyrrolide complexes notably in their redox chemistry. As is well known, porphyrins are produced from the oxidation of porphyrinogens which lack octaalkyl *meso*-substituents. The transformation is completed after the removal of six protons from a porphyrinogen precursor including four protons from the *meso*-positions and two from opposite pyrrole rings. Under normal conditions, porphyrinogens are robust with respect to oxidation if eight alkyl groups occupy the *meso*-positions. However, with the assistance of late transition metals, *meso*-octaalkylporphyrinogens are oxidised through pyrrolide ring coupling without *meso*-carbon proton loss. This oxidation with the removal of two electrons leads to an artificial porphyrinogen **(LXXVI)** containing a cyclopropyl ring. Further oxidation with the removal of an additional two electrons results another artificial porphyrinogen **(LXXVII)** containing two cyclopropyl rings, as shown in Scheme 8.
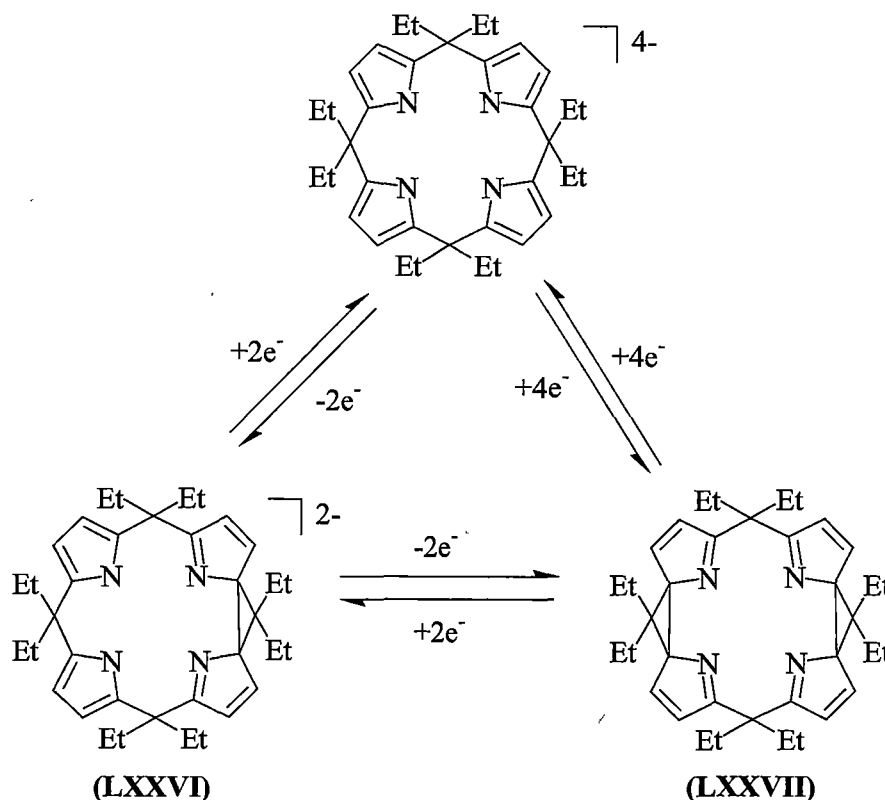
Scheme 8

Scheme 9 details the two and four electron oxidations of *meso*-octaethylporphyrinogen macrocycles through Ni, Co and Cu coordination. Copper

dichloride or quinone is employed as the oxidising reagent. The oxidation is reversible and the cyclopropyl units can be cleaved to recover the starting porphyrinogen macrocyclic complex. The formula of the four electron oxidised porphyrinogen is significant, with the $[Cu_4Cl_5]^-$ cluster formed as an unusual anion[47b, 48].
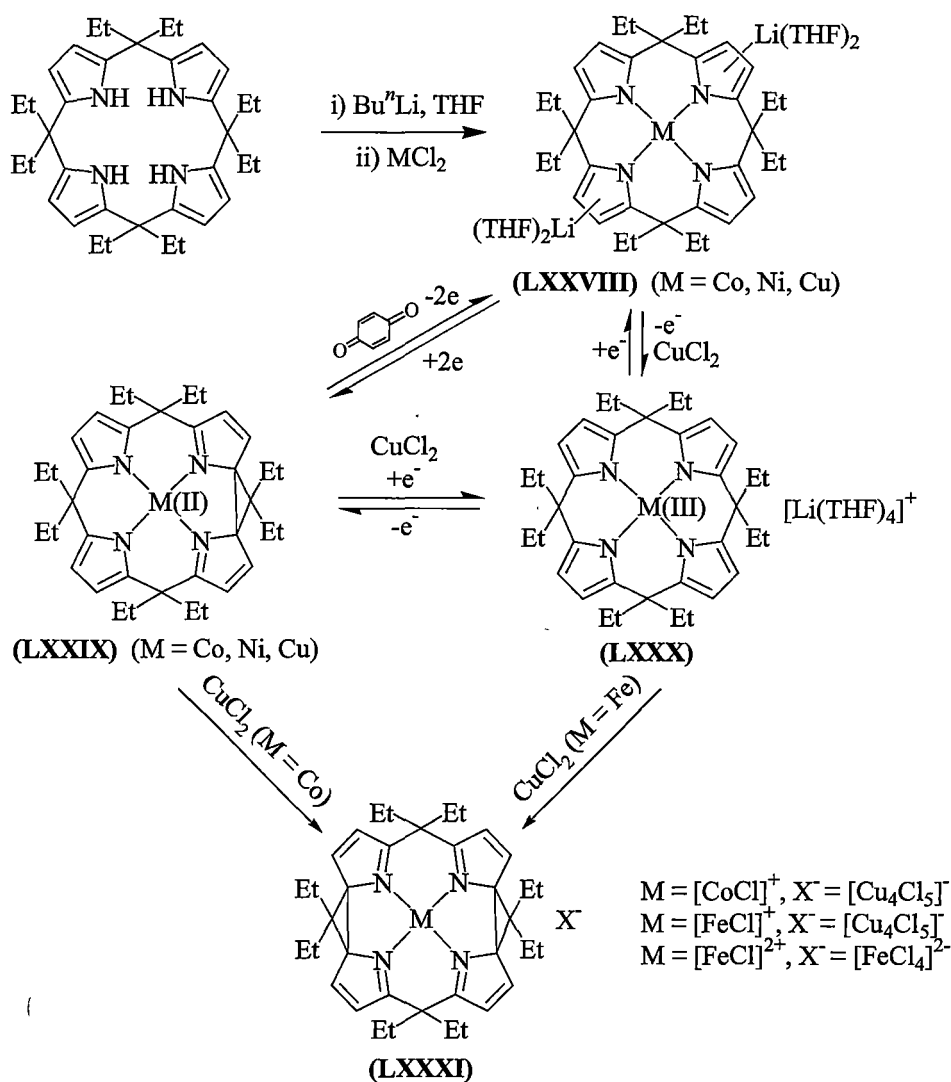
Scheme 9

The cobalt complex $[(Me_8O_2N_2)Co(THF)_2]$, **(LXXXII)** featuring dimetallated *trans*-difuranyl-*meso*-octamethylporphyrinogen, is the only transition metal complex of this ligand system to be reported with full characterisation[49]. The macrocycle binds to the metal by η^1:η^1:η^1:η^1-interactions through nitrogen and oxygen centres of the pyrrolide and the furanyl rings with the macrocycle adopting a partially flattened double cone conformation, as shown in Figure 7. Complex **(LXXXII)** has no

retention of alkali metal cations, which is a significant difference from mononuclear complexes of tetrametallated porphyrinogens featuring metals in oxidation states of less than four.
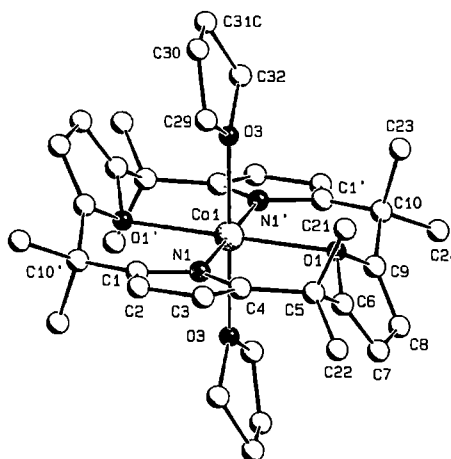
Figure 7: Crystal structure of [(Me$_8$O$_2$N$_2$)Co(THF)$_2$], **(LXXXII)**[49].

1.4 References

[1]   G. Wilkinson, J.M. Birmingham, *J. Am. Chem. Soc.*, 1954, **76**, 6210.

[2]   a. H. Gysling, M. Tsutsui, *Adv. Organomet. Chem.*, 1970, **9**, 361.

b. R.G. Hayes, J.L. Thomas, *Organomet. Chem. Rev. A,* 1971, **7**, 1.

c. M. Tsutsui, N. Ely, R. Dubois, *Acc. Chem. Res.*, 1976, **9**, 217.

d. S.A. Cotton, *J. Organomet. Chem.*, 1977, **3**, 189.

e. T.J. Marks, *Progr. Inorg. Chem.*, 1978, **24**, 51.

f. H. Schumann, In *Organometallics of the f-Elements*; T.J. Marks, R.D. Fischer, Eds. Reidel: Dordrecht, 1979, p 81.

g. W.J. Evans, In *The Chemistry of the Metal-Carbon Bond;* F.R. Hartley, S. Patai, Eds. John Wiley & Sons: London, 1982; Vol. X, Ch 12.

h. T.J. Marks, R.D. Ernst, In *Comprehensive Organometallic Chemistry*; F.G.A. Stone, G. Wilkinson, E.W. Abel, Eds. Pergamon Press: Oxford, 1982; Vol. 3, Chapter 21.

i. H. Schumann, W. Genthe, In *Handbook on the Physics and Chemistry of the Rare Earths*; K.A. Gschneidner, L. Eyring, Eds. Elsevier: Amsterdam, 1984; Vol. 7, Ch 53.

j. H. Schumann, *Angew. Chem., Int. Ed. Engl.,* 1984, **23**, 474.

k. M.N. Bochkarev, G.S. Kalinina, L.N. Bochkarev, *Russ. Chem. Rev.* 1985, **54**, 802.

l. W.J. Evans, *Adv. Organomet. Chem.*, 1985, **24**, 131.

m. A. Streitwieser, Jr. In *Fundamental and Technological Aspects of Organo-f-Element Chemistry*; T.J. Marks, I.L. Fragalà, Eds. NATO ASI Series D; Reidel: Boston, MA, 1985; Vol. 155, p 1.

n. R.D. Rogers, L.M. Rogers, *J. Organomet. Chem.*, 1993, **457**, 41.

o. R. Poli, *Chem. Rev.*, 1991, **91**, 509.

p. C.J. Schaverien, *Adv. Organomet. Chem.*, 1994, **36**, 283.

q. H. Schumann, J.A. Meese-Marktscheffel, L. Esser, *Chem. Rev.*, 1995, **95**, 865.

[3]   a. F.T. Edelmann, *Angew. Chem., Int. Ed. Engl.*, 1995, **34**, 2466.

b. C. Eaborn, K. Izod, J.D. Smith, *J. Organomet. Chem.,* 1995, **500**, 89.

c. M.P. Hogerheide, J. Boersma, G. van Koten, *Coord. Chem. Rev.*, 1996, **155**, 87.

d. S.A. Cotton, *Coord. Chem. Rev.*, 1997, **160**, 93.

e. L.N. Zakharov, Y.T. Struchkov, *J. Organomet. Chem.*, 1997, **536**, 65.

f. W.J. Evans, *New J. Chem.*, 1995, **19**, 525.

g. F. Nief, *Coord. Chem. Rev.*, 1998, **178**, 13.

h. F. Nief, *Eur. J. Inorg. Chem.*, 2001, 891.

[4]   **a.** G.W. Rabe, C.S. Strissel, L.M. Liable-Sands, T.E. Concolino, A.L. Rheingold, *Inorg. Chem.*, 1999, **38**, 3446.

b. G.W. Rabe, C.D. Bérubé, G.P.A. Yap, K.-C. Lam, T.E. Concolino, A.L. Rheingold, *Inorg. Chem.*, 2002, **41**, 1446.

[5]   **a.** T.I. Gountchev, T.D. Tilley, *Organometallics*, 1999, **18**, 2896.

b. T.I. Gountchev, T.D. Tilley, *Organometallics*, 1999, **18**, 5661.

[6]   C.J. Schaverien, N. Meijboom, A.G. Orpen, *J. Chem. Soc., Chem. Commun.*, 1992, 124.

[7]   M.D. Fryzuk, G. Giesbrecht, S.J. Rettig, *Organometallics*, 1996, **15**, 3329.

[8]   D.D. Graf, W.M. Davis, R.R. Schrock, *Organometallics*, 1998, **17**, 5820.

[9]   **a.** R. Duchateau, T. Tuinstra, E.A.C. Brussee, A. Meetsma, P.T. van Duijnen, J.H. Teuben, *Organometallics*, 1997, **16**, 3511.

b. R. Duchateau, E.A.C. Brussee, A. Meetsma, J.H. Teuben, *Organometallics*, 1997, **16**, 5506.

c. M. Veith, *Angew. Chem., Int. Ed. Engl.*, 1987, **26**, 1.

d. A. Recknagel, A. Steiner, S. Brooker, D. Stalke, F.T. Edelmann, *J. Organomet. Chem.*, 1991, **415**, 315.

[10] **a.** R. Taube, H. Windisch, F.H. Görlitz, H. Schumann, *J. Organomet. Chem.*, 1993, **445**, 85.

b M. Brunelli, S. Poggio, U. Pedretti, G. Lugli, *Inorg. Chim. Acta*, 1987, **131**, 281.

c. Z. Huang, M. Chen, W. Qiu, W. Wu, *Inorg. Chim. Acta*, 1987, **139**, 203.

d. R. Taube, S. Maiwald, J. Sieler, *J. Organomet. Chem.*, 1996, **513**, 37.

e. R. Taube, H. Windisch, S. Maiwald, H. Hemling, H. Schumann, *J. Organomet. Chem.*, 1996, **513**, 49.

f. R. Taube, S. Maiwald, J. Sieler, *J. Organomet. Chem.*, 2001, **621**, 327.

g. R. Taube, H. Windisch, H. Weissenborn, H. Hemling, H. Schumann, *J. Organomet. Chem.*, 1997, **548**, 229.

h. R. Taube, H. Windisch, *J. Organomet. Chem.*, 1994, **472**, 71.

i. H. Windisch, J. Scholz, R. Taube, B. Wrackmeyer, *J. Organomet. Chem.*, 1996, **520**, 23.

j. H. Reddmann, H.-D. Amberger, B. Kanellakopulos, S. Maiwald, R. Taube, *J. Organomet. Chem.*, 1999, **584**, 310.

k. W. Wu, M. Chen, P. Zhou, *Organometallics*, 1991, **10**, 98.

l. B. Hamann-Gaudinet, J.-L. Namy, H.B. Kagan, *J. Organomet. Chem.*, 1998, **567**, 39.

[11]   a. R. Duchateau, C.T. van Wee, A. Meetsma, J.H. Teuben, *J. Am. Chem. Soc.*, 1993, **115**, 4931.

b. F.T. Edelmann, *J. Alloys Compd.*, 1994, **207**, 182.

c. F.T. Edelmann, *Coord. Chem. Rev.*, 1994, **137**, 403.

d. R. Duchateau, C. T. van Wee, A. Meetsma, P.T. van Duijnen, J.H. Teuben, *Organometallics*, 1996, **15**, 2279.

e. R. Duchateau, C.T. van Wee, J.H. Teuben, *Organometallics*, 1996, **15**, 2291.

f. J.R. Hagadorn, J. Arnold, *Organometallics*, 1996, **15**, 984.

g. S. Bambirra, M.J.R. Brandsma, E.A.C. Brussee, A. Meetsma, B. Hessen, J.H. Teuben, *Organometallics*, 2000, **19**, 3197.

h. S. Bambirra, A. Meetsma, B. Hessen, J.H. Teuben, *Organometallics*, 2001, **20**, 782.

i. Y. Zhou, G.P.A. Yap, D.S. Richeson, *Organometallics*, 1998, **17**, 4387.

[12]   a. P.B. Hitchcock, M.F. Lappert, S. Tian, *J. Organomet. Chem.*, 1997, **549**, 1.

b. C.F. Caro, M.F. Lappert, P.G. Merle, *Coord. Chem. Rev.*, 2001, **219**, 605.

[13]   a. L.W.M. Lee, W.E. Piers, M.R.J. Elsegood, W. Clegg, M. Parvez, *Organometallics*, 1999, **18**, 2947.

b. P.W. Roesky, *J. Organomet. Chem.*, 2000, **603**, 161.

c. P.W. Roesky, *Inorg. Chem.*, 1998, **37**, 4507.

[14]   a. C.J. Schaverien, *Adv. Organomet. Chem.*, 1994, **36**, 283.

b. F.T. Edelmann, In *Comprehensive Organometallic Chemistry II*; F.G.A. Stone, G. Wilkinson, E.W. Abel, Eds.; Pergamon Press: Oxford, U.K., 1995; Vol. 4, Ch 2.

c. F.T. Edelmann, *Angew. Chem., Int. Ed. Engl.*, 1995, **34**, 2466.

d. F.T. Edelmann, *New J. Chem.*, 1995, **19**, 535.

e. A.L. Wayda, S. Cheng, I. Mukerji, *J. Organomet. Chem.*, 1987, **330**, C17.

f. A. Streitwieser, Jr. In *Fundamental and Technological Aspects of Organo-f-Element Chemistry*; T.J. Marks, I.L. Fragalà, Eds. NATO ASI Series D; Reidel: Boston, MA, 1985; Vol. 155, p 77.

g. A. Streitwieser, Jr., T.R. Boussie, *Eur. J. Solid State Inorg. Chem.*, 1991, **28**, 399.

[15]   **a.** W.J. Evans, G.W. Rabe, J.W. Ziller, *Organometallics*, 1994, **13**, 1641.

b. G.B. Deacon, C.M. Forsyth, B.M. Gatehouse, P.A. White, *Aust. J. Chem.*, 1990, **43**, 795.

c. C.T. Abrahams, G.B. Deacon, B.M. Gatehouse, G.N. Ward, *Acta Crystallogr., Sect. C (Cryst. Struct. Commun.)*, 1994, **50**, 504.

[16]   **a.** C.N. Eigenbrot, Jr., K.N. Raymond, *Inorg. Chem.*, 1981, **20**, 1553.

b. C.N. Eigenbrot, Jr., K.N. Raymond, *Inorg. Chem.*, 1982, **21**, 2653.

c. H. Schumann, P.K. Lee, J. Löbel, *Angew. Chem., Int. Ed. Engl.*, 1989, **28**, 1033.

d. G.B. Deacon, B.M. Gatehouse, S. Nickel, S.N. Platts, *Aust. J. Chem.*, 1991, **44**, 613.

e. J.E. Cosgriff, G.B. Deacon, B.M. Gatehouse, *Aust. J. Chem.*, 1993, **46**, 1881.

f. J.E. Cosgriff, G.B. Deacon, B.M. Gatehouse, H. Hemling, H. Schumann, *Angew. Chem., Int. Ed. Engl.*, 1993, **32**, 874.

g. J.E. Cosgriff, G.B. Deacon, B.M. Gatehouse, H. Hemling, H. Schumann, *Aust. J. Chem.*, 1994, **47**, 1223.

h. J.E. Cosgriff, G.B. Deacon, G.D. Fallon, B.M. Gatehouse, H. Schumann, R. Weimann, *Chem. Ber.*, 1996, **126**, 953.

i. G.B. Deacon, E.E. Delbridge, G.D. Fallon, C. Jones, D.E. Hibbs, M.B. Hursthouse, B.W. Skelton, A.H. White, *Organometallics*, 2000, **19**, 1713.

j. G.B. Deacon, E.E. Delbridge, C.M. Forsyth, *Angew. Chem. Int. Ed.*, 1999, **38**, 1766.

k. G.B. Deacon, A. Gitlits, B.W. Skelton, A.H. White, *Chem. Commun.*, 1999, 1213.

l. G.B. Deacon, E.E. Delbridge, B.W. Skelton, A.H. White, *Eur. J. Inorg. Chem.*, 1998, 543.

m. G.B. Deacon, E.E. Delbridge, B.W. Skelton, A.H. White, *Eur. J. Inorg. Chem.*, 1999, 751.

n. G.B. Deacon, E.E. Delbridge, B.W. Skelton, A.H. White, *Angew. Chem. Int. Ed.*, 1998, **37**, 2251.

n. X. Zhou, H. Ma, X. Yuang, X. You, *J. Chem. Soc., Chem. Commun.*, 1995, 2483.

o. X. Zhou, W. Ma, Z. Huang, R. Cai, X. You, X. Huang, *J. Organomet. Chem.*, 1997, **545**, 309.

p. H. Schumann, J. Loebel, J. Pickart, C. Quian, Z. Xie, *Organometallics*, 1991, **10**, 215.

[17]   a. G. Ferrence, J. Takats, *J. Organomet. Chem.*, 2002, **647**, 84.

b. F.T. Edelmann, *Angew. Chem., Int. Ed. Engl.*, 1995, **34**, 2466.

c. X. Zhang, R. McDonald, J. Takats, *New J. Chem.*, 1995, **19**, 573.

d. A.C. Hillier, X.W. Zhang, G.H. Maunder, S.Y. Liu, T.A. Eberspacher, M.V. Metz, R. McDonald, A. Domingos, N. Marques, V.W. Day, A. Sella, J. Takats, *Inorg. Chem.*, 2001, **40**, 5106 (and references therein).

e. S. Trofimenko, J.C. Calabrese, J.K. Kochi, J.D. Korp, S. Wolowiec, F.B. Hulsbergen, J. Reedijk, *Inorg. Chem.*, 1992, **31**, 3943.

f. S. Trofimenko, *Scorpionates: The Coordination Chemistry of Polypyrazolylborate Ligands*, Eds. Imperial College Press: London, 1999.

g. L. Hasinoff, J. Takats, X.W. Zhang, A.H. Bond, R.D. Rogers, *J. Am. Chem. Soc.*, 1994, **116**, 8833.

h. G.H. Maunder, A. Sella, D.A. Tocher, *J. Chem. Soc., Chem. Commun.*, 1994, 2689.

[18]   a. F. Nief, L. Ricard, *J. Chem. Soc., Chem. Commun.*, 1994, 2723.

b. P. Desmurs, M. Visseaux, D. Baudry, A. Dormond, F. Nief, L. Ricard, *Organometallics*, 1996, **15**, 4178.

c. P. Desmurs, A. Dormond, F. Nief, D. Baudry, *Bull. Soc. Chim. Fr.*, 1997, **134**, 683.

[19]   a. P.L. Arnold, F.G.N. Cloke, P.B. Hitchcock, J.F. Nixon, *J. Am. Chem. Soc.*, 1996, **118**, 7630.

b. P.L. Arnold, F.G.N. Cloke, J.F. Nixon, *Chem. Commun.*, 1998, 797.

[20]   G.B. Deacon, E.E. Delbridge, G.D. Fallon, C. Jones, D.E. Hibbs, M.B. Hursthouse, B.W. Skelton, A.H. White, *Organometallics*, 2000, **19**, 1713.

[21]   a. L. Lee, D.J. Berg, G.W. Bushnell, *Organometallics*, 1995, **14**, 8.

b. L. Lee, D.J. Berg, F.W. Eisenstein, R.J. Batchelor, *Organometallics*, 1997, **16**, 1819.

[22]   a. Z. Xie, Z. Liu, K. Chiu, F. Xue, T.C.W. Mak, *Organometallics*, 1997, **16**, 2460.

b. K. Chiu, Z. Zhang, T.C.W. Mak, Z. Xie, *J. Organomet. Chem.*, 2000, **614**, 107.

c. Z. Xie, Z. Liu, Q. Yang, T.C.W. Mak, *Organometallics*, 1999, **18**, 3603.

[23]   F.G. Bordwell, G.E. Drucker, H.E. Fried, *J. Org. Chem.*, 1982, **35**, 941.

[24]   R. Vann Bynum, W.E. Hunter, R.D. Rogers, J.L. Atwood, *Inorg. Chem.*, 1980, **19**, 2368.

[25]   R.B. King, M.B. Bisnette, *Inorg. Chem.*, 1964, **3**, 796.

[26]   M.D. Fayer, C.B. Harris, *Inorg. Chem.*, 1969, **8**, 2792.

[27]   K.K. Joshi, P.L. Pauson, A.R. Qazi, W.H. Stubbs, *J. Organomet. Chem.*, 1964, **30**, 211.

[28]   N.I. Pyshnograeva, V.N. Setkina, V.G. Andrianov, Y.T. Struchkov, D.N. Kursanov, *J. Organomet. Chem.*, 1977, **128**, 381.

[29]   a. N. Kuhn, M. Kockerling, S. Stubenrauch, D. Blaser, R. Boese, *J. Chem. Soc., Chem. Commun.*, 1991, 1368.

b. N. Kuhn, G. Henkel, J. Kreutzberg, S. Stubenrauch, C. Janiak, *J. Organomet. Chem.*, 1993, **456**, 97.

c. N. Kuhn, K. Jendral, R. Boese, D. Blaser, *Chem. Ber.*, 1991, **124**, 89.

[30]   a. H. Schumann, J. Gottfriedsen, J. Demtschuk, *Chem. Commun.*, 1999, 2091.

b. N. Kuhn, G. Henkel, S. Stubenrauch, *Angew. Chem., Int. Ed. Engl.*, 1992, **31**, 778.

c. N. Kuhn, G. Henkel, S. Stubenrauch, *J. Chem. Soc., Chem. Commun.*, 1992, 760.

[31]   a. H. Felkin, J. Zakrzewski, *J. Am. Chem. Soc.*, 1985, **107**, 3374.

b. J. Zakrzewski, *Heterocycles*, 1990, **31**, 383.

c. J. Zakrzewski, *J. Organomet. Chem.*, 1987, **326**, C17.

[32]	T. Dubé, D. Freckmann, S. Conoci, S. Gambarotta, G.P.A. Yap, *Organometallics*, 2000, **19**, 209.

[33]	M. Tayebani, S. Conoci, K. Feghali, S. Gambarotta, G.P.A. Yap, *Organometallics*, 2000, **19**, 4568.

[34]	K.K. Dailey, G.P.A. Yap, A.L. Rheingold, T.B. Rauchfuss, *Angew. Chem., Int. Ed. Engl.*, 1996, **35**, 1833.

[35]	P.A. Gale, J.L. Sessler, V. Král, V. Lynch, *J. Am. Chem. Soc.*, 1996, **118**, 5140.

[36]	Y.D. Wu, D.F. Wang, J. Sessler, *J. Org. Chem.*, 2001, **66**, 3739.

[37]	**a.** Y.S. Jang, H.J. Kim, P.H. Lee, C.H. Lee, *Tetrahedron Letters*, 2000, **41**, 2919.
	b. Y. Furusho, H. Kawasaki, S. Nakanishi, T. Aida, T. Takata, *Tetrahedron Letters*, 1998, **39**, 3537.

[38]	L. Bonomo, E. Solari, R. Scopelliti, C. Floriani, *Chem.-Eur. J.*, 2001, **7**, 1322.

[39]	L. Bonomo, O. Dandin, E. Solari, C. Floriani, R. Scopelliti, *Angew. Chem. Int. Ed.* 1999, **38**, 914.

[40]	J.M. Benech, L. Bonomo, E. Solari, R. Scopelliti, C. Floriani, *Angew. Chem. Int. Ed.*, 1999, **38**, 1957.

[41]	S. De Angelis, E. Solari, C. Floriani, A. Chiesi-Villa, C. Rizzoli, *Angew. Chem., Int. Ed. Engl.*, 1995, **34**, 1092.

[42]	D. Jacoby, C. Floriani, A. Chiesi-Villa, C. Rizzoli, *J. Am. Chem. Soc.*, 1993, **115**, 3595.

[43]	S. Isoz, C. Floriani, K. Schenk, A. Chiesi-Villa, C. Rizzoli, *Organometallics*, 1996, **15**, 337.

[44] **a**. D. Jacoby, S. Isoz, C. Floriani, A. Chiesi-Villa, C. Rizzoli, *J. Am. Chem. Soc.*, 1995, **117**, 2805.

b. D. Jacoby, S. Isoz, C. Floriani, K. Schenk, A. Chiesi-Villa, C. Rizzoli, *Organometallics*, 1995, **14**, 4816.

[45] **a**. D. Jacoby, C. Floriani, A. Chiesi-Villa, C. Rizzoli, *J. Am. Chem. Soc.*, 1993, **115**, 7025.

b. D. Jacoby, S. Isoz, C. Floriani, A. Chiesi-Villa, C. Rizzoli, *J. Am. Chem. Soc.*, 1995, **117**, 2793.

[46] C. Floriani, *Chem. Commun.*, 1996, **11**, 1257.

[47] **a**. J. Jubb, D. Jacoby, C. Floriani, A. Chiesi-Villa, C. Rizzoli, *Inorg. Chem.*, 1992, **31**, 1306.

b. S. De Angelis, E. Solari, C. Floriani, A. Chiesi-Villa, C. Rizzoli, *J. Am. Chem. Soc.*, 1994, **116**, 5702.

c. L. Bonomo, E. Solari, M. Latronico, R. Scopelliti, C. Floriani, *Chem.-Eur. J.*, 1999, **5**, 2040.

[48] J. Jubb, C. Floriani, A. Chiesi-Villa, C. Rizzoli, *J. Am. Chem. Soc.*, 1992, **114**, 6571.

[49] R. Crescenzi, E. Solari, C. Floriani, A. Chiesi-Villa, C. Rizzoli, *Inorg. Chem.*, 1996, **35**, 2413.

CHAPTER 2

SYNTHESIS OF MODIFIED PORPHYRINOGENS

2.1 INTRODUCTION

As early as 1886, Baeyer reported the first porphyrinogen (I) (R = Me), *meso*-octamethylporphyrinogen, by the condensation of pyrrole and acetone in the presence of acid[1] (in 88% yield using methanesulfonic acid was reported later by Gage[2]), as shown in Equation 1. Surprisingly, the chemistry of porphyrinogens remained dormant for a century until the 1990s, except for a very limited number of studies. Most studies so far are still related to unmodified systems, or simply modified examples through substituent variations at the *meso*-carbon positions. Only limited effort has been applied to the modification of porphyrinogens for applications restricted mainly to supramolecular chemistry based areas including sensors and separation science[3]. Several review articles have appeared on porphyrinogen chemistry[4], including synthetic/molecular recognition chemistry[5] and coordination chemistry[6]. The review in this chapter is focused on the modification of porphyrinogens. The 'modification' of porphyrinogens here includes both the direct preparation of modified porphyrinogens and those formed by the modification of simpler porphyrinogens.

(I) (R = Me)
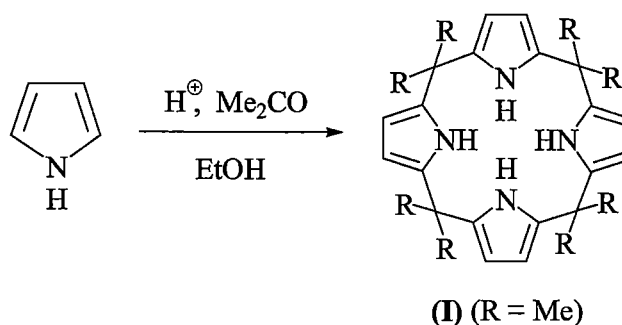
Equation 1

Modifications of porphyrinogens include those at the *meso*-carbons, 'C-rim' modifications at β-positions of the pyrrolide rings and 'N-rim' modifications through N-substitution of pyrrolide rings. More dramatic modifications involve substitution of pyrrole rings with other aromatic rings such as furan, thiophene or pyridine *etc.*

Meso-carbon modifications of porphyrinogens can be achieved by the use of different ketones in acid-catalysed condensations with pyrrole. Porphyrinogens featuring R = Et (*meso*-octaethylporphyrinogen), 2R = -(CH$_2$)$_5$- (*meso*-

tetraspirocyclohexylporphyrinogen) are most commonly utilised in porphyrinogen chemistry studies. More notably, modification at the *meso*-carbon with functionalised groups has been achieved recently[7]. For example, the condensation of Cbz-protected 3-aminoacetophenone, 3-pentanone and pyrrole in the presence of $BF_3 Et_2O$, followed by deprotection with Pd-C gave the mono-amine functionalised porphyrinogen (II) in 21% overall yield.

Generally speaking, lower yields of *meso*-substituted porphyrinogens are observed for ketones other than acetone in the acid-catalysed condensations. The *meso*-R groups alter the electrophilic addition characteristics of the carbonyl carbon centre through their electron donating and steric effects.

(II)

(III)
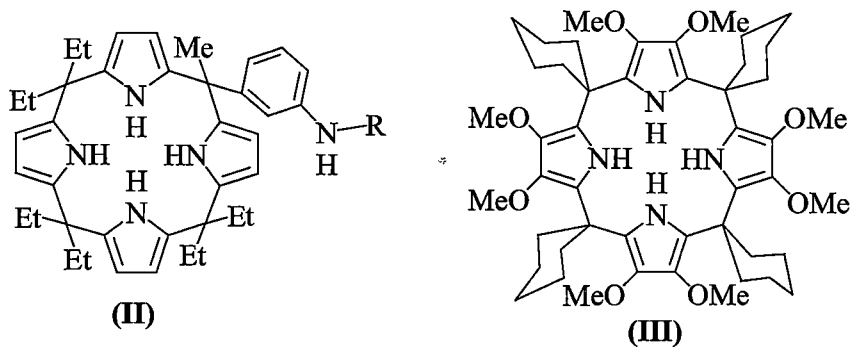
C-rim modifications can be obtained directly by the condensation of β-substituted pyrroles with ketones[8]. For example, the condensation of 3,4-dimethoxypyrrole with cyclohexanone in glacial acetic acid led to β-octamethoxy-*meso*-tetraspirocyclohexylporphyrinogen (III) in 8% yield. β-Octabromo-*meso*-octaethylporphyrinogen was prepared in high yield by the reaction of *meso*-octaethylporphyrinogen with *N*-bromosuccinimide.

The syntheses of mono β-substituted porphyrinogens have been achieved by organometallic[9] and organic synthetic[10] methods. The former case involves the reaction of *meso*-octamethylporphyrinogen (I) with 4 equivalents of *n*-butyllithium followed by the addition of ethyl bromoacetate giving macrocycle (IV) in 35% after hydrolysis, as shown in Scheme 1. The latter case gave the mono-iodo derivative obtained from the reaction of (II) with iodine-[bis(trifluoroacetoxy)iodo]benzene.

(I)

(IV) (R = CH$_2$CO$_2$Et)
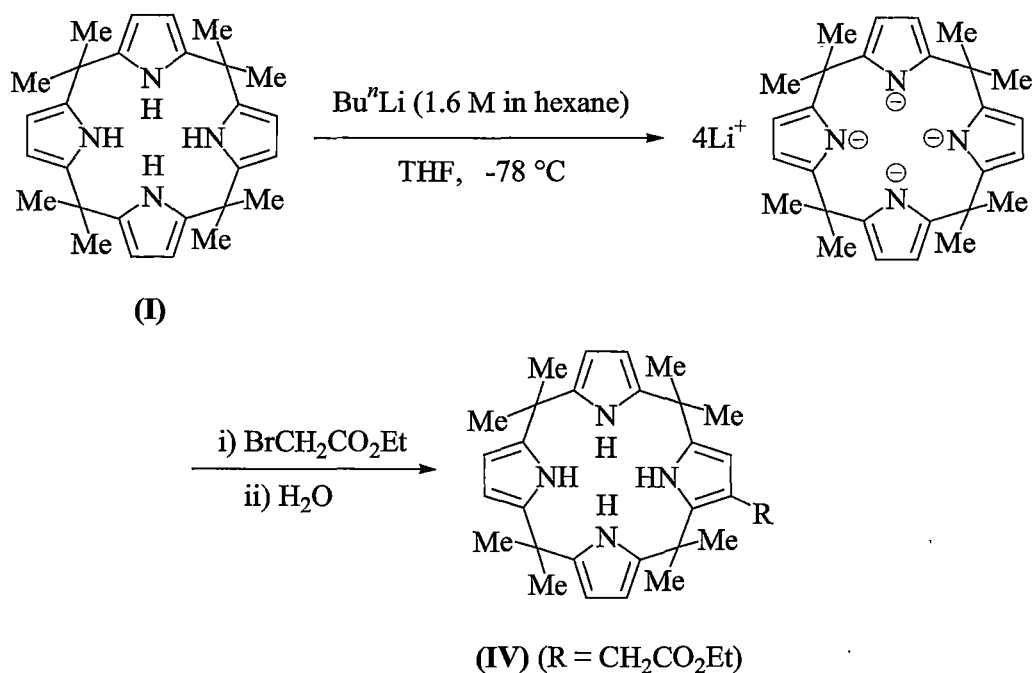
Scheme 1: Synthesis of macrocycle **(IV)**

An early N-rim modification *via* an acid-catalysed condensation was reported where a N,N',N'',N'''-tetramethylporphyrinogen **(V)** was prepared from the condensation of N-methylnorporphobilinogen in 17% yield[11], as shown in Equation 2. The macrocycle does not convert to the related porphyrin owing to the conformational restrictions placed by the N-methyl substituents.

(V) (R = CH$_2$COOH)
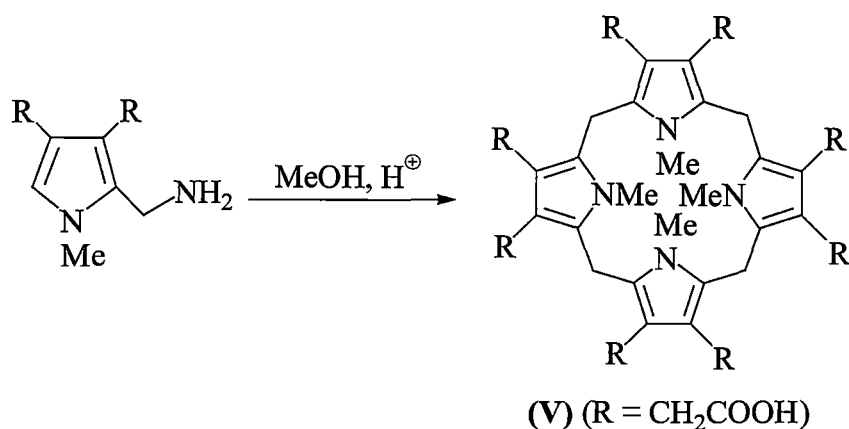
Equation 2

The synthesis of the two fold N,N'-bridged porphyrinogen **(VI)** was reported in 1987[12]. The macrocycle was achieved in 9% yield from the acid-catalysed condensation of a dialcohol derived from the reduction of the dialdehyde precursor,

as shown in Equation 3. The dialdehyde precursor was prepared from the reaction of potassium 3,4-diethyl-2-formylpyrrolide with 1,3-dibromopropane. The molecule experiences forcing geometrical restraints related to two N,N'-alkyl linkages. As a consequence, **(VI)** is also inert to oxidation and thus cannot be transformed to the corresponding planar porphyrin, as would normally occur for porphyrinogens lacking *meso*-substituents. In addition, the N-alkylation further prevents the oxidation of **(VI)** owing to the absence of labile N-H moities.

$$\text{MeOH, H}^{\oplus}$$

(VI) (R = Et)
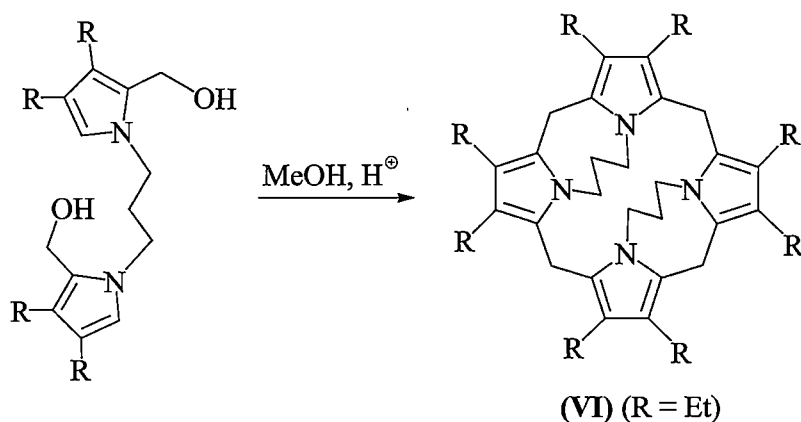
<div align="right">**Equation 3**</div>

As shown in Scheme 1 for the synthesis of the β-substituted porphyrinogen **(IV)**, C-rim substitution results from the reaction of the tetralithiated porphyrinogen with electrophiles. N-Rim modifications have proven to be inaccessible using nucleophilic substitution methodologies involving alkali metal salts of porphyrinogens with electrophiles under normal conditions. However, this reaction can be directed towards high yielding N-rim substitutions, rather than C-rim substitution, under very specific conditions. In 1998, Takata and coworkers reported the N-alkylation of *meso*-octaethylporphyrinogen by the reaction of the tetrasodium salt of the porphyrinogen with methyl or ethyl iodide in the presence of four stoichiometric equivalents of 18-crown-6[13]. Six N-alkylated porphyrinogens, **(VII)**, were prepared by this methodology. *Trans-N,N'*-dimethyl-*meso*-octaethylporphyrinogen is used extensively in this project and further synthetic details are shown in Section 2.2.2.

(VII)

$R = Me, R^1 = R^2 = R^3 = H;$

$R = R^1 = Me, R^2 = R^3 = H;$

$R = R^2 = Me, R^1 = R^3 = H;$

$R = R^1 = R^2 = Me, R^3 = H;$

$R = R^1 = R^2 = R^3 = Me;$

$R = Et, R^1 = R^2 = R^3 = H.$
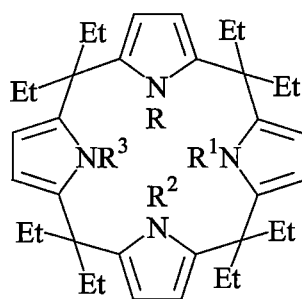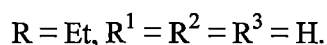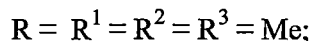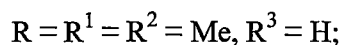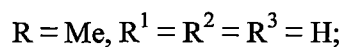
The earliest porphyrinogen modification by substitution of pyrrolyl rings with furanyl rings was reported in 1958 by Brown et al.[14]. Porphyrinogens (XI), (XII) and (XIII) were prepared by the condensation of furanyl and pyrrolyl precursors. The trans-dioxaporphyrinogen (XI) was formed from the acid catalysed condensation of 2-(2'-furanyl)-2-(2''-pyrrolyl)propane (IX) with acetone in 15% yield. The alternative condensation of 2,5-bis(dimethylhydroxymehtyl)furan and pyrrole led to the same macrocycle (XI) in a similar yield. The cis-dioxaporphyrinogen (XII) was synthesised from the condensation of (VIII) and (X), while the trioxaporphyrinogen (XIII) was obtained from the reaction between (X) and (IX). The syntheses of the all the oxaporphyrinogens (XI) - (XIII) were in rather low yields with poor control over the formation of byproducts such as polymeric species.
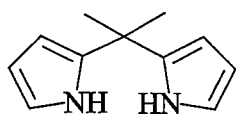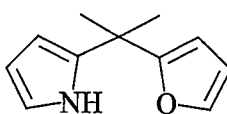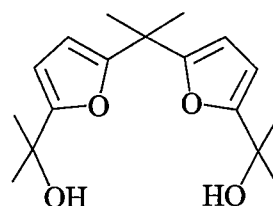
(VIII)   (IX)   (X)
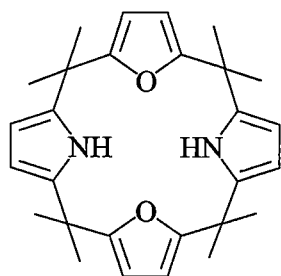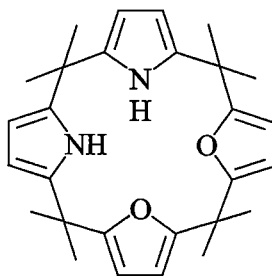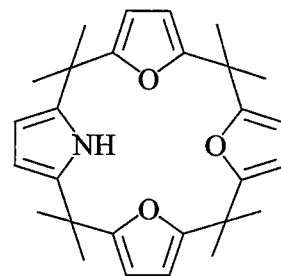
(XI)   (XII)   (XIII)

The so called '3+1' approach was reported to be an efficient way to prepare porphyrinogens, even for oxaporphyrinogens without *meso*-substituents, which are hardly accessible by other means[15]. In this more controlled procedure, the preparation of the *trans*-dioxaporphyrinogen **(XI)**[16] has been improved to 46% yield, as shown in Scheme 2. The hexameric **(XV)** and octameric **(XIV)** oxaporphyrinogens (X = O) were controlled to 11% and 9% content. The corresponding thiophene substituted macrocycles (X = S) have also been achieved in slightly lowered yields in the analogous reactions.
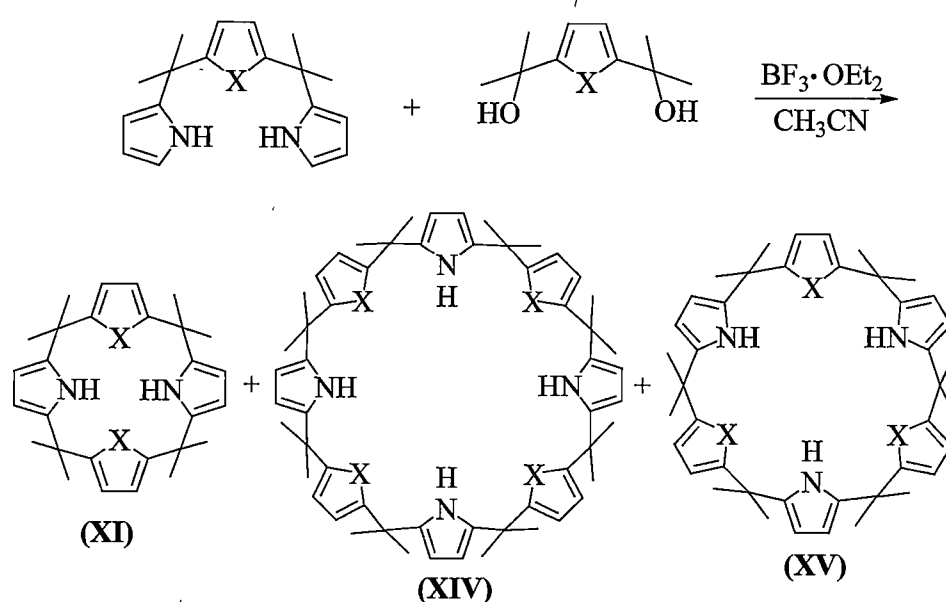
Scheme 2: Synthesis of the *trans*-dioxaporphyrinogen **(XI)**

The crystal structures of *trans-N,N'*-dimethyl-*meso*-octaethylporphyrinogen **(VII)** (R = R^2 = Me, R^1 = R^3 = H)[13] and *meso*-octamethyl-*trans*-dioxaporphyrinogen **(XI)** (X = O)[16] have been determined. The structures feature similar 1,3-alternate macrocyclic conformations. The *N*-H pyrrole rings pair towards one side of the macrocyclic cavities, while the *N*-methylpyrrole or furanyl rings pair towards the opposite side, as shown in Figure 1.
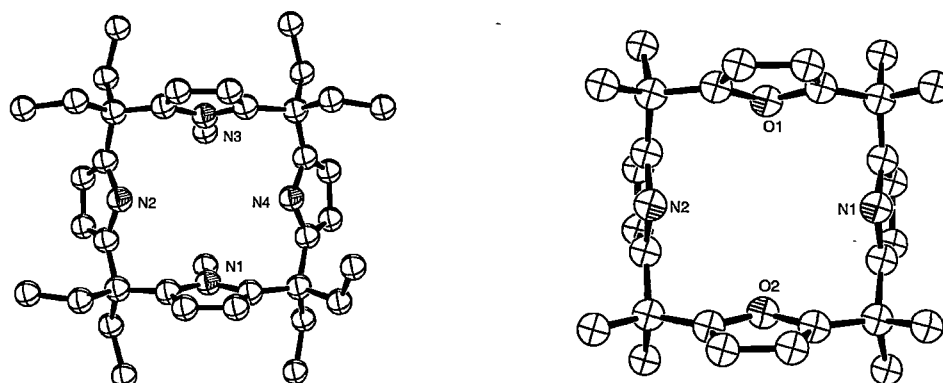
Figure 1: Molecular structures of *trans-N,N'*-dimethyl-*meso*-octaethylporphyrinogen **(VII)**[13] (R = R^2 = Me, R^1 = R^3 = H) and *meso*-octamethyl-*trans*-dioxaporphyrinogen **(XI)** (X = O)[16]. All protons have been removed. Atoms are shown as isotropic representations.

2.2 RESULTS AND DISCUSSION

2.2.1 Modified porphyrinogen syntheses

2.2.1.1 *Meso*-octaethyl-*trans*-dioxaporphyrinogen, Et$_8$O$_2$N$_2$H$_2$, (3)

The synthesis of the macrocycle *meso*-octaethyl-*trans*-dioxaporphyrinogen, Et$_8$O$_2$N$_2$H$_2$ **(3)**, was performed according to Scheme 3 in a similar manner to the reported procedure for the preparation of the *meso*-octamethyl analogue, Me$_8$O$_2$N$_2$H$_2$ **(XI)**[16].
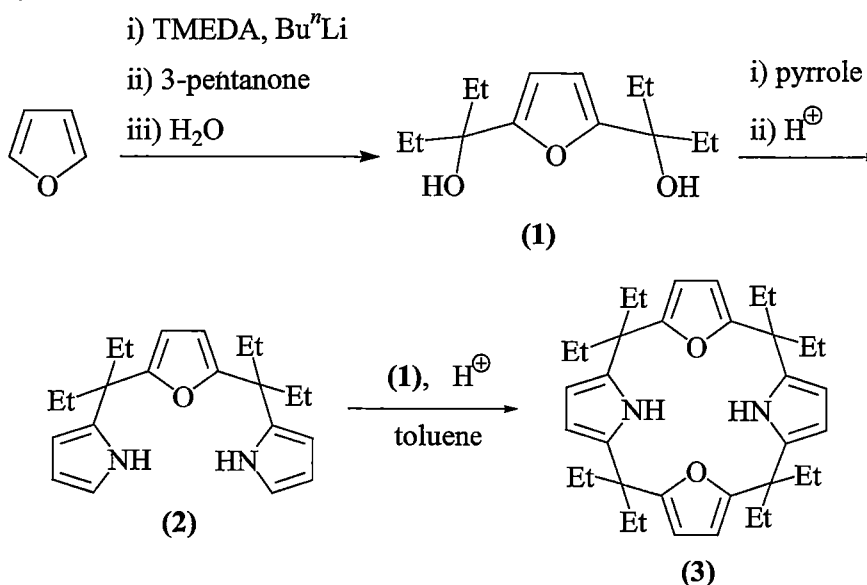
Scheme 3: Synthesis of *meso*-octaethyl-*trans*-dioxaporphyrinogen, Et$_8$O$_2$N$_2$H$_2$ **(3)**.

Furan was deprotonated at the 2 and 5 positions with 2.5 molar equivalents of *n*-butyllithium in the presence of TMEDA. The nuleophilic addition of the dilithiated furan to 3-pentanone followed by hydrolysis led to the dialcohol 2,5-bis(hydroxydiethylmethyl)furan, **(1)**, in 50% yield. Condensation of the dialcohol **(1)** with pyrrole in degassed ethanol in the presence of trifluoroacetic acid affords the tricyclic molecule 2,5-bis{(2'-pyrrolyl)diethylmethyl}furan, **(2)**. Tricycle **(2)** condenses with the dialcohol **(1)** in toluene in the presence of trifluoroacetic acid yielding the desired macrocycle *meso*-octaethyl-*trans*-dioxaporphyrinogen, $Et_8O_2N_2H_2$ **(3)**, in 20% yield.

Compared with the synthesis of the analogous *meso*-octamethyl-*trans*-dioxaporphyrinogen, $Me_8O_2N_2H_2$ **(XI)**[16], the synthesis of **(3)** was achieved in a reduced yield under the similar '3+1' method. The reaction carried out under the same conditions as in the synthesis of **(XI)** (CH_3CN as solvent and boron trifluoride diethyl etherate as the acid catalyst), led to the product in much lower yield (5%). Using toluene as solvent, the yield was improved to 18% and a similar yield (20%) was obtained using trifluoroacetic acid as the catalyst. The optimised yield of **(5)** is still lower than the reported yield of **(XI)** at 46%.

The *Meso*-alkyl substituents of the dioxaporphyrinogens obviously affect the yields of the condensation reactions greatly. The same trend has been seen often in the condensation of pyrrole with ketones leading to porphyrinogens. Namely, the condensation of pyrrole with acetone forms *meso*-octamethylporphyrinogen in about 85% yield in comparison to the synthesis of the *meso*-octaethyl analogue in only 67% yield with 3-pentanone[17]. The reduced stability of 2,5-bis(hydroxydiethylmethyl)furan **(1)** relative to 2,5-bis(hydroxydimethylmethyl)furan in acidic conditions due to the existence of hydrogens β- to the hydroxy group leads to partial decomposition by an elimination reaction.

Compounds **(1)**, **(2)** and **(3)** were characterised by IR, ^1H and ^{13}C NMR spectroscopies, and a X-ray crystal structure determination in the case of **(3)** (see Section 2.2.2). The infrared spectra feature bands at 3353 cm^{-1} for the OH stretch in **(1)**, 3752 and 3896 cm^{-1} for the NH stretches in **(2)**, and 3427 and 3444 cm^{-1} for the NH stretches in **(3)**. The ^1H and ^{13}C NMR spectral data for **(1)** - **(3)** are summarised in Tables 1 and 2. Of note is the occurrence of resonances for only a single *meso*-ethyl group for the macrocycle **(3)**. This is consistent with a dynamic structure in which the macrocycle has a fluctional conformation at room temperature on the

NMR time scales, which renders the geminal *meso*-ethyl groups chemically equivalent.

Compound number	OH/NH	=CH, fur	=CH, pyr	CH$_2$	CH$_3$
(1)	1.92 (broad)	6.11	-	1.79	0.80
(2)	7.99	6.06-6.61		2.00	0.79
(3)	6.57 broad	6.08	6.57	1.82	0.61

Table 1: ^{1}H NMR spectral data for compounds **(1)**, **(2)** and **(3)** (C$_6$D$_6$ for **(1)** and CDCl$_3$ for **(2)** and **(3)**, 399.694 MHz, 298 K, ppm).

Compound number	=CH, fur	=CR, fur	=CH, pyr	=CR, pyr	CEt$_2$	CH$_2$	CH$_3$
(1)	105.8	157.3	-	-	74.9	31.9	7.8
(2)	105.9, 106.0, 107.4, 116.3, 135.6, 157.8				44.5	28.8	8.5
(3)	104.0, 106.2, 134.0, 158.3				43.8	26.8	7.9

Table 2: ^{13}C NMR spectral data for compounds **(1)**, **(2)** and **(3)** (C$_6$D$_6$ for **(1)** and CDCl$_3$ for **(2)** and **(3)**, 100.512 MHz, 298 K, ppm).

2.2.1.2 *Trans-N,N'*-dimethyl-*meso*-octaethylporphyrinogen, Et$_8$N$_4$Me$_2$H$_2$ (6)

The syntheses of *meso*-octaethylporphyrinogen, Et$_8$N$_4$H$_2$ (**4**)[17], and *trans-N,N'*-dimethyl-*meso*-octaethylporphyrinogen, Et$_8$N$_4$Me$_2$H$_2$ (**6**), have been achieved in the similar manner to that reported in the literature[13], as shown in Scheme 4.

(4)

i) NaH,18-Crown-6
ii) MeI
iii) NH_4Cl, H_2O

(6)

other *N*-methylated porphyrinogens
((**5**), (**7**) and (**8**))

+
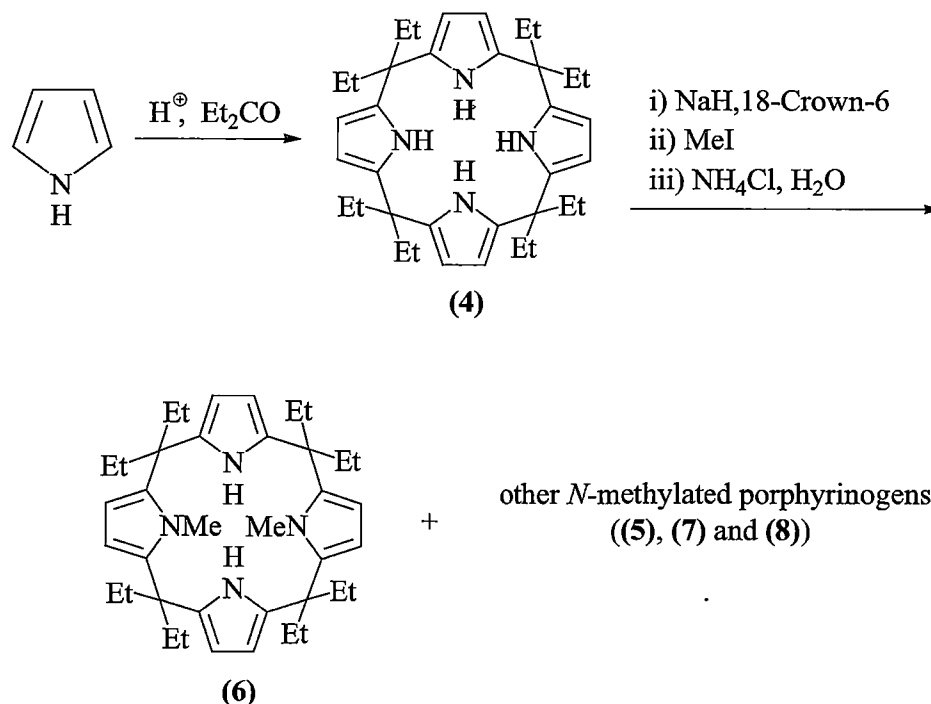
Scheme 4: Syntheses of $Et_8N_4H_4$ **(4)** and *trans-N,N'*-dimethyl-*meso*-octaethylporphyrinogen, $Et_8N_4Me_2H_2$ **(6)**.

The condensation of pyrrole with 3-pentanone in the presence of methyl sulfonic acid in degassed ethanol yielded *meso*-octaethylporphyrinogen, $Et_8N_4H_4$ **(4)**, in 62% yield. The porphyrinogen **(4)** reacted with four molar equivalents of sodium hydride in dried THF resulting, presumably, in the tetrasodium complex. Four equivalents of 18-crown-6 was added, followed by the dropwise addition of 2.5 molar equivalents of methyl iodide giving the *N,N'*-dimethylated porphyrinogen **(6)** as the major isolated product by flash chromatography in 46% yield.

(5)   **(7)**   **(8)**
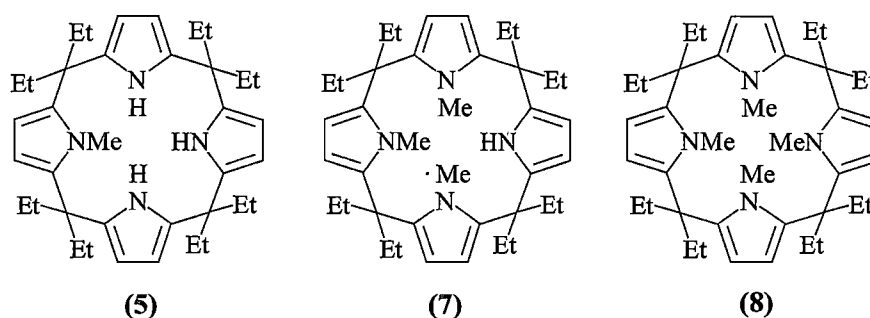
The synthesis of the *trans-N,N'*-dimethylated porphyrinogen $Et_8N_4Me_2H_2$, **(6)**, in this manner is accompanied by the other *N*-methylated products *N*-methyl-*meso*-octaethylporphyrinogen, $Et_8N_4MeH_3$ **(5)**, *N,N',N''*-trimethyl-*meso*-octaethylporphyrinogen, $Et_8N_4Me_3H$ **(7)**, and *N,N',N'',N'''*-tetramethyl-*meso*-

octaethylporphyrinogen, $Et_8N_4Me_4$, **(8)**. The *cis-N,N'*-dimethylated porphyrinogen((**VII**) (R = R^1 = Me, R^2 = R^3 = H) was also observed in low yield, but was not isolated. The reaction was qualitatively monitored by TLC in order to maximise the yield of **(6)** (eluent: dichloromethane/hexane = 1:6; v/v) with the result that the addition of 2.5 molar equivalents of methyl iodide improved the isolated yield of **(6)** to 46% (*c.f.*, 30% using 2 molar equivalents following the literature conditions). The yield distribution of each of the compounds **(4)** - **(8)** using 2 and 2.5 molar equivalents of methyl iodide to *meso*-octaethylporphyrinogen, $Et_8N_4H_4$ **(4)**, is listed in Table 3.

Molar ratio MeI:(4)	(4)	(5)	(VII)*	(6)	(7)	(8)
2:1	18.8	14.1	5.6	34.4	12.8	2.0
2.5:1	1.5	7.4	6.7	58.4	17.8	3.5

Table 3: Yield distribution of products in the *N*-methylation of *meso*-octaethylporphyrinogen, $Et_8N_4H_4$ **(4)**, (GC analysis) ((**VII**)* (R = R^1 = Me, R^2 = R^3 = H)).

The presence of 18-crown-6 plays a vital role in controlling the location of methylation of the porphyrinogen **(4)**. The methylation occurs at the nitrogen position rather than at β-positions only in the presence of a stoichiometric amount (in pyrrolide units) of 18-crown-6. In the absence of 18-crown-6, an inseparable mixture including a, presumed, large portion of β-methylated products is obtained. The strategy of changing NaH to different metalating reagents to control the β-methylation, which is an effective way of improving the yield of *N*-methylpyrrole from unsubstituted pyrrole itself, was unsuccessful in the case of the macrocyclic porphyrinogen. For example, using KH or *n*-butyllithium instead of NaH in the absence of 18-crown-6, the methylation gives an inseparable mixture containing β-methylation products. Other chelating Lewis bases, including TMEDA, were unsuccessfully substituted for 18-crown-6 to control β-methylation. Dibenzo-18-crown-6 addition shows the same effect as 18-crown-6 in controlling the *N*-methylation, however, it offers no advantages.

The difficulty in directing the alkylation of **(4)** towards the nitrogen centres stems from the apparent high formation constant of the macrocycle towards binding both sodium and potassium, which arises from the conformational freedom that the macrocycle possesses in changing its binding mode to host metals of various sizes. As a result, only another suitably sized macrocycle, such as 18-crown-6 is capable of removing all the alkali metal cations from within the macrocycle cavity to allow N-methylation to proceed. Thus, in the absence of 4 equivalents of 18-crown-6, the β-positions, even though bearing lower electron density, are left exposed and react with methyl iodide rather than the nitrogen centres.
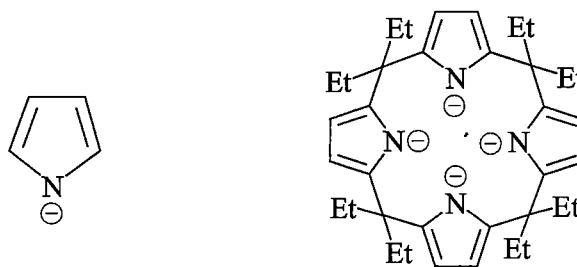
Figure 2: The pyrrolide anion and the *meso*-octaethylporphyrinogen tetraanion

The N-methylated porphyrinogens **(5)** - **(8)** have been characterised by Takata *et al.* by ^{1}H NMR spectroscopy, mass spectrometry, and an X-ray crystal structure determination in the case of **(6)**. Additional characterisation details are presented herein, including X-ray crystal structure determinations for **(7)** and **(8)** (see Sections 2.2.2.2 and 2.2.2.3). The ^{1}H NMR spectral data of compounds **(5)** - **(8)** are listed in Table 4.

Compound number	NH	=CH pyrMe	=CH pyr	NCH$_3$	CH$_2$	CH$_3$
Et$_8$N$_4$H$_4$, (4)	7.13	-	5.97	-	1.75	0.67
Et$_8$N$_4$MeH$_3$, (5)	6.03	5.82-6.02		2.58	1.73-1.95	0.56-0.76
Et$_8$N$_4$Me$_2$H$_2$, (6)	7.24 (broad)	6.05	5.99	2.83	1.69-2.00	0.60, 0.71
Et$_8$N$_4$Me$_3$H, (7)	7.05	5.89-6.00		2.36, 2.82(6H)	1.6-2.1	0.4-0.7
Et$_8$N$_4$Me$_4$, (8)	-	6.08	-	2.83	1.92	0.65

Table 4: ^{1}H NMR spectral data for the N-methylated porphyrinogens (4), (5), (6), (7) and (8) (in C$_6$D$_6$, 399.694 MHz, 298 K, ppm).

2.2.2 Molecular structures of modified porphyrinogens Et$_8$O$_2$N$_2$H$_2$, (3), Et$_8$N$_4$Me$_3$H, (7), Et$_8$N$_4$Me$_4$, (8).

2.2.2.1 Molecular structure of *meso*-octaethyl-*trans*-dioxaporphyrinogen, Et$_8$O$_2$N$_2$H$_2$ (3)

Colourless crystals of Et$_8$O$_2$N$_2$H$_2$, (3), suitable for X-ray crystal structure determination were grown overnight from a saturated hexane/diethyl ether solution (5:1, v/v). The crystals belong to the monoclinic space group $P2_1/n$ (No. 14), a = 21.106(2), b = 14.224(2), c = 11.230(3) Å, β = 104.719(6)°, with four molecules in the unit cell. The asymmetric unit contains one molecule of (3). The molecular structure of (3) is shown in Figure 3.
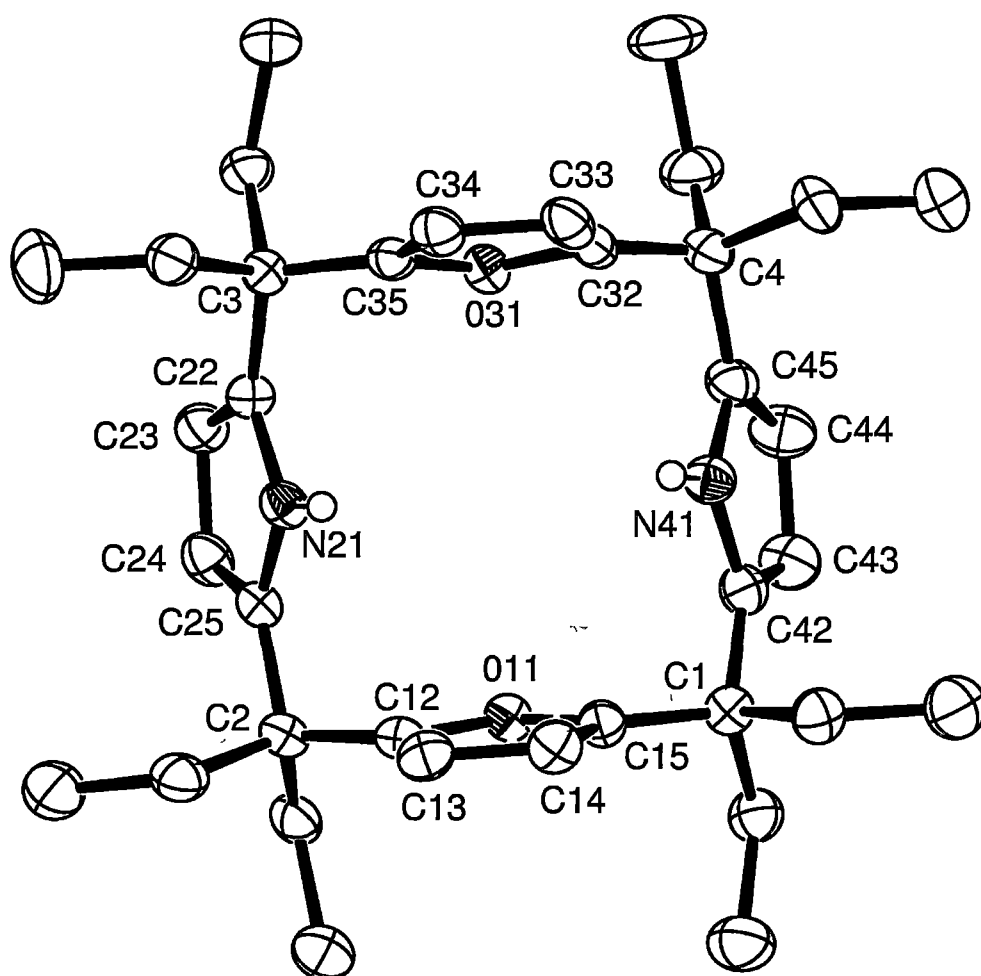
Figure 3: Molecular structure of *meso*-octaethyl-*trans*-dioxaporphyrinogen, $Et_8O_2N_2H_2$ (**3**), with thermal ellipsoids drawn at the level of 50% probability, protons (except *N*-H protons) have been omitted for clarity.

Molecules of (**3**) in the solid state adopt a 1,3-alternate macrocyclic conformation, as was also found for the *meso*-octamethyl analogue[16]. The two opposite pyrrole rings are directed to one side of the macrocyclic cavity, while the two furan rings are directed to the opposite side.

The size of the macrocyclic cavity of (**3**) can be gauged by the cross-cavity N···N and O···O distances between opposing pyrrolyl or furanyl rings and the dihedral angles, or 'tilt angles', of each ring to the average plane of the macrocycle defined by the *meso*-carbon centres. These quantities are listed in Table 5, along with those for (**XI**) and (**6**) for comparison of the relative shapes of the macrocyclic cavities. Compared with the analogous *meso*-octamethyl-*trans*-dioxaporphyrinogen (**XI**), the

distances between the oxygen centres of the opposite furanyl rings are substantially longer while the two N···N distances of the opposite pyrrolyl rings are shorter in (3) by a large extent. The ring tilt angles are also significantly different in both analogous dioxaporphyrinogens, with furanyl rings in (3) being substantially steeper than those in (XI) but two other opposite pyrrolyl rings are much flatter in (3) than those in (XI). In comparison with *trans-N,N'*-dimethyl-*meso*-octaethylporphyrinogen (6), the macrcyclic cavity of (3) has closer N-H pyrrolyl contacts and a longer distance between the oxygen centres of the two furanyl rings than the nitrogen centres of the N-methylpyrrolyl rings. The N-H pyrrolyl rings lie flatter than the furanyl rings in (3). The two furanyl rings in (3) are steeper than the N-methyl pyrrolyl rings in (6) and the N-H pyrrolyl rings in (3) are also steeper than those in (6).

Compound number	Furan or N-methyl pyrrole rings		Pyrrole rings	
	Cross-cavity O···O or N···N distance (Å)	Ring tilt angles (°)	Cross-cavity N···N distance (Å)	Ring tilt angles (°)
$Et_8O_2N_2H_2$, (3)	4.85_7	79.0_3, 79.4_9	4.65_1	65.5_1, 67.1_1
$Me_8O_2N_2H_2$, (XI)	4.69_8	71.7_3, 73.1_1	4.93_0	76.3_2, 78.7_5
$Me_8N_4Me_2H_2$, (6)	4.73_3	73.5_9, 74.0_3	4.83_1	53.5_1, 57.3_1

Table 5: Cross-cavity N···N/O···O distances and heterocycle ring tilt angles for $Et_8O_2N_2H_2$, (3), $Me_8O_2N_2H_2$, (XI), and $Et_8N_4Me_2H_2$, (6).

2.2.2.2 Molecular structure of N,N',N''-trimethyl-*meso*-octaethylporphyrinogen, $Et_8N_4Me_3H$ (7)

Colourless crystals of N,N',N''-trimethyl-*meso*-octaethylporphyrinogen, $Et_8N_4Me_3H$ (7), suitable for X-ray crystal structure determination were grown overnight from a hexane/dichloromethane solution (6:1, v/v). The crystals belong to the triclinic space group $P\bar{1}$ (No. 2), $a = 12.611(1)$, $b = 12.878(1)$, $c = 22.466(3)$ Å, $\alpha = 83.700(2)$, $\beta = 79.166(2)$, $\gamma = 78.354(2)°$, with four molecules in the unit cell. The asymmetric unit contains two molecules of (7), which are both similar in

structural detail. Both molecules of (7) display a 50:50% two-fold disorder of the unique N-H pyrrolyl ring across opposite pyrrole locations, which has been removed from the structure shown in Figure 4 (molecule 1).
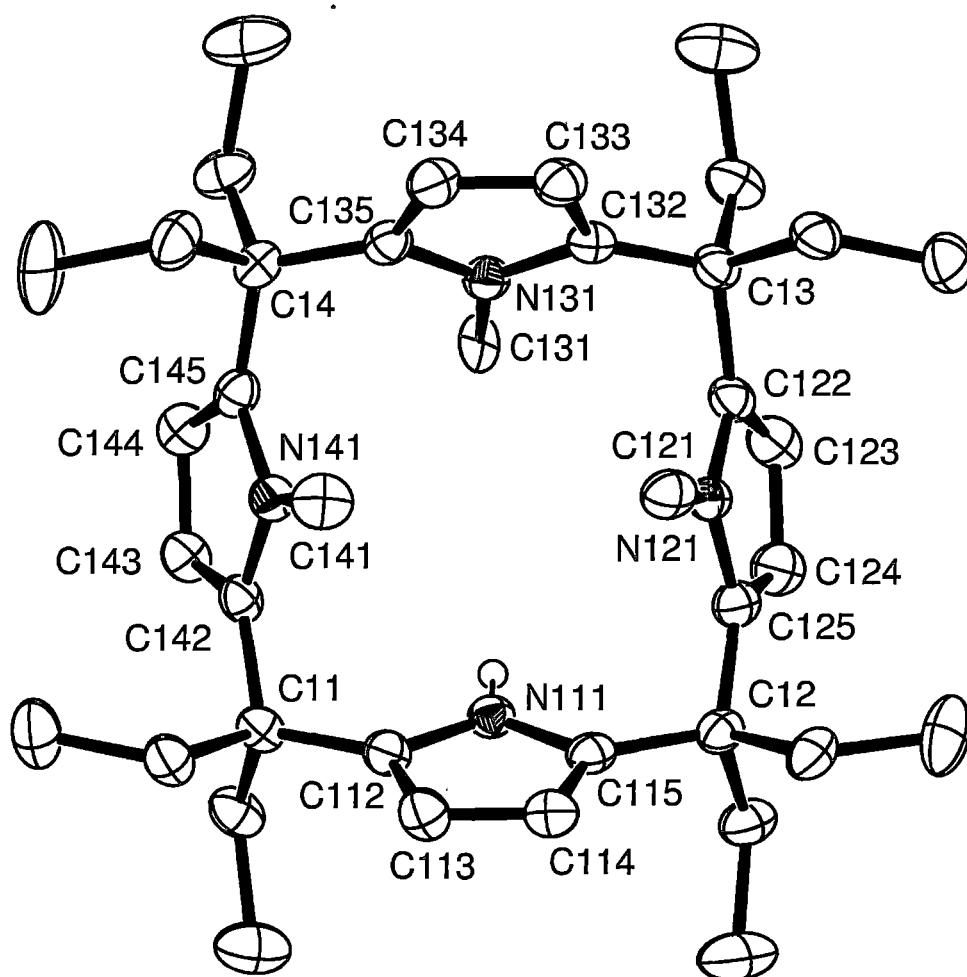
Figure 4: Molecular structure of N,N',N''-trimethyl-*meso*-octaethylporphyrinogen, Et$_8$N$_4$Me$_3$H (7), with thermal ellipsoids drawn at the level of 50% probability, protons (except N-H protons) and the N-H pyrrolyl disorder have been removed for clarity.

Molecules of (7) adopt 1,3-alternate macrocyclic conformations. The two opposite N-methylpyrrolyl rings are directed to the same side of the macrocyclic cavity, while the other two opposite rings (one N-H pyrrolyl and one N-methylpyrrolyl ring) are both directed towards the other side.

Compared to the related *trans-N,N'*-dimethylated porphyrinogen (6), the macrocyclic cavity of (7) is more symmetrical with respect to the cross-cavity N· N

distances of opposite tetracyclic ring pairs, as shown in Table 6. The tilt angles of the heterocyclic rings to the plane of the macrocycle are also very similar in (7). These conformational similarities are in accord with the disorder of the unique N-H pyrrolyl ring in both molecules of (7).

Compound number	N-Methyl pyrrole		N-Methyl pyrrole (or pyrrole)	
	Cross-cavity $N \cdots N$ distance (Å)	Ring tilt angles (°)	Cross-cavity $N \cdots N$ distance (Å)	Ring tilt angles (°)
$Et_8N_4Me_3H$, (7) (Molecule 1)	4.87_4	68.4_2, 69.2_1	4.84_5	58.9_3, 60.1_7
$Et_8N_4Me_3H$, (7) (Molecule 2)	4.86_1	62.6_8, 63.3_4	4.85_2	60.3_4, 60.9_9
$Me_8N_4Me_2H_2$, (6)	4.73_3	73.5_9, 74.0_3	4.83_1	53.5_1, 57.3_1

Table 6: Cross-cavity $N \cdots N$ distances and heterocycle ring tilt angles for $Et_8N_4Me_3H$, (7), and $Et_8N_4Me_2H_2$, (6).

2.2.2.3   Molecular   structure   of N,N',N'',N'''-tetramethyl-*meso*-octaethylporphyrinogen, $Et_8N_4Me_4$ (8).

Colourless crystals of $Et_8N_4Me_4$, (8), suitable for X-ray crystal structure determination were grown overnight from a hexane/dichloromethane solution (6:1, v/v). The crystals belong to triclinic space group $P\bar{1}$ (No. 2), $a = 12.591(1)$, $b = 12.942(1)$, $c = 22.570(2)$ Å, $\alpha = 83.463(2)$, $\beta = 79.093(2)$, $\gamma = 78.093(2)°$, with four molecules in the unit cell. Two molecules of (8) are again found in the asymmetric unit. Both molecules of (8) have similar geometries, Figure 5 shows the structure of molecule 1.
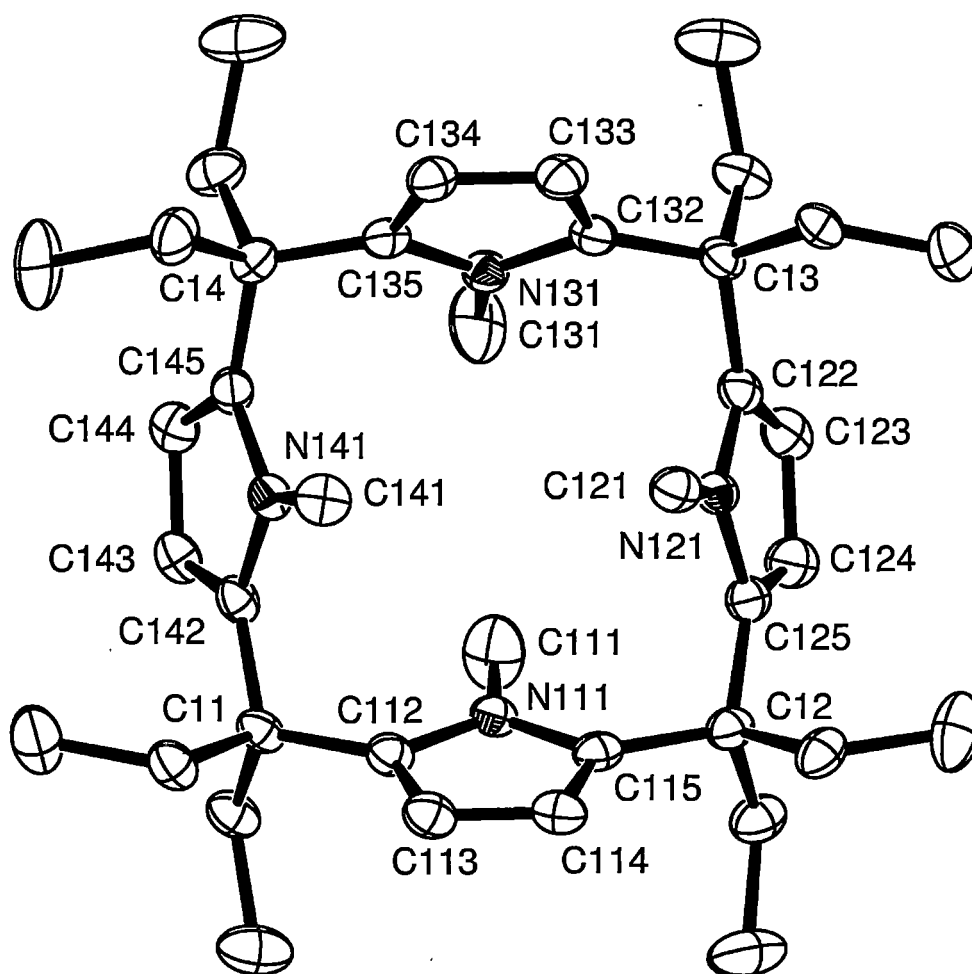
Figure 5: Molecular structure of N,N',N'',N'''-tetramethyl-*meso*-octaethylporphyrinogen, $Et_8N_4Me_4$ **(8)**, with thermal ellipsoids drawn at the level of 50% probability, all protons have been removed for clarity.

The molecules of **(8)** again adopt 1,3-alternate macrocyclic conformations. The two opposite N-methylpyrrolyl rings are directed toward one side of the plane of the macrocycle defined by the four *meso*-carbon centres, while the other two opposite N-methylpyrrolyl rings are directed to the other side of the macrocycle.

As shown in Table 7, the macrocyclic cavity of **(8)** is very symmetrical with regard to the cross-cavity N⋯N distances and the heterocycle tilt angles with respect to the plane of the macrocycle. The cross-cavity N⋯N distances of the two pairs of the opposite pyrrolyl rings in **(8)** have similar values to those of the N-methyl pyrrole rings and are larger than those of the nonmethylated pyrrole rings in **(6)** and **(7)**. The

tilt angles of each of the pyrrolyl rings in **(8)** are more similar than those seen in other methylated porphyrinogens **(6)** and **(7)**.

Compound number	N-Methyl pyrroles	
	Cross-cavity N $\cdots$ N distance (Å)	Ring tilt angles ($^\circ$)
$Et_8N_4Me_4$, **(8)** (Molecule 1)	4.83_7 4.82_9	65.9_4, 68.3_7 59.2_2, 60.8_7
$Et_8N_4Me_4$, **(8)** (Molecule 2)	4.81_7 4.83_6	61.1_2, 62.9_4 60.2_9, 60.7_7

Table 7: Cross-cavity N$\cdots$N distances and heterocycle ring tilt angles for $Et_8N_4Me_4$, **(8)**

2.3 Experimental

Synthesis of 2,5-bis(hydroxydiethylmethyl)furan, **(1)**

To a flask (1 L) containing furan (12.7 g, 0.20 mol), TMEDA (53.9 g, 0.50 mol) and hexane (100 mL), n-butyllithium solution in hexane (1.6 M, 0.50 mol) was added with stirring under nitrogen at 5°C. The mixture was stirred for half an hour after being allowed to warm to room temperature. The mixture was refluxed for another half an hour and allowed to cool to room temperature. 3-Pentanone (49.6 mL, 40.4 g, 0.50 mol) was added dropwise at ambient temperature over half an hour. After stirring for two hours at the same temperature, distilled water (9.0 g, 0.50 mol) was added dropwise to the mixture and the mixture kept stirring for one hour. The undissolved solid waste was filtered off and extracted three times with diethyl ether (40 mL). The hexane and diethyl ether solutions were combined and dried over anhydrous Na_2CO_3. The solvent was removed to leave a crude product, which was recrystallised from a diethyl ether/hexane solution (1:2; v/v) to afford **(1)** as a pure colourless solid product (22.5 g, 50%).

> **^{1}H NMR** (C_6D_6, 399.694 MHz, 298 K, ppm): 0.80 (t, ^3J = 7.33 Hz, 12H, CH_3), 1.79 (m, 8H, CH_2), 1.92 (broad s, 2H, OH), 6.11 (s, 2H, C_4H_2O).
> **^{13}C NMR** (C_6D_6, 100.512 MHz, 298 K, ppm): 7.8 (CH_3), 31.9 (CH_2), 74.9 (COH), 105.8 (=CH, fur), 157.3 (=CR, fur).
> **IR** (υ (cm^{-1}), KBr): 770 (m), 960 (s), 1110 (m), 1017 (m), 1138 (m), 1209 (w), 1326 (m), 1375 (w), 1420 (w), 1458 (s), 2878 (w), 2940 (s), 2965 (s), 3353 (b, s, OH).
> **MS** (esi): m/z 263 (M+Na).

Synthesis of 2,5-bis{(2'-pyrrolyl)diethylmethyl}furan, **(2)**

To a flask containing pyrrole (5.00 g, 74.00 mmol) and 2,5-bis(hydroxydiethylmethyl)furan, **(1)**, (4.80 g, 20.00 mmol) in degassed absolute ethanol (50 mL), trifluoroacetic acid (0.84 g, 7.40 mmol) was added. After the resulting mixture was refluxed for six hours, ethanol was removed by rotary evaporation and the residue was dissolved in diethyl ether. The ethereal solution was washed with saturated $NaHCO_3$ solution, brine and dried over anhydrous Na_2CO_3. Solvent and excess pyrrole were removed by evaporation to afford a brown oil of crude 2,5-bis{(2'-pyrrolyl)diethylmethyl}furan, **(2)**, (6.37 g, 94%), which was used in the next reaction without further purification.

^{1}H NMR (CDCl$_3$, 399.694 MHz, 298 K, ppm): 0.79 (t, ^{3}J = 7.36 Hz, 12H, CH$_3$), 2.00 (m, 8H, 4CH$_2$), 6.06-6.61 (m, 8H, =CH, pyr and fur), 7.99 (broad s, 2H, 2NH).

^{13}C NMR (CDCl$_3$, 100.512 MHz, 298 K, ppm): 8.5 (CH$_3$), 28.8 (CH$_2$), 44.5 (CEt$_2$), 105.0, 105.9, 107.4, 116.3, 135.6, 157.8 (=CR and =CH).

IR (υ (cm^{-1}), KBr): 743 (s), 780 (s), 1034 (s), 1380 (m), 1544 (m), 1554 (m), 2936 (m), 2964 (m), 3752 (m, NH), 3896 (m, NH).

MS (esi): m/z 339 (M+H)

Synthesis of *meso*-octaethyl-*trans*-dioxaporphyrinogen, Et$_8$O$_2$N$_2$H$_2$ **(3)**

To a flask containing crude 2,5-bis{(2'-pyrrolyl)diethylmethyl}furan, **(2)**, (6.37 g, 19.00 mmol), from the previous reaction, 2,5-bis(hydroxydiethylmethyl)furan, **(1)**, (7.00 g, 24.00 mmol) was added, followed by degassed toluene (40 mL). Trifluoroacetic acid (0.8 g, 7.4 mmol) was added dropwise with stirring. The mixture was stirred at 60°C for six hours. The solution was washed with saturated NaHCO$_3$ solution and brine, and then dried over anhydrous Na$_2$CO$_3$. The solvent was removed *in vacuo*, leaving the crude product which was recrystallised from a hexane/toluene solution (5:1, v/v) to obtain pure product (2.06 g, 20 %) (m.p. 200-203°C).

^{1}H NMR (CDCl$_3$, 399.694 MHz, 298 K, ppm): 0.61 (t, ^{3}J = 7.38 Hz, CH$_3$), 1.82 (m, 16H, CH$_2$), 5.78 (d, 2H, =CH, pyr), 6.08 (d, 2H, =CH, fur), 6.57 (broad, s, 2H, NH).

^{13}C NMR (CDCl$_3$, 100.512 MHz, 298 K, ppm): 7.9 (CH$_3$), 26.8 (CH$_2$), 43.8 (CEt$_2$), 104.0 (=CH), 106.2 (=CH), 134.0 (=CR), 158.3 (=CR).

IR (υ (cm^{-1}), KBr): 706 (m), 757 (s), 787 (m), 832 (w), 924 (w), 964 (w), 1024 (m), 1103 (m), 1201 (m), 1284 (w), 1330 (w), 1378 (s), 1462 (s), 1550 (m), 1579 (w), 2853 (s), 2922 (s), 3427 (m, NH), 3444 (m, NH).

MS (esi): m/z 543 (M+H).

Synthesis of *meso*-octaethylporphyrinogen, Et$_8$N$_4$H$_4$ **(4)**

To a flask containing pyrrole (21.0 mL, 303.0 mmol) and 3-pentanone (32.0 mL, 303.0 mmol) in ethanol (85 mL), methylsulfonic acid (2 mL) was added dropwise with stirring. The stirred mixture was refluxed for 6 hours under argon, during which time some product precipitated. The mixture was cooled in the freezer

(-30°C) yielding more solid. The solid was collected by filtration and washed with ethanol until the dark brown solid became a colourless pure product (26.20 g, 64%).

^{1}H NMR (C_6D_6, 399.694 MHz, 298 K, ppm): 0.67 (t, 24 H, CH_3), 1.75 (m, 16H, CH_2), 5.97 (m, 8H, =CH), 7.13 (s, broad, 2H, NH).

Synthesis of N-methyl-$meso$-octaethylporphyrinogen, $Et_8N_4MeH_3$ (5)

Following the same procedure as for the synthesis of $trans$-N,N'-dimethyl-$meso$-octaethylporphyrinogen, $Et_8N_4Me_2H_2$ (6), the product was isolated as a colourless solid (5) (0.03 g, 6%; 7.4% by GC).

^{1}H NMR (C_6D_6, 399.694 MHz, 298 K, ppm): 0.76-0.56 (m, 24 H, CH_3), 1.95-1.73 (m, 16H, CH_2), 2.58 (s, 3H, CH_3), 5.82-6.02 (m, 8H, =CH, pyr and pyrMe), 6.03 (s, 1H, NH).

Synthesis of $trans$-N,N'-dimethyl-$meso$-octaethylporphyrinogen, $Et_8N_4Me_2H_2$ (6)

A THF (50 mL) suspension of $meso$-octaethylporphyrinogen, (4), (5.40 g, 10.0 mmol) and sodium hydride (60% oil dispersion, 1.60 g, 40.0 mmol) was stirred under an argon atmosphere at 50°C for 1.5 hrs and then the mixture was cooled to room temperature. 18-crown-6 (11.00 g, 40.0 mmol) was added and stirring continued for 30 min. Methyl iodide was added (4.00 g, 25.0 mmol) and the resulting mixture was stirred overnight. The mixture was poured into a saturated NH_4Cl solution and then extracted with diethyl ether. The extract was washed with $NaHCO_3$ solution followed by brine. The solution was then evaporated to dryness. The crude product was separated by chromatography over silica gel (DCM/hexane=1:10 then 2:10) to give (6) as a colourless solid (3.20 g, 46%; 58.4% by GC).

^{1}H NMR (C_6D_6, 399.694 MHz, 298 K, ppm): 0.60 (t, ^3J = 14.88 Hz, 12H, CH_3), 0.71 (t, ^3J = 14.68 Hz, 12H, CH_3), 1.69-2.00 (m, 16H, CH_2), 2.83 (s, 6H, CH_3), 5.99 (d, 4H, =CH, pyr), 6.05 (d, 4H, =CH, pyrMe), 7.24 (s, broad, 2H, NH).
^{13}C NMR (C_6D_6, 100.512 MHz, 298 K, ppm): 7.9, 7.7 (CH_3), 30.0, 24.3 (CH_2), 31.9 (NCH_3), 42.9 (CEt_2), 104.6 (=CH), 106.6 (=CH), 135.4 (=CR), 136.4 (=CR).

IR (υ (cm^{-1}), KBr): 655 (s), 748 (m), 766 (s), 853 (s), 982 (s), 1048 (m), 1189 (w), 1205 (w), 1330 (m), 1377 (m), 1415 (w), 1466 (w), 1490 (w), 2873 (s), 2934 (s), 2965 (s), 3433 (m, NH).

Synthesis of N,N',N''-trimethyl-*meso*-octaethylporphyrinogen, Et$_8$N$_4$Me$_3$H (7)

Following the same procedure as for the synthesis of *trans*-N,N'-dimethyl-*meso*-octaethylporphyrinogen, Et$_8$N$_4$Me$_2$H$_2$ (6), the product was isolated as a colourless solid (7) (0.10 g, 14%; 17.8% by GC).

^{1}H NMR (CDCl$_3$, 399.694 MHz, 298 K, ppm): 0.45-0.65 (m, 24H, CH$_3$), 1.80-2.07 (m, 16H, CH$_2$), 2.36 (s, 3H, NCH$_3$), 2.82 (s, 6H, NCH$_3$), 5.88-6.00 (m, 4H, =CH, pyr and pyrMe), 7.04 (s, broad, 1H, NH).
IR (υ (cm^{-1}), KBr): 527 (m), 760 (m), 751 (s), 768 (s), 882 (w), 925 (w), 1050 (m), 1090 (w), 1184 (w), 1217 (w), 1281 (m), 1301 (m), 1329 (s), 1381 (s), 1441 (w), 1486 (m), 1572 (w), 1965 (s), 2872 (m), 2931 (m), 3440 (m).

Synthesis of N,N',N'',N'''-tetramethyl-*meso*-octaethylporphyrinogen, Et$_8$N$_4$Me$_4$ (8)

Following the same procedure as for the synthesis of *trans*-N,N'-dimethyl-*meso*-octaethylporphyrinogen, Et$_8$N$_4$Me$_2$H$_2$ (6), the product was isolated as a colourless solid (8) (0.02 g, 3%; 3.5% by GC).

^{1}H NMR (C$_6$D$_6$, 399.694 MHz, 298 K, ppm): 0.65 (q, 24H, CH$_3$), 1.92 (m, 8H, CH$_2$), 2.03 (m, 8H, CH$_2$), 2.83 (s, 12H, CH$_3$), 6.08 (s, 8H, =CH, Pyr).
IR (υ (cm^{-1}), KBr): 701 (m), 755 (s), 883 (m), 925 (m), 1043 (m), 1227 (m), 1283 (m), 1299 (s), 1331 (s), 1383 (s), 1443 (m), 1469 (s), 1487 (s), 2872 (m), 2960 (m).

2.4 References

[1]   A. Baeyer, *Ber. Dtsch. Chem. Ges.*, 1886, **19**, 2184.

[2]   P. Rothemund, C.L. Gage, *J. Am. Chem. Soc.*, 1955, **77**, 3340.

[3]   **a.** P.A. Gale, J.L. Sessler, V. Král, V. Lynch, *J. Am. Chem. Soc.*, 1996, **118**, 5140.
b. P. Anzenbacher, A.C. Try, H. Miyaji, K. Jursikova, V.M. Lynch, M. Marquez, J.L. Sessler, *J. Am. Chem. Soc.*, 2000, **122**, 10268.
c. W.E. Allen, P.A. Gale, C.T. Brown, V.M. Lynch, J.L. Sessler, *J. Am. Chem. Soc.*, 1996, **118**, 12471.
d. V. Král, J.L. Sessler, T.V. Shishkanova, P.A. Gale, R. Volf, *J. Am. Chem. Soc.*, 1999, **121**, 8771.
e. P.D. Beer, P.A. Gale, G.Z. Chen, *J. Chem. Soc., Dalton Trans.,* 1999, **12**, 1897.
f. J.L. Sessler, A. Gebauer, P.A. Gale, *Gazz. Chim. Ital.*, 1997, **127**, 723.
g. Z. Chen, P.A. Gale, P.D. Beer, *J. Electroanal. Chem.*, 1995, **393**, 113.

[4]   **a.** P.A. Gale, P. Anzenbacher, J.L. Sessler, *Coord. Chem. Rev.*, 2001, **222**, 57.
b. P.A. Gale, J.L. Sessler, V. Král, *Chem. Commun.*, 1998, 1.
c. V. Král, J.L. Sessler, R.S. Zimmerman, D. Seidel, V. Lynch, B. Andrioletti, *Angew. Chem. Int. Ed.*, 2000, **39**, 1055.
d. W. Sliwa, *Heterocycles,* 2002, **57**, 169.

[5]   J.L. Sessler, P. Anzenbacher, H. Miyaji, K. Jursikova, E.R. Bleasdale, P.A. Gale, *Ind. Engng. Chem. Res.*, 2000, **39**, 3471.

[6]   **a.** C. Floriani, *Chem. Commun.*, 1996, 1257.
b. R. Crescenzi, E. Solari, C. Floriani, A. Chiesi-Villa, C. Rizzoli, *J. Am. Chem. Soc.*, 1999, **121**, 1695.
c. F.T. Edelmann, D.M.M. Freckmann, H. Schumann, *Chem. Rev.*, 2002, **102**, 1851.

[7]   **a.** J.L. Sessler, A. Andrievsky, P.A. Gale, V. Lynch, *Angew. Chem., Int. Ed. Engl.*, 1996, **35**, 2782.
b. P. Anzenbacher, K. Jursikova, J.L. Sessler, *J. Am. Chem. Soc.*, 2000, **122**, 9340.

[8]   P.A. Gale, J.L. Sessler, W.E. Allen, N.A. Tvermoes, V.M. Lynch, *Chem. Commun.*, 1997, 665.

[9]   P. Anzenbacher, K. Jursikova, H. Shriver, H. Miyaji, V.M. Lynch, J.L. Sessler, *J. Org. Chem.*, 2001, **65**, 7641.

[10]   **a**. H. Miyaji, W. Sato, J.L. Sessler, V.M. Lynch, *Tetrahedron Letters*, 2000, **41**, 1369.
       b. W. Sato, H. Miyaji, J.L. Sessler, *Tetrahedron Letters*, 2000, **41**, 6731.

[11]   B. Franck, C. Wegner, *Angew. Chem., Int. Ed. Engl.*, 1975, **14**, 424.

[12]   R. Timmermann, R. Mattes, B. Franck, *Angew. Chem., Int. Ed. Engl.*, 1987, **26**, 64.

[13]   Y. Furusho, H. Kawasaki, S. Nakanishi, T. Aida, T. Takata, *Tetrahedron Letters*, 1998, **39**, 3537.

[14]   W.H. Brown, W.N. French, *Can. J. Chem.*, 1958, **36**, 371.

[15]   **a**. S. Taniguchi, H. Hasegawa, M. Nishimura, M. Takahashi, *Synlett*, 1999, **1**, 73.
       b. S. Taniguchi, H. Hasegawa, S. Yanagiya, Y. Tabeta, Y. Nakano, M. Takahashi, *Tetrahedron*, 2001, **57**, 2103.

[16]   **a**. Y.S. Jang, H.J. Kim, P.H. Lee, C.H. Lee, *Tetrahedron Letters*, 2000, **41**, 2919.
       b. N. Arumugam, Y.S. Jang, C.H. Lee, *Organic Letters*, 2000, **2**, 3115.

[17]   D. Jacoby, C. Floriani, A. Chiesivilla, C. Rizzoli, *J. Am. Chem. Soc.*, 1993, **115**, 3595.

CHAPTER 3

GROUP 1 METAL COMPLEXES OF MODIFIED PORPHYRINOGENS

3.1 INTRODUCTION

Recently π-interactions with alkali metal cations have received considerable attention in the context of biology[1]. It is clear that these π-interactions play an important role among various noncovalent binding forces that determine the solvation of the metal ions.

Alkali metal coordination chemistry with pyrrolide ligand systems, including examples featuring π-interactions, have witnessed noticeable progress in the last decade. The achievements in this area is reviewed in two parts, (i) alkali metal pyrrolide complexes as homometallic species, and, (ii) alkali metals retained from reactants in metathetical exchange reactions, coexisting with anionic pyrrolide complexes of other metals.

3.1.1 Alkali metal pyrrolide complexes as homometallic species

Due to the general σ-bonding preference of simple pyrrolides, most studies have focused on substituted pyrroles, e.g., 2,5-disubstituted pyrroles, to explore new coordination possibilities.

The structurally characterised sodium 2,3,4,5-tetramethylpyrrolide (I) was reported by Kuhn et al. in 1996[2]. The complex features both σ- and π- bonding of the pyrrolide anion with sodium cations. It was prepared from the reaction between 2,3,4,5-tetramethylpyrrole with an equimolar amount of sodium hydride, resulting in a colourless crystalline complex as a solvent free polymer, as shown in Equation 1.

$$\text{(structure: 2,3,4,5-tetramethylpyrrole, Me groups at 2,3,4,5 positions, N–H)} \quad \xrightarrow[-1/2\ H_2]{NaH\ /\ THF} \quad 1/n\ (C_4Me_4NNa)_n$$

$$(\textbf{I})$$
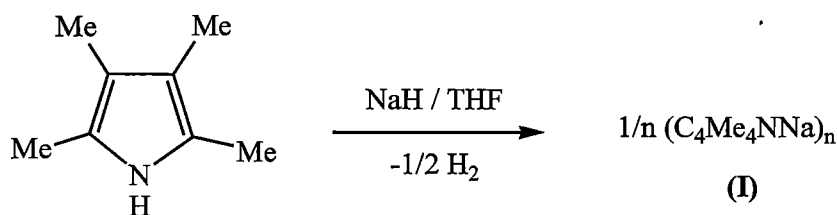
Equation 1

The crystals of complex **(I)** adopt a double chain structure, consisting of alternating sodium and nitrogen atoms, as shown in Figure 1. Each 2,3,4,5-tetramethylpyrrolide bridges three sodium cations with two σ-bonds through nitrogen atoms and one η^5-coordination mode. The two Na-N bonds involving η^1-bonding are of different lengths even though the two η^1-bonded sodium atoms lie outside the plane of the linking pyrrolide ligand to the same extent. The η^5-bonding distance (Na-centroid) is 2.694(1) Å, with the sodium cation being slipped towards the β-carbon atoms. The roughly planar Na_2N_2 quadrilaterals formed by the double chains result in a layer structure resembling a distorted rope ladder.
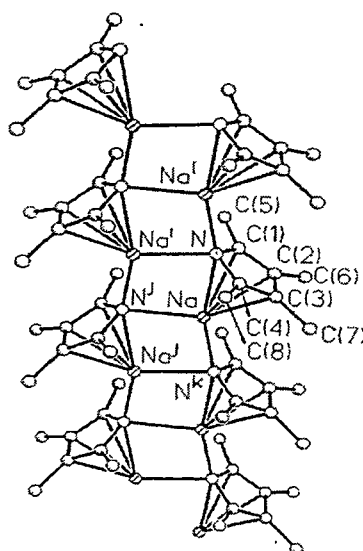
Figure 1: Crystal structure of sodium 2,3,4,5-tetramethylpyrrolide, **(I)**[2].

Lithium, however, opts only for η^1-interactions with pyrrolides even when bulky *tert*-butyl groups substituents are present in the 2 and 5 positions of the pyrrolide ring, for example, the monomeric bis(THF) adduct of lithium 2,5-di(*tert*-butyl)pyrrolide **(II)**[3].

When the pyrrolide unit coordinates to Lewis acidic centres, the lone pair electrons in the sp^2 orbital of the nitrogen atom are less available for further coordination, which changes the possible binding modes dramatically. While the lithium cations bind to the pyrrolide unit with η^1-binding modes in dilithium bis(dimethylamino)bis(1-pyrrolyl)diborate, **(III)**[4], it uses η^5-bonds in the case of [(Et$_2$O)Li(C$_4$H$_4$N)B(C$_6$F$_5$)$_3$], **(IV)**[5], as shown in Figure 2, and [Li{(C$_4$Me$_4$N)AlMe$_2$}$_2$(μ-Cl)], **(V)**[6].

(II)

(III)

(V)
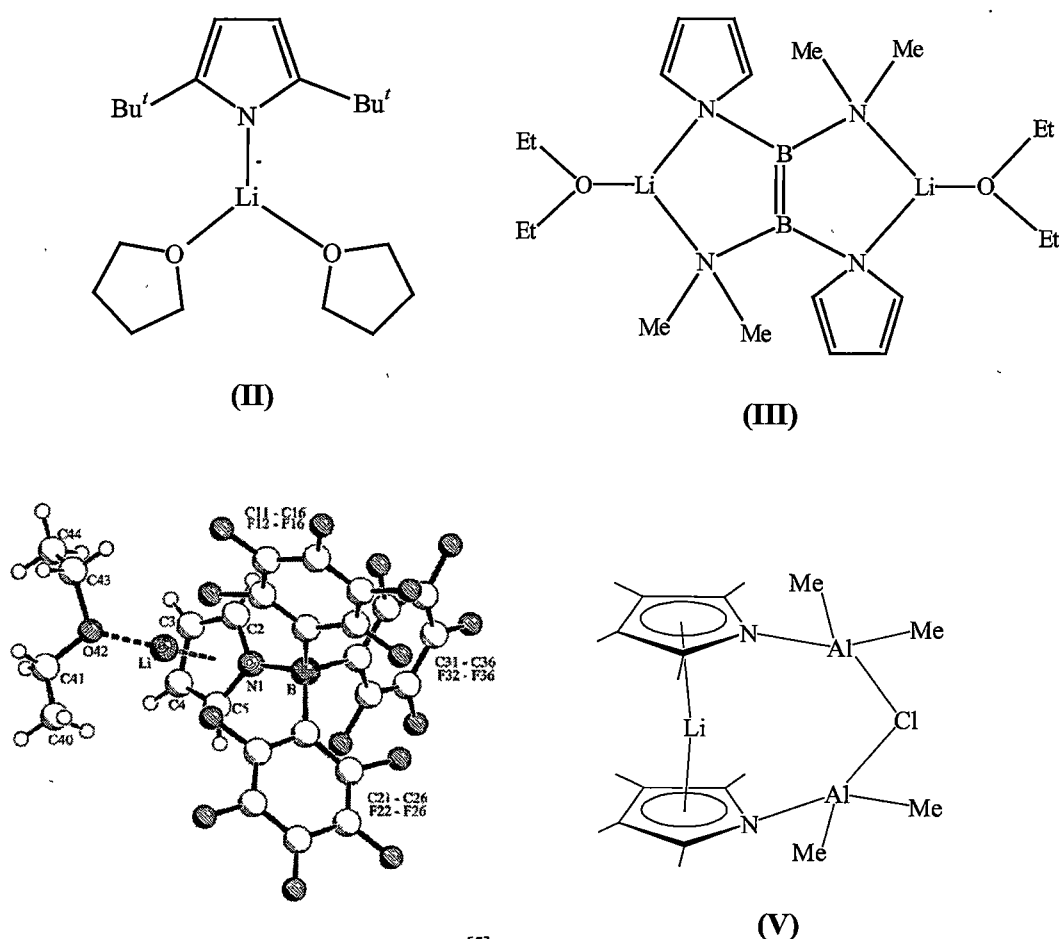
Figure 2: Molecular structure of **(IV)**[5].

Alkali metal complexes of porphyrinogens have been reported by both the groups of Floriani and Gambarotta since 1994. These species were characterised by limited means in most cases, as the authors' main interest in these compounds has been their utility as reagents for subsequent methathetical exchange reactions for the preparation of transition metal and lanthanide complexes.

Several tetralithiated complexes of *meso*-octaethylporphyrinogen or *meso*-tetraspirocyclohexylporphyrinogen, prepared from the reaction of porphyrinogen with *n*-butyllithium, have been reported with full structural characterisation[7]. The tetralithium complex derived from *meso*-octaethylporphyrinogen was isolated initially with four coordinated THF molecules, as shown in Equation 2. Three of the coordinated THF molecule are firmly bound, while the fourth can be lost either by prolonged drying *in vacuo* or when recrystallised from hydrocarbons, *e.g.*, toluene, giving the tris(THF) adduct **(VI)**.

$$\text{Et}_8\text{N}_4\text{H}_4 + 4\,\text{LiBu}^n \xrightarrow[-4\,\text{C}_4\text{H}_{10}]{\text{THF}} [\text{Et}_8\text{N}_4\text{Li}_4(\text{THF})_4] \xrightarrow[-\text{THF}]{\text{toluene}} [\text{Et}_8\text{N}_4\text{Li}_4(\text{THF})_3]$$

(4)   (VI)
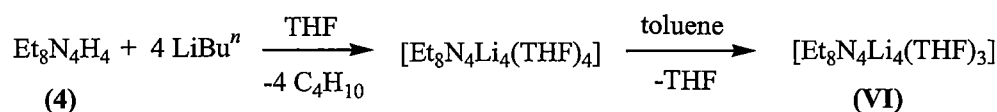
Equation 2

The crystal structure of **(VI)** revealed a quite flattened macrocyclic conformation that is remarkably different from the 1,3-alternate conformation found for the porphyrinogen itself, as shown in Figure 3. One of the lithium cations, Li(1), is η^1-bound to four nitrogen atoms with significantly shorter distances to N(1) and N(4) than to N(2) and N(3), due to the asymmetry of the binding of the other three lithium cations in the macrocyclic cavity. The cations Li(2), Li(3) and Li(4) are η^2-bound to pyrrolide rings through C-N bonds and η^1-bound to the nitrogen centre of an adjacent pyrrolide ring. The coordination spheres of Li(2), Li(3) and Li(4) are each completed by a single THF molecule.
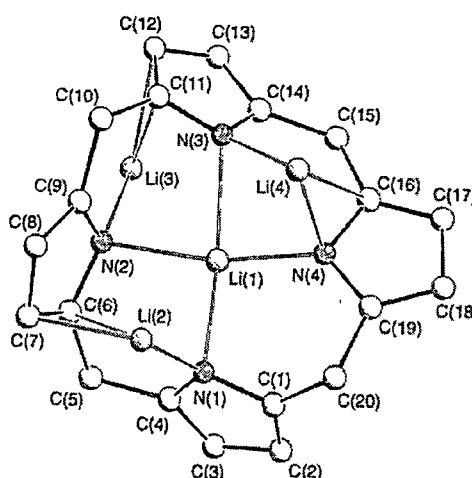
Figure 3: Crystal structure of [Et$_8$N$_4$Li$_4$(THF)$_3$], **(VI)**[7] (*meso*-ethyl groups and coordinated THF molecules are omitted for clarity).

While the molecular structure of [Et$_8$N$_4$Li$_4$(THF)$_4$] has not been determined, the structural details of the related complex [{(-CH$_2$-)$_5$}$_4$N$_4$Li$_4$(THF)$_4$], **(VII)**, have been reported[8], as shown in Figure 4. Complex **(VII)** was obtained from a similar synthetic procedure as that used for [Et$_8$N$_4$Li$_4$(THF)$_4$], and also as byproduct from the synthesis of a samarium complex. The structure of **(VII)** features a slightly distorted 1,3-alternate macrocyclic conformation. Each lithium has one coordinated THF molecule and binds one pyrrolide ring with an η^5-bonding mode and is also η^1-bound to an adjacent pyrrolide ring.
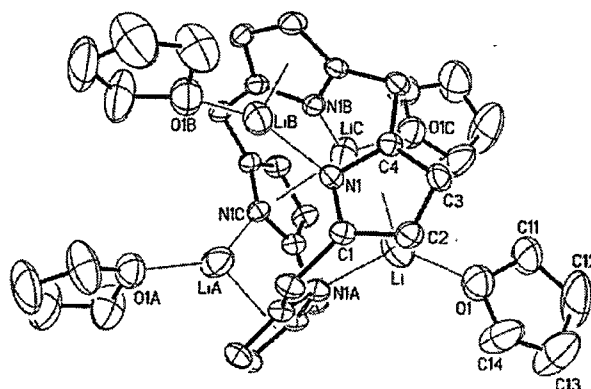
Figure 4: Crystal structure of [{(-CH$_2$-)$_5$}$_4$N$_4$Li$_4$(THF)$_4$], **(VII)**[8] (*meso*-(-CH$_2$-)$_5$ groups are omitted for clarity).

A solvent free tetralithiated complex **(VIII)** featuring incorporation of *tert*-butyllithium has been prepared from the reaction between the porphyrinogen and *tert*-butyllithium in hexane rather than THF, as shown in Equation 3[9].

$$Et_8N_4H_4 + 6\,LiBu^t \xrightarrow[-4\,HCMe_3]{Hexane} [Et_8N_4Li_4(Bu^tLi)_2]$$
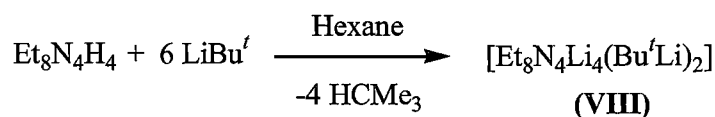
(VIII)

Equation 3

The crystal structure of **(VIII)** features an unusual 'chaise longue' macrocycle conformation, as shown in Figure 5. The four pyrrolide rings bind to four lithium cations (Li2, Li2*, Li3, Li3*) with η^5-binding modes, while the other two lithium cations (Li1, Li1*) reside symmetrically above and below the symmetry centre of the complex and are η^1-bound to two nitrogen atoms of two adjacent pyrrolide rings. The *tert*-butyl anions tribridge lithium cations to complete the coordination sphere of the metal centres.
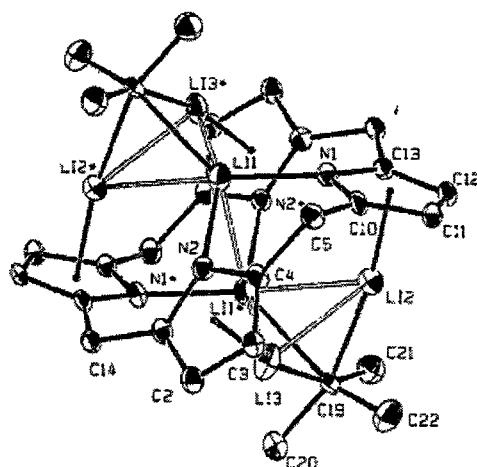
Figure 5: Crystal structure of [Et$_4$N$_4$Li$_4$(Bu^{t}Li)$_2$], (VIII)[9] (*meso*-ethyl groups are omitted for clarity).

An enolate containing lithium porphyrinogen complex (IX) was isolated after refluxing [Et$_8$N$_4$Li$_4$] in THF overnight, as shown in Equation 4. The reaction shows that the unsolvated form behaves as a 'superbase' capable of decomposing THF to the lithium enolate ('LiOCH=CH$_2$') identified in the aggregate (IX)[10].

$$Et_8N_4H_4 + 4LiBu^n \xrightarrow[\text{-4 } C_4H_{10}]{\text{hexane}} [Et_8N_4Li_4] \xrightarrow{\text{THF}} [Et_8N_4Li_4(LiOCH=CH_2)_2(THF)_4]$$
$$(IX)$$
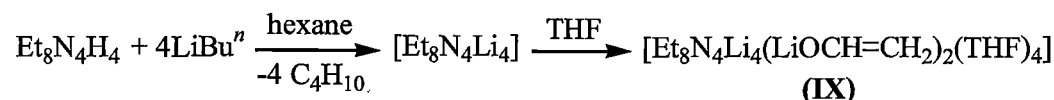
Equation 4

The tetrametallated porphyrinogen (IX) displays again a 'chaise longue' conformation, as shown in Figure 6. Two pairs of adjacent pyrrolide rings face the same direction and opposite pyrroles are almost parallel resulting in a 1,2-alternate macrocyclic conformation. The six lithium cations are arranged in two sets, three above and three below the N$_4$ planar core. Each set of lithium atoms are triply bridged by the oxygen atoms of the enolate groups. The two sets of three lithium cations display the same overall bonding mode to the porphyrinogen unit. Both Li(1) and Li(2) bridge two adjacent pyrrolide rings through η^1-binding to nitrogen centres of a pyrrolide ring and are η^2-bound to C-N units of another pyrrolide ring. Analogously, Li(4) and Li(5) form η^2-bonds to C$_\alpha$-C$_\beta$ units respectively, while Li(3) and Li(6) are η^1-bound to the nitrogens centres of opposite pyrrolide rings. The structure strongly resembles that of the *tert*-butyl lithium containing derivative (VIII), except for the presence of η^2-binding interactions in place of the η^5-interactions seen in the former case.
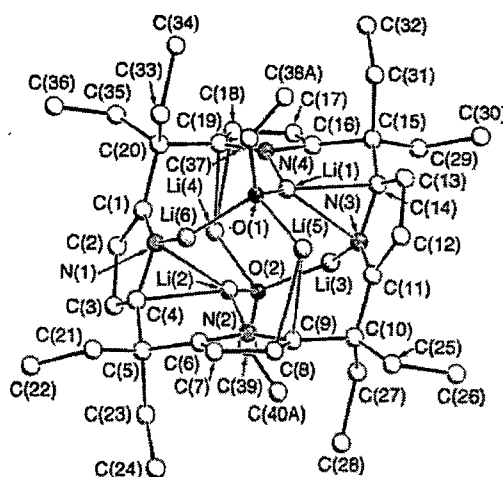
Figure 6: Crystal structure of $[Et_8N_4Li_6(OCH=CH_2)_2(THF)_4]$, **(IX)**[10] (coordinated THF molecules are omitted for clarity).

Several potassium complexes of porphyrinogens were reported by Floriani in 2001[11]. The complexes were prepared from the reaction between the porphyrinogens and potassium metal in the presence of naphthalene as an electron transfer reagent, as shown in Equation 5. Three forms of potassium complexes **(X)**, **(XI)** and **(XII)** were obtained by recrystallisation from the solvents DME, THF and diglyme, respectively.

$$R_8N_4H_4 \quad \xrightarrow[{-2\,H_2}]{K,\ naphthalene} \quad R_8N_4K_4(L)_n$$
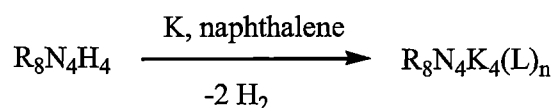
Equation 5

(X): $(Bu^n)_8N_4K_4(DME)_3$ (R = Bu^n, L = DME)

(XI): $(Bz)_8N_4K_4(THF)_5$ (R = Bz, L = THF)

(XII): $[(Bz)_8N_4K_2][K(diglyme)_3)]_2$ (R = Bz, L = diglyme)

The molecular complexity of the potassium derivatives **(X)** - **(XII)** in the solid state is quite different. Complexes **(X)** and **(XI)** adopt polymeric forms while **(XII)** is a solvent separated ionic species. The three complexes are, however, similar in containing both *endo-* and *exo-*cavity-bound potassium cations involving both σ- and π-bonding modes between potassium cations and the metallated porphyrinogens. The porphyrinogen core skeleton displays a partial cone conformation in **(X)**, while 1,3-alternate conformations are seen for both **(XI)** and **(XII)**.

In complex **(X)**, two potassium cations reside in the macrocyclic cavity with K1 and K2 being $\eta^1{:}\eta^1{:}\eta^1{:}\eta^5$, $\eta^5{:}\eta^1{:}\eta^5{:}\eta^1$-bound to the four pyrrolide rings

respectively, as shown in Figure 7. The *exo*-bound-potassium cations bridge two adjacent macrocyclic units with η^5-binding modes to pyrrolide rings of each macrocycle, to form a polymeric chain. A coordinated DME molecule bridges macrocyclic units through K1 and K2 to complete a two-dimensional network, while the remaining potassium cation is chelated by two DME molecules and is η^5-bound to a pyrrolide ring in *exo*-fashion.
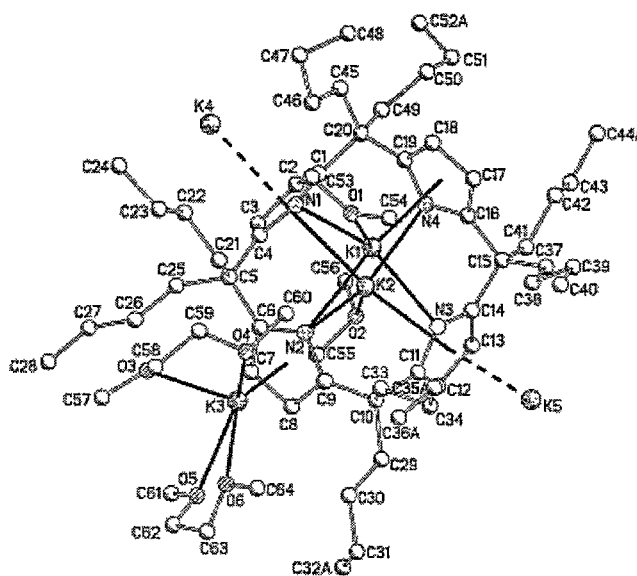
Figure 7: Crystal structure of [(Bu^n)$_8$N$_4$K$_4$(DME)$_3$], (**X**)[11] (K1-N1 = 2.880(3), K1-N2 = 2.953(3), K1-N3 = 2.901(3), K1-η^5 (Pyr) = 2.823(2), K2-η^5 (Pyr) = 2.973(2), K2-N2 = 2.985(3), K2-η^5 (Pyr) = 2.910(2), K2-N4 = 2.812(3) Å).

The *endo*-bound-potassium cations in the ionic complex (**XII**) choose η^5:η^1:η^5:η^1-binding modes to the four pyrrolide rings, as shown in Figure 8[11]. Two opposite pyrrolide rings are η^5-bound to one potassium cation and are η^1-bound to the other potassium cation, and *vice versa* for the other potassium cation. The macrocycle thus adopts a 1,3-alternate macrocyclic conformation.
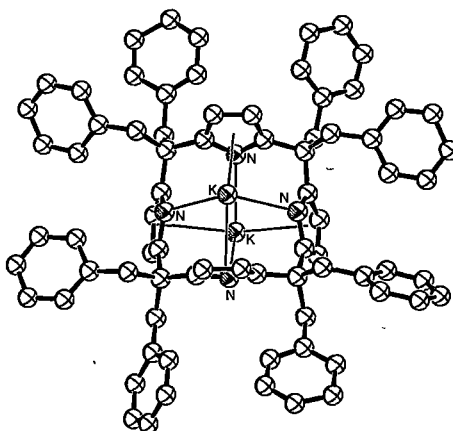
Figure 8: Crystal structure of $[(Bz)_8N_4K_2]^{2-}$, **(XII)**[11] ($[K(diglyme)_3]_2$ not shown). Atoms are shown as isotropic representations.

The disodium complex $[Me_8O_2N_2Na_2(DME)_2]$, **(XIII)**, of dimetallated *meso*-octamethyl-*trans*-dioxaporphyrinogen was reported by Floriani[12]. This compound was synthesised from the reaction of the dioxaporphyrinogen with excess sodium hydride under overnight reflux in THF. The THF adduct $[Me_8O_2N_2Na_2(THF)]$ was isolated and recrystallised from DME leading to the colourless crystalline DME adduct **(XIII)**, as shown in Equation 6.

$$Me_8O_2N_2H_2 \ + \ NaH \ \xrightarrow[-2\,H_2]{DME} \ (Me_8O_2N_2)Na_2(DME)_2$$
$$\textbf{(XIII)}$$
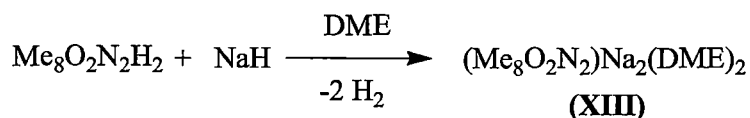
Equation 6

The molecular structure of $[Me_8O_2N_2Na_2(DME)_2]$, **(XIII)**, has been determined, as shown in Figure 9. The 1,3-alternate macrocyclic conformation found in the solid state for the protonated dioxaporphyrinogen is altered to a doubly flattened partial cone conformation in the disodium complex. Each sodium cation, one above and the other below the N_2O_2 core, is σ-bound to the nitrogen centres of the dibridging pyrrolide rings and is η^5-bound to a single furan ring (bonds not shown in Figure 9). The chelating DME molecules fill the remaining coordination sites of the sodium cations.
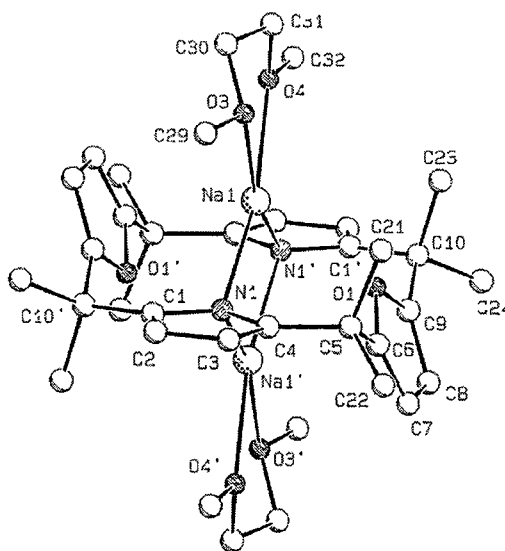
Figure 9: Crystal structure of [Me$_8$O$_2$N$_2$Na$_2$(DME)$_2$], **(XIII)**[12].

Porphyrins and related macrocyclic ligands, such as **(XIV)**, invariably bind alkali metal cations via four σ-bonds through the nitrogen centres[13]. Lithium complexes adopt two structural types, (i) a single lithium resides at the centre of the macrocyclic cavity forming an anionic complex while the other lithium cation is present as a solvated separated cation in the solid state, and (ii) two lithium cations bind through σ-bonding modes residing above and below the N$_4$ core. The larger alkali metals, sodium and potassium, choose the second way to bind with porphyrins.

(XIV)
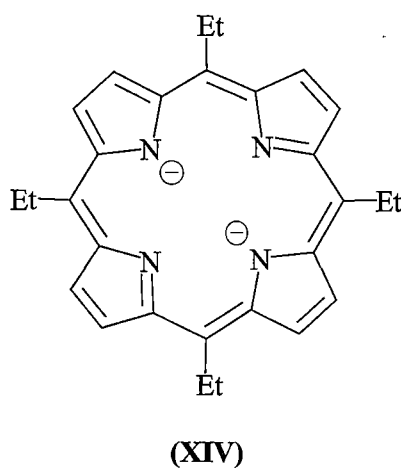
Alkali metal complexes have also been reported for the related macrocycles[14] *meso*-octaethyltris(pyrrole)-monopyridine, **(XV)**, the artificial porphyrin **(XVI)** and the porphodimethene **(XVII)**. The alkali metals display coordination chemistry resembling both porphyrinogen and porphyrin complexes

with these macrocyclic ligands in different respects.

(XV)   (XVI)   (XVII)
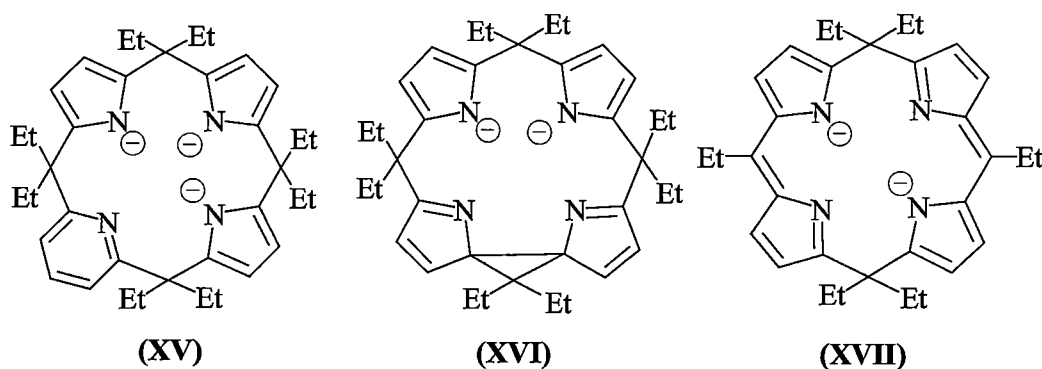
3.1.2 Alkali metals coexisting with other metals in pyrrolide complexes

Alkali metal incorporation in s-[11][15], p-[14h][16], d-[14b][14c][17] and f-[8][10][18] block metal porphyrinogen complexes is very common owing to the frequently used metathetical exchange synthesis of such complexes involving alkali metal reagents, which has been discussed in Chapter 1. This is primarily due to the high tetraanionic charge of the macrocycle in its fully deprotonated form and the preponderance of complexes studied that have featured metals in oxidation states of less than +4. Even for complexes featuring metals of oxidation states of +4 or higher, alkali metal inclusion is still very likely owing to the presence of potential coordination sites *endo-* or *exo-* to the macrocyclic cavity. The presence of the alkali metal cations has significant structural and reactivity influences, which has partly been reviewed in Chapter 1.

The retention of alkali metals in complexes of other metals is also common for other pyrrolide based ligand systems[19], such as dipyrrolide[20] (see Section 4.1) and tripyrrolide systems[21] (see Section 5.1). However, porphyrin complexes typically do not retain alkali metal cations in a similar way, with one exception having been found among the myriad of complexes that have been studied[22].

3.2 RESULTS AND DISCUSSION

3.2.1 Complex syntheses

The synthesis of dimetallated modified porphyrinogen complexes featuring the alkali metals lithium, sodium and potassium have been carried out as shown in
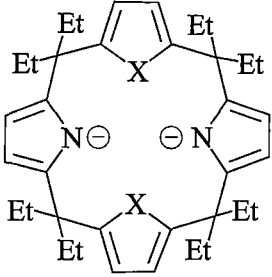
Scheme 1, using *n*-butyllithium, sodium hydride and potassium metal, respectively, using THF or toluene as solvents.

$(Et_8O_2N_2)M_2L_n$, (X = O), **(9) - (10)**

or

$(Et_8N_4Me_2)M_2L_n$, (X = NMe), **(11) - (14)**

(M = Li, Na, K; L = THF or TMEDA)

(3) X = O
(6) X = NMe
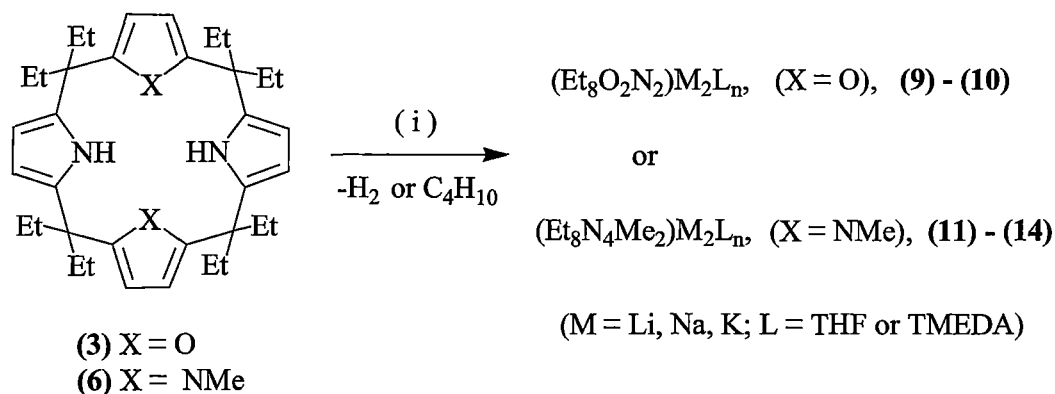
Scheme 1: Synthesis of Group 1 metal complexes of modified porphyrinogens. (i) Bu^{n}Li, NaH or K; THF or toluene with or without the presence of TMEDA.

As shown in Scheme 1, the macrocycles studied are *meso*-octaethyl-*trans*-dioxaporphyrinogen $Et_8O_2N_2H_2$,   **(3)**,   and   *trans*-*N,N'*-dimethyl-*meso*-octaethylporphyrinogen $Et_8N_4Me_2H_2$, **(6)**. The general molecular formula $(Et_8O_2N_2)M_2L_n$ represents Group 1 metal complexes of **(3)** and $(Et_8N_4Me_2)M_2L_n$ the complexes of **(6)**. 'M' is a general symbol of the Group 1 metals Li, Na or K. L represents coordinated solvent molecules (THF or TMEDA), whose presence is typically such that 'n' is 2, except for complex **(11)** where n = 1. Each dianionic macrocyclic unit, as expected, is countered by two monovalent Group 1 metals in the complexes, rather than four in the corresponding tetrametallated parent porphyrinogen complexes, and no additional alkali metal containing fragments are present.

Six Group 1 metal complexes have been synthesised and are listed in Table 1. Complexes **(9)** and **(10)** are derived from *meso*-octaethyl-*trans*-dioxaporphyrinogen **(3)**, while **(11)**, **(12)**, **(13)** and **(14)** are derived from *trans*-*N,N'*-dimethyl-*trans*-octaethylporphyrinogen, **(6)**. The Group 1 metal complexes are very air and moisture sensitive, colourless or light brown and mainly crystalline THF or TMEDA adducts (the latter isolated in the presence of TMEDA). The complexes were characterised by IR, ^1H and ^{13}C NMR spectroscopy, microanalysis, and X-ray crystal structure determinations in the cases of **(10)** and **(14)**.

Complex.	X	M	L	n
(9)	O	Li	TMEDA	2
(10)	O	K	TMEDA	2
(11)	NMe	Li	THF	1
(12)	NMe	Li	TMEDA	2
(13)	NMe	Na	THF	2
(14)	NMe	K	THF	2

$\{(M^+)_2L_n\}$

X = O, NMe

Table 1: Synthesised Group 1 metal complexes of modified porphyrinogens.

The dilithiation of both macrocyclic ligands **(3)** and **(6)** were carried out in THF or toluene using Bu^nLi in hexane. The homogenous lithiating reagent Bu^nLi is an ideal metallation reagent for the acidic pyrrolic hydrogens of the modified porphyrinogens as it is efficient, convenient to handle and commercially available. One dilithium complex $[(Et_8O_2N_2)Li_2(TMEDA)_2]$, **(9)**, derived from macrocycle **(3)** and the two dilithium complexes $[(Et_8N_4Me_2)Li_2(THF)]$, **(11)**, and $[(Et_8N_4Me_2)Li_2(TMEDA)_2]$, **(12)**, derived from macrocycle **(6)** were obtained. The lithium complexes were isolated in moderate yield of 60% for **(9)**, 65% for **(11)** and 80% for **(12)**.

The formation of the dilithium compound $[(Et_8O_2N_2)Li_2(TMEDA)_2]$, **(9)**, was synthesised from the reaction between the dioxaporphyrinogen **(3)** and Bu^nLi (1.6 M solution in hexane) in THF. A slight excess of the lithiating reagent (2.4:1 molar ratio to the macrocycle) was added to ensure the full transformation of the macrocycle. The reaction had reached completion after the mixture was stirred for 30 minutes at 0°C followed by three hours at ambient temperature. To minimise the formation of unnecessary byproduct from the reaction between Bu^nLi and THF, the reaction was carried out at lower temperature before warming to room temperature. Attempts to isolate the crystalline THF adduct from the mixture failed, but the isolation of the alternative TMEDA containing compound was achieved in the presence of TMEDA. Thus 6 molar equivalents of TMEDA were added to the concentrated THF solution, followed by the addition of 40/60°C petroleum ether (4:1, v/v, to THF). The mixture was kept at -4°C for two weeks and the crystalline light brown product **(9)** was collected in 60% yield.

The dilithiated complex $[(Et_8N_4Me_2)Li_2(THF)]$, **(11)**, was obtained from the lithiation of the *trans-N,N'*-dimethylated porphyrinogen $Et_8N_4Me_2H_2$, **(6)**. The

reaction is slower than that of the dioxaporphyrinogen (3) with Bu^{n}Li and had transformed only partly to (11) using the same conditions as those used for (3). The reaction in THF stirred for a longer time at room temperature, or at higher temperature, results in a complicated mixture which contained substantial side product formed from the reaction between Bu^{n}Li and THF. To avoid the unwanted byproduct, toluene was employed for the reaction in place of THF. Thus the mixture of (6) and n-butyllithium reagent in toluene was kept at 40°C for five hours to reach completion and the dilithiated product (Et$_8$N$_4$Me$_2$)Li$_2$ precipitated from the solution as colourless solid which was separated by removal of the clear, colourless solution after the undissolved product settled from standing overnight. The solid product was washed twice with toluene and recrystallised from a minimum amount of THF leading to the pure colourless dilithiated product as a mono THF adduct in 65% yield. The TMEDA adduct of the dilithium complex [(Et$_8$N$_4$Me$_2$)Li$_2$(TMEDA)$_2$], (12), was isolated in the presence of 6 molar equivalents of TMEDA.

The synthesis of the disodium complex of the dioxaporphyrinogen (3) was not included in this work. The *meso*-octamethyl analogue [(Me$_8$N$_2$O$_2$)Na$_2$(DME)$_2$], (XIII), was, however, reported in the literature and its characterisation has been quoted for comparison when needed. The formation of the disodium complex [(Et$_8$N$_4$Me$_2$)Na$_2$(THF)$_2$], (13), was carried out by the reaction between the *trans-N,N'*-dimethylated porphyrinogen (6) and sodium hydride in THF-d^8 on an NMR scale. The reaction did not proceed under the same reflux conditions used for the preparation of [(Et$_8$N$_4$Me$_2$)K$_2$(THF)$_2$]$_n$, (14). However, the synthesis of (13) was achieved with sonication at 55°C with the reaction approaching completion after seven hours. The alternative reaction to prepare (13), using sodium metal instead of sodium hydride, is a much slower reaction under the same conditions.

The colourless dipotassium complexes [(Et$_8$O$_2$N$_2$)K$_2$(TMEDA)$_2$], (10), and [(Et$_8$N$_4$Me$_2$)K$_2$(THF)$_2$]$_n$, (14), were obtained from the reactions of the modified porphyrinogens with potassium metal in high yield (88% for (10) and 95% for (14)). Potassium metal, the only potassium metallating reagent to be used, shows high reactivity towards the deprotonation of the porphyrinogens compared with sodium metal in the case of the *trans-N,N'*-dimethylated porphyrinogen. Other advantages of using potassium metal include easy observation of the extent of completion and convenient separation.

Potassium metal was added to the solution of the dioxaporphyrinogen (3) in THF and mild effervescence (presumably hydrogen gas) was noticed. Reflux for

three hours resulted in completion of the reaction. Six molar equivalents of TMEDA were added to the concentrated THF solution, followed by 40/60°C petroleum ether. The mixture was brought to -4°C affording the colourless crystalline dipotassium product $[(Et_8O_2N_2)K_2(TMEDA)_2]$, (10), which was collected after storage for two weeks at -4°C. These crystals were suitable for X-ray crystal structure determination.

The reaction of the $trans$-N,N'-dimethylated porphyrinogen (6) with potassium appears, again, slower than that of the analogous reaction involving the dioxaporphyrinogen (3). No effervescence was observed from the contact of potassium metal with the solution of the macrocycle in THF and a longer reflux time of six hours was needed to complete the reaction, after which time two molar equivalents of the added potassium metal had been consumed. The dipotassium complex was only slightly soluble in THF and most product precipitated during reflux. Samples of the colourless crystalline product $[(Et_8N_4Me_2)K_2(THF)_2]_n$, (14), were obtained through the dropwise addition of toluene to its saturated THF solution followed by storage at room temperature for two hours. These crystals were suitable for X-ray crystal structure determination.

In terms of the reactivity towards Group 1 metal reagents, the dioxaporphyrinogen (3) is consistently slower than that of the parent porphyrinogens which have more acidic protons and similar steric bulk. However, the metallation of (3) is still much faster than the $trans$-N,N'-dimethylated porphyrinogen (6) due to the difference in their molecular structures. The responsible factors contributing to the reactivity differences relate to the macrocyclic cavity formed by the furan and pyrrole rings in the dioxaporphyrinogen (3), which is considered to be more accessible, allowing more ready metallation of the pyrrole units in comparison with the $trans$-N,N'-dimethylated porphyrinogen (6), where the bulky N-methyl groups make it more difficult to metallate the acidic N-H pyrrolic protons. Neighbouring assistance, a factor suggested for some metallation processes, is considered to promote the reactivity of the dioxaporphyrinogen (3). The oxygen donor atoms in the neighbouring position to the pyrrolic units coordinate to the metallating reagents, thus holding the strong base in close proximity to the molecule. In this case, the strong base is at an advantageous position to remove the active N-H protons from the pyrrole functionalities, as shown in Figure 10. No neighbouring assistance exists in the $trans$-N,N'-dimethylated porphyrinogen (6) due to the presence of the two bulky N-methyl pyrrole units replacing the furan rings in (3).
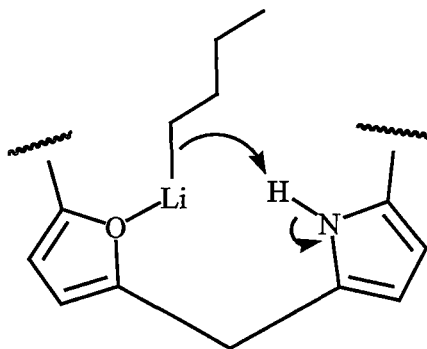
Figure 10: Neighbouring assistance in the metallation of **(3)** (only the part structures of **(3)** and the metallating reagents are shown, Bu^{n}Li used as an example).

The IR spectra of complexes **(9)** - **(14)** confirm that the metallation has removed all *N*-H protons of the macrocycles **(3)** and **(6)**. Complexes **(9)**, **(10)**, **(11)** and **(13)** have given satisfactory microanalytical results, but compound **(14)** showed low carbon analysis.

3.2.2 NMR spectroscopic characterisation

The ^{1}H NMR spectral data of the Group 1 metal complexes featuring the macrocycle **(3)** are listed in Table 2 and complexes featuring **(6)** are given in Table 3 (^{1}H NMR spectral data of macrocycles **(3)** and **(6)** are also given for comparison; resonances of coordinating THF or TMEDA molecules are not listed). The resonances of all protons in the molecules have been assigned through gCOSY, gHMQC, gHMBC and gNOESY NMR spectra. Furanyl and pyrrolide ring protons occur in the range δ = 5.50-6.50 ppm, the *N*-methyl protons occur between δ = 2.80-3.70 ppm, while the *meso*-ethyl group protons resonate at between δ = 1.60-2.40 ppm for CH_2 and 0.40-1.00 ppm for CH_3 protons.

Compound number	NH	=CH, fur	=CH, pyr	CH$_2$	CH$_3$
Et$_8$O$_2$N$_2$H$_2$ (3)	6.57 (broad)	6.08	5.78	1.82	0.61
[(Et$_8$O$_2$N$_2$)Li$_2$(TMEDA)$_2$] (9)	-	6.38	5.84	2.02-2.20	0.88
[(Et$_8$O$_2$N$_2$)K$_2$(TMEDA)$_2$] (10)	-	6.18	5.89	1.97-2.11	0.64 0.78

Table 2: ^{1}H NMR spectral data for Group 1 metal complexes (9) and (10) (THF-d^8 for (10), pyridine-d^5 for (9), 399.694 MHz, 298 K, ppm, protons of TMEDA are not listed). ^{1}H NMR data for Et$_8$O$_2$N$_2$H$_2$, (3) (CDCl$_3$, 399.694 MHz, 298 K, ppm) are included for reference.

Compound number	NH	=CH pyrMe	=CH pyr	NCH$_3$	CH$_2$	CH$_3$
Et$_8$N$_4$Me$_2$H$_2$ (6)	7.24 (broad)	6.05	5.99	2.83	1.75-1.92	0.60 0.71
[(Et$_8$N$_4$Me$_2$)Li$_2$(THF)] (11)	-	6.41	5.68	3.67	2.04, 2.16, 2.30(8H)	0.71 0.97
[(Et$_8$N$_4$Me$_2$)Li$_2$(TMEDA)$_2$] (12)	-	6.41	5.68	3.68	2.06, 2.18, 2.32(8H)	0.71 0.99
[(Et$_8$N$_4$Me$_2$)Na$_2$(THF)$_2$] (13)	-	5.76	5.55	2.95	1.65, 1.88	0.45 0.47
[(Et$_8$N$_4$Me$_2$)K$_2$(THF)$_2$]$_n$ (14)	-	5.89	5.75	3.05	1.91-2.15	0.69

Table 3: ^{1}H NMR spectral data for Group 1 metal complexes (11), (12), (13) and (14) (THF-d^8 for (13) and (14), pyridine-d^5 for (11) and (12), 399.694 MHz, 298 K, ppm, protons of THF and TMEDA are not listed). ^{1}H NMR data for Et$_8$N$_4$Me$_2$H$_2$, (6), (CDCl$_3$, 399.694 MHz, 298 K, ppm) are included for reference.

The ^{1}H NMR spectra of complexes (9) - (14) indicate that the metallation results in the removal of both of the active N-H protons from the pyrrole rings of the

porphyrinogens. The N-H resonances at $\delta = 6.57$, 7.24 ppm (broad) for (3) and (6) are absent in all of the complexes.

Both of the dilithium complexes of *trans-N,N'*-dimethylated porphyrinogen (6), the THF adduct (11) and the TMEDA adduct (12), have very similar ^{1}H NMR spectroscopic characteristics in terms of the resonances of the macrocyclic units. The similarity in the ^{1}H NMR spectra of analogous Lewis base adducts has also been found for the reported compounds [(Me$_8$O$_2$N$_2$)Na$_2$(THF)] and [(Me$_8$O$_2$N$_2$)Na$_2$(DME)$_2$], (XIII)[12]. This suggests that the coordinated Lewis bases have little effect on the overall structural features of the complexes in solution.

The coordination of lithium and sodium with the dioxaporphyrinogen (3) markedly increases the ^{1}H NMR chemical shift separation of the furanyl and pyrrolide proton resonances, as shown in Figure 11. The potassium complex, however, having similar ^{1}H NMR spectral features to the protonated macrocycle (3), has its aromatic proton resonances at closer chemical shifts. The chemical shift differences between the furanyl and pyrrolide protons are 0.54, 0.75 and 0.29 ppm for (9), [(Me$_8$O$_2$N$_2$)Na$_2$(THF)] (or [(Me$_8$O$_2$N$_2$)Na$_2$(DME)$_2$]), and (10), respectively (compared to 0.30 for (3) and 0.20 for Me$_8$O$_2$N$_2$H$_2$). For the Group 1 metal complexes featuring the macrocycle (6), the two lithium complexes (11) and (12) display the same trend in large separation between the aromatic proton resonances of the N-methyl pyrrole and pyrrolide rings as noted for the dilithium complex (9) of the dioxaporphyrinogen (3). However, the ^{1}H NMR spectral feature of the sodium complex (13) is similar to the potassium complex (14), showing slight separations between the proton resonances. The chemical shift differences between N-methyl pyrrole and pyrrolide resonances are 0.73, 0.73, 0.21 and 0.14 ppm for compounds (11), (12), (13) and (14), respectively, compared with 0.06 ppm for the macrocycle (6).
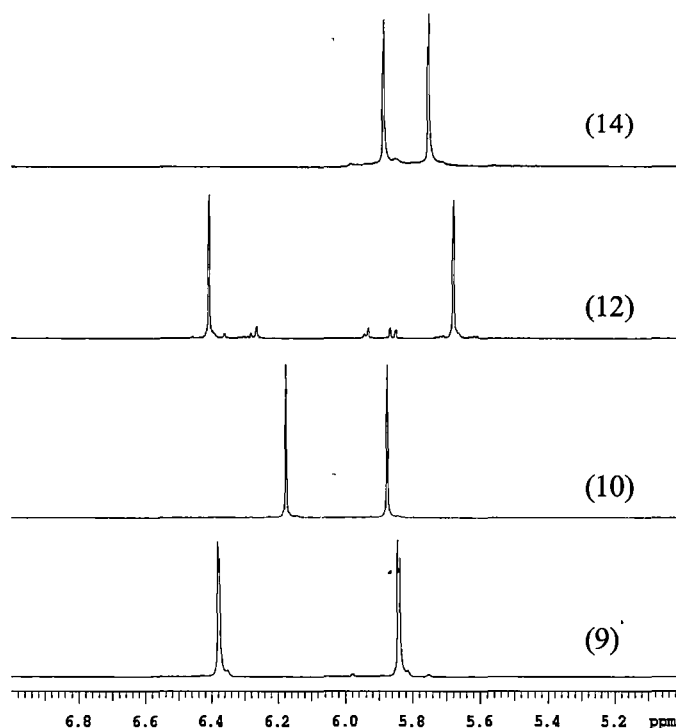
Figure 11: Aromatic region of the ^{1}H NMR spectra of complexes **(9)**, **(10)**, **(12)** and **(14)** (pyridine-d^5 for **(9)** and **(12)**, THF-d^8 for **(10)** and **(14)**, 399.694 MHz, 298 K, ppm).

The different ^{1}H NMR spectral patterns existing amongst the Group 1 metal complexes, in terms of the chemical shift separation of the resonances from two types of aromatic protons, are very likely caused by different bonding modes between the metals and the macrocycles, resulting in different macrocycle conformation, as shown in Figure 12.

It is likely that the lithium and sodium complexes featuring the dioxaporphyrinogen **(3)** have analogous structures in which the macrocycles adopt partially flattened double cone conformations, similar to the sodium complex **(XIII)** which differs from that found for the potassium complex **(10)** (see Section 3.2.3.1) in which the pyrrolide rings partake in both η^5- and η^1-bonding interactions, as shown in Figure 19 (depicted is the likely variation for the smaller lithium cation). Similarly, for the N,N'-dimethylated porphyrinogen complexes, the similarity of the spectral features of the sodium complex **(13)** to the structurally authenticated potassium complex **(14)** may suggest analogous macrocyclic conformations and metal binding modes. Whereas the structure of the dilithium complexes may be somewhat similar to the structure of **(9)**, featuring a partially flattened double cone

macrocycle conformation, thus accounting for the differences in comparison to the ^{1}H NMR spectra of the sodium and potassium complexes.

(10)   **(14)**

(9)   **(11), (12)**
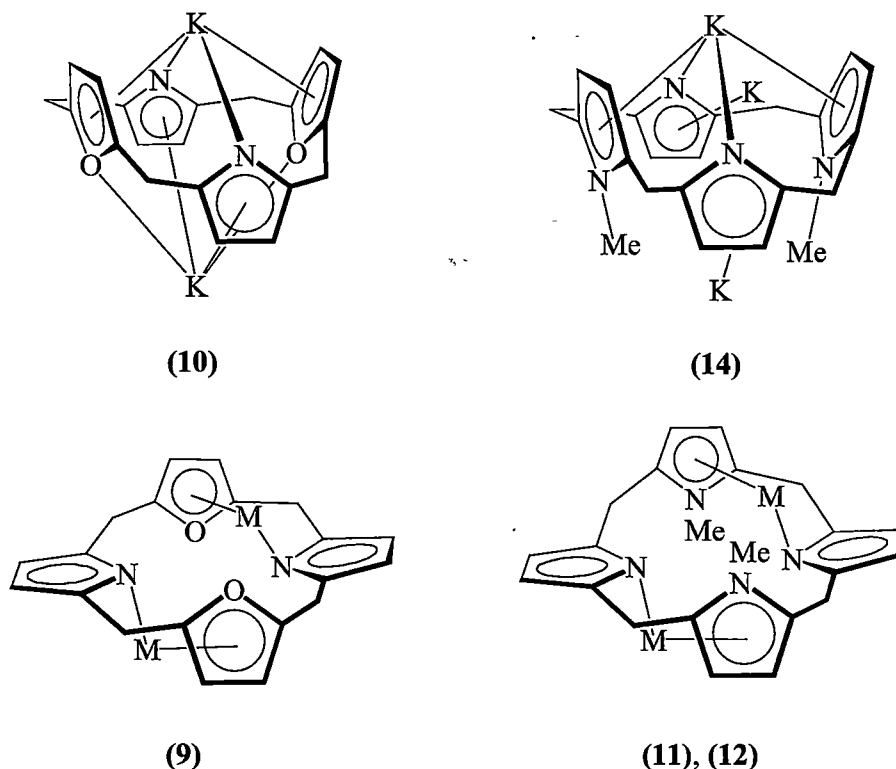
Figure 12. Established, **(10)** and **(14)**, and proposed **(9)**, **(11)** and **(12)** structures based on ^{1}H NMR spectral feature (solvent molecules not shown).

The N-methyl protons of lithium complex of **(6)** resonant at a much higher chemical shift than that of corresponding sodium, potassium complexes and the porphyrinogen itself (3.67, 3.68 ppm for **(11)** and **(12)**, 2.95, 3.05, 2.83 ppm for **(13)**, **(14)** and **(6)** respectively). This demonstrates again the different bonding and structural features in solution among these metal complexes.

The observation of two singlet resonances for the β-pyrrolic and furanyl protons in the ^{1}H NMR spectra of complexes **(11)** – **(14)** suggests that all the structures of the Group 1 metal complexes average to be C_{2v} symmetric in solution. Thus, the structure of associated complexes such as $[(Et_8N_4Me_2)K_2(THF)_2]_n$, **(14)**, have a different structure in solution from that in solid state (see Section 3.2.3.2, Figure 22). In solution, one metal cation resides symmetrically in the cavity while the other one is presumably solvated and dissociated from the macrocycle or is fluxional in its *exo*-cavity binding mode.

Inequivalent ethyl groups attached to the *meso*-carbons are observed in the ^{1}H NMR spectra of the Group 1 metal complexes **(10)** - **(14)** of the modified porphyrinogens **(3)** and **(6)**, as shown in Figure 13. The molecular structures of all complexes in solution are highly symmetric in terms of the C_{2v} symmetry axis through the N_4 or N_2O_2 macrocyclic planes, but are asymmetric with respect to the N_4 or N_2O_2 planes. Thus, each *meso*-carbon and its substituents are equivalent, but the two geminal ethyl groups of the each *meso*-carbon residing on each side of N_4 or N_2O_2 planes are chemically inequivalent. This will be further discussed below in relation to variable temperature studies. Complex **(9)** displays a rapid fluxional process, resulting in chemically equivalent *meso*-ethyl substituents at room temperature. Complex **(14)** exhibits overlap of the methyl protons of the *meso*-ethyl groups at room temperature, giving the appearance of a more symmetric solution structure.
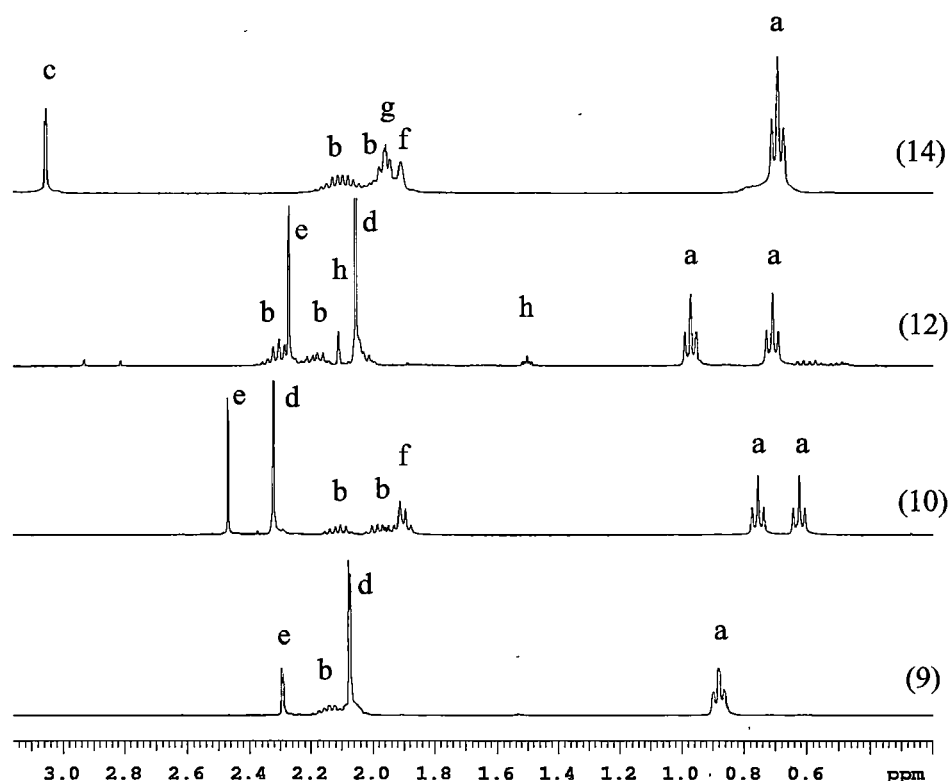
Figure 13: *Meso*-ethyl region of the ^{1}H NMR spectra of selected complexes (pyridine-d^5 for **(9)** and **(12)** or THF-d^8 for **(10)** and **(14)**, 399.694 MHz, 298 K, ppm) (a. CH_3 of *meso*-ethyl group, b. CH_2 of *meso*-ethyl group, c. NCH_3 of macrocycle, d. NCH_3 of TMEDA, e. NCH_2 of TMEDA, f. THF-d^8, g. THF, h. impurity).

The ^{13}C NMR spectra of the series of Group 1 metal complexes (9) - (14) support the presumption of the features of the molecular structures deduced from the ^{1}H NMR spectra. Four aromatic carbon resonances are found in the spectra of each compound for the pyrrolide and furanyl (or N-methyl pyrrolyl) units. The ^{13}C NMR spectral data of the ethyl groups in selected compounds are listed in Table 4 and shown in Figure 14. Two different ethyl groups are observed in the ^{13}C NMR spectra of compounds (10), (11), (12) and (14).

Compound number	CH_2	CH_3
$Et_8O_2N_2H_2$ (3)	28.8	8.5
$[(Et_8O_2N_2)Li_2(TMEDA)_2]$ (9)	33.9	10.1
$(Et_8O_2N_2)K_2(TMEDA)_2$ (10)	28.2 30.0	8.7 9.6
$Et_8N_4Me_2H_2$ (6)	24.3 30.0	7.7 7.9
$[(Et_8N_4Me_2)Li_2(THF)]$ (11)	27.0 32.3	9.7 9.9
$[(Et_8N_4Me_2)Li_2(TMEDA)_2]$ (12)	27.0 32.3	9.7 9.9
$[(Et_8N_4Me_2)K_2(THF)_2]_n$ (14)	27.0 31.8	9.6 9.8

Table 4: ^{13}C NMR spectral data of the *meso*-ethyl groups in selected compounds (pyridine-d^5 for (9), (11) and (12), THF-d^8 for (10) and (14), 100.512 MHz, 298 K, ppm).
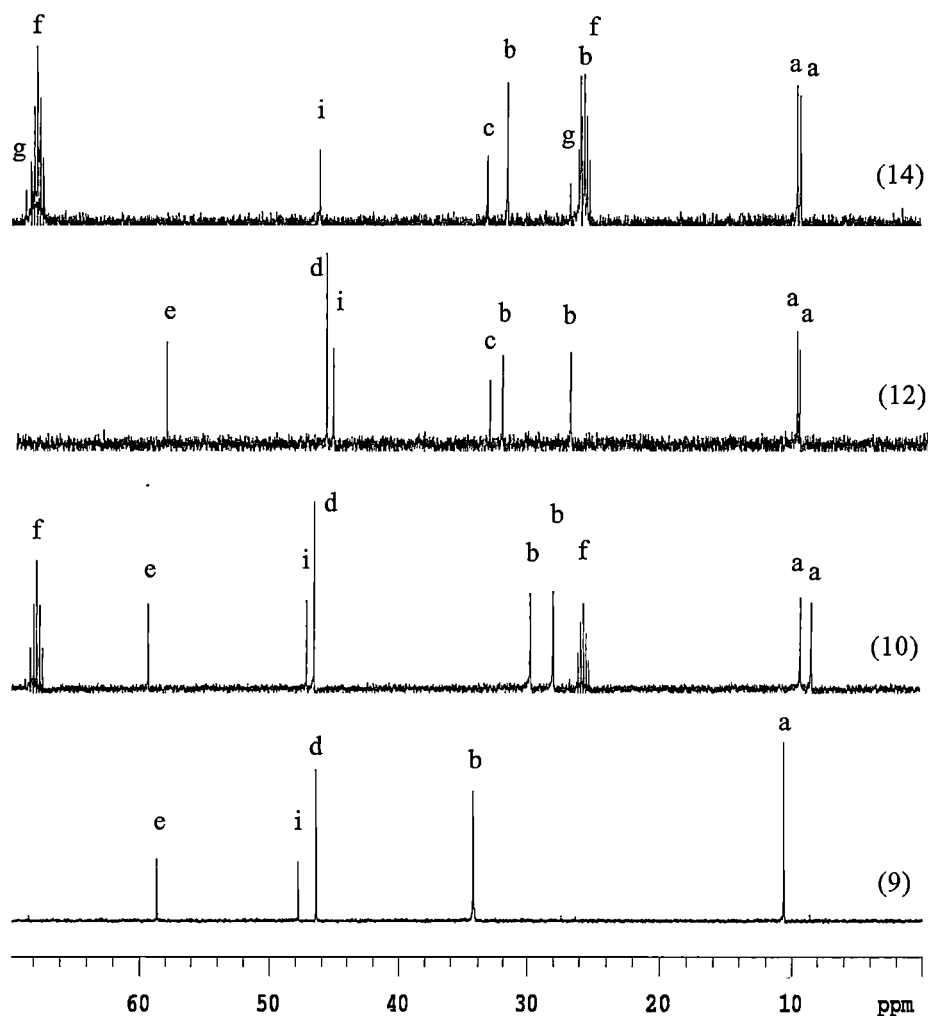
Figure 14: *Meso*-ethyl region of the ^{13}C NMR spectra of selected complexes **(9)**, **(10)**, **(12)** and **(14)** (pyridine-d^5 for **(9)** and **(12)**, THF-d^8 for **(10)** and **(14)**, 100.512 MHz, 298 K, ppm) (a. CH$_3$ of *meso*-ethyl group, b. CH$_2$ of *meso*-ethyl group, c. NCH$_3$ of macrocycle, d. NCH$_3$ of TMEDA, e. NCH$_2$ of TMEDA, f. THF-d^8, g. THF, i. CEt$_2$).

Chemically equivalent ethyl groups are noted for the dioxaporphyrinogen **(3)** and **(9)** based on their room temperature ^{13}C NMR spectra. It is presumed that a fluxional process involving the flipping of the furan or pyrrole rings in these two compounds is less constrained than in the other complexes, for example, the complexes of the *trans-N,N'*-dimethylatedporphyrinogen **(6)** in which *N*-methyl groups are expected to hinder such a fluxional process. As a result of this rapid fluxional process, the molecules feature time-averaged symmetry across the N$_2$O$_2$ plane by ^{1}H and ^{13}C NMR spectroscopy at room temperature. Complex **(10)**, of the large potassium cation, prevents such a rapid fluxional process. Thus the time-averaged symmetry across the N$_2$O$_2$ plane no longer exists, leading to inequivalent

meso-ethyl substituents at room temperature. The room temperature ^{1}H NMR spectrum reported for the disodium complex **(XIII)** derived from the dioxaporphyrinogen **(3)** contains a single *meso*-methyl resonance, indicating that the fluxional process is also rapid in this case.
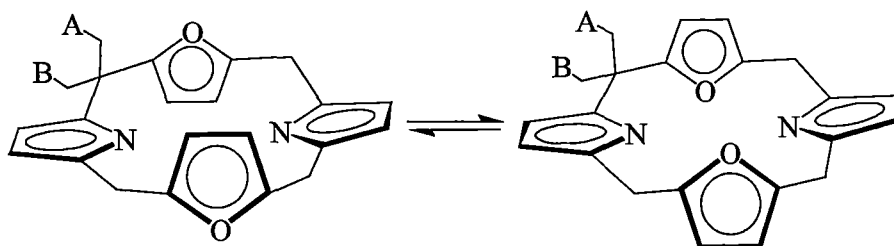
Figure 15: Proposed flipping of the macrocyclic conformations for compounds **(3)** and **(9)** accounting for the exchange of chemically inequivalent *meso*-ethyl groups A and B (some parts of the molecules are omitted for clarity).

gCOSY, gHMQC, gHMBC NMR spectra on most of the complexes **(9)** - **(14)** were performed to fully assign the ^{1}H and ^{13}C NMR spectra. As an example of the stereochemical assignments that were made, the gNOESY spectrum at 25°C of **(10)** shows correlation between the aromatic β-pyrrolide protons (δ = 5.89 ppm) directly attached to the β-carbons (δ = 102.9 ppm) and protons of one of the methyl groups (δ = 0.64 ppm) directly attached to a methyl carbon (δ = 8.7 ppm) of one of the *meso*-ethyl groups, as shown in Figure 16.
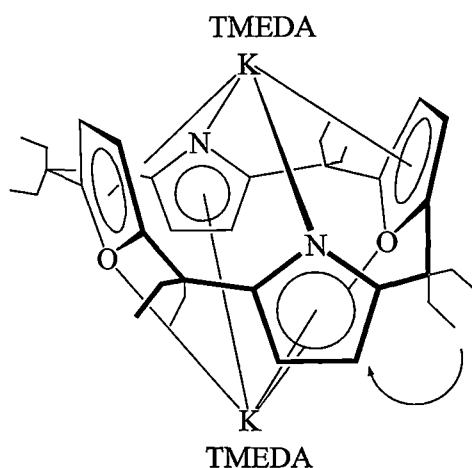
Figure 16: NOE correlation observed in the gNOESY NMR spectrum of [Et$_8$O$_2$N$_2$)K$_2$(TMEDA)$_2$], **(10)** (correlation of other *meso*-ethyl groups have not been shown for clarity)

Variable temperature ^{1}H NMR spectra of complex **(14)** show only a minor temperature dependence for the chemical shifts of the CH$_3$ protons of the *meso*-ethyl groups. The CH$_3$ protons display various patterns arising from overlap of the triplets in the range of temperatures studies as shown in Figure 17. This study resolves the apparent chemical inequivalence of the protons as resulting from signal overlap at room temperature.
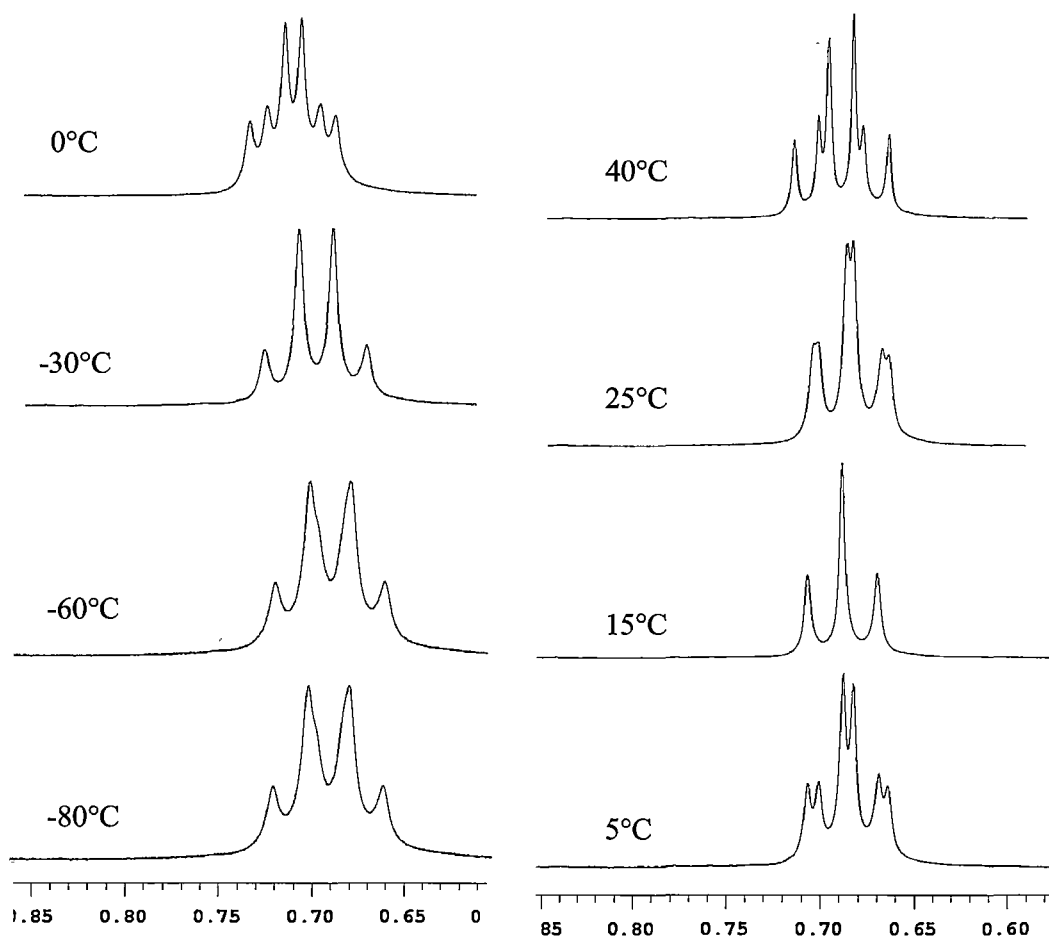
Figure 17: Variable temperature ^{1}H NMR spectra of the methyl region of the *meso*-ethyl groups in [(Et$_8$N$_4$Me$_2$)K$_2$(THF)$_2$]$_n$, **(14)** (THF-d^8, 399.694 MHz, ppm).

^{1}H NMR spectra of the potassium complex **(10)** show no noticeable changes in the temperature between -50°C to 35°C. However, at temperatures above 35°C, the CH$_3$ protons of the *meso*-ethyl groups merge and coelesce at *ca.* 65°C. This indicates that a fluxional process in the molecule is becoming faster as the temperature rises and, as a result, the *meso*-ethyl groups are equivalent at higher temperatures. Unfortunately, with the boiling point limitation of THF, higher temperature studies could not be undertaken.
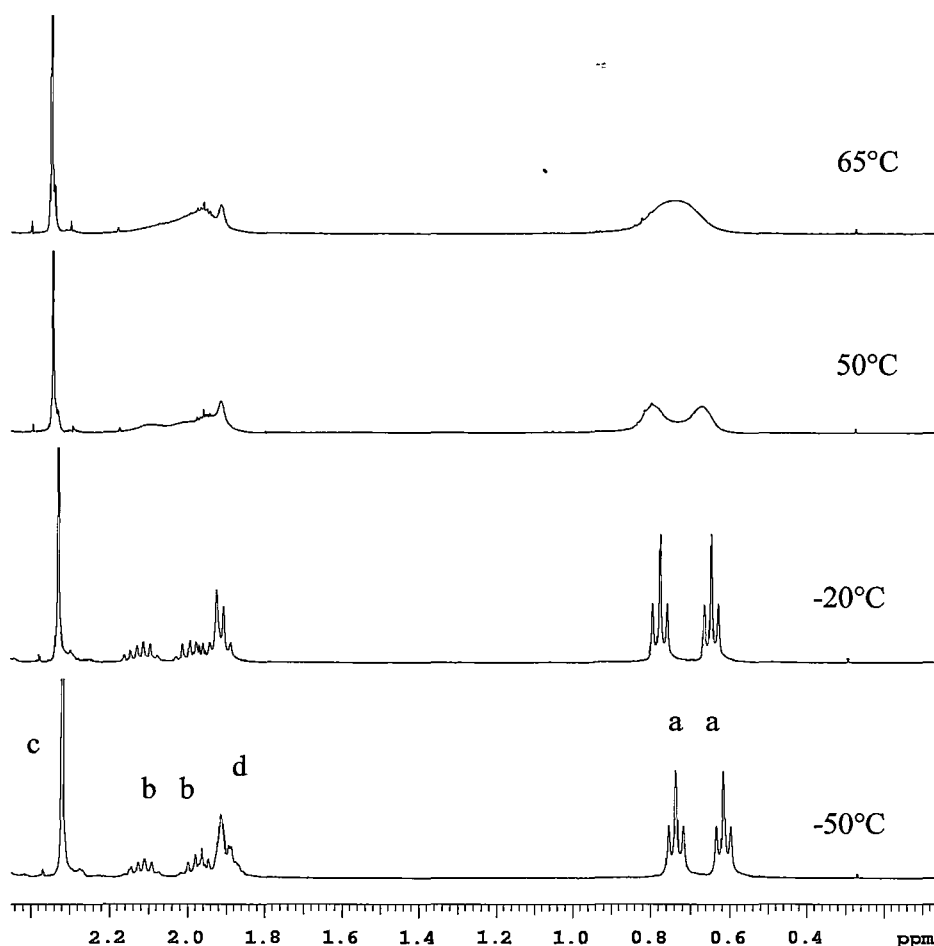
Figure 18: Variable temperature ^1H NMR spectra of the *meso*-ethyl group region in complex **(10)** (THF-d^8, 399.694 MHz, ppm), (a. CH_3 of *meso*-ethyl group, b. CH_2 of *meso*-ethyl group, c. NCH_3 of TMEDA, d. THF-d^8).

Variable temperature ^1H NMR spectroscopic studies of complexes **(12)** - **(14)** show that the macrocyclic conformations of the Group 1 metal complexes of the *trans-N,N'*-dimethylated porphyrinogen **(6)** are rigid. No significant changes were noted in the variable temperature ^1H NMR spectra in the temperature range from 65°C to -50°C. This result is consistent with the steric restrictions imposed by the *N*-Me substituents, which prevents fluxional processes similar to those noted above for complexes **(9)** and **(10)** derived from the less bulky dioxaporphyrinogen **(3)**.

3.2.3 Molecular structures of [(Et$_8$O$_2$N$_2$)K$_2$(TMEDA)$_2$], (10), and [(Et$_8$N$_4$Me$_2$)K$_2$(THF)$_2$]$_n$, (14)

3.2.3.1 Molecular structure of [(Et$_8$O$_2$N$_2$)K$_2$(TMEDA)$_2$], (10)

Colourless crystals of [(Et$_8$O$_2$N$_2$)K$_2$(TMEDA)$_2$], **(10)**, suitable for X-ray crystal structure determination were grown by storing a THF/40-60°C petroleum ether (1:2, v/v) solution at -4°C for two weeks. The crystals were isolated and mounted in sealed thin-walled glass capillaries under an argon atmosphere. The crystals belong to the triclinic space group P$\bar{1}$ (No. 2), a = 12.194(3), b = 12.608(3), c = 17.834(5) Å, α =80.359(4), β = 80.055(4), γ = 68.722(4)°, with two molecules in
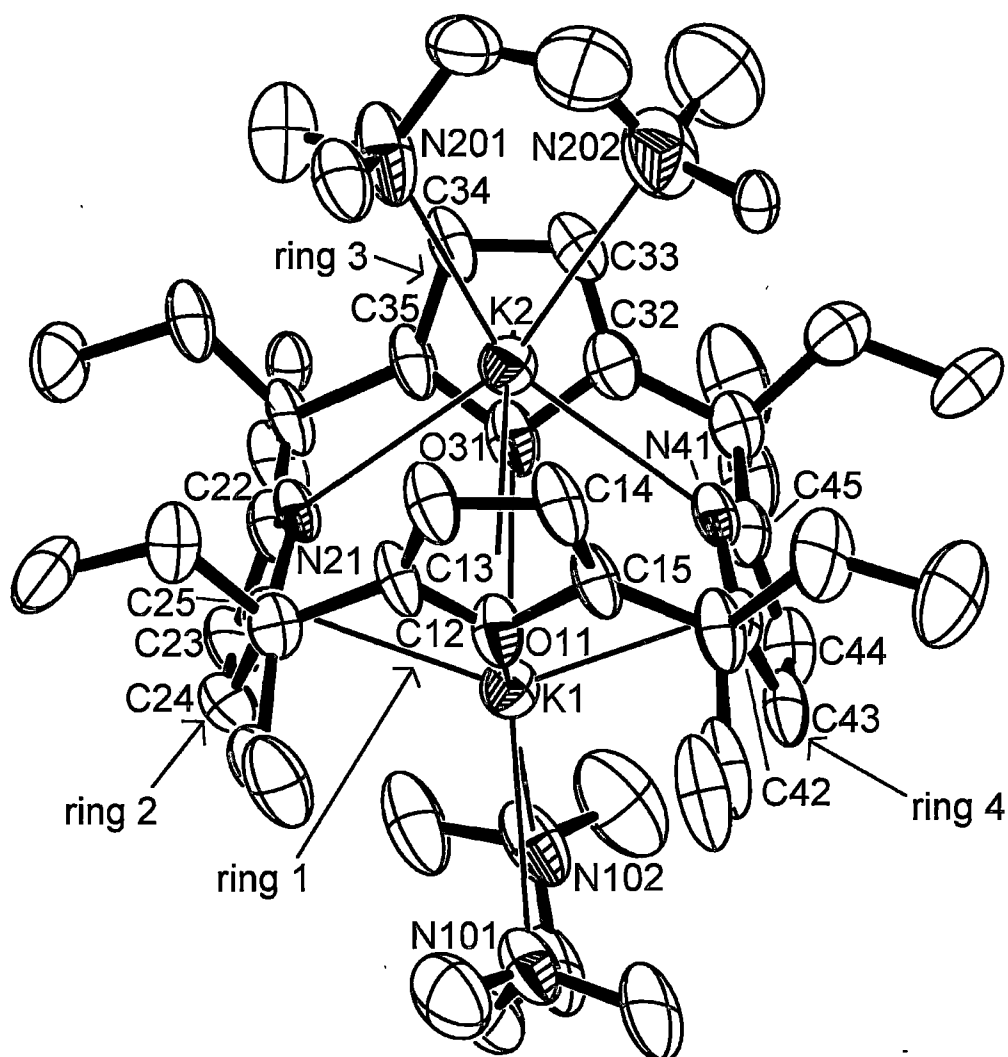
Figure 19: Molecular structure of [(Et$_8$O$_2$N$_2$)K$_2$(TMEDA)$_2$], **(10)**, with thermal ellipsoids drawn at the level of 50% probability (protons and disorder in a TMEDA molecule have been removed for clarity).

the unit cell, the asymmetric unit consisting of one molecule of $[(Et_8O_2N_2)K_2(TMEDA)_2]$, **(10)**, as shown in Figure 19.

Complex **(10)** adopts a monomeric structure in the solid state. The macrocycle has a 1,3-alternate conformation (the two oxygen atoms in the two furan rings are "down" and the two nitrogen atoms in the two pyrrolide rings are "up"). The two potassium cations reside inside the macrocyclic cavity on either side of the average N_2O_2 plane, each displaying the same $\eta^5:\eta^1:\eta^5:\eta^1$-bonding sequence to the macrocycle. Thus one potassium features η^5-binding to the nitrogen centres of both pyrrolide units and σ-binding to the oxygen centres of both furan units and vice versa for the other potassium. Chelating TMEDA molecules complete the coordination spheres of both potassium cations in two perpendicular directions, with each dividing the space between two η^5-binding pyrrolide or η^5-bonding furan rings.

The structure of complex **(10)** is different from the reported structure of corresponding disodium complex **(XIII)** of the *meso*-octamethyl analogue of the dioxaporphyrinogen[12]. The conformational change underlying the observed binding modes of the potassium cations in **(10)** is in response to providing an increased macrocyclic cavity size to bind the larger cations. In the sodium complex, both nitrogen centres are involved in bridging the sodium cations through the macrocyclic cavity, with the pyrrolide units lying flat with respect to the macrocyclic cavity. Each sodium centre is bound in η^5-fashion to a single furan ring and further coordinated by a 1,2-dimethoxyethane molecule, defining a partially flattened double cone conformation for the macrocycle. The same conformation exists for a cobalt(II) complex, the only other structurally characterised metal complex of the dioxaporphyrinogen[12].

Complex **(10)** has its two potassium cations residing in the macrocyclic cavity. This structural feature is different from the corresponding parent tetrapotassium complexes derived from **(4)**, in which two potassiums bind *exo-* to the cavity and the remaining two cations reside within the cavity as for those in the complex **(10)**. Thus, the structure of **(10)** featuring the modified divalent porphyrinogen is more akind to those of the dinuclear alkaline earth metal complexes of calcium, strontium and barium, rather than the alkali metal complexes[11] of **(4)**.

Figures 20 and 21 show alternative views of complex **(10)** from different angles. These figures provide pertinent information about the macrocyclic conformation defining the macrocyclic cavity comprised by the furan and pyrrolide

rings and the position of potassium cations relative to these rings in the complex. Each potassium cation can be seen to partake in a bent metallocene coordination environment with additional coordination offered by the σ-bound heterocycles (in addition to the chelating TMEDA molecules).
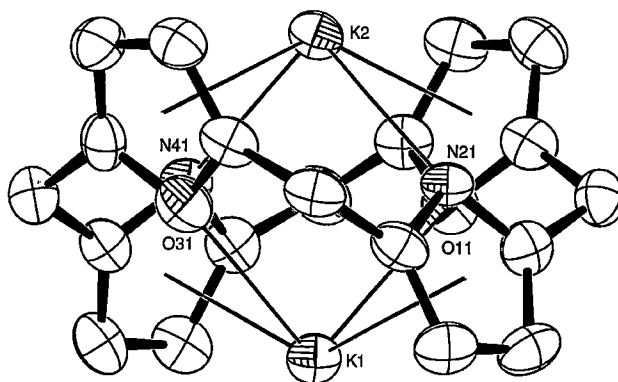
Figure 20: Side view of the molecular structure of [(Et₈O₂N₂)K₂(TMEDA)₂], **(10)**, with thermal ellipsoids drawn at the level of 50% probability (TMEDA molecules, ethyl groups and protons have been removed for clarity).
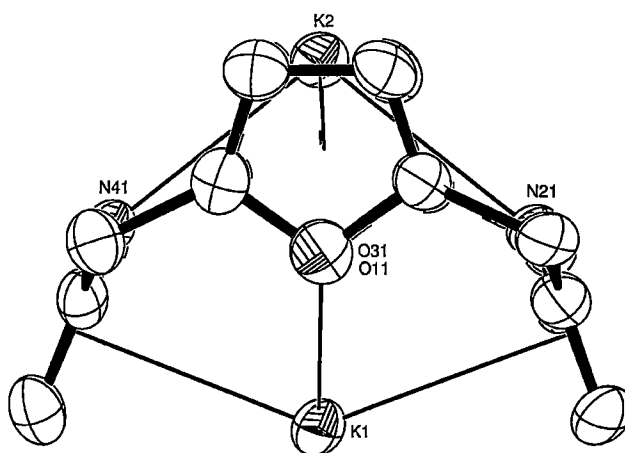
Figure 21: Side view of the molecular structure of [(Et₈O₂N₂)K₂(TMEDA)₂], **(10)**, with thermal ellipsoids drawn at the level of 50% probability (TMEDA molecules, ethyl groups and protons have been removed for clarity).

Significantly different σ-bond distances are found between the potassium cation and the pyrrolide, with K(2)-N(21) and K(2)-N(41) distances of 2.898(4) and 2.952(4) Å, respectively, while the σ-bond distances involving the furan rings of K(1)-O(11) and K(1)-O(31) are similarly longer at 2.976(4) and 2.972(4) Å,

respectively. The furan-based η^5-contacts to K(2) are similar at K(2)-η^5(O11) = 2.91$_0$ and K(2)-η^5(O31) = 2.92$_3$ Å, but those to K(1) involving the pyrrolide rings are shorter and vary slightly, K(1)-η^5(N21) = 2.88$_1$ and K(1)-η^5(N41) = 2.93$_1$ Å.

The closer σ-coordination between K(2) and two pyrrolide rings play a key role for the upper part of the structure (as shown in Figure 19) of the molecule. The TMEDA molecule coordinated to K(2) displays two disparate bond distances K(2)-N(202) = 3.076(8) being longer than K(2)-N(201) = 2.952(4) Å, while the other chelating TMEDA coordinated to K(1) has quite similar bonding distances of K(1)-N(101) = 3.046(7) and K(1)-N(102) = 3.080(7) Å. The closer coordination between K(2) and the two pyrrolide rings tend to bring the TMEDA molecule deeper into the cavity resulting in close contact of a N-methyl group of TMEDA with an ethyl group attached to a *meso*-position of the macrocycle. The compromise result is that the TMEDA molecule is unevenly positioned relative to the cavity with disparate K-N bond distances. Consistent with this asymmetry feature of the upper part of the structure, the related angles about K(2), N(21)-K(2)-N(201) = 100.6(1)° and N(41)-K(2)-N(202) = 95.3(2)° differ. In contrast, the other two nearly identical corresponding angles about K(1), N(101)-K(1)-O(11) = 99.4(1)° and N(102)-K(1)-O(31) = 99.3(1)° is a result of the even position of this TMEDA molecule from the bottom side of the macrocyclic cavity. The upper TMEDA molecule chelates the metal with a bite angle of 60.4(2)°, which is slightly larger than the corresponding bite angle relating to the TMEDA molecule bound to K(1) at 59.4(2)° and consistent with the short K(2)-N(201) bond distance noted above.

The angle formed between the two σ-bonds to the macrocycle and K(1), O(11)-K(1)-O(31) = 101.9(1)°, is smaller than that involving K(2), N(21)-K(2)-N(41) = 103.7(1)°, which is consistent with the longer K-O bond lengths compared with the K-N bond lengths. The angle formed between the two η^5-bound heterocycles and K(1), η^5(N21)-K(1)-η^5(N41) = 138.$_3$°, is slightly smaller than that involving K(2), η^5(O11)-K2-η^5(O31) = 140.$_7$°, which is again consistent with K(2) lying deeper in the macrocyclic cavity.

Comparison of the cavity shape of [(Et$_8$O$_2$N$_2$)K$_2$(TMEDA)$_2$], (10), and the protonated macrocycle (3) reveals that the oxygen centres of the two furanyl rings are drawn significantly closer through bonding with the potassium cations, with the cross-cavity distance of the two oxygen atoms being 0.24 Å shorter in the complex, with the tilt angles of the furanyl rings with respect to the plane of the macrocycle also being reduced in the complex in consequence. The cross-cavity pyrrolide

nitrogen contacts are also slightly closer than in **(3)**, but the pyrrolide rings lie steeper than those rings in **(3)**, as shown in Table 5.

Compound number	Furanyl ring		Pyrrolide ring	
	Cross-cavity $O \cdots O$ distance (Å)	Ring tilt angles (°)	Cross-cavity $N \cdots N$ distance(Å)	Ring tilt angles (°)
$[(Et_8O_2N_2)K_2(TMEDA)_2]$, **(10)**	4.61_7	67.5_6, 67.7_2	4.60_2	70.0_2, 68.1_9
$Et_8O_2N_2H_2$, **(3)**	4.85_7	79.4_9, 79.0_3	4.65_1	65.5_1, 67.1_1

Table 5: Cross-cavity $O \cdots O/N \cdots N$ distances and heterocycle ring tilt angles for $[(Et_8O_2N_2)K_2(TMEDA)_2]$, **(10)**, and $Et_8O_2N_2H_2$, **(3)**.

3.2.3.2 Molecular structure of $[(Et_8N_4Me_2)K_2(THF)_2]_n$, (14)

Colourless crystals of $[(Et_8N_4Me_2)K_2(THF)_2]_n$, **(14)**, suitable for X-ray crystal structure determination were grown in two hours after the addition of an equivalent volume of toluene to a saturated THF solution of **(14)**. The crystals were isolated and mounted in sealed thin-walled glass capillaries under an argon atmosphere. The crystals belong to space group P_{nma} (No. 62), $a = 23.941(3)$, $b = 17.131(2)$, $c = 10.832(1)$ Å, with four molecules in the unit cell, the asymmetric unit comprising one half of a monomeric unit residing on a mirror plane on (x, 1/4, z), as shown in Figure 22.

Complex **(14)** adopts a linear polymeric structure in the solid state. One potassium cation is bound within the macrocyclic cavity and the other potassium cation necessarily binds outside of the cavity in consequence of the inhibition of access to the opposite opening of the cavity by the N-methyl substituents. The macrocycle adopts the 1,3-alternate conformation. The *endo*-cavity-bound potassium exhibits $\eta^5:\eta^1:\eta^5:\eta^1$-binding, with η^5-interactions to both N-methyl pyrrole rings and σ-binding to both nitrogen centres of the pyrrolide rings. A disordered THF molecule also coordinates to the *endo*-cavity-bound potassium. The *exo*-cavity-bound potassium bridges two porphyrinogen units by η^5- and η^2- bonding modes (the latter to the β carbons). In addition, the *exo*-cavity-bound potassium is coordinated by a THF molecule and has close contacts with two methyl groups of the adjacent *meso*-ethyl substituents of the macrocycle to which it is η^5-bound.
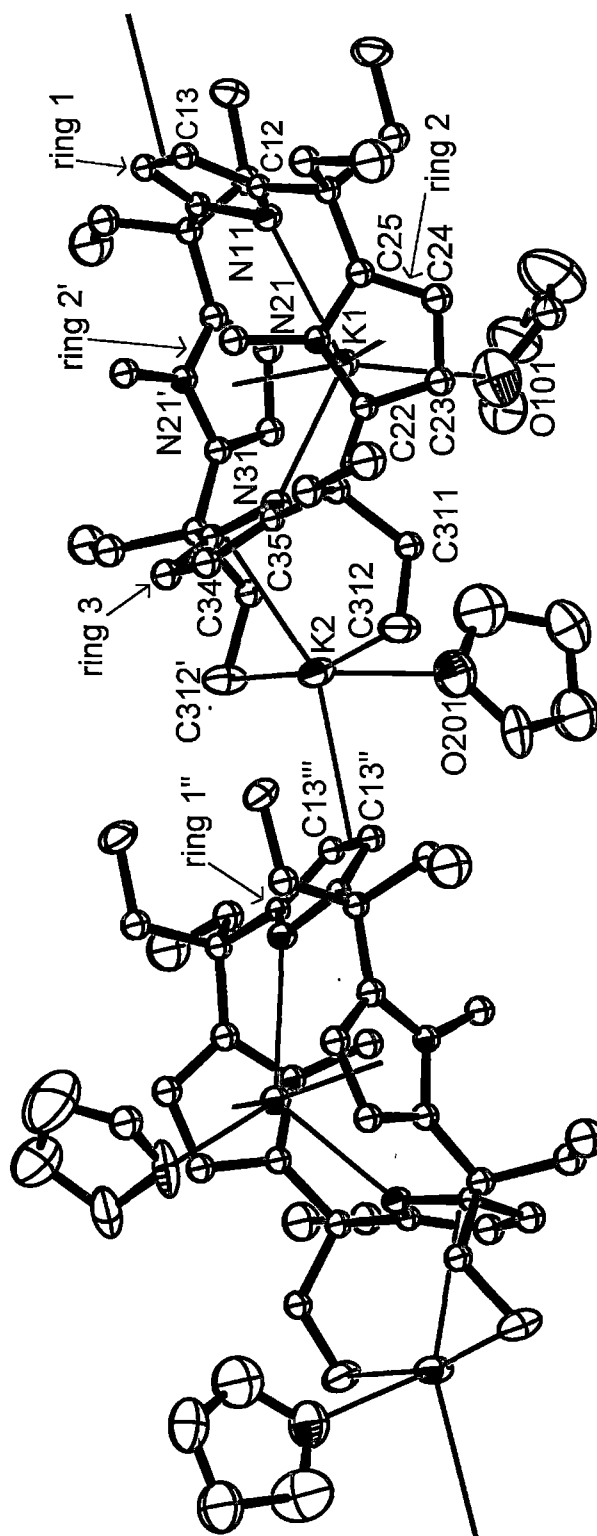
Figure 22: Molecular structure of $[(Et_8N_4Me_2)K_2(THF)_2]_n$, **(14)**, with thermal ellipsoids drawn at the level of 50% probability (protons and disorder in a THF molecule have been removed for clarity).

Complex **(14)** has both *endo*- and *exo*-cavity bound potassium cations like the tetrapotassium complexes of the parent tetraanionic porphyrinogen derived from **(4)**[11]. However, complex **(14)** of the divalent modified porphyrinogen has only one potassium cation in the macrocyclic cavity and only one potassium cation found outside the cavity rather than two potassium cations inside and two more outside the cavity as found in the parent tetraanionic porphyrinogen complexes.

Figure 23 displays spacefilling representations of part of the structure of $[(Et_8N_4Me_2)K_2(THF)_2]_n$, **(14)**, from different angles. These figures provide pertinent information about the shape of the macrocyclic cavity formed by the pyrrolide and *N*-methyl pyrrole rings and the coordination conditions of the *endo*-cavity-bound potassium cation. The representations clearly highlight the one sided, single opening nature of the cavity.

(a)   (b)
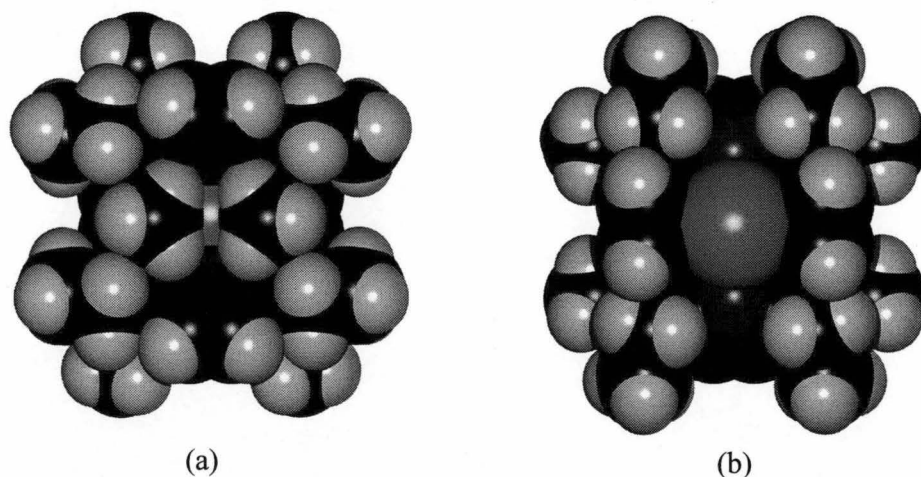
Figure 23: Space filling representations of the partial molecular structure of $[(Et_8N_4Me_2)K_2(THF)_2]_n$, **(14)**, (a) viewed from *N,N'*-dimethyl substituents blocked side of the cavity, (b) viewed from the potassium containing open side of the cavity (THF and the *exo*-bound potassium cation is removed for clarity).

The *endo*-cavity-bound potassium cation K(1) coordinates two pyrrolides with similar σ-bond distances of K(1)-N(11) = 2.820(2) and K(1)-N(31) = 2.815(2) Å, at an angle of N(11)-K(1)-N(31) = 119.98(5)°. K(1) also coordinates with both *N*-methyl pyrrole rings through η^5-bonding modes at a distance of 2.82_2 Å, with the metallocene bend angle formed being 150.2_1°.

The *exo*-cavity-bound potassium cation K(2) η^5-binds to a pyrrolide ring with the K-centroid distance of 2.77_8 Å. Short contact distances exist for K(2) and two

methyl groups of two *meso*-ethyl groups of K(2)-C(312) = 3.143(2), K(2)-C(311) = 3.371(2), K(2)-H(312c) = 2.70(2) and K(2)-H(312b) = 3.15(2) Å. K(2) is also η^2-bound to a pyrrolide ring in an adjoining macrocyclic unit at a distance of K(2)-η^2(C13) = 3.065(2) Å.

One THF molecule is bound to the *exo*-cavity bound potassium K(2) with a shorter distance, K(2)-O(201) = 2.678(2) Å, than which the THF binds to the *endo*-cavity bound potassium K(1), K(1)-O(101) = 2.757(3) Å. The orientation of the THF residing in the macrocyclic cavity is quite different from other porphyrinogen complexes, with the THF molecule lying in a direction that results in closer contact with the two η^5-bound *N*-methyl pyrrole units rather than the direction parallel to the two *N*-methyl pyrrole units. This unusual structural feature is apparently due to the effect of the *exo*-cavity-potassium-bound THF molecule which adopts a parallel orientation to the neighbouring ethyl groups. The *endo*-cavity-potassium-bound THF molecule is also propelled away from the other THF, however, the K-O bond of the *endo*-cavity-bound THF is inclined towards the *exo*-cavity bound THF. Thus the angle N(31)-K(1)-O(101), 115.87(8)°, is smaller than the opposite counterpart N(11)-K(1)-O(101), 123.57(8)°.

The nonbonding cross-cavity distances in complex (14) show that the coordination of the potassium cations has the effect of lengthening the distance between the nitrogen centres of the two *N*-methylpyrrole rings and slightly reducing their tilt angles. The two pyrrolide rings, however, are drawn slightly closer by potassium cation coordination with the ring involved in η^2-bonding to the *exo*-cavity-bound potassium being considerably at a steeper tilt angle to the macrocyclic plane.

Compound number	*N*-methylpyrrolide ring		Pyrrolide ring	
	Cross cavity N···N distance (Å)	Ring tilt angles (°)	Cross cavity N···N distance (Å)	Ring tilt angles (°)
[(Et$_8$N$_4$Me$_2$)K$_2$(THF)$_2$]$_n$, **(14)**	4.87_6	72.7_1, 72.7_1	4.76_8	56.1_0 66.5_5
Et$_8$N$_4$Me$_2$H$_2$ **(6)**	4.73_3	74.0_3, 73.5_9	4.83_1	53.5_1 57.3_1

Table 6: Cross-cavity N···N distances and heterocycle ring tilt angles for [(Et$_8$N$_4$Me$_2$)K$_2$(THF)$_2$]$_n$, **(14)**, and Me$_8$N$_4$Me$_2$H$_2$, **(6)**.

3.3 EXPERIMENTAL

Synthesis of [(Et$_8$O$_2$N$_2$)Li$_2$(TMEDA)$_2$], (9)

To a flask containing *meso*-octaethyl-*trans*-dioxaporphyrinogen, Et$_8$O$_2$N$_2$H$_2$
(3), (1.63 g, 3.00 mmol) in THF (40 mL), Bu^{n}Li (2.25 mL, 1.6 M solution in hexane,
3.6 mmol) was added while stirring. After stirring continuously overnight, the
solution was concentrated *in vacuo* to 10 mL. TMEDA (2.1 g, 2.7 mL, 18 mmol) was
added, followed by 40/60°C petroleum ether (40 mL). Storage for two weeks at -4 °C
yielded [(Et$_8$O$_2$N$_2$)Li$_2$(TMEDA)$_2$], (9), as a light brown crystalline product (1.42 g,
60%).

> ^{1}H NMR (pyridine-d^5, 399.694 MHz, 298 K, ppm): 0.88 (t, ^{3}J = 7.20 Hz,
> 24H, CH$_3$), 2.20-2.02 (m, 16H+12H, 8CH$_2$+4NCH$_3$), 2.29 (d, 8H, 4NCH$_2$),
> 5.84 (q, 4H, =CH, pyr), 6.38 (q, 4H, =CH, fur).
> ^{13}C NMR (pyridine-d^5, 100.512 MHz, 298 K, ppm): 10.1 (CH$_3$), 33.9 (CH$_2$),
> 46.0 (NCH$_3$), 47.3 (CEt$_2$), 58.2 (NCH$_2$), 101.9 (=CH, pyr), 105.1 (=CH, fur),
> 142.7 (=CR, pyr), 161.4 (=CR, fur).
> **IR** (υ (cm^{-1}), Nujol): 696 (w), 716 (s), 788 (s), 840 (m), 884 (w), 924 (m),
> 948   (s),   974   (s),
> 982 (w), 1030 (s), 1058 (m), 1100 (w), 1128 (m), 1158 (m), 1182 (m),
> 1194 (m), 1264 (m), 1248 (m), 1286 (s), 1318 (s), 1552 (m).
> **Anal.** Calcd.: C, 73.25; H, 10.25; N, 10.68 (C$_{48}$H$_{80}$Li$_2$N$_6$O$_2$, MW 787.06).
>   Found: C, 73.19; H, 10.11; N, 10.56.

Synthesis of [(Et$_8$O$_2$N$_2$)K$_2$(TMEDA)$_2$], (10)

Potassium metal (0.29 g, 7.20 mmol) was added to a solution of *meso*-
octaethyl-*trans*-dioxaporphyrinogen, Et$_8$O$_2$N$_2$H$_2$ (3), (1.63 g, 3.00 mmol) in THF (60
mL) and refluxed for 3 hrs. The solution was filtered from the excess potassium and
other undissolved species and concentrated to *ca.* 20 mL *in vacuo*. Addition of
TMEDA (2.10 g, 2.70 mL, 18.00 mmol), followed by 40-60°C petroleum ether (40
mL) and storage for one week at -4°C yielded [(Et$_8$O$_2$N$_2$)K$_2$(TMEDA)$_2$], (10), as
colourless crystals (2.25 g, 88%). Crystals suitable for X-ray crystal structure
determination were grown in two hours after adding an equivalent volume of toluene
to a saturated THF solution of (10).

¹H NMR (THF-d⁸, 399.694 MHz, 298 K, ppm): 0.64 (t, ^3J = 7.20 Hz, 12H, CH₃), 0.78 (t, ^3J = 7.20 Hz, 12H, CH₃), 1.90-2.10 (m, 16H, 8CH₂), 2.32 (s, 24H, NCH₃), 2.48 (s, 8H, NCH₂), 5.89 (d, 4H, =CH, pyr), 6.18 (s, 4H, =CH, fur).

¹³C NMR (THF-d⁸, 100.512 MHz, 298 K, ppm): 9.6, 8.7 (CH₃), 30.0, 28.2 (CH₂), 46.8 (NCH₃), 47.4 (CEt₂), 59.5 (NCH₂), 102.9 (=CH, pyr), 105.5 (=CH, fur), 145.0 (=CR, pyr), 164.5 (=CR, fur).

IR (υ (cm⁻¹), Nujol): 782 (s), 830 (m), 886 (m), 1028 (s), 922 (w), 964 (m), 1042 (s), 1062 (w), 1082 (w), 1100 (s), 1136 (m), 1152 (m), 1172 (w), 1196 (w), 1212 (w), 1266 (m), 1296 (m), 1324 (m), 1554 (m).

Anal. Calcd: C, 67.72; H, 9.47; N, 9.87 (C₄₈H₈₀K₂N₆O₂, MW 851.38).
    Found: C, 67.69; H, 9.51; N, 9.79.

Synthesis of [(Et₈N₄Me₂)Li₂(THF)], **(11)**

To a solution of *trans-N,N′*-dimethyl-*meso*-octaethylporphyrinogen, Et₈N₄Me₂H₂ **(6)**, (1.14 g, 2.00 mmol) in toluene (50 mL), Bu^{n}Li (3.0 mL, 1.6 M solution in hexane, 4.8 mmol) was added and the reaction stirred overnight. The clear colourless solution was decanted by cannula wire after all the solid had precipitated and settled. The remaining solid was washed with hexane (2 × 40 mL) and collected. The solid was recrystallised from a minimum amount of THF to obtain the pure product [(Et₈N₄Me₂)Li₂(THF)], **(11)**, (0.85 g, 65%).

¹H NMR (pyridine-d⁵, 399.694 MHz, 298 K, ppm): 0.71 (t, ^3J = 7.60 Hz, 12H, CH₃), 0.97 (t, ^3J = 7.60 Hz, 12H, CH₃), 1.48-1.53 (m, 4H, THF), 2.04 (m, 4H, 2CH₂), 2.16 (m, 4H, 2CH₂), 2.30 (m, 8H, 4CH₂), 3.52-3.57 (m, 4H, THF), 3.67 (s, 6H, NCH₃), 5.68 (s, 4H, =CH), 6.41 (s, 4H, =CH).

¹³C NMR (pyridine-d⁵, 100.512 MHz, 298 K, ppm): 9.7, 9.9 (CH₃), 25.8 (THF), 27.0, 32.3 (CH₂), 33.4 (NCH₃), 45.4 (CEt₂), 67.8 (THF), 101.9 (=CH), 106.5 (=CH), 139.7 (=CR), 145.6 (=CR).

IR (υ (cm⁻¹), Nujol): 680 (w), 710 (w), 726 (s), 748 (s), 792 (w), 810 (w), 844 (m), 884 (s), 926 (s), 946 (m), 980 (w), 1032 (s), 1094 (m), 1186 (w), 1126 (w), 1168 (w), 1220 (m), 1254 (m), 1274 (s), 1288 (s), 1322 (s), 1488 (m).

Anal. Calcd.: C, 77.27; H, 9.57; N, 8.58 (C₄₂H₆₂Li₂N₄O, MW 652.85).
    Found: C, 77.31; H, 9.61; N, 8.49.

Synthesis of [(Et₈N₄Me₂)Li₂(TMEDA)₂], **(12)**

To a solution of [(Et$_8$N$_4$Me$_2$)Li$_2$(THF)], **(11)**, (0.65 g, 1.00 mmol) in the minimum amount of THF required to dissolve all the complex, six equivalents TMEDA (0.70 g, 0.90 mL, 6.00 mmol) was added. Recrystallisation from THF gave [(Et$_8$N$_4$Me$_2$)Li$_2$(TMEDA)$_2$], **(12)** (0.65 g, 80%).

^{1}H NMR (pyridine-d^5, 399.694 MHz, 298 K, ppm): 0.71 (t, ^{3}J = 7.20 Hz, 12H, CH$_3$), 0.99 (t, ^{3}J = 7.20 Hz, 12H, CH$_3$), 2.05 (s, 24H, NCH$_3$), 2.06 (m, 4H, 2CH$_2$), 2.18 (m, 4H, 2CH$_2$), 2.27 (s, 8H, NCH$_2$), 2.32 (m, 8H, 4CH$_2$), 3.68 (s, 6H, NCH$_3$), 5.68 (s, 4H, =CH), 6.41 (s, 4H, (=CH).

^{13}C NMR (pyridine-d^5, 100.512 MHz, 298 K, ppm): 9.7 (CH$_3$), 9.9 (CH$_3$), 27.0, 32.3 (CH$_2$), 33.4 (NCH$_3$), 45.4 (CEt$_2$), 45.9 (NCH$_3$), 58.2 (NCH$_2$), 101.9 (=CH), 106.5 (=CH), 139.8 (=CR), 145.6 (=CR).

Synthesis of [(Et$_8$N$_4$Me$_2$)Na$_2$(THF)$_2$], **(13)**

To a solution of *trans-N,N'*-dimethyl-*meso*-octaethylporphyrinogen, Et$_8$N$_4$Me$_2$H$_2$ **(6)**, (0.01 g, 0.02 mmol) in THF-d^8 (0.60 mL) was added NaH (0.05 g, 0.20 mmol), and the mixture heated at 45°C overnight with sonication.

^{1}H NMR (THF-d^8, 399.694 MHz, 298 K, ppm): 0.47 (m, 24H, CH$_3$), 1.65 (m, 8H, CH$_2$), 1.73 (m, 8H, THF), 1.88 (m, 8H, CH$_2$), 2.95 (s, 6H, NCH$_3$), 3.57 (m, 8H, THF), 5.55 (s, 4H, =CH, pyr or pyrMe), 5.76 (s, 4H, =CH, pyr or pyrMe).

Synthesis of [(Et$_8$N$_4$Me$_2$)K$_2$(THF)$_2$]$_n$, **(14)**

Potassium metal (0.24 g, 6.0 mmol) was added to a solution of *trans-N,N'*-dimethyl-*meso*-octaethylporphyrinogen, Et$_8$N$_4$Me$_2$H$_2$ **(6)**, (1.70 g, 3.0 mmol) in THF (100 mL) and refluxed for 6 hrs. THF was removed *in vacuo* and the solid washed with toluene (2 × 40 mL). Drying *in vacuo* gave the product (2.25 g, 95%). Crystals suitable for X-ray analysis were obtained by the addition of an equal volume of toluene to a saturated THF solution.

^{1}H NMR (THF-d^8, 399.694 MHz, 298 K, ppm): 0.69 (t, ^{3}J = 7.20 Hz, 24H, CH$_3$), 1.91-2.15 (m, 16H, CH$_2$ and THF), 3.05 (s, 6H, CH$_3$), 3.76-3.82 (m, 8H, THF), 5.75 (s, 4H, =CH, pyr), 5.89 (s, 4H, =CH, pyrMe).

^{13}C NMR (THF-d^8, 100.512 MHz, 298 K, ppm): 9.8, 9.6 (CH$_3$), 26.0 (THF), 27.0, 31.8 (CH$_2$), 33.5 (NCH$_3$), 46.4 (CEt$_2$), 68.9 (THF), 101.1 (=CH, pyr), 104.6 (=CH, pyrMe), 142.5 (=CR, pyrMe), 144.5 (=CR, pyr).

IR (υ (cm^{-1}), Nujol): 720 (m), 730 (m), 752 (m), 884 (m), 946 (w), 972 (w), 1024 (m), 1048 (m), 1218 (m), 1272 (m), 1298 (m), 1326 (m).

Anal. Calcd.: C, 70.00; H, 8.94; N, 7.10 (C$_{46}$H$_{70}$K$_2$N$_4$O$_2$, MW 789.28).

Found: C, 67.64; H, 8.99; N, 6.85.

3.4 REFERENCES

[1]   **a.** J.C. Ma, D.A. Dougherty, *Chem. Rev.*, 1997, **97**, 1303.
        b. D.A. Dougherty, *Science,* 1996, **271**, 163.
        c. J. Sunner, K. Nishizawa, P. Kebarle, *J. Phys. Chem.*, 1981, **85**, 1814.
        d. S.K. Burley, G.A. Petsko, *FEBS Lett.*, 1986, **203**, 139.

[2]   N. Kuhn, G. Henkel, J. Kreutzberg, *Angew. Chem., Int. Ed. Engl.*, 1990, **29**, 1143.

[3]   M. Westerhausen, M. Wieneke, H. Nöth, T. Seifert, A. Pfitzner, W. Schwarz, O. Schwarz, J. Weidlein, *Eur. J. Inorg. Chem.*, 1998, 1175.

[4]   H. Nöth, J. Knizek, W. Ponikwar, *Eur. J. Inorg. Chem.*, 1999, 1931.

[5]   G. Kehr, R. Rosemann, R. Frohlich, C. Holst, G. Erker, *Eur. J. Inorg. Chem.*, 2001, 535.

[6]   H.-D. Hausen, J. Todtmann, J. Weidlein, *J. Organomet. Chem.*, 1994, **466**, C1.

[7]   S. De Angelis, E. Solari, C. Floriani, A. Chiesi-Villa, C. Rizzoli, *J. Chem. Soc., Dalton Trans.*, 1994, 2467.

[8]   J. Guan, T. Dubé, S. Gambarotta, G.P.A. Yap, *Organometallics*, 2000, **19**, 4820.

[9]   J. Jubb, P. Berno, S. Hao, S. Gambarotta, *Inorg. Chem.*, 1995, **34**, 3563.

[10]   J. Jubb, S. Gambarotta, R. Duchateau, J.H. Teuben, *J. Chem. Soc., Chem. Commun.*, 1994, 2641.

[11]   L. Bonomo, E. Solari, R. Scopelliti, C. Floriani, *Chem.-Eur. J.*, 2001, **7**, 1322.

[12]   R. Crescenzi, E. Solari, C. Floriani, A. Chiesi-Villa, C. Rizzoli, *Inorg. Chem.*, 1996, **35**, 2413.

[13] a. R.F. Ziolo, W.H.H. Gunther, J.M. Troup, *J. Am. Chem. Soc.*, 1981, **103**, 4629.

b. A. Gebauer, D.Y. Dawson, J. Arnold, *J. Chem. Soc., Dalton Trans.*, 2000, 111.

c. H. Huckstadt, C. Jaouen, M. Goldner, U. Cornelissen, A. Tutass, H. Homborg, *Z. Anorg. Allg. Chem.*, 2000, **626**, 671.

d. J. Arnold, D.Y. Dawson, C.G. Hoffman, *J. Am. Chem. Soc.*, 1993, **115**, 2707.

e. B. Latte, B. Assmann, H. Homborg, *Z. Anorg. Allg. Chem.*, 1997, **623**, 1281.

[14] a. R. Crescenzi, E. Solari, C. Floriani, N. Re, A. Chiesi-Villa, C. Rizzoli, *Organometallics*, 1999, **18**, 606.

b. R. Crescenzi, E. Solari, C. Floriani, A. Chiesi-Villa, C. Rizzoli, *Inorg. Chem.*, 1998, **37**, 6044.

c. L. Bonomo, E. Solari, R. Scopelliti, C. Floriani, N. Re, *J. Am. Chem. Soc.*, 2000, **122**, 5312.

d. L. Bonomo, E. Solari, R. Scopelliti, M. Latronico, C. Floriani, *Chem. Commun.*, 1999, 2229.

e. R. Crescenzi, E. Solari, C. Floriani, A. Chiesi-Villa, C. Rizzoli, *J. Am. Chem. Soc.*, 1999, **121**, 1695.

f. J.-M. Benech, L. Bonomo, E. Solari, R. Scopelliti, C. Floriani, *Angew. Chem. Int. Ed.*, 1999, **38**, 1957.

g. U. Piarulli, E. Solari, C. Floriani, A. Chiesi-Villa, C. Rizzoli, *J. Am. Chem. Soc.*, 1996, **118**, 3634.

[15] L. Bonomo, O. Dandin, E. Solari, C. Floriani, R. Scopelliti, *Angew. Chem., Int. Ed.*, 1999, **38**, 914.

[16] J. Jubb, C. Floriani, A. Chiesi-Villa, C. Rizzoli, *J. Am. Chem. Soc.*, 1992, **114**, 6571.

[17] a. J. Jubb, S. Gambarotta, *J. Am. Chem. Soc.*, 1993, **115**, 10410.

b. J. Jubb, S. Gambarotta, *Inorg. Chem.*, 1994, **33**, 2503.

c. E. Solari, F. Musso, C. Floriani, A. Chiesi-Villa, C. Rizzoli, *J. Chem. Soc., Dalton Trans.*, 1994, 2015.

d. L. Bonomo, E. Solari, M. Latronico, R. Scopelliti, C. Floriani, *Chem.-Eur. J.*, 1999, **5**, 2040.

e. L. Bonomo, C. Stern, E. Solari, R. Scopelliti, C. Floriani, *Angew. Chem. Int. Ed.*, 2001, **40**, 1449.

f. C. Floriani, E. Solari, G. Solari, A. Chiesi-Villa, C. Rizzoli, *Angew. Chem. Int. Ed.*, 1998, **37**, 2245.

g. D. Jacoby, C. Floriani, A. Chiesi-Villa, C. Rizzoli, *J. Am. Chem. Soc.*, 1993, **115**, 7025.

h. G. Solari, E. Solari, C. Floriani, A. Chiesi-Villa, C. Rizzoli, *Organometallics*, 1997, **16**, 508.

i. D. Jacoby, C. Floriani, A. Chiesi-Villa, C. Rizzoli, *J. Am. Chem. Soc.*, 1993, **115**, 3595.

j. J. Jubb, L. Scoles, H. Jenkins, S. Gambarotta, *Chem.-Eur. J.*, 1996, **2**, 767.

k. L. Bonomo, E. Solari, R. Scopelliti, C. Floriani, *Angew. Chem. Int. Ed.*, 2001, **40**, 2529.

l. D. Jacoby, S. Isoz, C. Floriani, A. Chiesi-Villa, C. Rizzoli, *J. Am. Chem. Soc.*, 1995, **117**, 2793.

m D. Jacoby, S. Isoz, C. Floriani, A. Chiesi-Villa, C. Rizzoli, *J. Am. Chem. Soc.*, 1995, **117**, 2805.

n. D. Jacoby, S. Isoz, C. Floriani, K. Schenk, A. Chiesi-Villa, C. Rizzoli, *Organometallics*, 1995, **14**, 4816.

n. M. Dionne, J. Jubb, H. Jenkins, S. Wong, S. Gambarotta, *Inorg. Chem.*, 1996, **35**, 1874.

[18] a. E. Campazzi, E. Solari, R. Scopelliti, C. Floriani, *Chem. Commun.*, 1999, 1617.

b. E. Campazzi, E. Solari, R. Scopelliti, C. Floriani, *Inorg. Chem.*, 1999, **38**, 6240.

c. T. Dubé, J. Guan, S. Gambarotta, G.P.A. Yap, *Chem.-Eur. J.*, 2001, **7**, 374.

d. E. Campazzi, E. Solari, C. Floriani, R. Scopelliti, *Chem. Commun.*, 1998, 2603.

e. J. Jubb, S. Gambarotta, *J. Am. Chem. Soc.*, 1994, **116**, 4477.

f. T. Dubé, S. Gambarotta, G.P.A. Yap, *Organometallics*, 2000, **19**, 817.

g. T. Dubé, S. Gambarotta, G.P.A. Yap, *Organometallics*, 2000, **19**, 121.

h. I. Korobkov, S. Gambarotta, G.P.A. Yap, *Organometallics*, 2001, **20**, 2552.

[19] H. Schumann, J. Winterfeld, H. Hemling, N. Kuhn, *Chem. Ber.*, 1993, **126**, 2657.

[20]   **a**. T. Dubé, D. Freckmann, S. Conoci, S. Gambarotta, G.P.A. Yap, *Organometallics*, 2000, **19**, 209.

b. T. Dubé, S. Conoci, S. Gambarotta, G.P.A. Yap, G. Vasapollo, *Angew. Chem. Int. Ed.*, 1999, **38**, 3657.

c. M. Ganesan, C.D. Berube, S. Gambarotta, G.P.A. Yap, *Organometallics*, 2002, **21**, 1707.

d. D.M.M. Freckmann, T. Dubé, C.D. Berube, S. Gambarotta, G.P.A. Yap, *Organometallics*, 2002, **21**, 1240.

e. M. Ganesan, M.P. Lalonde, S. Gambarotta, G.P.A. Yap, *Organometallics*, 2001, **20**, 2443.

[21]   M. Tayebani, S. Conoci, K. Feghali, S. Gambarotta, G.P.A. Yap, *Organometallics*, 2000, **19**, 4568.

[22]   C.S. Alexander, S.J. Rettig, B.R. James, *Organometallics*, 1994, **13**, 2542.

CHAPTER 4

SAMARIUM(II) COMPLEXES
OF MODIFIED PORPHYRINOGENS

4.1 INTRODUCTION

Schumann *et al.* reported in 1993 the synthesis of divalent lanthanide complexes of the pyrrolide ligand derived from deprotonation of 2,5-di-*tert*-butylpyrrole[1]. The composition of the complexes were determined by ^{1}H and ^{13}C NMR spectroscopy and microanalysis, but without X-ray structural results.

$$LnI_2(THF)_x + 2\ Na[NC_4H_2(Bu^t_2\text{-}2,5)] \xrightarrow[\text{-2 NaI}]{THF} [\{NC_4H_2(Bu^t_2\text{-}2,5)\}_2Ln(THF)]$$

$$\textbf{(I)} \quad \begin{array}{l} (Ln = Sm, x = 2; \\ Ln = Yb, x = 2, 3) \end{array}$$
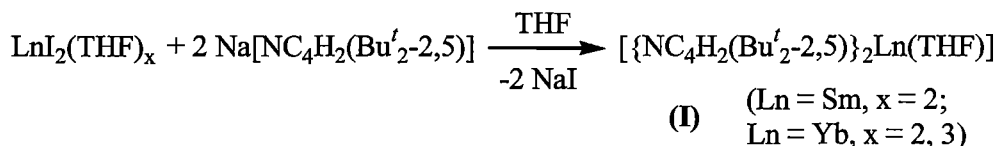
Recently, Gambarotta *et al.* reported the coordination of divalent samarium and ytterbium with the less bulky 2,5-dimethyl pyrrolide ligand[2]. Treatment of $SmCl_3(THF)_3$ and $YbCl_3(THF)_3$ with two equivalents of an alkali metal salt of 2,5-dimethylpyrrole followed by reduction in THF using the same alkali metal or the reaction of $SmI_2(THF)_2$ and $YbI_2(THF)_2$ with the alkali metal pyrrolide salts led to the formation of mono- and polynuclear complexes. The divalent lanthanide complexes **(II)**, **(III)** and **(IV)** were synthesised according to Scheme 1.

(i) Bu^{n}Li,
(ii) SmCl$_3$/THF,
(iii) Li   **(II)**

(i) NaH,
(ii) SmCl$_3$/THF,
(iii) Na   **(III)**

(i) KH/THF,
(ii) YbI$_2$ **(IV)**
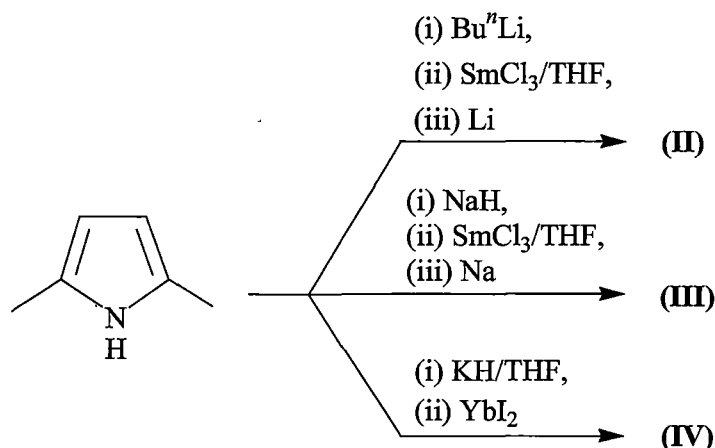
Scheme 1

Structural analyses of complexes (II) – (IV) indicate that the bonding modes adopted by the pyrrolide ligands are dependent on the nature of the alkali metal cations retained in the structures. In the lithium retained complex (II), the pyrrolide fragments exclusively form η^5-contacts to samarium centres, while the pyrrolide nitrogens are η^1-bound to the lithium centres. The utilisation of sodium containing bases instead of lithium, such as in complex (III), results in the samarium centre being both π- and σ- bound to the pyrrolide units while sodium adopts the reverse π- and σ- bonding modes to the pyrrolide units. The presence of potassium, as in (IV), results in the lanthanide metal exclusively forming σ-interactions with the pyrrolide units, in turn, potassium adopts π-bonding modes with the pyrrolide units. The polymeric structure is further built up via μ_2-THF bridges to the potassium centres (not shown in the figure).
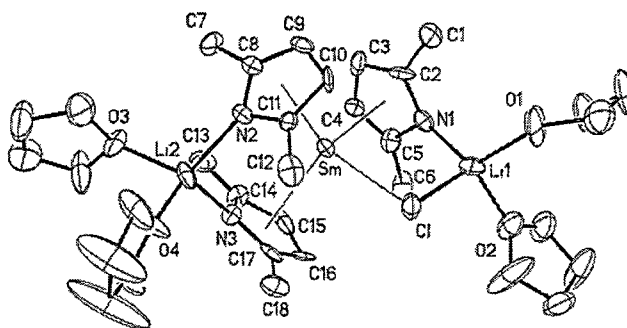
$[(\mu\text{-}\eta^1:\eta^5\text{-}Me_2C_4H_2N)_3Sm(\mu\text{-}Cl)\{Li(THF)_2\}_2]$, (II)[2]
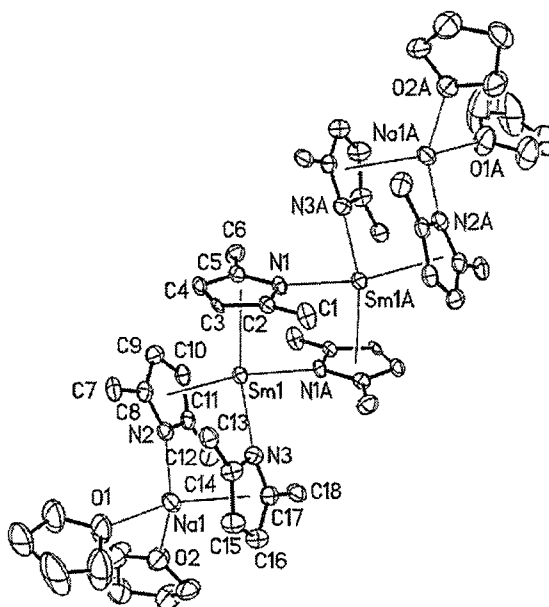
$[\{(THF)_2Na(\mu\text{-}\eta^1:\eta^5\text{-}Me_2C_4H_2N)_2Sm\}_2(\mu\text{-}\eta^1:\eta^5\text{-}Me_2C_4H_2N)_2]$, (III)[2]

$$[\{(\mu\text{-THF})K\}_2\{(\mu\text{-}\eta^1\text{:}\eta^5\text{-}Me_2C_4H_2N)_4Yb\}]_n, \mathbf{(IV)}^{[2]}$$
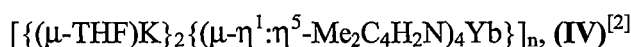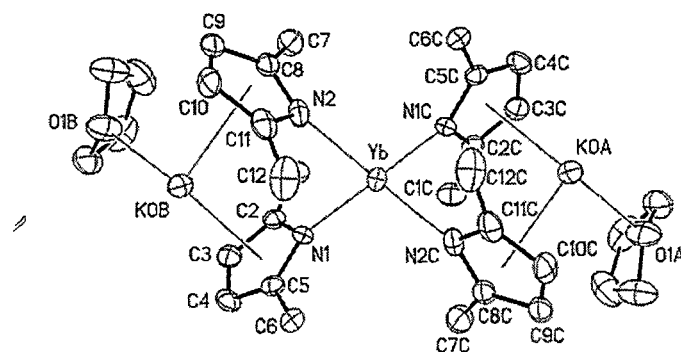
The dimeric imine coordinated samarium(II) dipyrrolide complex **(V)** has been reported recently[3]. The reaction of $[Sm\{N(SiMe_3)_2\}_2(THF)_2]$ with 1,2-ethanediamine-N,N'-bis(pyrrol-2-yl)ethylidene was carried out in THF at room temperature over several days, affording yellow crystals of **(V)**.

$$\mathbf{(V)}^{[3]}$$
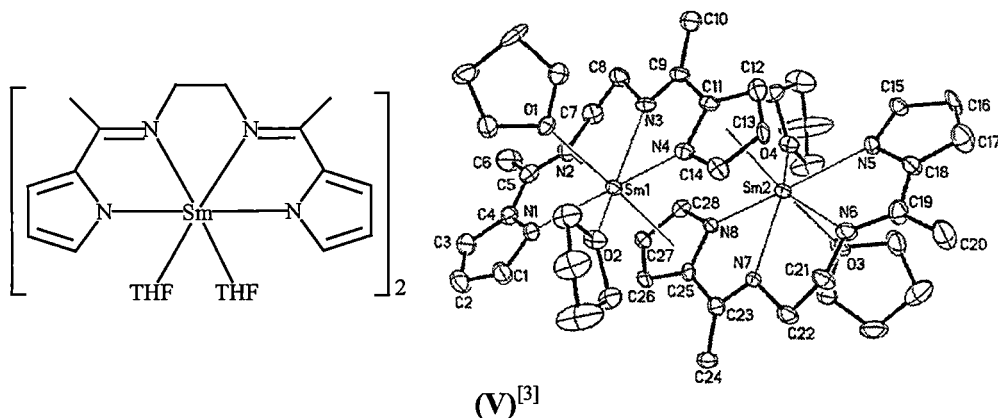
Complex **(V)** is dimeric, formed through two η^5-pyrrolide samarium interactions. Each monomeric unit is composed of a Sm(II) centre σ-bound to a tetradentate ligand, which defines the equatorial plane of the pentagonal bipyramidally coordinated samarium, with one molecule of THF occupying the fifth position of the equatorial plane. The two axial positions are occupied by a second THF and a η^5-bound pyrrolide ligand.

In 2000, Gambarotta *et al.* introduced doubly deprotonated di(2'-pyrrolyl)methane ligands into organolanthanide chemistry, which has revealed many interesting structural features and remarkable reactivity stemming from the geometrically restrained dianionic ligand system[4].

Reaction of [{(SiMe$_3$)$_2$N}$_2$Sm(THF)$_2$] with one equivalent of 1,1-di-(2'-pyrrolyl)diphenylmethane or 1,1-di-(2'-pyrrolyl)cyclohexane in THF under an argon atmosphere afforded (VI) as a hexameric cluster in moderate yield and (VII) as an octameric cluster in very good yield, as shown in Scheme 2. The 'empty' divalent samarium clusters, are highly active, being devoid of halogen and alkali metal cations, representing rare examples of lanthanide cyclic clusters. Upon exposure to N$_2$, solutions of (VI) and (VII) rapidly formed the tetranuclear dinitrogen complexes (VIII) in good yield. The analogous preparation of (VI) and (VII), conducted under nitrogen rather than argon, formed the nitrogen complexes (VIII) directly.

In the molecular structures of complexes (VI) and (VII), groups of three and four samarium(II) centres respectively adopt flat planes divided into two alternate sets with and without coordinating THF molecules. Each samarium centre without coordinated THF is bridged to the next samarium(II) centre (with coordinated THF) by one dipyrrolide unit, the pyrrolide rings are in turn π-bound to one samarium centre and σ-bound to the next samarium centre. As a result, the coordination geometry around each samarium atom is strongly reminiscent of that of a bent samarocene with one pyrrolide ring from each ligand being σ-bound and the other η^5-coordinated. The samarium centres bearing coordinated THF molecules display a trigonal bipyramidal geometry, with centroids of two π-bound pyrrolide rings and the oxygen atoms of the coordinated THF defining the equatorial plane, while the nitrogen atoms of the two σ-bound pyrrolide rings are in the axial positions.

Molecules of (VIII) are tetranuclear, with four samarium(III) centres arranged to form a rhombohedron. Samarium centres bind with the dipyrrolide ligand with the same bonding modes seen in (VI) and (VII). Each of the two chemically inequivalent samarium centres bind dinitrogen in a different manner, the samarium centres bearing no THF display side-on η^2-interactions, whereas end-on η^1-interactions are seen for the THF coordinated samarium centres.

Treatment of SmCl$_3$(THF)$_3$ with sodium salts of 1,1-di-(2'-pyrrolyl)diphenylmethane in the presence of N$_2$, followed by reduction with sodium, led to the formation of an ionic tetranuclear divalent samarium hydride cluster (IX) as dark purple crystals, as shown in Scheme 3. Similar reaction between dilithium or disodium salts of 1,1-di-(2'-pyrrolyl)diphenylmethane with an equivalent of SmCl$_3$(THF)$_3$ in THF under argon, followed by reduction with metallic lithium or

$$[\{(Me_3Si)_2N\}_2Sm(THF)_2]$$

(VI)

(VII)

(VIII) (R = Ph, -(CH$_2$)$_5$-)

Scheme 2

(IX)

(X) (M = Li, n = 2;
M = Na, n = 1)

(XI) (2R = -(CH$_2$)$_5$-)
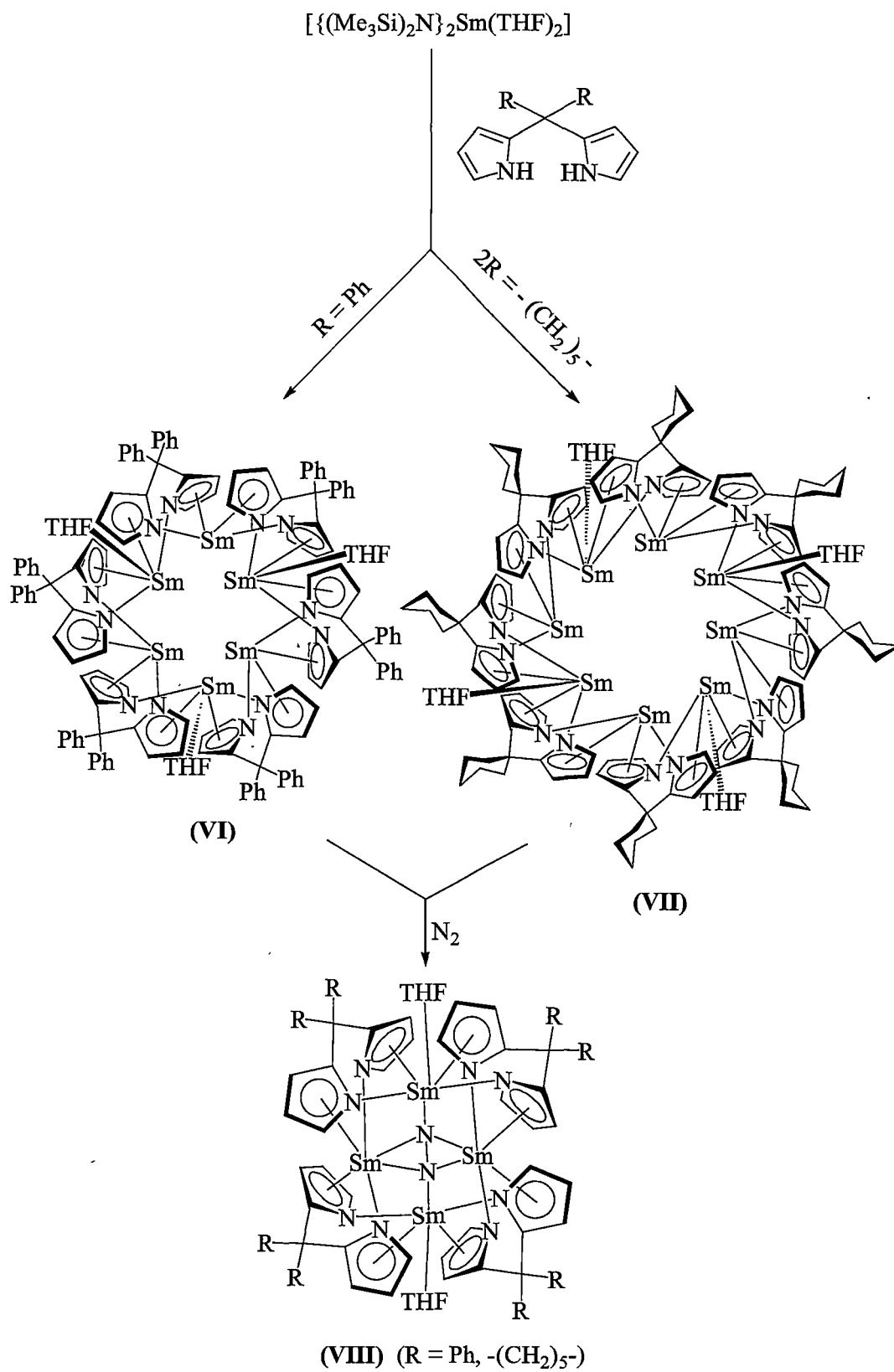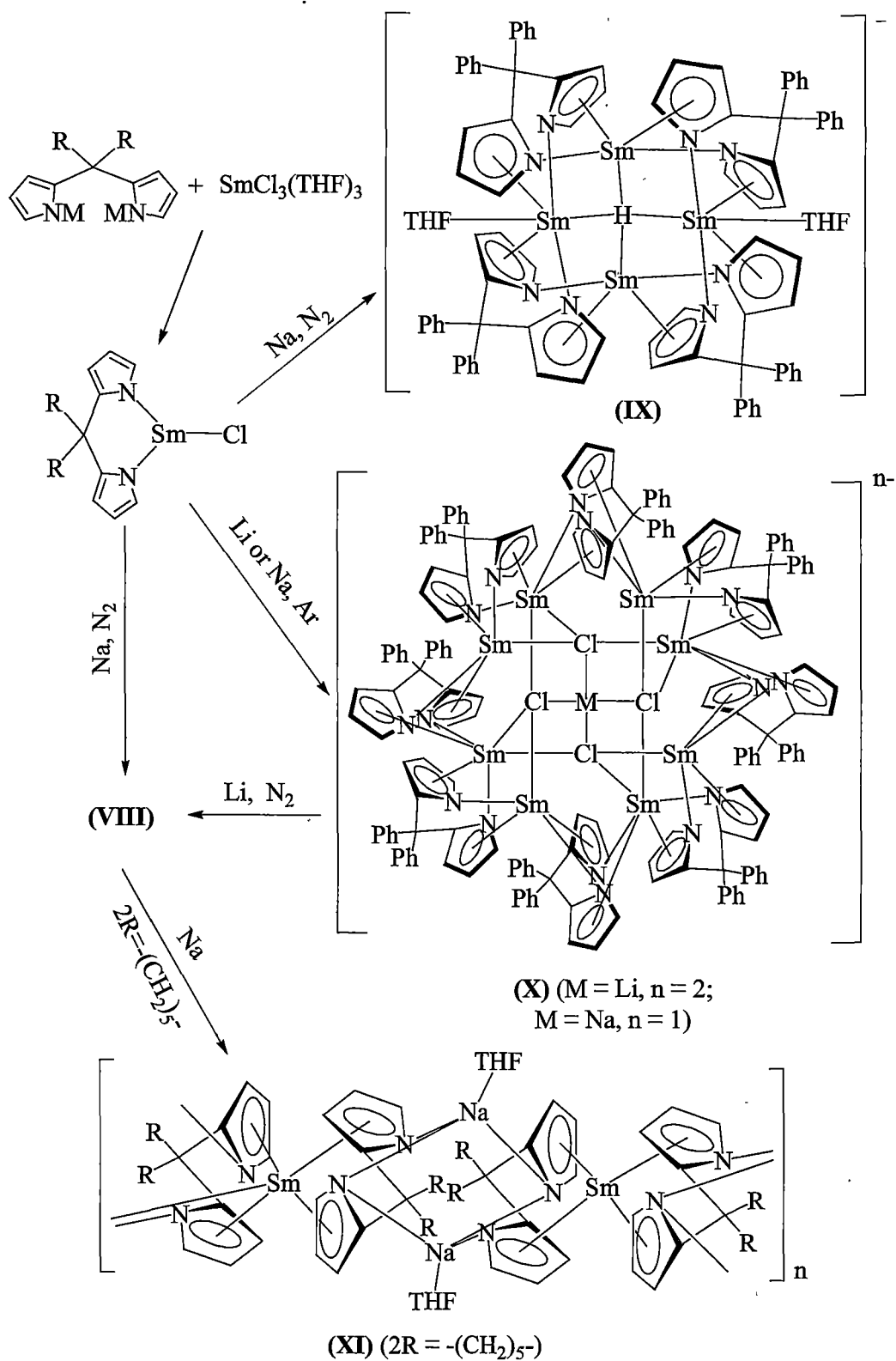
Scheme 3

sodium produced **(X)** (M = Li, n = 2; M = Na, n = 1). The lithium and sodium complexes of **(X)** are mixed valent species. The lithium complex formally contains seven divalent samarium centres and one trivalent samarium centre while the sodium complex is composed of six divalent samarium centres and two trivalent samarium centres. The mixed valent samarium complexes **(X)** show no reactivity towards N_2, as expected owing to their 'filled' chluster-type structure. The lithium complex can be further reduced to release samarium(II) units which form **(VIII)** when exposed to N_2.

The reaction of sodium salts of 1,1-di-(2'-pyrrolyl)cyclohexane with $SmCl_3$, followed by reduction with sodium under nitrogen led to the dinitrogen complex **(VIII)**. Extensive reduction of **(VIII)** leads to the linear polymeric divalent samarium(II) complex **(XI)** containing sodium cations.

Molecules of **(IX)**, adopt a tetranuclear form with a rhombohedral type structure similar to **(VIII)**. Samarium centres bind with the dipyrrolide with the usual bonding modes seen in other compounds such as **(VI)**, **(VII)** and **(VIII)**.

The X-ray crystal structures of complexes **(X)** reveal octameric molecules consisting of eight [{Ph_2C(C_4H_3N)_2}Sm] units with the samarium centres arranged in an overall bowl conformation. The bonding modes between the samarium centres and the dipyrrolide are again usual, as seen in the structures of **(VI)**, **(VII)** and **(VIII)**. A samarocene-type environment is established with each samarium centre coordinated by two π-bound and two σ-bound pyrrole rings from two adjacent dipyrrolides. Four chloride centres are arranged within the cavity formed by the eight samarium centres such that each chloride bridges three adjacent samarium centres. The four chlorides are, in turn, bridged by a single lithium or sodium cation which is located in the centre of the cluster and is nearly coplanar with the four chlorine atoms.

The composition of **(XI)** resembles that of the Yb(II) complex [{(THF)K}_2{(μ-η^1:η^5-Me_2C_4H_2N)_4Yb}]_n, **(IV)**, except for some variations in the bonding modes of the pyrrolides and THF molecules. These differences are most likely in response to the steric and constrained geometry differences between the pyrrolides and the lowered tendency for sodium to form π-interactions compared with potassium. In the linear polymeric complex **(XI)**, samarium centres are surrounded by four π-coordinated pyrrolide rings from two dipyrrolides. The coordination geometry around each samarium centre is therefore pseudo-tetrahedral,

with the centroids of the four pyrrolide rings defining the vertices of the coordination tetrahedron. The two nitrogen centres of a dipyrrolide are σ-bound to two THF coordinated sodium centres, which are in turn, σ-bonded to two other nitrogen centres of another dipyrrolide, thus building a polymeric structure where the samarium centres form a nearly linear array.

Pentanuclear samarium(II) complexes (**XII**) having different structural features were prepared from an alternative synthetic route. The reaction between SmI$_2$ and potassium salts of the dipyrrolide dianions derived from 1,1-di-(2'-pyrrolyl)diphenylmethane and 1,1-di-(2'-pyrrolyl)phenylethane led to the two analogous samarium(II) complexes (**XII**) (R = R^1 = Ph; R = Ph, R^1 = Me). The complexes feature the five samarium centres pentagonally arranged around a central iodide centre. However, when chloride is retained in the molecule instead of iodide, a tetranuclear species (**XIII**) was obtained which has a similar structure to the hydride complex (**IX**).

(**XII**)   (**XIII**)
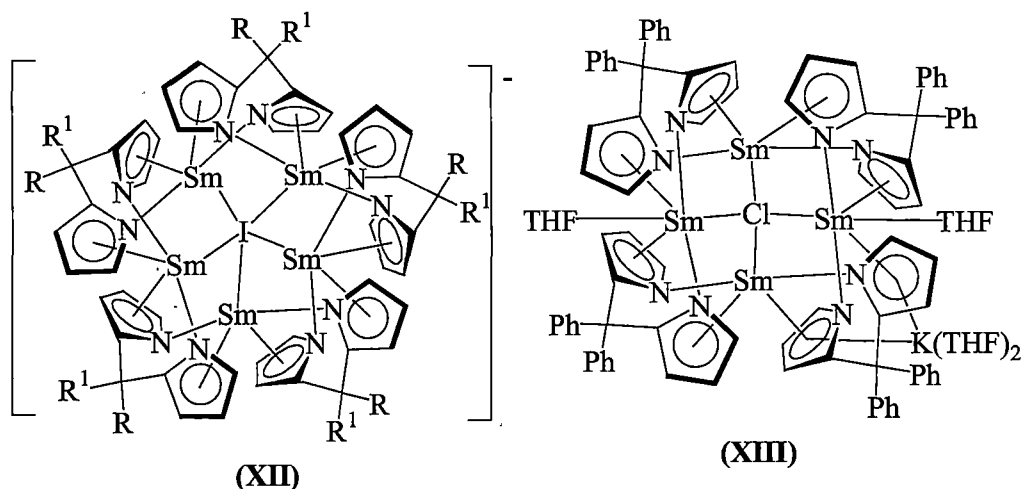
Several samarium(II) complexes of porphyrinogens have been synthesised as THF and diethyl ether adducts[5]. The dimetallic complexes (**XIV**) are alkali metal and halide free species. The complexes have been synthesised by various approaches which include, (i) reaction between Sm{N(SiMe$_3$)$_2$}$_2$ with half an equivalent of Et$_8$N$_4$H$_4$, (**4**), (ii) reduction of trivalent samarium(III) complexes using lithium or lithium aluminium hydride and, (iii) metathetical exchange of samarium diiodide with half an equivalent of the tetralithium salt of the porphyrinogen.
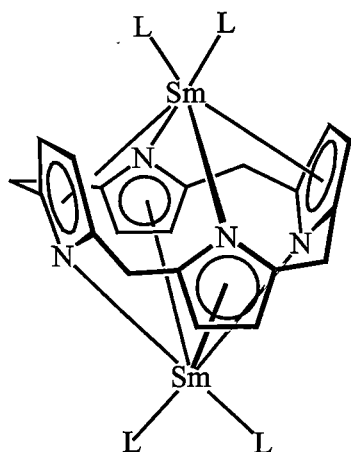
(XIV) (L = THF,
2L = diethyl ether)
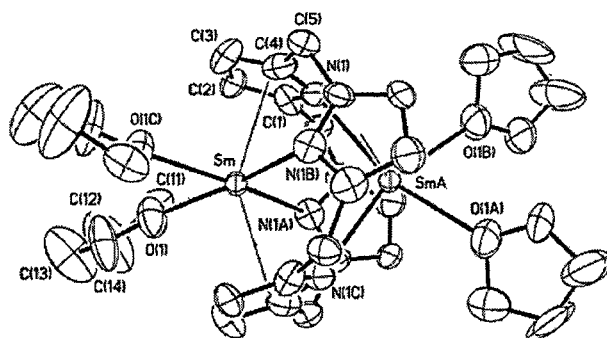
(XIV)[5] (L = THF)

The complexes (XIV) feature the samarium(II) centres residing on either side of the macrocyclic cavity of the porphyrinogen adopting an almost symmetric arrangement. The porphyrinogen tetraanions adopt 1,3-alternate conformations. The molecules feature bent samarocene like structures with the macrocyclic unit binding the two samarium centres with η^5:η^1:η^5:η^1-interactions. Thus each pyrrole ring σ-binds one samarium centre, η^5-binds the other samarium centre, and *vice versa* for adjacent pyrrolide rings. The Sm-Sm distances are short in the two complexes, suggesting possible Sm-Sm interactions. However, other geometry parameters suggest repulsive effects between the metal centres (see Section 4.2.3.1)

In comparison to the reactivity of related lanthanide(II) porphyrinogen complexes retaining alkali metal cations, both complexes (XIV) show no reactivity towards nitrogen. This result suggests that alkali metal cations may play some role in N_2 reduction chemistry, even though examples are known in which the alkali metal cations are not bound to the reduced dinitrogen in the complex[6].

The samarium(II) complex (XV), which retains chloride and lithium ions can be conveniently prepared *via* reduction of the samarium(III) chloride precursor with lithium under argon, as shown in Scheme 4. Compound (IV) has also been prepared from the decomposition of alkenyl samarium(III) complexes[5b, 7].

$Et_8N_4Li_4$ $\xrightarrow{\text{i) SmCl}_3\text{(THF)}_3\text{ ii) Li}}$ (XV)

(XV) (L = THF)
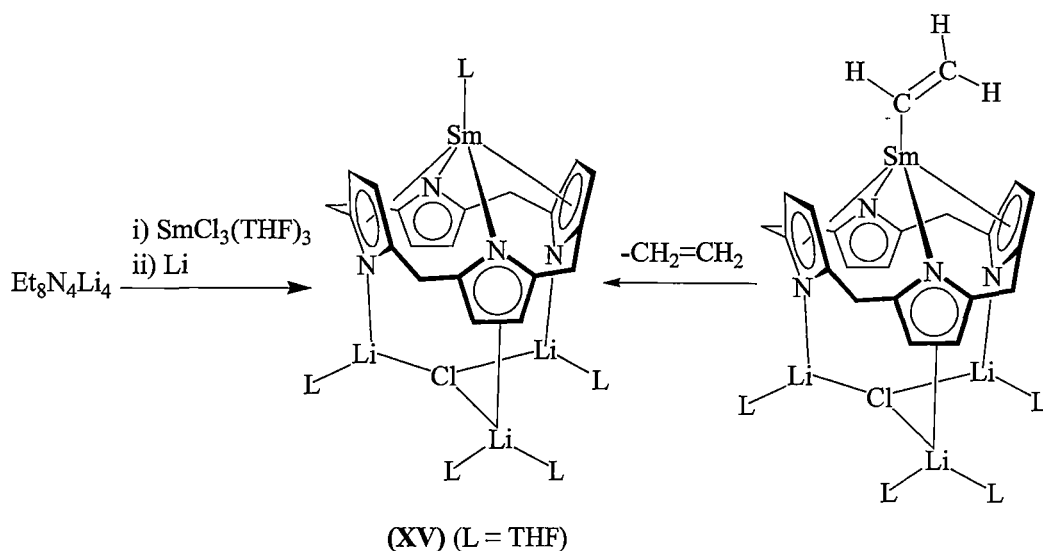
Scheme 4

While the samarium(II) complex **(XV)** is stable when stored under argon at room temperature, dark green solutions of **(XV)** in hexane/THF solvent mixtures exposed to nitrogen led to a dinitrogen complex (see also Section 5.1).

Dark red crystals of the Sm(II) enolate derivative **(XVI)** were formed by the reaction of **(XV)** with THF. The structure of **(XVI)** is closely related to **(XV)**, the major difference between the two compounds being the presence of the enolate group bridging the three lithium centres instead of the bridging chloride and the hapticity of some lithium - macrocycle interactions. Complex **(XVI)**, isolated from a toluene solution, can be transformed to another form of the Sm(II) enolate **(XVII)** bearing an additional two THF molecules by recrystallisation from THF.
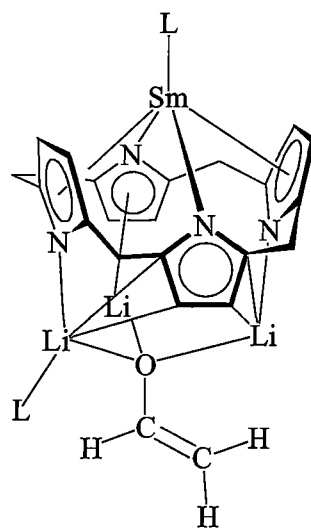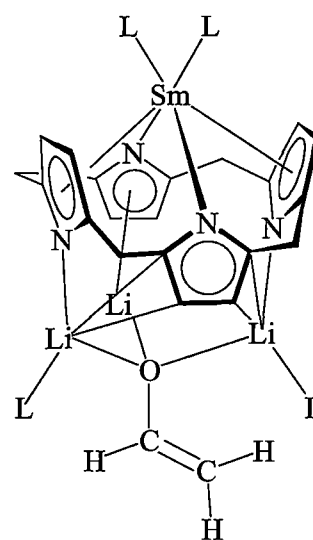
(XVI) (L = THF)   (XVII) (L = THF)

4.2 RESULTS AND DISCUSSION

4.2.1 Complex syntheses

The green divalent samarium complex [{(THF)$_2$K(Et$_8$O$_2$N$_2$)Sm(μ-I)}$_2$], (15), of the dioxaporphyrinogen (3) and the related dark purple complex [(Et$_8$N$_4$Me$_2$)Sm(THF)$_2$], (16), derived from the N,N'-dimethylatedporphyrinogen (6), have been obtained from metathesis reactions between the dipotassium complexes of the modified porphyrinogens with samarium(II) diiodide, as shown in Scheme 5.

(10) X = O, n = 4
(14) X = NMe, n = 2
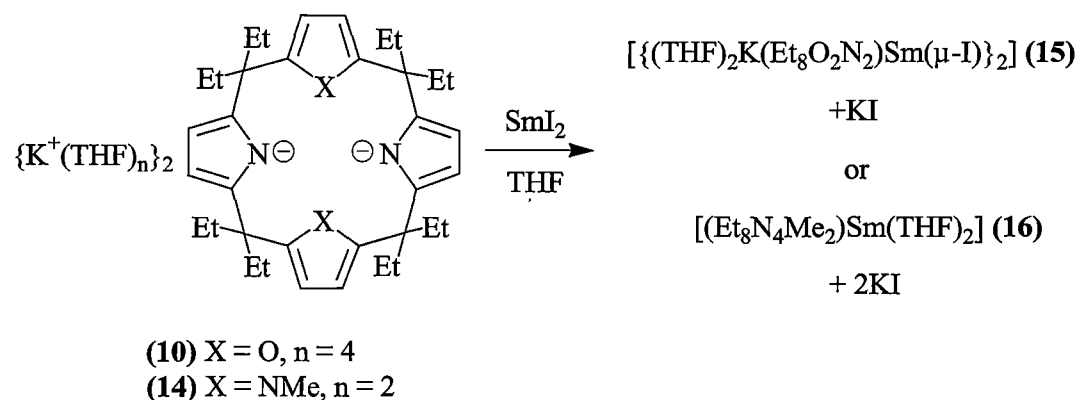
Scheme 5: Syntheses of [{(THF)$_2$K(Et$_8$O$_2$N$_2$)Sm(μ-I)}$_2$], (15), and [(Et$_8$N$_4$Me$_2$)Sm(THF)$_2$], (16).

The homogeneous reaction between the dipotassium complex (10) and samarium diiodide in THF giving [{(THF)$_2$K(Et$_8$O$_2$N$_2$)Sm(μ-I)}$_2$], (15), reaches completion after three hours at ambient temperature, during which time the colour of the solution changed gradually to green. The reaction between the dipotassium complex (14) and samarium diiodide in THF is, however, a heterogeneous reaction due to the poor solubility of the dipotassium compound (14) in THF and is slower than the former reaction, requiring overnight stirring to reach completion with the colour changing slowly to purple.

The dipotassium reactants (10) and (14), prepared *in situ* from the metallation of the porphyrinogens (3) and (6) using potassium metal in THF, were used directly in the reactions with samarium diiodide without further purification (except for filtration in the case of (15)). The one-pot reactions from the porphyrinogens formed the samarium(II) complexes in good yields of 71% for (15) and 80% for (16) as crystalline products after filtration from the potassium iodide byproduct and recrystallisation from THF. A noticeably smaller amount of potassium iodide precipitate is noticed for the formation of (15), in keeping with the incorporation of an equivalent of the byproduct in the product.

Both complexes (15) and (16) have different solubilities. Complex (15) is moderately soluble in THF but insoluble in toluene or hexane. Complex (16) is very soluble in toluene and moderately soluble in THF and hexane.

Both complexes (15) and (16) gave satisfactory microanalyses for the proposed formulations. The structures of (15) and (16) have been confirmed by X-ray crystal structure determinations. Complex (16) was also characterised by ^{1}H and ^{13}C NMR spectroscopy. The poor solubility of (15) prevented its characterisation by NMR spectroscopy.

The samarium(II) complexes (15) and (16) of the two modified porphyrinogens have strikingly different molecular structures. The general formula [{(THF)$_2$K(Et$_8$O$_2$N$_2$)Sm(μ-I)}$_2$], (15) represents a dimeric samarium complex. The complex incorporates two potassium cations, each of them bearing two coordinating THF molecules. Two samarium coordinated iodide centres, incorporated as counter anions to the potassium cations, bridge the two samarium(II) centres. The formula [(Et$_8$N$_4$Me$_2$)Sm(THF)$_2$], (16), represents a monomeric samarium complex in which no potassium iodide is incorporated, with the remaining samarium coordination sites

being occupied by two THF molecules. Three dimensional representations of the two samarium(II) complexes are shown in Figure 1.

(15)

(16)
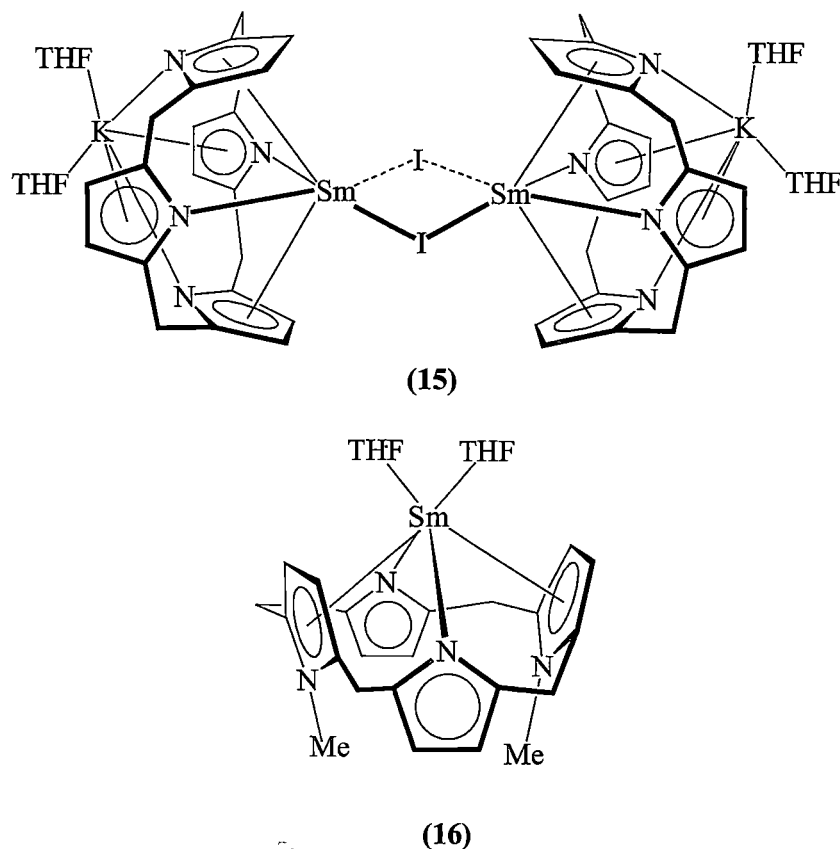
Figure 1: Three dimensional representations of the samarium(II) complexes [{(THF)$_2$K(Et$_8$O$_2$N$_2$)Sm(μ-I)}$_2$], **(15)**, and [(Et$_8$N$_4$Me$_2$)Sm(THF)$_2$], **(16)**.

Complex **(16)** loses the coordinated THF molecules only under extreme conditions. Attempted sublimation of the complex results in loss of THF above 165°C (5×10^{-5} mbar) to leave a brown solid, presumably [(Et$_8$N$_4$Me$_2$)Sm], as shown in Equation 3. This brown solid is soluble in benzene, but remains poorly characterised due to a non-assignable ^{1}H NMR spectrum in deuterated benzene, presumably arising from paramagnetic effects. Above 220°C (5×10^{-5} mbar), the brown residue changes further to a white solid, presumably by decomposition.

$$[(Et_8N_4Me_2)Sm(THF)_2] \longrightarrow [(Et_8N_4Me_2)Sm] + 2\ THF$$
(16)
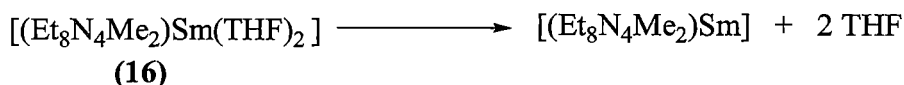
Equation 3

4.2.2 NMR spectroscopic characterisation

Complex **(15)** could not be characterised by NMR due to its poor solubility. The ^{1}H NMR spectrum of complex **(16)** in deuterated benzene shows a series of variously broadened and shifted resonances in the range -21 to 43 ppm at room temperature which have been partially assigned, as shown in Figure 2. The singlet resonance at 42.91 ppm is assigned to the *N*-methyl group, while the aromatic protons from the pyrrolide and *N*-methyl pyrrole rings appear at 1.12 and 19.22 ppm. The multiplets at -21.07, -4.89, 1.26 and 5.17 ppm are attributable to CH$_2$ protons of the *meso*-ethyl groups. The broad resonances at 10.83 and 4.51 ppm are from coordinating THF and the two triplets at -8.21 and 0.89 ppm belong to CH$_3$ protons of the *meso*-ethyl groups. The ^{13}C NMR spectrum has also been assigned through gCOSY, gHMQC and gHMBC experiments except for the *N*-methyl groups and the THF molecules, which were not located presumably owing to the paramagnetic shift effect of the nearby samarium centre. The resonances at 44.3, 68.2, 108.7 and 188.0 ppm are from the aromatic carbons of the pyrrolide and *N*-methylpyrrole rings. The resonance at 50.0 ppm is assigned to the *meso*-carbons, signals at 21.3 and 32.0 ppm belong to methylene carbons and overlapping resonances at 10.8 ppm are attributable to the methyl groups.
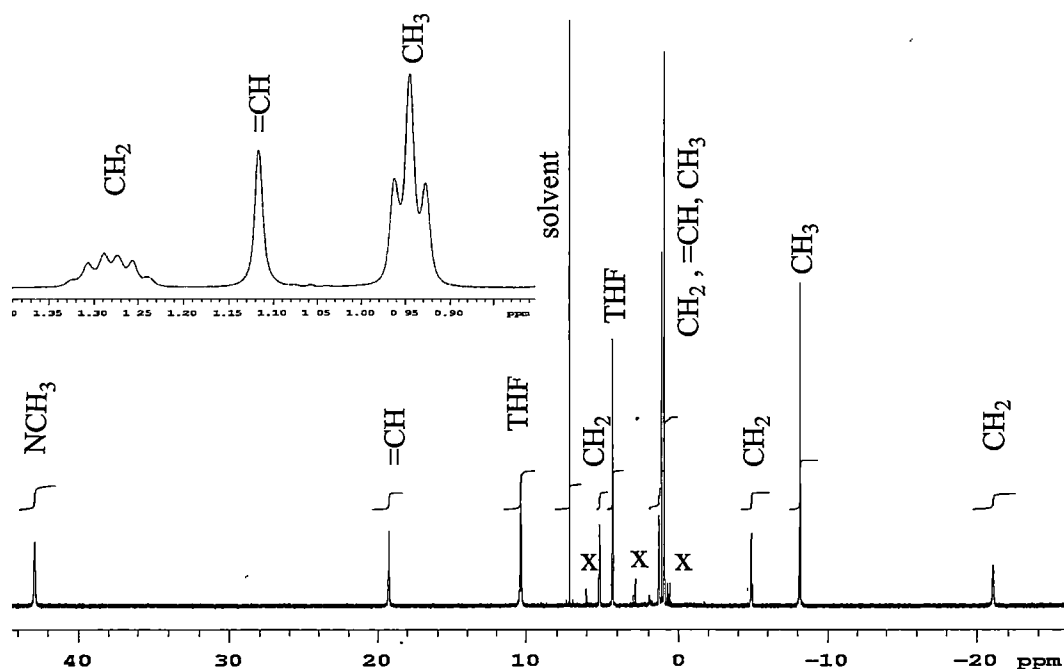
Figure 2: ^{1}H NMR spectrum of complex [(Et$_8$N$_4$Me$_2$)Sm(THF)$_2$], **(16)** (C$_6$D$_6$, 399.694 MHz, 298 K, ppm) (x = impurity).

Variable temperature ^{1}H NMR spectroscopic studies of [(Et$_8$N$_4$Me$_2$)Sm(THF)$_2$], (16), in the temperature range of between -50 to 50°C have also been investigated. The chemical shift variation of each proton in the molecule versus the inverse of the absolute temperature is shown in Figure 3. The resonances of all protons vary quite linearly with 1/T following the Curie-Weiss law. The absence of any dramatic changes in the spectra is an indication of no major changes to the average molecular structure in solution in the range of temperatures studied.
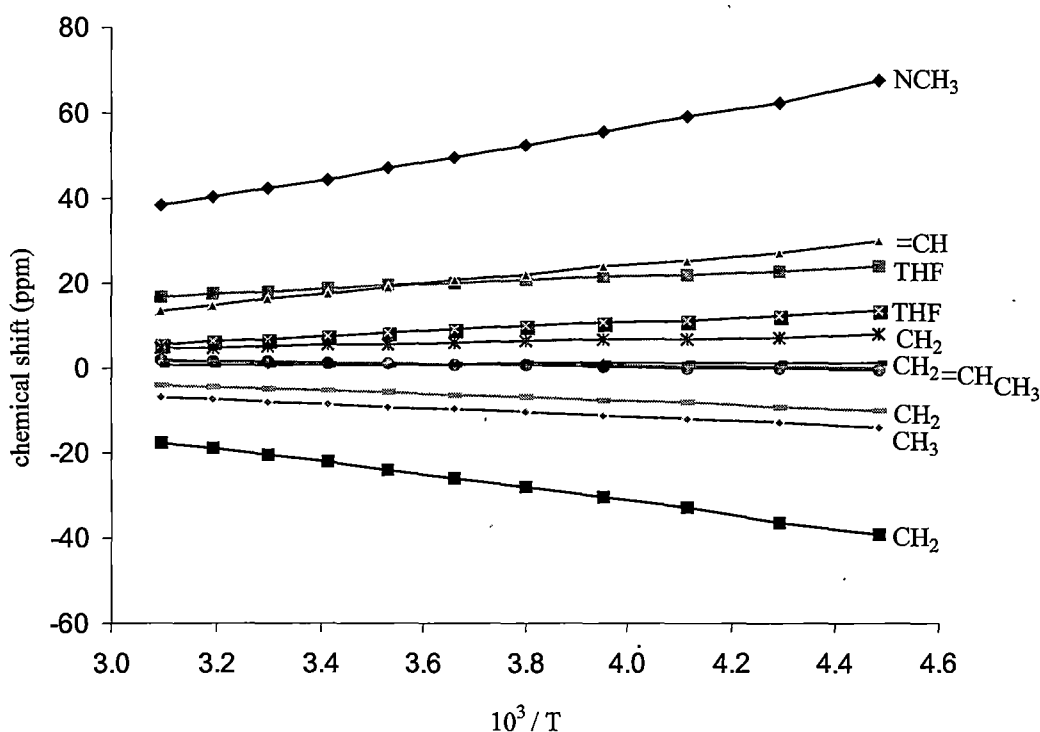
Figure 3: Variable temperature ^{1}H NMR spectra of [(Et$_8$N$_4$Me$_2$)Sm(THF)$_2$], (16) (toluene-d^8, 399.694 MHz, ppm).

At -50°C, the proton resonances of (16) are spread across the range of -40 to 68 ppm, with the greatest paramagnetic shift effects being noted for those protons in close proximity to the samarium(II) centre. Notably only one of the aromatic proton resonances of the pyrrolide and N-methyl pyrrole rings exhibits a large chemical shift temperature dependence, which perhaps allows assignment of the resonance at 19.22 ppm (at 25°C) to the protons of the η^5-bound N-methyl pyrrole rings and the protons of the η^1-bound pyrrolide rings to the resonance at 1.12 ppm (at 25°C).

4.2.3 Molecular structures

4.2.3.1 Molecular structure of [{(THF)$_2$K(Et$_8$O$_2$N$_2$)Sm(μ-I)}$_2$], (15)

Green crystals of [{(THF)$_2$K(Et$_8$O$_2$N$_2$)Sm(μ-I)}$_2$], (15), suitable for X-ray crystal structure determination were grown from a hot saturated THF/toluene (2:1) solution which was allowed to cool slowly to ambient temperature and stood for two days. The crystals belong to the orthorhombic space group *Fmmm* (No. 69), $a =$ 19.0780(3), $b = 21.4190(3)$, $c = 26.7020(4)$ Å, with four molecules in the unit cell, the asymmetric unit consisting of one eighth of a molecule of [{(THF)$_2$K(Et$_8$O$_2$N$_2$)Sm(μ-I)}$_2$], (15), residing on *mmm* symmetry sites. The structure of (15) is shown in Figures 4 and 5.

The accuracy of the molecular structure of (15) is poor owing to disorder related to the high crystallographic symmetry of the structure, but nevertheless, the structure is qualitatively defined in all senses except for the relative location of the pyrrolide and furanyl rings and hence their binding modes to the Sm(II) and K centres. Figures 4 and 5 show the furanyl rings being σ-bound to the Sm centres, only in the assumption of this being seen in all Sm(III) derivatives prepared (see Section 5.2.3.4). Disordered potassium coordinated THF molecules and non-coordinated solvent molecules (modelled as THF molecules) were also present in the structure, but have been omitted from Figures 4 and 5.
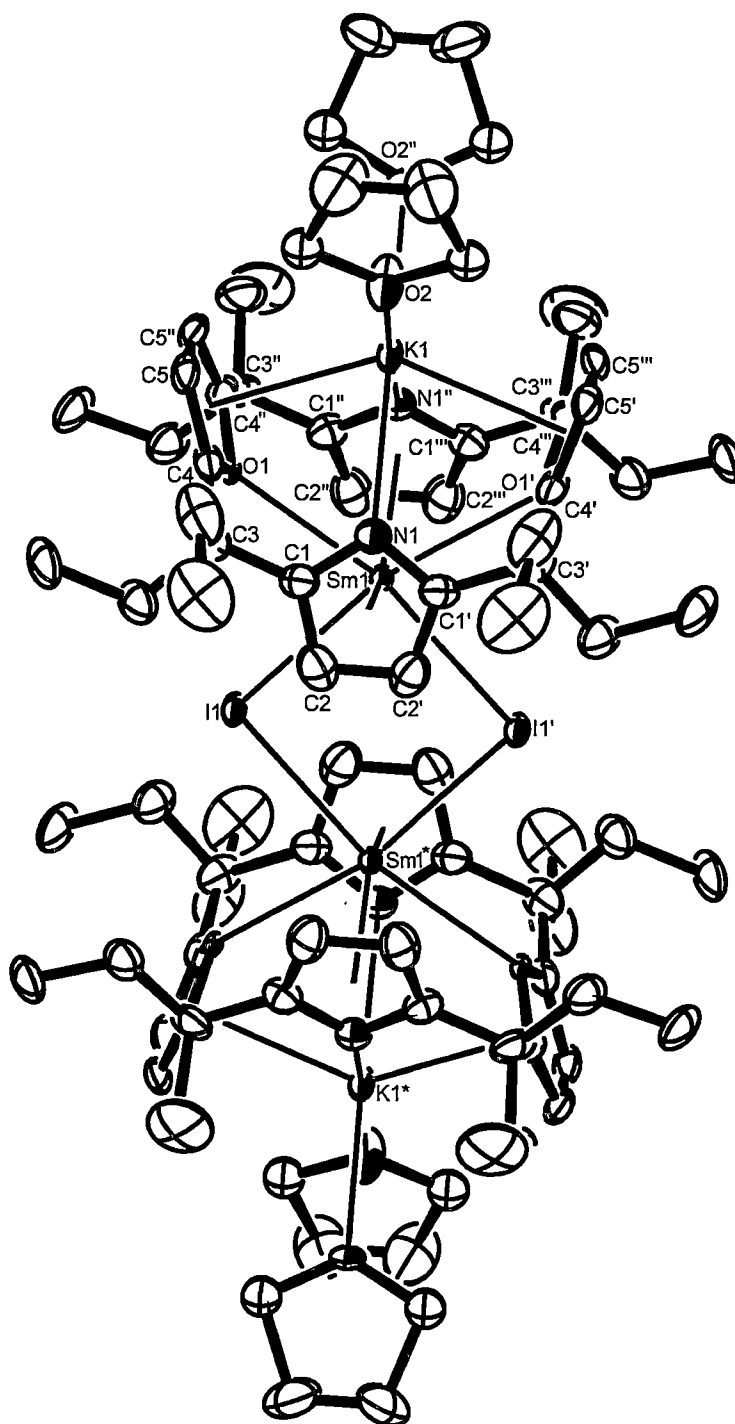
Figure 4: Molecular structure of [{(THF)$_2$K(Et$_8$O$_2$N$_2$)Sm(μ-I)}$_2$], **(15)**, with thermal ellipsoids drawn at the level of 50% probability (atoms are partly labelled, protons have been removed for clarity and disorder in the coordinated THF molecules is omitted).

(a)   (b)
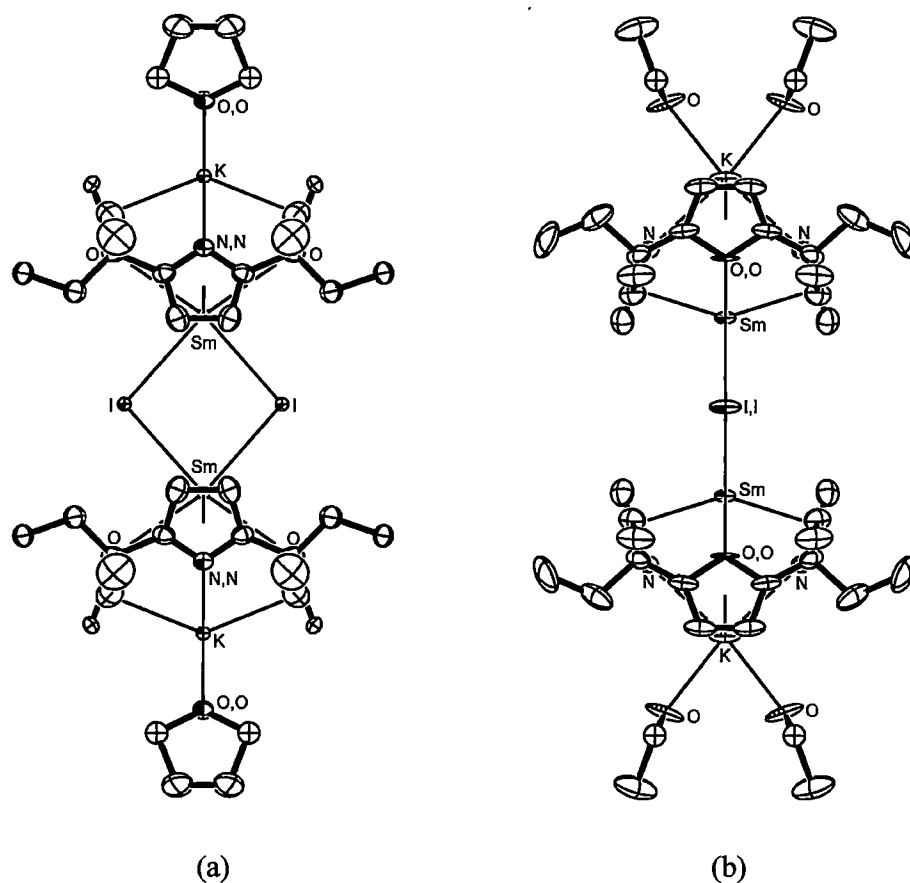
Figure 5: Side views of the molecular structure of [{(THF)$_2$K(Et$_8$O$_2$N$_2$)Sm(μ-I)}$_2$], **(15)**, with thermal ellipsoids drawn at the level of 50% probability (protons have been removed for clarity and disorder in the coordinated THF molecules is omitted): (a) in the direction perpendicular to the Sm$_2$I$_2$ plane, (b) in the direction through the Sm$_2$I$_2$ plane.

Complex **(15)** adopts a dimeric structure in solid state, as shown in Figures 4 and 5. Two samarium atoms and two bridging iodide atoms form a 4-membered ring linking the two macrocyclic units. Both macrocyclic units adopt 1,3-alternate conformations and the two samarium centres use the same η^5:η^1:η^5:η^1-bonding modes to pyrrolide and furanyl rings, alternatively. Potassium cations bind to the macrocyclic unit using η^1:η^5:η^1:η^5-bonding modes with pyrrolide and furan rings in opposite fashion to the bonding modes seen for the samarium centres. The remaining coordination sites of each potassium cation are occupied by two THF molecules.

The central Sm$_2$I$_2$ four-membered rings contain equal Sm-I distances of 3.2961(12) Å, Sm-I-Sm angles of 96.81(4)° and I-Sm-I angles of 83.19(4)°. The samarium centre is σ-bound to the furanyl rings with distances of 2.907(10) Å

(Sm(1)-O(1)) and η^5-bound to the pyrrolide rings with samarium-centroid distances of 2.65_2 Å. The O-Sm-O angles are 110.1(4)°, while the centroid-Sm-centroid angle is 145.1_4°. Potassium centres coordinate to the macrocyclic units with η^1-interactions to the pyrrolide nitrogen centres at distances of 2.928(16) Å (K-N) and η^5-interactions to the furanyl rings at distances of 2.98_9 Å (K-centroid distance). The N-K-N angle is 93.9(6)°, while the centroid-Sm-centroid angle is 136.3_4°. The four THF molecules coordinate to the potassium centres with equivalent K-O distances of 2.74(2) Å, and equivalent O-K-O angles of 78.1(15)°.

The non-bonding cross-cavity heteroatom distances defining the size of the cavity of the macrocycle are 4.75_7 Å, measured for opposite oxygen centres, and 4.26_3 Å, for opposing nitrogen centres. The furanyl and pyrrolide rings adopt tilt angles of 70.3_9 and 70.2_8°, respectively, relative to the plane of the macrocycle. The macrocyclic cavity of (15) is smaller than (3) (4.85_7 Å, for oxygen centres, and 4.65_1 Å, for nitrogen centres). The pyrrolide rings of (15) lie steeper than those of (3) (65.5_1 and 67.1_1°) and furan rings are flatter than (3) (79.4_9 and 79.0_3°). The shrunken macrocyclic cavity of (15) indicates that the samarium(II) coordination has drawn the macrocyclic unit inwards towards the metal through conformational adjustments.

4.2.3.2 Molecular structure of [(Et$_8$N$_4$Me$_2$)Sm(THF)$_2$], (16)

Dark purple crystals of [(Et$_8$N$_4$Me$_2$)Sm(THF)$_2$], (16), suitable for X-ray crystal structure determination were grown from a hot saturated THF solution that was allowed to cool slowly to ambient temperature and stood overnight. The crystals belong to the orthorhombic space group *Pbna* (No. 60), $a = 10.5498(1)$, $b = 18.5892(2)$, $c = 21.3197(2)$ Å, with four molecules in the unit cell, the asymmetric unit consisting of half of a molecule of [(Et$_8$N$_4$Me$_2$)Sm(THF)$_2$], (16), residing on a crystallographic C_2 symmetry axis. The molecule has approximate C_{2v} symmetry, except for the orientations of the THF molecules and a minor twist of the macrocycle. The structure of (16) is shown in Figure 6.
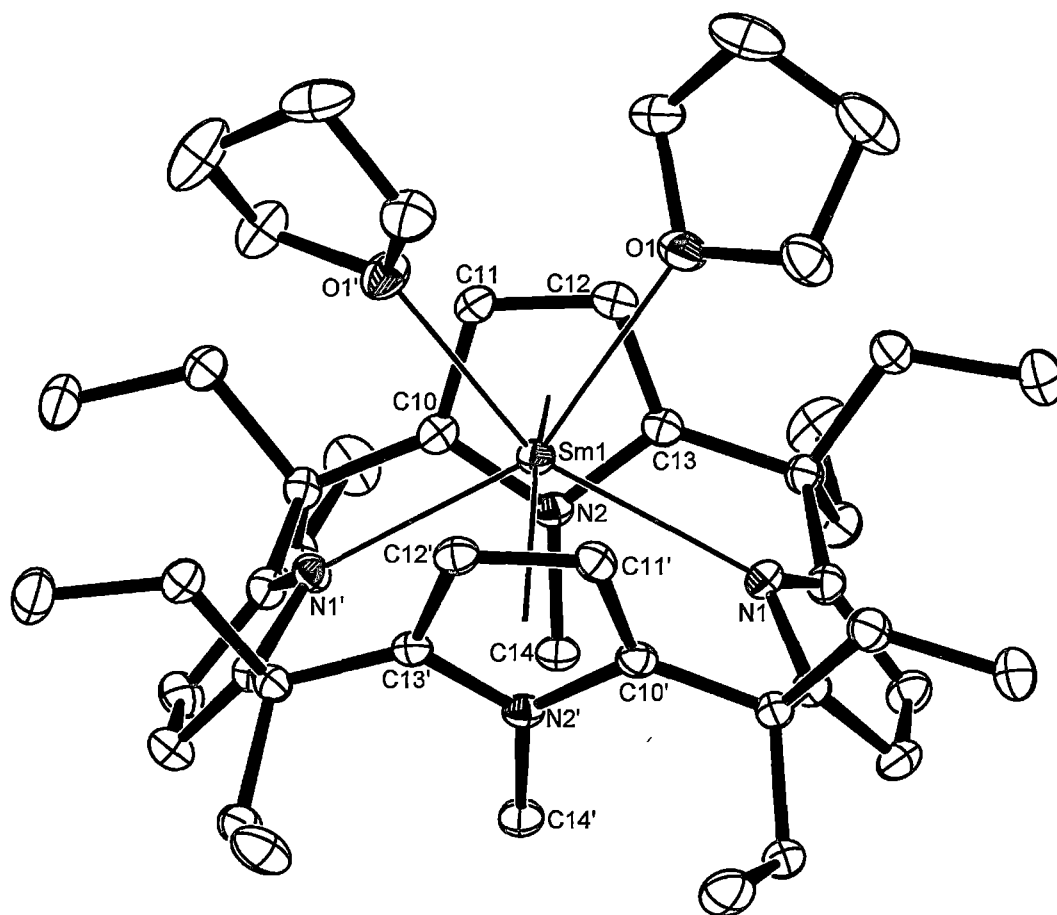
Figure 6: Molecular structure of [(Et₈N₄Me₂)Sm(THF)₂], **(16)**, with thermal ellipsoids drawn at the level of 50% probability (protons have been removed for clarity).

The structure of the samarium(II) complex **(16)** shows it to be a monomeric species. The samarium centre is bound within the macrocyclic cavity by a η^5:η^1:η^5:η^1-bonding mode. Two coordinating THF molecules occupy the remaining coordinating sites of the samarium centre. In a similar way to the *endo*-cavity-bound potassium centre in the dipotassium complex **(14)**, the samarium(II) centre is forced to adopt η^5-interactions to both *N*-methyl pyrrole rings and is σ-bound to both nitrogen centres of the pyrrolide rings owing to the *N*-methyl substitutents which preclude the formation of the alternative η^5:η^1:η^5:η^1 arrangement with π-bound pyrrolide units. The macrocyclic unit adopts a 1,3-alternate conformation, with the two *N*-methyl groups directed towards (and blocking) one face of the macrocyclic cavity.

Molecules of **(16)** viewed from N,N'-dimethyl substituent blocked side of the cavity, as shown in Figure 7(a), highlight the sterically hindered face of the macrocyclic cavity arising from the two N-methyl groups. The shielding feature of the two N-methyl groups in the macrocycle is a key factor in the control of the coordination of the samarium centre with the N,N'-dimethylated porphyrinogen unit. As the N-methyl groups protect the samarium centre from coordination by other ligands, the samarium centre in the macrocyclic cavity can only be further coordinated on one side of the macrocyclic cavity which is occupied by two THF molecules. Further, the macrocyclic cavity can host only one metal centre.

(a)   (b)
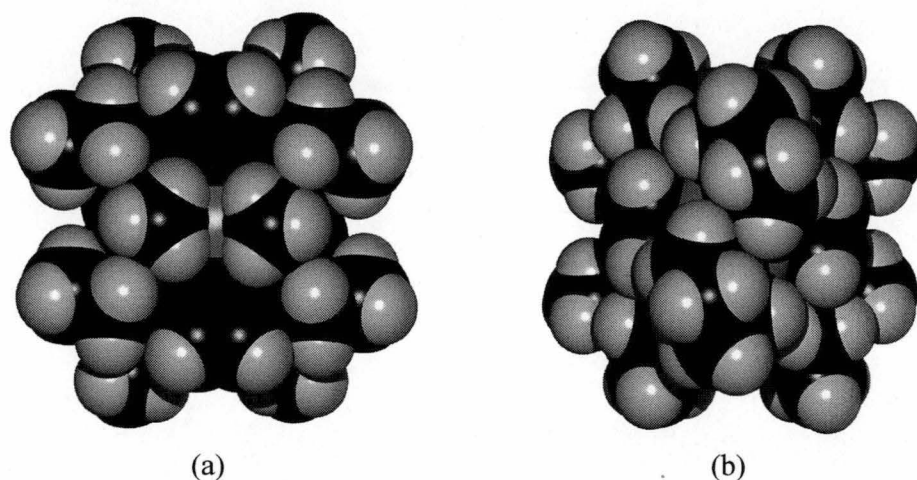
Figure 7: Space filling representations of the molecular structure of $[(Et_8N_4Me_2)Sm(THF)_2]$, **(16)**, (a) viewed from the direction of two N-methyl groups; (b) viewed down the bisector of the O-Sm-O angle.

Compared with the dinuclear samarium(II) complex **(15)**, the monomeric complex **(16)** displays a better controlled coordination. The samarium(II) complex **(15)** based on the dioxaporphyrinogen **(3)**, in which two furan rings exist as a replacement of the two N-methyl pyrrole rings in **(16)**, allows potassium cations with two coordinating THF molecules to bind within the macrocyclic cavity. With one more cation (monovalent) bound in the macrocyclic cavity the samarium(II) complex must contain an additional anionic group, an iodide centre, which bridges two samarium centres giving rise to the dimeric structure.

The structure of complex **(16)** viewed down the bisector of the O-Sm-O angle, as shown in Figure 7(b), highlights the orientation of the coordinating THF molecules. To avoid contact with the π-bound pyrrolide rings, the THF molecules try

to be as parallel as possible to the N-methyl pyrrolide rings. However, van der Waals interactions between two THF molecules prevent them from lying in the same plane. The compromise reached is that the two THF molecules are twisted slightly.

The samarium centre in the macrocyclic cavity is σ-bound to the two pyrrolide rings through the nitrogen centres with equal distances of 2.6671(16) Å, while it is η^5-bound to N-methyl pyrrole rings with a Sm-centroid distance of 2.75_6 Å. The two σ-bonds to the samarium centre form a N-Sm-N angle of 120.03(7)°, while the centroid-Sm-centroid angle associated with the two N-methyl pyrrolide rings is 154.4_4°. The two THF molecules σ-coordinate through the oxygen centres to the samarium centre with equal bond lengths of 2.6552(14) Å, forming an O-Sm-O angle of 70.13(6)°. The η^5-bound N-methyl pyrrole interaction is slipped somewhat from the centroid, with the samarium lying slightly towards the nitrogen centre (Sm(1)-N(2) = 2.9047(15) Å, Sm(1)-C(10) = 2.9988(18) Å, Sm(1)-C(11) = 3.06_4 Å, Sm(1)-C(12) = 3.0553(19) Å, Sm(1)-C(13) = 2.9761(17) Å).

As shown in Table 1, complex (16) has greatly shorter Sm-N σ-bonds and similar η^5-interaction distances compared with the related dinuclear samarium(II) complex (XIV) of porphyrinogen (4) (Sm-N = 2.748(4) Å and Sm-centroid = 2.7_6 Å). The metallocene bend angle in complex (16) (centroid-Sm-centroid) is larger than (XIV) ($149._5$°), while the THF molecules coordinate to the samarium centre with a smaller O-Sm-O angle in complex (16) (74.1_8° for (XIV)) with two slightly longer Sm-O bonds in complex (16) (2.634(4) Å for (XIV)). The macrocyclic cavity of complex (16) is larger than in (XIV) (cross cavity N··N distance is 4.42_3 Å for (XIV)), further indicating the conformational changes associated with the tetrametallated porphyrinogen hosting two samarium(II) centres versus the steric effects of the N,N'-dimethyl groups in the mononuclear complex (16).

(XIV) (L = THF)		(16)	
Sm-O(1)	2.634(4)	Sm(1)-O(1)	2.6552(14)
Sm-N(1a)	2.748(4)	Sm-N(1)	2.6671(16)
Sm(1)-η^5(N1)	2.7_6	Sm(1)-η^5(N2)	2.75_6
Sm-Sm(a)	3.4417(9)	-	-
η^5(N1)-Sm(1)-η^5(N1c)	$149._5$	η^5(N2)-Sm(1)-η^5(N2′)	154.4_4
N(1)-Sm-N(1c)	107.47(17)	N(1)-Sm-N(1′)	120.03(7)
O(1)-Sm(1)-O(1c)	74.1_8	O(1)-Sm(1)-O(1′)	70.13(6)
N(1)···N(1c)	4.42_3	N(1)···N(1′), N(2)···N(2′)	$4.67_5, 4.62_0$

Table 1: Selected bond lengths (Å) and angles (°) for compounds [(Et$_8$N$_4$){Sm(THF)$_2$}$_2$], **(XIV)**, and [(Et$_8$N$_4$Me$_2$)Sm(THF)$_2$], **(16)**

Compared to the mononuclear samarium(II) complex **(XV)**, **(16)** has a smaller metallocene bend angle ($166._4$° for **(XV)**), a longer Sm-centroid distance (2.6_5 Å for **(XV)**) and a longer η^1-bond distance (Sm-N = 2.541(9) and 2.567(9) Å for **(XV)**). Only one THF coordinates to the samarium centre in **(XV)** with a shorter Sm-O distance of 2.612(8) Å. The macrocyclic cavity of **(16)** is more symmetrical than **(XV)** (cross cavity N···N distances are 4.5_6 Å and 4.9_0 Å).

Some features of **(16)** are worthy of mention in comparison to the structure of [(η^5-C$_5$Me$_5$)$_2$Sm(THF)$_2$], **(XVIII)**[8]. Complex **(16)** has a larger coordination number (10 compared with 8 for **(XVIII)** and has the geometrical constraints of the macrocyclic unit. An approximate C_{2v} symmetry is noted for **(16)** (except for the two THF molecules), while **(XVIII)** dismisses this symmetry by the staggering of the pentamethylcyclopentadienyl rings of 36°, as shown in Figure 8.

(a)

(b)

(c)
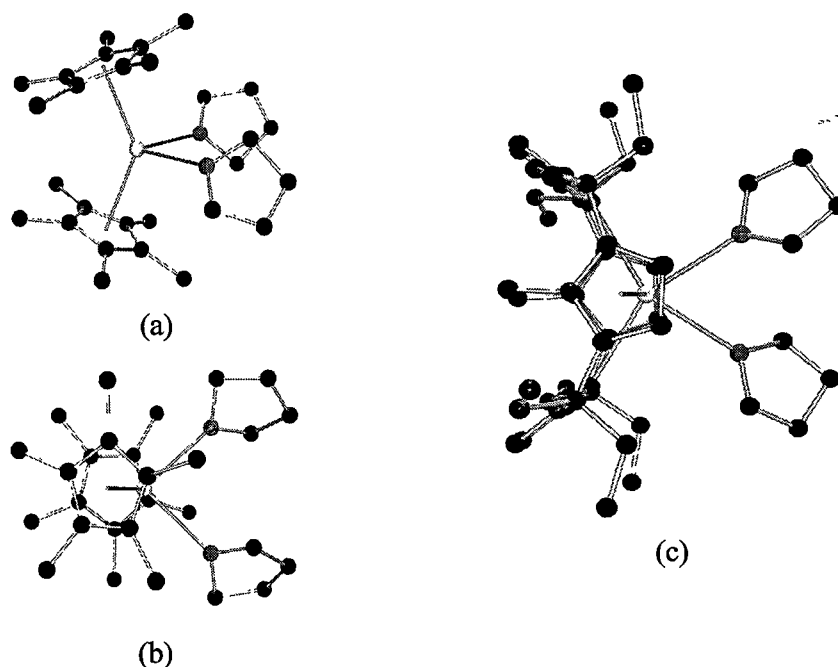
Figure 8: Projections of the molecular structures of $[(\eta^5\text{-}C_5Me_5)_2Sm(THF)_2]$, **(XVIII)**, (a) and (b) and $[(Et_8N_4Me_2)Sm(THF)_2]$, **(16)**, (c). Views (b) and (c) show projections eclipsing the η^5-bound ligands.

The Sm-centroid distance in complex **(16)** of 2.75_6 Å is much longer than those in **(XVIII)** which measure 2.60_3 Å and 2.59_5 Å. The two coordinated THF molecules in **(16)** form an O-Sm-O angle of $70.13(6)°$ compared with $82.7(4)°$ for **(XVIII)**, mainly due to the steric effect of the *meso*-ethyl groups in **(16)**. The Sm-O bond distances of $2.620(9)$ Å in **(XVIII)** are shorter than in **(16)** $2.6552(14)$ Å. The metallocene bend angle (centroid-Sm-centroid) of $136.7_0°$ in **(XVIII)** is small compared with $154.4_4°$ in **(16)**. These geometry variations are consistent with the coordination number variations in the two complexes and the geometrical restraints of the macrocyclic ligand in **(16)**.

Compared with the reported crystal structure of the protonated N,N'-methylated porphyrinogen **(6)**, complex **(16)** displays reduced distances between both opposing nitrogens of the N-methyl pyrrole and pyrrolide rings, as shown in Table 2. The tilt angles of the four heterocyclic rings are flattened slightly in **(16)**, with the N-methylpyrrole rings remaining steeper than the pyrrolide rings in accord with repulsions between the N-methyl groups.

Compound number	N-Methylpyrrolide ring		Pyrrolide ring	
	Cross-cavity $N \cdots N$ distance (Å)	Ring tilt angles (°)	Cross-cavity $N \cdots N$ distance (Å)	Ring tilt angles (°)
(6)	4.73_3	$74.0_3, 73.5_9$	4.83_1	$57.3_1, 53.5_1$
(16)	4.67_5	73.0_4	4.62_0	50.3_7

Table 2: Cross-cavity $N \cdots N$ distances and heterocycle ring tilt angles for compounds $Et_8N_4Me_2H_2$, (6), and $[(Et_8N_4Me_2)Sm(THF)_2]$, (16)

4.3 EXPERIMENTAL

Synthesis of [{(THF)$_2$K(Et$_8$O$_2$N$_2$)Sm(μ-I)}$_2$], (15)

Potassium metal (0.19 g, 4.8 mmol) was added to *meso*-octaethyl-*trans*-dioxaporphyrinogen, (3), (1.09 g, 2.00 mmol) in THF (80 mL) and refluxed for 6 hours. Excess potassium metal and other undissolved impurities were filtered off and samarium diiodide (0.1 M solution in THF, 20 mL, 2.0 mmol) was added to the solution dropwise over 20 minutes while stirring. The mixture was stirred for three hours during which time the colour of the solution changed gradually from blue to green. A white precipitate, presumably potassium iodide, was filtered off and the mixture was concentrated *in vacuo* to *ca.* 40 mL and crystallisation from THF at ambient temperature giving a pure green product (yield 1.42 g, 71%). Crystals suitable for X-ray crystal structure determination were grown from a solution of THF and toluene (v/v, 2:1).

Anal. Calcd.: C, 52.78; H, 6.44; N, 2.80 (C$_{88}$H$_{128}$I$_2$K$_2$N$_4$O$_8$Sm$_2$, MW 2002.7). Found: C, 52.59; H, 6.62; N, 2.71.

Synthesis of [(Et$_8$N$_4$Me$_2$)Sm(THF)$_2$], (16)

Potassium metal (0.16 g, 4.1 mmol) was added to a solution of *trans-N,N'*-dimethyl-*meso*-octaethylporphyrinogen, (6), (1.14 g, 2.00 mmol) in THF (80 mL) and refluxed for 6 hours. At that stage all the potassium had been consumed and a small amount of the dipotassium compound had precipitated from the solution. Samarium diiodide (0.1 M solution in THF, 20 mL, 2.0 mmol) was added dropwise with stirring at ambient temperature. The reaction was stirred continuously overnight and a white precipitate presumably potassium iodide, was filtered off. The purple solution was concentrated *in vacuo* to *ca.* 20 mL and crystallised from THF at ambient temperature giving a pure dark purple crystalline product (1.38 g, 80%) which were suitable for X-ray crystal structure determination.

^{1}H NMR (C$_6$D$_6$, 399.694 MHz, 298 K, ppm): -21.07 (m, 4H, 2CH$_2$), -8.15 (t, 12H, 4CH$_3$), -4.89 (m, 4H, 2CH$_2$), 0.93 (t, 12H, 4CH$_3$), 1.12 (s, 4H, =CH, pyrMe or pyr), 1.26 (m, 4H, 2CH$_2$), 4.51 (s, broad, 8H, THF), 5.17 (m, 4H, 2CH$_2$), 10.83 (s, broad, 8H, THF), 19.22 (s, 4H, =CH, pyrMe or pyr), 42.91 (s, 6H, 2NCH$_3$).

^{13}C NMR (C_6D_6, 100.512 MHz, 298 K, ppm): 10.8 (CH_3), 21.3 (CH_2), 32.0 (CH_2), 44.3 (=CH, pyrMe or pyr), 50.0 (CEt_2), 68.2 (=CH, pyrMe or pyr), 108.7 (=CR, pyrMe or pyr), 188.0 (=CR, pyrMe or pyr).

Anal. Calcd.: C, 64.14; H, 8.19; N, 6.50 ($C_{46}H_{70}N_4O_2Sm$, MW 861.43)

Found: C, 63.98; H, 8.27; N, 6.43.

4.4 REFERENCES

[1]   H. Schumann, J. Winterfeld, H. Hemling, N. Kuhn, *Chem. Ber.*, 1993, **126**, 2657.

[2]   M. Ganesan, C.D. Berube, S. Gambarotta, G.P.A. Yap, *Organometallics*, 2002, **21**, 1707.

[3]   C.D. Berube, S. Gambarotta, G.P.A. Yap, *Organometallics*, 2003, **22**, 434.

[4]   **a.** T. Dubé, M. Ganesan, S. Conoci, S. Gambarotta, G.P.A. Yap, *Organometallics*, 2000, **19**, 3716.
        b. T. Dubé, S. Conoci, S. Gambarotta, G.P.A. Yap, G. Vasapollo, *Angew. Chem. Int. Ed.*, 1999, **38**, 3657.
        c. T. Dubé, D.M.M. Freckmann, S. Conoci, S. Gambarotta, G.P.A. Yap, *Organometallics*, 2000, **19**, 209.
        d. D.M.M. Freckmann, T. Dubé, C.D. Berube, S. Gambarotta, G.P.A. Yap, *Organometallics*, 2002, **21**, 1240.
        e. T. Dubé, S. Gambarotta, G.P.A. Yap, S. Conoci, *Organometallics*, 2000, **19**, 115.
        f. M. Ganesan, S. Gambarotta, G.P.A. Yap, *Angew. Chem. Int. Ed.*, 2001, **40**, 766.
        g. T. Dubé, S. Conoci, S. Gambarotta, G.P.A. Yap, *Organometallics*, 2000, **19**, 1182.
        h. M. Ganesan, M.P. Lalonde, S. Gambarotta, G.P.A. Yap, *Organometallics*, 2001, **20**, 2443.

[5]   **a.** J.-I. Song, S. Gambarotta, *Angew. Chem. Int. Ed. Engl.*, 1995, **34**, 2141.
        b. T. Dubé, S. Gambarotta, G.P.A. Yap, *Organometallics*, 2000, **19**, 817.

[6]   E. Campazzi, E. Solari, C. Floriani, R. Scopelliti, *Chem. Commun.*, 1998, 2603.

[7]   T. Dubé, S. Gambarotta, G.P.A. Yap, *Organometallics*, 2000, **19**, 121.

[8]   **a.** W.J. Evans, J.W. Grate, H.W. Choi, I. Bloom, W.E. Hunter, J.L. Atwood, *J. Am. Chem. Soc.*, 1985, **107**, 941.

b. W.J. Evans, I. Bloom, W.E. Hunter, J.L. Atwood, *J. Am. Chem. Soc.*, 1981, **103**, 6507.

c. R.E. Marsh, *Acta Crystallogr., Sect. B: Struct. Sci.*, 1995, **51**, 897.

CHAPTER 5

SAMARIUM(III) COMPLEXES
OF MODIFIED PORPHYRINOGENS

5.1 INTRODUCTION

Trivalent organolanthanide chemistry featuring simple pyrrolides has been explored only to a very limited extent so far. π-Bonding modes between lanthanide(III) centres and simple pyrrolides (including 2,5-disubstituted pyrrolides) were only realised in 1993. The complexes $[(\eta^5\text{-}C_5H_5)_2Yb(NC_4H_4)(THF)]$ and $[(\eta^5\text{-}C_5H_5)_2Lu\{NC_4H_2(Bu^t_2\text{-}2,5)\}(THF)]$, (I), are examples of fully structurally characterised simple trivalent lanthanide pyrrolide complexes in which the pyrrolides adopt σ-bonding modes to the lanthanide centres[1].

(I)   (II)
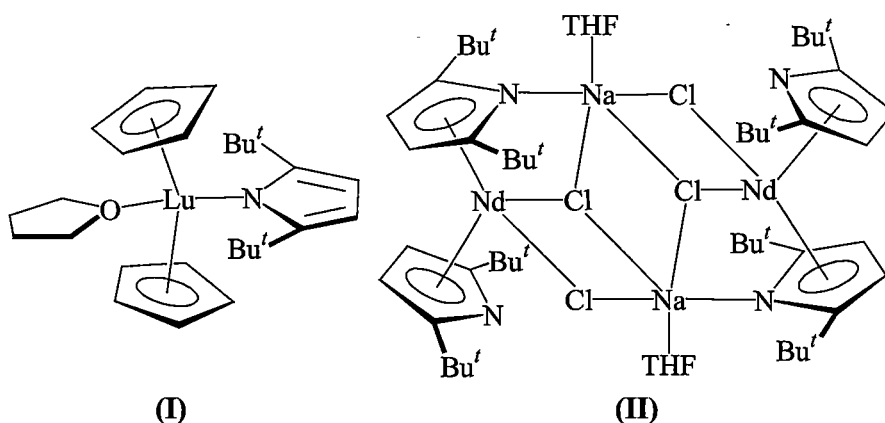
Schumann et al. reported the first trivalent lanthanide complex featuring a π-bound simple pyrrolide, $[\{[NC_4H_2(Bu^t_2\text{-}2,5)]_2Nd(\mu\text{-}Cl)_2[\mu\text{-}Na(THF)]\}_2]$ (II)[2]. The complex was prepared from the reaction between neodymium trichloride and two molar equivalents of sodium 2,5-bis(tert-butyl)pyrrolide in THF. Complex (II) adopts a dimeric form with two bent neodynocene type units in which each pair of pyrrolide rings are π-bound to the neodymium centres. The central four-membered ring is composed of two sodium and two chloride centres bridging the two metallocene units via two Nd-Cl units. Each sodium cation is σ-bound to a pyrrolide nitrogen centre and is bridged to a neodymium centre by a μ_2-chloride centre. The similar reaction of ytterbium(III) trichloride with one equivalent of the sodium pyrrolide formed the Yb(III) π-bound pyrrolide complex (III) of without the presence of sodium cations. The complex adopts a monomeric form containing only one η^5-coordinated pyrrolide ring[3].

(III)   **(IV)**
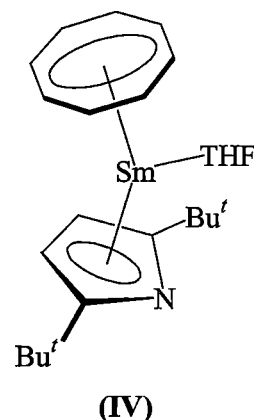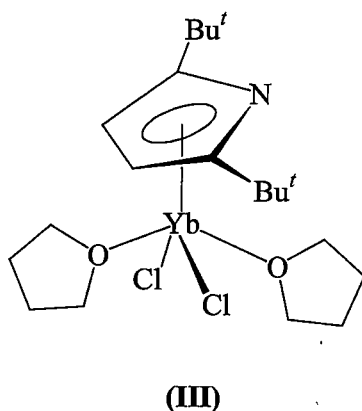
Later, Schumann *et al.* reported further results of halide free η^5-bound pyrrolide lanthanide(III) complexes. Treatment of a dimeric cyclooctatetraene lanthanide chloride, [{(C$_8$H$_8$)LnCl(THF)}$_2$] with Na[NC$_4$H$_2$(Bu$^t_2$-2,5)] afforded [{(C$_8$H$_8$)Ln{NC$_4$H$_2$(Bu$^t_2$-2,5)}(THF)] (Ln = Sm, Tm, Lu). In the samarium(III) complex **(IV)**, the samarium(III) centre is pseudo trigonal planar coordinated by one η^8-bound cyclooctatetraendiyl, one η^5-bound pyrrolide and one THF molecule[4].

Trivalent lanthanide complexes featuring 1,1-di(2'-pyrrolyl)methanes have been unexpectedly made in attempts to prepare divalent species. Other examples arise from a limited number of studies of oxidised products from the corresponding divalent complexes since the initial interest has been centred on the study of lanthanide(II) complexes for this ligand system[5]. As trivalent complexes of samarium or ytterbium complexes are typically more stable than the corresponding divalent complexes, trivalent lanthanide species could only be partly reduced to divalent species and thus mixed valent lanthanide complexes resulted (see Section 4.1). With the high reactivity of samarium(II) complexes towards reduction chemistry, they are very prone to oxidation, resulting in trivalent derivatives, *e.g.*, dinitrogen complexes[6] or unexpected oxidation even in the absence of added oxidising reagents. The following example shows that the reaction intended to make a divalent samarium complex led unexpectedly to a mixed valent complex **(V)** in which samarium(II) and samarium(III) oxides coexist without the intended employment of any oxidising reagents. The reaction of disodium salts of 1,1-di(2'-pyrrolyl)cyclohexane with SmCl$_3$, followed by reduction with sodium under argon led to complex **(V)**. The presence of oxygen atoms is considered to arise from cleavage of THF used as a solvent.
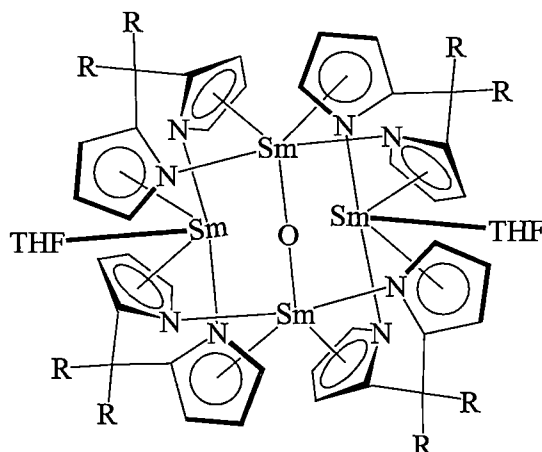
(V) (2R = -(CH$_2$)$_5$-)

The unusual oxidised samarium(III) product **(VI)** was recently identified from the reaction of another dipyrrolide ligand 1,2-benzenediamine-N,N'-bis(1H-pyrrol-2-yl)methylene with [{(Me$_3$Si)$_2$N}$_2$Sm(THF)$_2$] in THF[7], as shown in Equation 1. Interestingly, a closely related dipyrrolide has led to a divalent samarium complex from a similar reaction (see Section 4.1).
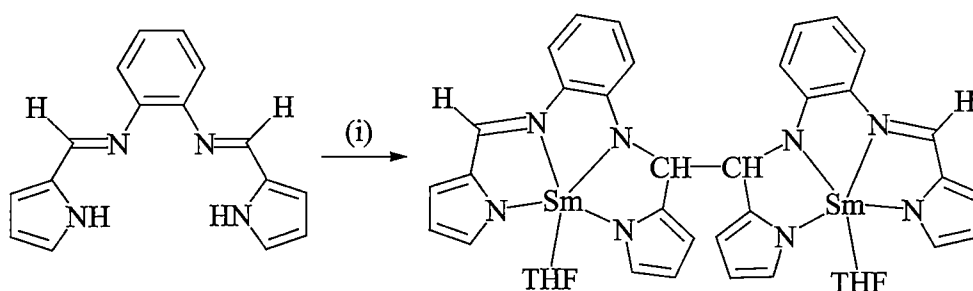
(VI) ((i), [{(Me$_3$Si)$_2$N}$_2$Sm(THF)$_2$], THF)

Equation 1

Lanthanide(III) coordination chemistry of porphyrins is well established. Invariably, lanthanide(III) porphyrin complexes, **(VII)**, adopt σ-bonding modes through the pyrrolic nitrogen centres[8]. Of particular note is the position of the lanthanide centres being out of the plane of the macrocycle owing to their large ionic radii. The remaining coordination sites of the lanthanide centres can be occupied by other chemical groups such as alkyls, halogens, arenes, alkoxides, and so on, which can feature both σ- and π-bonding modes. Another general structural feature for these complexes is 'decker' type complexes, **(VIII)**, in which each lanthanide centre

bridges two porphyrins, with the porphyrin ligands remaining planar owing to the delocalised π-bonding within the dianionic macrocyclic framework.

(VII)   **(VIII)**
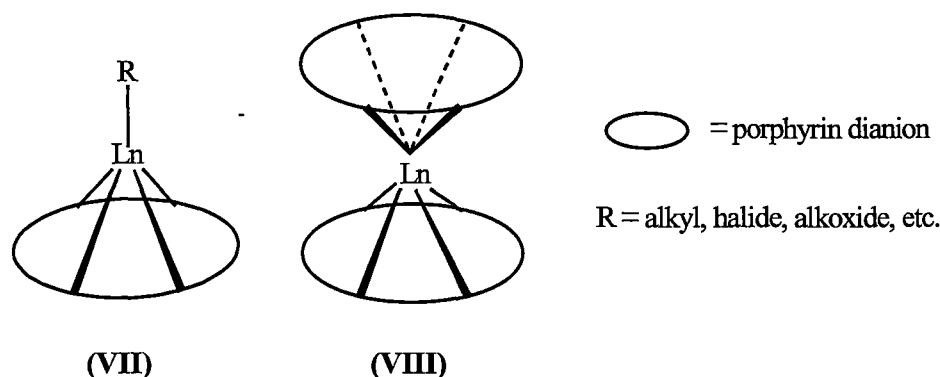
Lanthanide(III) coordination chemistry of porphyrinogens has witnessed a more recent establishment and has revealed a rich variety of bonding features between the lanthanide centres and the macrocycles. Porphyrinogens usually use both σ- and π-bonding modes to bind lanthanide centres with the 1,3-alternate macrocyclic conformation usually being observed. Another general feature for these complexes is the retention of alkali metal cations or the formation of dinuclear complexes in consequence of the tetraanionic status of the deprotonated ligands and the lower oxidation states of the lanthanide centres.

The reported research achievements in this field by the groups of Floriani and Gambarotta include complexes featuring, (i) only Lewis base solvent molecules bound to lanthanide centres, (ii) anionic ligands, such as alkyl, halide or anions of oxygen donor atoms, *etc.*, bound to lanthanide centres, and, (iii) activated small molecules such as dinitrogen and acetylene. The lanthanide(III) complexes are described below under these categories.

(i) Lanthanide(III) complexes featuring only coordinated solvent molecules

Lanthanide(III) complexes without functional groups have been mainly achieved from reactions between [(Et$_8$N$_4$)Na$_4$(THF)$_3$] and LnCl$_3$(THF)$_2$ in THF or DME. A variety of structural types have been established for lanthanide(III) complexes of porphyrinogens depending on the lanthanide reactants or the crystallisation solvent. When the reactions were carried out in THF and the final complex recrystallised from THF, monomeric complexes [η^3:η^1-(THF)$_2$Na(Et$_8$N$_4$)Ln(THF)], **(IX)**, (Ln = Pr, Nd, Sm, Eu, Gd, Yb) were obtained[9]. Recrystallisation of **(IX)** from DME/dioxane led to dimeric complexes [η^3:η^1-

Na(dioxane)(Et$_8$N$_4$)Ln(DME)(dioxane)$_{0.5}$]$_2$, **(X)**, (Ln = Nd, Sm), with dioxane bridging the sodium cations of the monomeric units. Under the same conditions, another category of lanthanide complexes [{η^2:η^3:η^1-Na(Et$_8$N$_4$)Ln(THF)}$_2$], **(XI)**, (Ln = Pr, Sm), were obtained. All three complexes types **(IX)**, **(X)** and **(XI)** contain the same monomeric fragment [η^3:η^1-Na(Et$_8$N$_4$)Ln] and differ from each other only by the solvation of the sodium cation. The lanthanide cations are η^5:η^1:η^5:η^1-bound to the porphyrinogen units with one coordinated THF solvent molecule. The sodium cations are invariably η^3-bound to one of the pyrrolide rings which is η^1-bound to the lanthanide centres and η^1-bound to one of the pyrrolide rings which is η^5-bound to the lanthanide centres. The coordination sphere of the sodium cation is completed by two THF molecules in **(IX)**, one bridging η^1-bound dioxane in **(X)** and η^2-bound to the C$_\beta$-C$_\beta$ bond of a pyrrolide ring which is η^1-bound to the lanthanide centres in **(XI)**. In complex **(XI)**, the two sodium cations are η^1:η^2:η^3-sandwiched by two [(Et$_8$N$_4$)Ln] units.

(IX)   (XI)
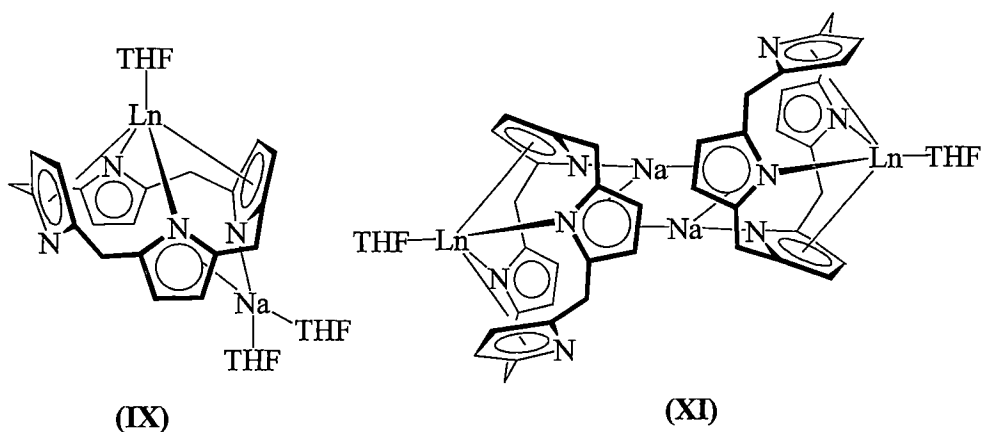
The recrystallisation of **(IX)** from DME led to solvent separated ionic complexes with a dianionic [Na(DME)$_2$]$_2$[{(Et$_8$N$_4$)Ln}$_2$], **(XII)**, (Ln = Pr, Nd, Sm, Eu, Gd), as a ion-separated complex. Further recrystallisation of complexes **(XII)** in THF led to highly novel complexes **(XIII)**, (Ln = Pr, Nd, Sm, Gd), in which two sodium cations are η^2-bound to β-carbons of a pyrrolide ring that is η^5-bound to the lanthanide centres. The macrocyclic units in complexes **(XIII)** have undergone a highly unusual rearrangement with a *meso*-carbon migrating to the β-carbon of a pyrrolide ring. However, when complexes **(XII)** was recrystallised from THF/dioxane, complexes [{η^2-Na(THF)}$_2$(μ-dioxane){(Et$_8$N$_4$)Ln}$_2$]$_n$, **(XIV)**, (Ln = Nd, Gd) were isolated as polymeric complexes in which the sodium cations are bridged by dioxane molecules.

(XIII)
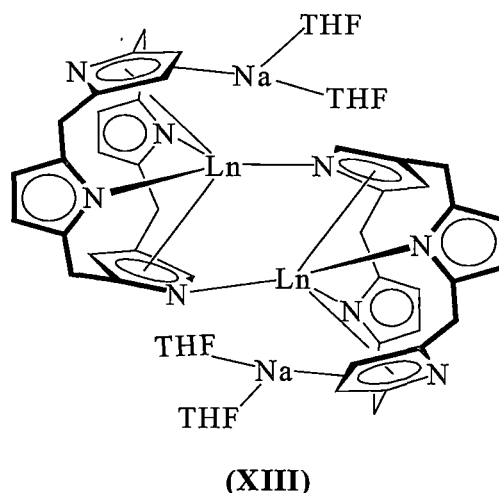
(ii) Lanthanide(III) complexes featuring anionic ligands

Treatment of $SmCl_3(THF)_2$ with half a molar equivalent of $[(Et_8N_4)Li_4(THF)_4]$ in THF led to the dinuclear samarium(III) chloride complex $[(Et_8N_4)\{Sm(\mu\text{-}Cl)_2Li(THF)_2\}_2]$, **(XV)**[10a]. The two samarium centres reside in the macrocyclic cavity above and below the mean plane of the macrocycle with the Sm-Sm distance being 3.391(3) Å. The macrocyclic unit adopts a 1,3-alternate conformation and binds to both the samarium centres with $\eta^5{:}\eta^1{:}\eta^5{:}\eta^1$-binding modes. The opposing pyrrolide rings adopt π-bonding interactions with one samarium centre, while using σ-bonding interactions to the other samarium centre and *vice versa* for the other pyrrolide units. Two chlorides bridge each of the samarium centres to lithium centres, which are in turn coordinated to two THF molecules.

Complex **(XV)** was reduced with half an equivalent of lithium aluminium hydride in THF, resulting in the formation of $[(THF)_2Li(\mu\text{-}Cl)_2Sm(Et_8N_4)Sm(THF)_2]$, **(XVI)**[10a], isolated as a dark red crystalline solid. The dimetallic complex is a mixed valent samarium(II/III) species with one part of the structure similar to the trivalent samarium complex **(XV)** and the other part being similar to its divalent samarium analogue $[(Et_8N_4)\{Sm(THF)_2\}_2]$, (see Section 4.1).

(XV)   (XVI)
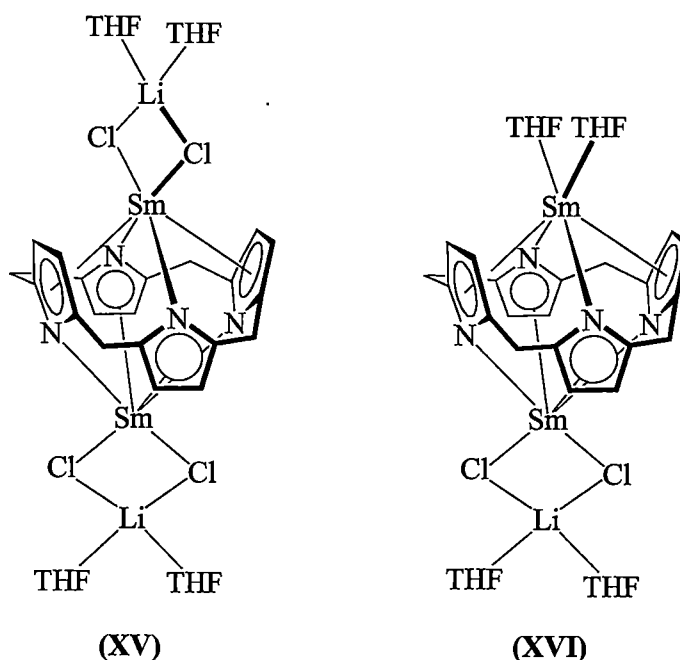
Treatment of $SmCl_3(THF)_2$ with one equivalent of $[(Et_8N_4)Li_4(THF)_4]$ in THF led to a samarium(III) chloride complex $[(Et_8N_4)Sm(Cl)_2Li_3(THF)_3]$, (XVII)[10b]. The formula of the complex is suggested by microanalytical data and the trivalent state of samarium was supported with magnetic moment measurements, but no crystal structure details are available for this complex. However, the analogous reaction using $[\{[(-CH_2-)_5]_4N_4\}Li_4(THF)_4]$ led to the samarium(III) chloride complex $[\{(THF)Li\}_3(\mu_3-Cl)\{[(-CH_2-)_5]_4N_4\}SmCl]$, (XVIII)[10c], which has been structurally characterised. Complex (XVIII) adopts a monomeric form with $\eta^5:\eta^1:\eta^5:\eta^1$-bonding between the samarium centre and the porphyrinogen. One chloride occupies the remaining coordination site of the samarium centre whereas two chlorides are coordinated in (XV) and (XVI). On the other face of the macrocycle, three lithium cations, each coordinated by one THF molecule, are bridged by a single tribridging chloride centre. A lithium cation is σ-bound to a pyrrolide unit which is π-bound to the samarium centre, the second lithium cation is π-bound to a pyrrolide ring which is σ-bound to the samarium centre, and the third lithium cation is bound to the other two pyrrolide rings (σ-bound to the pyrrolide ring which is π-bound to the samarium and π-bound to the pyrrolide ring which is σ-bound to the samarium centre).

(XVIII) (L = THF)   (XIX)
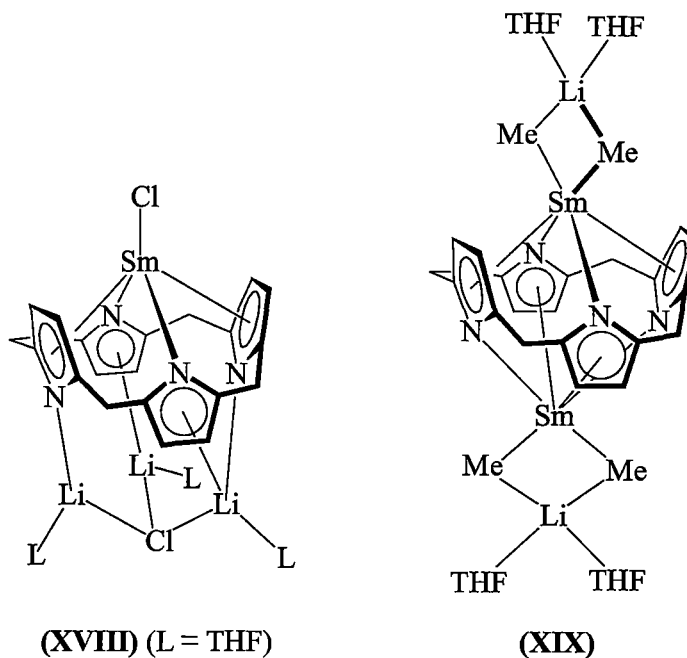
Samarium(III) alkyl complexes have been accessed in a limited number of cases. Reaction of the samarium(III) chloride (XV) with four equivalents of MeLi in diethyl ether led to yellow prisms of the tetramethyl analogue (XIX), whereas the reaction of the samarium(III) chloride (XVII) with an equivalent of RLi (R = Me, vinyl) in diethyl ether led to the yellow-orange or light yellow crystalline samarium(III) alkyl complexes [(THF)$_4$Li$_3$(μ_3-Cl)(Et$_8$N$_4$)SmR], (XX)[10b]. The structures of both alkyl complexes are very similar. The samarium centre is situated in the centre of the macrocycle and is bound to the four pyrrolide rings in $^{-}\eta^5{:}\eta^1{:}\eta^5{:}\eta^1$-fashion. The alkyl group occupies the remaining coordination site of the samarium centre on the same side of the macrocyclic cavity. On the opposite side of macrocyclic cavity, three lithium cations bridged by a single chloride are coordinated to three pyrrolide rings. Two lithium cations are σ-bound through nitrogen centres of pyrrolide rings, while the third lithium cation is π-bound to another pyrrolide ring. A total of four coordinated THF molecules complete the coordination geometry around the three lithium cations. Thus, the Li$_3$(Cl)(THF)$_n$ units in the complexes (XVIII) and (XX) display somewhat different bonding modes to the macrocycles, which highlights the variability that is introduced through alkali metal halide incorporation.

(XX) (R = Me, vinyl, L = THF)   **(XXI)**
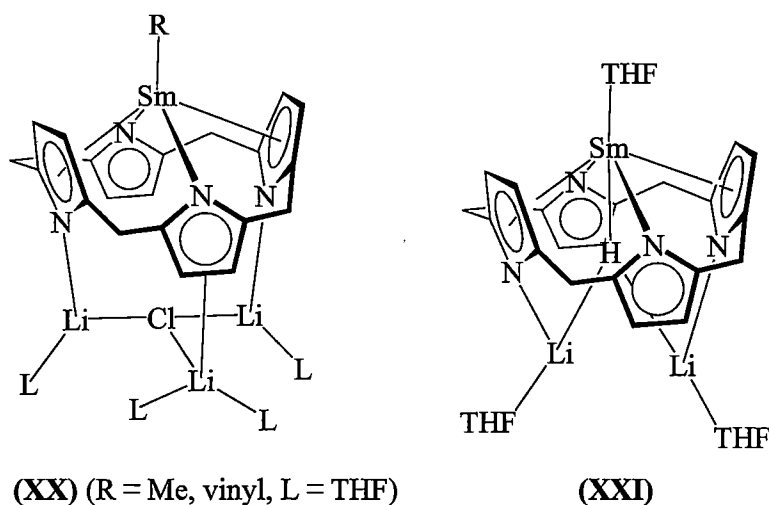
Exposure of a THF solution of **(XX)** (R = Me) to hydrogen gas (1 atm) at room temperature resulted in a rapid reaction from which the hydride derivative [(THF)$_2$Li$_2$(μ-H)(Et$_8$N$_4$)Sm(THF)], **(XXI)**, was isolated in good yield as a pale yellow crystalline solid[10b]. The reaction of **(XX)** with PhSiH$_3$, in place of hydrogen, led to the same product **(XXI)**. Complex **(XXI)** can also be prepared conveniently *via* the direct reaction of the samarium(III) precursor [(THF)$_2$Li(μ-Cl)$_2$Sm(Et$_8$N$_4$)Sm(THF)$_2$], **(XVI)**, with either LiAlH$_4$ or NaHBEt$_3$. The samarium centre in **(XXI)** binds to the macrocycle by a η^5:η^1:η^5:η^1-bonding mode. Each lithium cation is σ-bound to a pyrrolide ring which is π-bound to the samarium centre. Each lithium atom bears an additional coordinated THF molecule and one THF molecule is coordinated to the samarium centre. The hydride was located in the middle of the SmLi$_2$ triangle and is coaxial with the Sm-O vector. This special 'inwards' hydrogen arrangement is different from the alkyl or chloride ligands previously described in complexes **(XV)** to **(XX)** due to its small size and strong bonding with the lithium centres.

- A samarium(III) oxide **(XXII)** has been reported in which the source of the oxygen is believed to be from THF[10c]. An analogous complex is formed from [(η^5-C$_5$Me$_5$)$_2$Sm(THF)$_2$], but in that case the source of oxygen is believed to be from molecular dioxygen[11]. These two analogous oxide complexes are not a rarity, and many reactivity and structural similarities have now be reported between decamethyllanthanocenes and lanthanide porphyrinogen complexes.
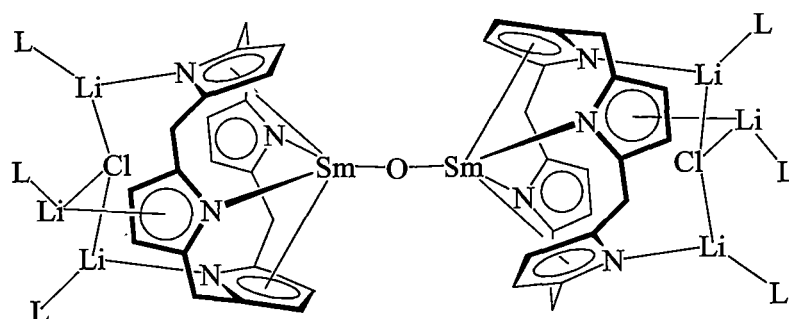
(XXII)

(iii) Lanthanide(III) complexes featuring coordinated activated small molecules

A number of dinitrogen complexes of lanthanide porphyrinogen complexes have been isolated[10c]. The reaction of the samarium(III) complex **(XVII)** with lithium in THF under argon, followed by exposure to nitrogen led to the tetralithium hydrazide complex **(XXIII)**[12a] with the formal four-electron reduction of dinitrogen. The dinitrogen reduced product **(XXIV)** has been obtained from the related samarium(III) precursor **(IX)** which features the retention of sodium cations through the reaction with sodium in the presence of naphthalene in THF under nitrogen. Complex **(XXIV)** contains the two electron reduced $(N_2)^{2-}$ species[12b].
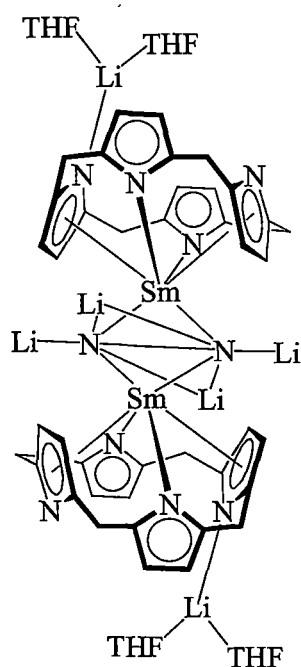
(XXIII)
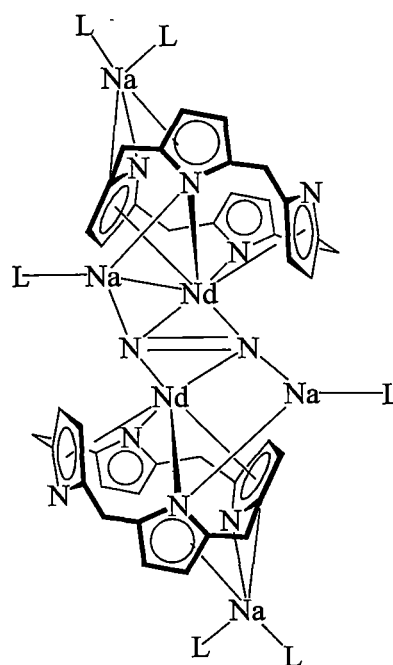
(XXIV) (L = dioxane)

Related reactions of lanthanide(II) porphyrinogen complexes (or *in situ* reduction of lanthanide(III) porphyrinogen complexes) with small molecules such as ethylene and acetylene have led to various forms of small molecule activated complexes somewhat analogous to the dinitrogen reduction chemistry[12c] which also have parallels in decamethyllanthanocene chemistry[13].

5.2 RESULTS AND DISCUSSION

5.2.1 Samarium(III) halide complexes of modified porphyrinogens

5.2.1.1 Syntheses of samarium(III) iodide or chloride complexes (17), (18) and (19)

The samarium(III) iodide complex [(Et$_8$O$_2$N$_2$)SmI], (17), derived from *meso*-octaethyl-*trans*-dioxaporphyrinogen (3), was prepared by oxidation of the divalent samarium precursor (15) with iodine in THF, as shown in Equation 2.

$$[\{(THF)_2K(Et_8O_2N_2)Sm(\mu\text{-}I)_2\}_2] \xrightarrow[\text{THF}]{I_2} 2\,[(Et_8O_2N_2)SmI] + 2\,KI + 4\,THF$$

$$\text{(15)} \qquad\qquad\qquad\qquad\qquad \text{(17)}$$
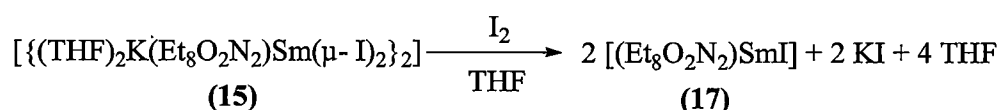
Equation 2

The reaction giving the samarium(III) iodide (17) is rapid and the stoichiometry was controlled through the distinct colour change observed. To a THF solution of the divalent samarium complex (15) of green colour, was added dropwise half a molar equivalent of iodine (1.0 M solution in THF) of brown colour. Upon the mixing of two reactants the brown colour of iodine dissipated. When half a molar equivalent of iodine had been added a yellow solution of complex (17) resulted. Complex (17) is moderately soluble in THF and is insoluble in toluene and hexane. Complex (17) was isolated by concentration of the THF solution *in vacuo* giving a light yellow powder of complex (17) in 85% yield.

The low solubility and paramagnetism of the samarium(III) complex (17) prevented even ^{1}H NMR spectroscopic characterisation. Microanalytical results show that complex (17) sample contains half a molar equivalent of potassium iodide (per Sm) that possibly arises from contamination with the byproduct rather than arising from a molecular component of the compound. The formulation of complex (17) is further supported by subsequent reaction producing the samarium amide complex (22) (see Section 5.2.3) that has been fully characterised including X-ray structure

determination, as containing no incorporated potassium iodide despite the open face of the macrocyclic cavity.

The samarium(III) chloride complex [(Et$_8$N$_4$Me$_2$)SmCl], (18), derived from *trans-N,N'*-dimethyl-*meso*-octaethylporphyrinogen (6) has been synthesised from the oxidation of divalent samarium precursor (16) using *tert*-butyl chloride as shown in Equation 3.

$$[(Et_8N_4Me_2)Sm(THF)_2] \xrightarrow[\text{THF/toluene}]{\text{Bu}^t\text{Cl}} [(Et_8N_4Me_2)SmCl]$$
$$\text{(16)} \hspace{4cm} \text{(18)}$$
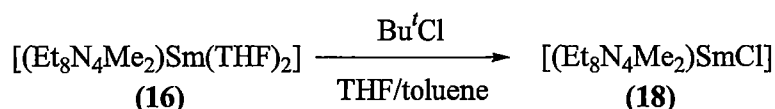
Equation 3

Oxidation of the samarium(II) complex (16) with *tert*-butyl chloride (1 M solution in THF, 1 molar equivalent) was carried out in toluene at ambient temperature. The completion of the reaction was indicated by a colour change from dark brown to light brown. The samarium complex (18) is sparingly soluble in THF and toluene, precipitating from the reaction mixture allowing its isolation by filtration as a light brown powder in 91% yield.

Poor solubility in THF and hydrocarbon solvents and/or the effect of the paramagnetic samarium centre prevented the NMR spectroscopic characterisation of complex (18). However, microanalytical data confirms the stoichiometry as the given formalism. Mass spectrometry (EI-MS) of complex (18), as shown in Figure 1, supports its monomeric formulation. Some ions in the spectrum (m/z = 753 (M$^+$), 726 (M-Et)$^+$) provide strong evidence for a monomeric form, as various mass spectral features expected of higher aggregated forms are absent, *e.g.*, dimers (which is expected to partially cleave to the ion [(Et$_8$N$_4$Me$_2$)SmCl$_2$]$^+$, m/z = 788).
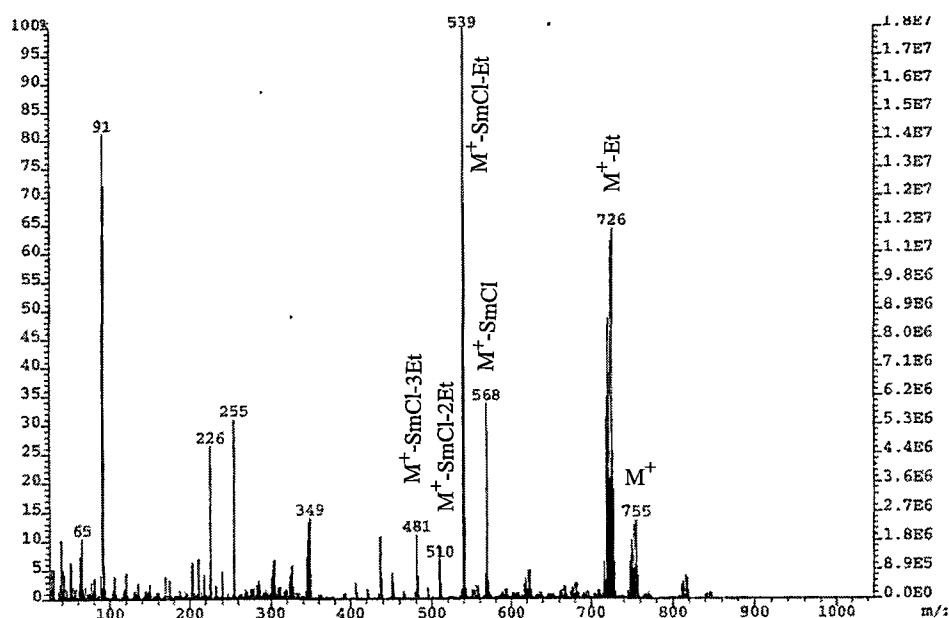
Figure 1: EI-MS spectrum of [(Et$_8$N$_4$Me$_2$)SmCl], **(18)**

The light brown coloured monomeric complex **(18)** partly undergoes slow conversion in THF or THF/toluene solution to the red coloured dimeric samarium(III) chloride complex [{(Et$_8$N$_4$Me$_2$)Sm(μ-Cl)}$_2$], **(19)**, as shown in Equation 4. A small amount of the red complex **(18)** was noticed after storage of the suspension of **(18)** in THF for several weeks at ambient temperature. Raising the temperature in toluene alone led to a faster and more complete transformation of **(18)** to **(19)**.

$$2 \ [(Et_8N_4Me_2)SmCl] \longrightarrow [\{(Et_8N_4Me_2)Sm(\mu\text{-}Cl)\}_2]$$

$$\textbf{(18)} \qquad\qquad\qquad\qquad\qquad \textbf{(19)}$$
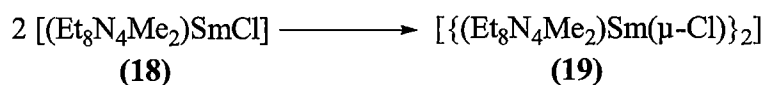
Equation 4

Complex **(19)** has also been prepared directly by the vapour phase diffusion of one equivalent of *tert*-butyl chloride into a toluene solution of [(Et$_8$N$_4$Me$_2$)Sm(THF)$_2$], **(16)**. The red crystalline dimeric complex [{(Et$_8$N$_4$Me$_2$)Sm(μ-Cl)}$_2$], **(19)**, is formed overnight as a main product and was isolated in 75% yield. Complex **(19)** prepared in this manner, is possibly formed directly from **(17)**, as shown in Equation 5, rather than the transformation according to Equation 4 in view of the known slow rate of Equation 4 under the similar conditions.

$$[(Et_8N_4Me_2)Sm(THF)_2] \xrightarrow{\text{Bu}^t\text{Cl/toluene}} [\{(Et_8N_4Me_2)Sm(\mu\text{-Cl})\}_2]$$
$$\textbf{(16)} \qquad\qquad\qquad\qquad\qquad \textbf{(19)}$$
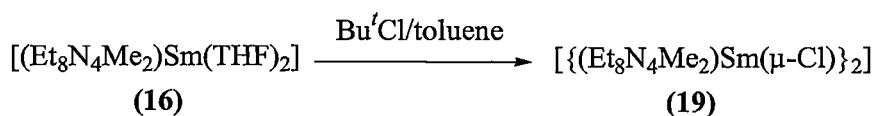
Equation 5

The solvent employed in the reactions giving complexes **(18)** and **(19)** plays a key role in determining the product distribution, through either Equation 3 or Equation 5. Indeed, the diffusion of *tert*-BuCl into the toluene solution of $[(Et_8N_4Me_2)Sm(THF)_2]$, **(16)**, resulted mainly to complex **(18)** rather than **(19)**. The formation of **(19)** in a coordinating solvent containing THF is possibly blocked by weakly coordinated THF molecules (coordinated THF is not indicated by the microanalytical and mass spectral data of complex **(18)** and it is presumably removed *in vacuo* during isolation or coordinates only in solution). The monomeric complex **(18)** with no coordinated solvent transforms more rapidly to **(19)** than the possible THF adduct **(18a)**.

(18a)   **(19)**
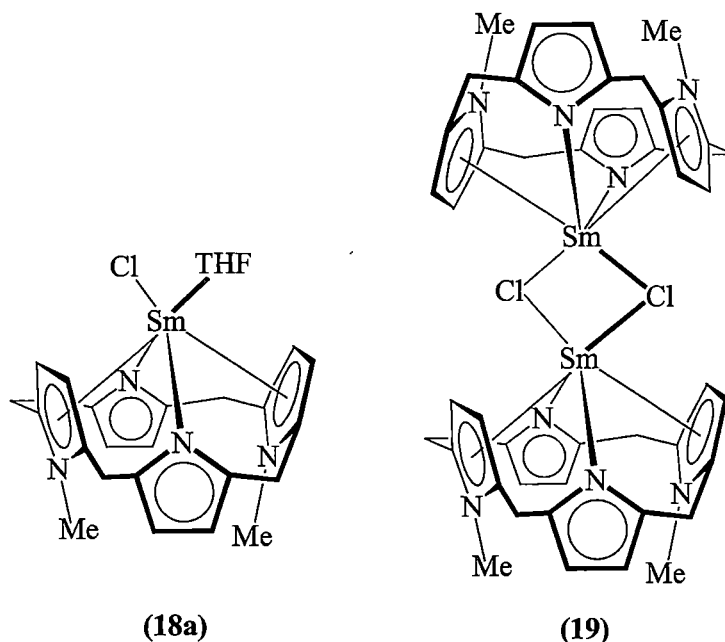
Complex **(19)** has poor solubility in THF and hydrocarbon solvents, as was the case for complex **(18)**. This poor solubility and/or the effect of paramagnetic samarium(III) centre prevented NMR spectroscopic characterisation. Complex **(19)** gave satisfactory microanalytical data. The molecular structure for complex **(19)** has been confirmed by X-ray crystal structure determination (see Section 5.2.1.2).

5.2.1.2 Molecular structure of [{(Et$_8$N$_4$Me$_2$)Sm(μ-Cl)}$_2$], (19)

Red crystals of [{(Et$_8$N$_4$Me$_2$)Sm(μ-Cl)}$_2$], **(19)**, suitable for X-ray crystal structure determination were grown from storage of a suspension of the pale brown complex **(18)** in toluene for three weeks at ambient temperature after it was heated gently for 30 minutes. The crystals were isolated and mounted in sealed thin-walled glass capillaries under an argon atmosphere. The crystals belong to the monoclinic
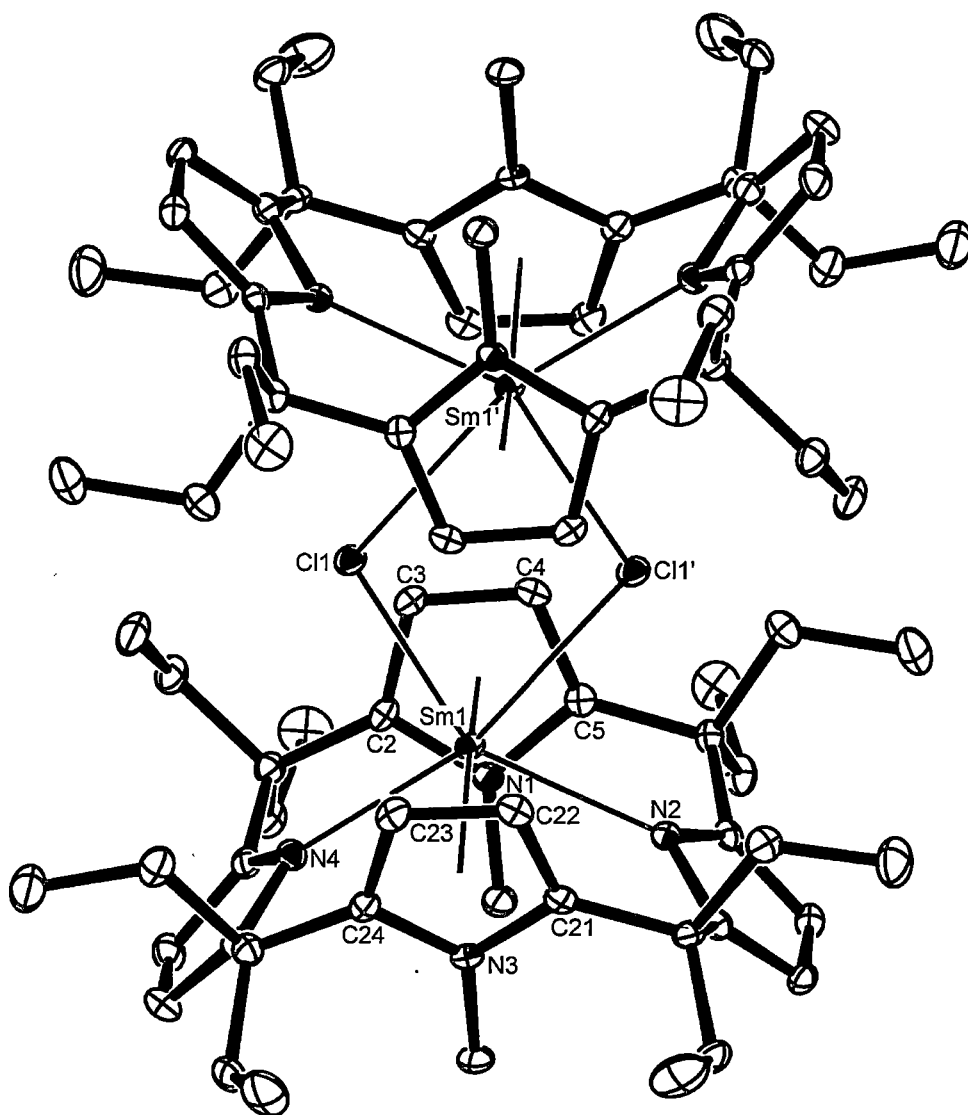
Figure 2: Molecular structure of [{(Et$_8$N$_4$Me$_2$)Sm(μ-Cl)}$_2$], **(19)**, with thermal ellipsoids drawn at the level of 50% probability (protons have been removed for clarity).

space group $C2/c$ (No. 15), $a = 19.4523(2)$, $b = 13.8795(1)$, $c = 26.9726(3)$ Å, $\beta = 106.1366(4)°$, with four molecules in the unit cell. The asymmetric unit comprises one half of the dimeric unit residing on an inversion centre, as shown in Figure 2.

The crystal structure of $[\{(Et_8N_4Me_2)Sm(\mu\text{-}Cl)\}_2]$, **(19)**, shows it to be a dimeric species in the solid state. The samarium centres are bound to the macrocyclic units by η^5:η^1:η^5:η^1-bonding modes. In the same way as was seen for the samarium(II) complex **(16)** derived from the *trans-N,N′*-dimethylated porphyrinogen **(6)**, η^5-interactions to both *N*-methyl pyrrole rings and η^1-binding to both nitrogen centres of pyrrolide rings to the samarium centres are observed for complex **(19)**. The two samarium centres and the two bridging chloride atoms form a Sm_2Cl_2 four-membered ring located at the central part of the molecule which is generated by a crystallographic inversion centre. The four bond lengths within the Sm_2Cl_2 four-membered ring are disparate, with two longer (2.9290(5) Å) and two shorter (2.7511(5) Å) Sm-Cl bonds. The remarkable difference between the two Sm-Cl bonds results from the steric interactions between the two macrocyclic units within the dimer, as shown in Figure 3. Through the formation of the central Sm_2Cl_2 four-membered ring, the β-carbons of the *N*-methyl pyrrole rings are brought in close proximity. As a result of the steric interactions, one macrocyclic unit with its coordinating partners shift slightly side ways to lessen the repulsion between the *N*-methyl pyrrole rings and can be seen to mesh together somewhat. The two angles relating to the Sm_2Cl_2 four-membered ring are Cl(1)-Sm(1)-Cl(1') = 69.923(16) and Sm(1)-Cl(1)-Sm(1') = 110.077(16)°.
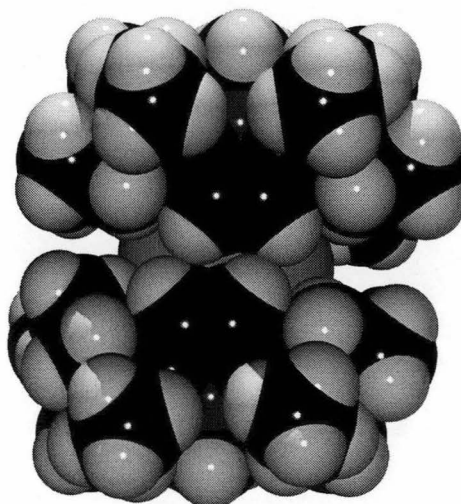
Figure 3: Space filling representation of the molecular structure of $[\{(Et_8N_4Me_2)Sm(\mu\text{-}Cl)\}_2]$, **(19)**.

Each samarium centre is η^1-bound to two pyrrolide units with distances of Sm(1)-N(2) = 2.4879(16) and Sm(1)-N(4) = 2.5378(16) Å through an angle of N(2)-Sm(1)-N(4) = 119.16(5)°. The disparate bond lengths are most likely the result of the asymmetry feature of the Sm_2Cl_2 four-membered ring core of the dimer, as discussed earlier. The η^5-bonding interactions between each samarium centre and two N-methyl pyrrolides measure Sm(1)-η^5(N1) = 2.63_8 and Sm(1)-η^5(N3) = 2.62_8 Å with metallocene bend angle of η^5(N1)–Sm-η^5(N3) = 162.3_3°. Each η^1- and η^5-interactions of (19) between the samarium(III) centre and the macrocyclic unit are shorter than in the related samarium(II) complex (16) (2.6671(16) Å for the η^1- and 2.75_6 Å for η^5-interactions), consistent with the smaller ionic radius of Sm(III) in comparison to Sm(II).

Complex (19) has strikingly different structural features from the samarium(III) complex (XVIII), derived from the unmodified porphyrinogen (4). Complex (XVIII) has two chlorides included in one molecule, and adopts a monomeric form with the inclusion of alkali metal cations[10c]. Complex (19) has relatively longer interactions between samarium(III) centres and the macrocyclic unit than seen in (XVIII) (Sm-N bond distances are 2.457(9) and 2.405(8) Å, while the Sm-centroid distances measure 2.53_0 and 2.54_9 Å). The Sm-Cl bond in (XVIII) (3.15(2) Å) is longer than both Sm-Cl bonds in (19).

In comparison to complex (19), $[\{(\eta^5\text{-}1,3\text{-}(Me_3Si)_2C_5H_3]_2Sm(\mu\text{-}Cl)\}_2]$, (XXV)[14], dimerises by symmetrical $(\mu_2\text{-}Cl)_2$- bridging, Sm-Cl = 2.758(2) Å and 2.771(2) Å. The dimeric $ansa$-metallocene derivative $[\{Ph_2Si(C_{13}H_8)(Bu^tC_5H_3)Y(\mu\text{-}Cl)\}_2]$, (XXVI), possesses similar steric conditions to (19) and also has disparate Y-Cl bond distances within the Y_2Cl_2 four-membered ring, with Y-Cl = 2.633(2) and 2.348(4) Å, while the related $[\{Me_2Si(C_{13}H_8)(C_5H_4)Y(\mu\text{-}Cl)\}_2]$ has two similar Y-Cl bond lengths, 2.649(2) and 2.638(2) Å.

The metallocene bend angle in (19) (162.3_3°) is larger than that of (16) (154.4_4°) and accord with the short Sm-macrocyclic interactions in (19), and much larger than that of (XXV) ($129._6$°), but smaller than that of (XVIII) (171.84°).

The pyrrolide or N-methylpyrrole rings defining the size of the macrocyclic cavity in complex (19) display the following opposing N⋯N nonbonding distances, 4.33_4 Å for N(2)⋯N(4) and 4.66_4 Å for N(1)⋯N(3). The tilt angles of the N-methylpyrrole rings are steeper (77.0_3° and 78.0_9°) than the pyrrolide units (46.8_4° and 43.5_4°) with respect to the average plane of the macrocycle. The cavity shape

data further reveal the closer interaction between the samarium(III) centre and the pyrrolide units compared with the samarium(II) complex (16) (see Section 4.2.3.2).

5.2.2 Samarium(III) alkyl complexes of modified porphyrinogens

5.2.2.1 Syntheses of samarium(III) alkyl complexes of modified porphyrinogens

The samarium(III) alkyl complexes [(Et$_8$N$_4$Me$_2$)SmMe], (20), and [(Et$_8$N$_4$Me$_2$)Sm(CH$_2$SiMe$_3$)], (21), have been synthesised as shown in Scheme 1.

i) Bu^{t}Cl

ii) RLi

(16)

(20) R = Me
(21) R = CH$_2$SiMe$_3$
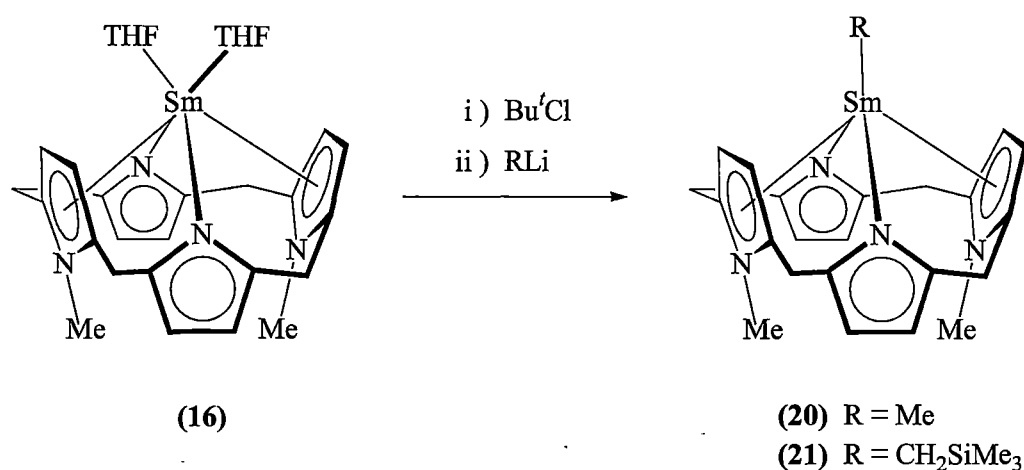
Scheme 1: Syntheses of [(Et$_8$N$_4$Me$_2$)SmMe], (20), and [(Et$_8$N$_4$Me$_2$)SmCH$_2$SiMe$_3$], (21).

The synthesis of the alkyl complexes (20) and (21) were achieved in one-pot reactions by oxidation of the samarium(II) complex (16) with *tert*-butyl chloride giving the samarium(III) chloride complex (18) (see also Section 5.2.1), which was used without further purification in the subsequent metathetical exchange reactions. Thus one equivalent of the alkyllithium reagent was added (a lower temperature of - 30°C is necessary for the synthesis of (20), while the room temperature reaction was sufficient for (21)) and stirred overnight at ambient temperature. An insoluble by-product, presumably lithium chloride, was filtered off and the products recrystallised from diethyl ether (for (20)) or 40-60°C petroleum ether (for (21)) giving compounds (20) and (21) as orange crystalline solids in moderate yields (54% for (20) and 62% for (21)). Both complexes are soluble in THF, diethyl ether and toluene. Complex (21) is only moderately soluble in 40-60°C petroleum ether while (20) is slightly soluble in 40-60°C petroleum ether. Both complexes appear to be moderately sensitive to air and moisture.

Complexes (20) and (21) have been characterised by ^{1}H NMR spectroscopy, microanalysis and single crystal X-ray structure determinations.

All resonances in the ^{1}H NMR spectra of (20) and (21) have been assigned, see Table 1. Resonances common to both (20) and (21) appear at very similar chemical shifts. The CH_2 or CH_3 protons directly bound to the samarium centres appear as broadened resonances at downfield chemical shifts of 8.94 and 9.56 ppm for (20) and (21), respectively. The resonances at 6.76 and 2.98 ppm for (20), 6.77 and 2.94 ppm for (21) are assigned to aromatic protons of pyrrolide or N-methylpyrrole rings. The N-methyl protons in both complexes appear at 3.69 and 3.50 ppm for (20) and (21), respectively. Four sets of multiplets for each complex are attributable to CH_2 protons of the meso-ethyl substituents at similar chemical shifts. The methyl protons of the meso-ethyl substituents appear as two triplets with different coupling constants (6.8 and 7.2 Hz, for (20), 6.8 and 7.6 Hz for (21)) at -0.56, 1.44 ppm for (20), and -0.53, 1.44 ppm for (21).

Compound number	SmCH$_2$/SmCH$_3$	=CH, pyr/pyrMe	NCH$_3$	CH$_2$	CH$_3$	SiCH$_3$
(20)	8.94, broad	2.98, 6.76	3.69	1.13, 1.53, 1.95, 2.50	-0.56, 1.44	-
(21)	9.56, broad	2.94, 6.77	3.50	1.18, 1.51, 1.96, 2.75	-0.53, 1.44	0.97

Table 1: ^{1}H NMR spectral data for complexes (20) and (21) (C$_6$D$_6$, 399.694 MHz, 298 K, ppm)

The gCOSY spectrum of complex (20) reveals that the CH_3 (δ = -0.56 ppm) and CH_2 protons (δ = 1.95 and 1.53 ppm) belong to one meso-ethyl group while the CH_3 (δ = 1.44 ppm) and CH_2 prorons (δ = 2.50 and 1.13 ppm) belong to the other meso-ethyl group. The CH_3 (δ = -0.53 ppm) and CH_2 protons (δ = 1.96 and 1.51 ppm) belong to one meso-ethyl group, while the CH_3 (δ = 1.44 ppm) and CH_2 protons (δ = 2.75 and 1.18 ppm) belong to the other meso-ethyl group.

5.2.2.2 Molecular structure of [(Et$_8$N$_4$Me$_2$)SmMe], (20)

Orange crystals of $[(Et_8N_4Me_2)SmMe]$, **(20)**, suitable for X-ray crystal structure determination were grown from a hot saturated toluene 40-60°C petroleum ether solution (1:1, v/v) which was allowed to cool slowly to ambient temperature and stood for overnight. The crystals were isolated and mounted in sealed thin-walled glass capillaries under an argon atmosphere. The crystals belong to the space group *Pnma* (No. 62), $a = 14.271(1)$, $b = 17.676(2)$, $c = 16.520(1)$ Å, with four molecules in the unit cell, with the asymmetric unit consisting one half of a molecule of $[(Et_8N_4Me_2)SmMe]$, **(20)**, which resides on a mirror plane. The overall molecular symmetry approximates to C_{2v}, as shown in Figure 4.

Figure 4: Molecular structure of $[(Et_8N_4Me_2)SmMe]$, **(20)**, with thermal ellipsoids drawn at the level of 50% probability, protons have been removed for clarity.

The samarium centre in complex **(20)** displays a $\eta^5:\eta^1:\eta^5:\eta^1$-bonding mode with the macrocyclic unit, which displays a 1,3-alternate conformation. The samarium centre adopts η^5-interactions to both *N*-methyl pyrrole rings and σ-bonding to both nitrogen centres of the pyrrolide rings. The methyl anion binds to the samarium centre on the opposite side of the macrocyclic cavity to the *N*-methyl substituents, blocking further coordination of metal centre within the macrocyclic cavity.

The samarium centre in complex (20) binds to methyl ligand with a Sm-C distance of 2.4242(51) Å. The samarium centre coordinates to the macrocyclic unit by two Sm-N interactions of the same distance, 2.4780(29) Å, and two η^5-interactions with Sm-centroid bond lengths of 2.59_3 and 2.60_9 Å. The related angles are C(0)-Sm-N(11) = 116.09(7)°, N(11)-Sm-N(11') = 127.82(9)° and the metallocene bend angle is 168.8_6°.

The methyl ligand binds to the samarium centre in (20) with shorter distances than in [(η^5-C$_5$Me$_5$)$_2$SmMe(THF)], (XXVII)[15], 2.484(14) Å, and (XX), 2.496(6) Å[10b]. The two Sm-N bond distances to the pyrrolide nitrogens in (20) are equivalent but those of (XX) are inequivalent and remarkably different at 2.465(5) Å and 2.716(5) Å, presumably a result of the cavity-bound lithium cations. The lengths of the two η^5-interactions between the samarium centre and two N-methylated pyrrole units are slightly longer than those in (XX) 2.56_9 and 2.60_2 Å. The metallocene bend angle formed by two η^5-interactions in (20) is slightly smaller than those of (XX) (170.7_1° and 171.0_7° for two independent molecules in crystal structure), but still much larger than in (XXVII), 134.$_9$°. This bend angle is also larger than in the samarium(II) complex (16), 154.4$_4$°, which is consistent with the closer interactions between the samarium(III) centre and macrocyclic unit in the case of (20).

The cross-cavity N⋯N distances between two pyrrolide nitrogen centres, N(11)⋯N(11'), is 4.44_8 Å and the two N-methylpyrrole nitrogens, N(21)⋯N(41) is 4.71_2 Å. The tilt angles of two N-methylpyrrole rings are steeper at 80.5_7 and 78.8_1° than the two pyrrolide rings at 50.15°. The cavity size differences in complex (20), in terms of the cross-cavity distances and tilt angles of the constituent rings, reveal again a closer interaction between the samarium centre and the macrocyclic unit compared with the samarium(II) complex (16) (see Section 4.2.3.2).

5.2.2.3 Molecular structure of [(Et$_8$N$_4$Me$_2$)SmCH$_2$SiMe$_3$], (21)

Orange crystals of [(Et$_8$N$_4$Me$_2$)SmCH$_2$SiMe)], (21), suitable for X-ray crystal structure determination were grown from a hot saturated 40-60°C petroleum ether solution which was allowed to cool slowly to ambient temperature and stood overnight. The crystals were isolated and mounted in sealed thin-walled glass capillaries under an argon atmosphere. The crystals belong to the triclinic space group $P\bar{1}$ (No. 2), a = 12.453(4), b = 16.999(5), c = 22.490(7) Å, α = 101.204(4), β = 104.691(4), γ = 101.691(4)°, with four molecules in the unit cell. The asymmetric unit consists of two molecules of [(Et$_8$N$_4$Me$_2$)SmCH$_2$SiMe$_3$], (21). Molecule 1

exhibits 50:50% occupational disorders in two of the *meso*-ethyl substituents, as shown in Figure 5. Molecule 2 has a similar geometry to molecule 1, however, it is extremely badly disordered which prevents any quantitative discussion of that molecule. The disorder in molecule 2 involves a 50:50% two-site occupational disorder of the whole macrocycle and the trimethylsilyl substituent, with each position rotated about the Sm-methyl bond vector by *ca.* 10-15°. As a result, all atoms in molecule 2 have only been refined isotropically.
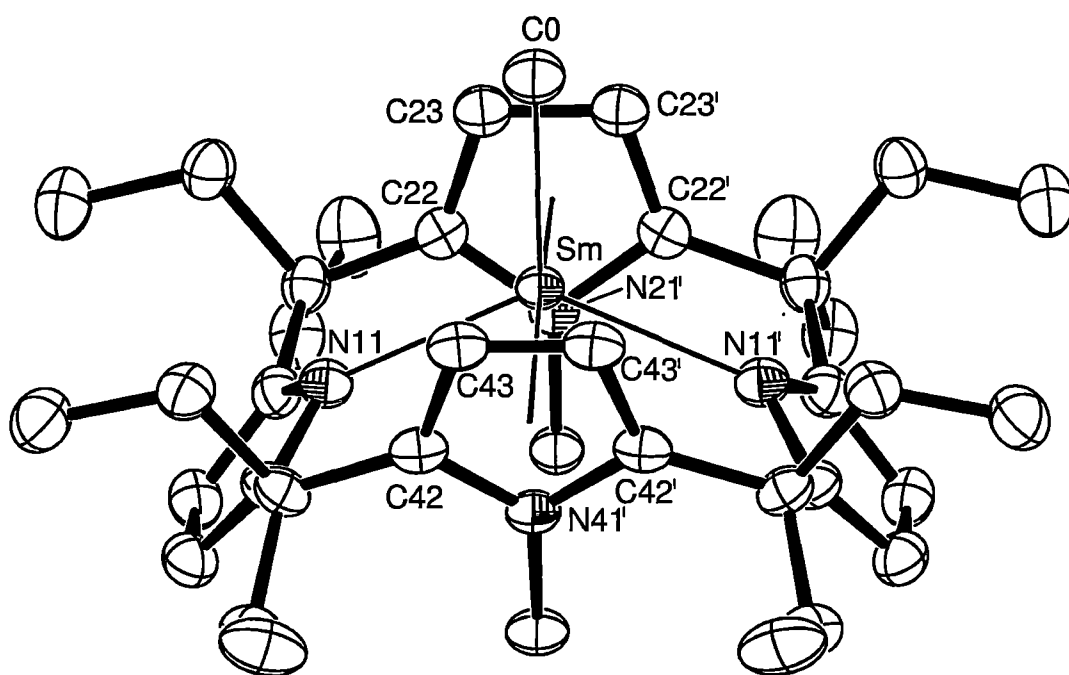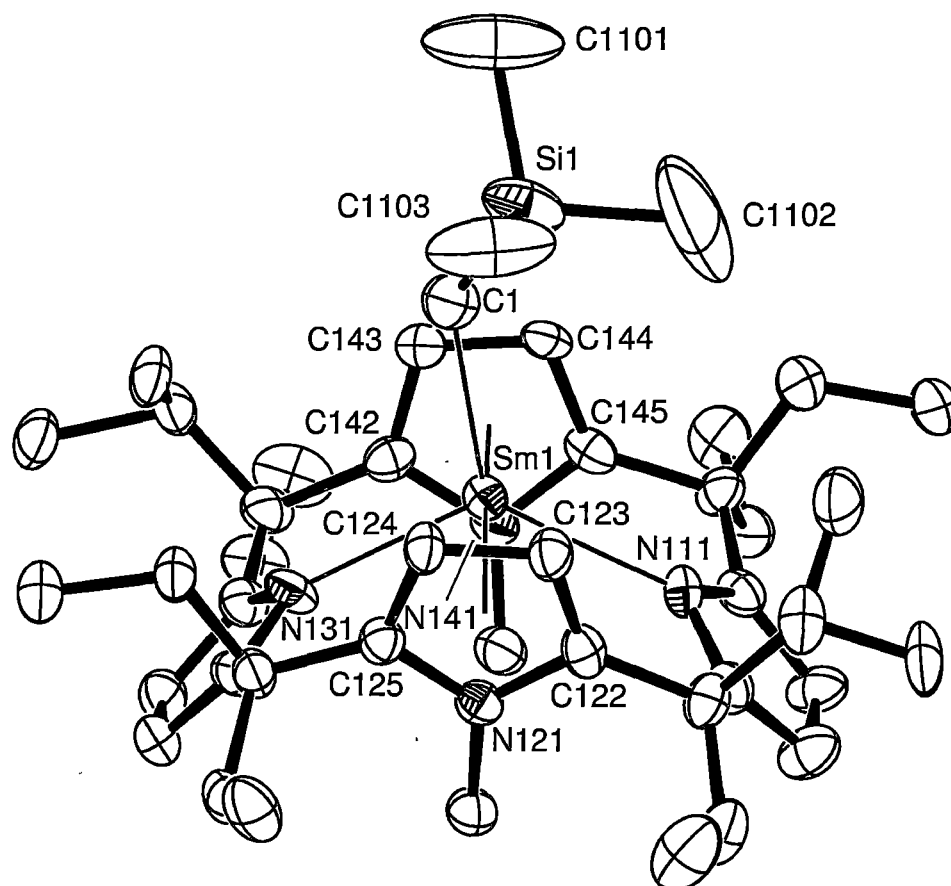

Figure 5: Molecular structure of [(Et$_8$N$_4$Me$_2$)SmCH$_2$SiMe$_3$], **(21)**, with thermal ellipsoids drawn at the level of 50% probability, protons have been removed for clarity. The 50:50% disorder in two of the *meso*-ethyl groups are shown.

The crystal structure of [(Et$_8$N$_4$Me$_2$)SmCH$_2$SiMe$_3$], **(21)**, shows it to be a monomeric species in the solid state. Similar to the methyl samarium(III) complex **(20)**, complex **(21)** chooses the same bonding mode between the samarium centre and the macrocyclic unit. The samarium centre is bound in η^5:η^1:η^5:η^1-fashion to the macrocyclic unit, forming a 1,3-alternate macrocyclic conformation. The trimethylsilylmethyl ligand binds to the samarium centre on the opposite side of the

macrocyclic cavity to the *N*-methyl groups which block further coordination inside the macrocyclic cavity.

The structure of complex **(21)** is very similar to that of complex **(20)**. The samarium centre in complex **(21)** is bound to the alkyl carbon with Sm-C = 2.453(7) Å and to the macrocyclic unit through two Sm-N bond distances of 2.501(5) and 2.485(6) Å and two η^5-interactions with Sm-centroid distances of 2.60_6 and 2.60_3 Å which are all slightly longer than those of **(20)**. This comparison indicates that the bulky trimethylsilylmethyl ligand in **(21)** forces a slight expulsion of the samarium centre out of the macrocyclic cavity. In consequence, the N(111)-Sm(1)-N(131) angle of 124.09(18)° and the metallocene bend angle (η^5(N121)-Sm(1)-η^5(N141)) of 166.7_5° are both slightly smaller than in **(20)**. Selected structural data for the two alkyl samarium(III) complexes **(20)** and **(21)** are listed in Table 2.

Complex **(20)**		Complex **(21)**	
Sm-C(0)	2.4242(51)	Sm(1)-C(1)	2.453(7)
Sm-N(11)	2.4780(29)	Sm(1)-N(111)	2.501(5)
		Sm(1)-N(131)	2.485(6)
Sm-η^5(N21)	2.59_3	Sm(1)-η^5(N121)	2.60_6
Sm-η^5(41)	2.60_9	Sm(1)-η^5(N141)	2.60_3
C(0)-Sm-N(11)	116.09(7)	C(1)-Sm(1)-N(111)	126.5(2)
		C(1)-Sm(1)-N(131)	109.4(2)
N(11)-Sm-N(11′)	127.82(9)	N(111)-Sm(1)-N(131)	124.09(18)
η^5(N21)-Sm-η^5(N41)	168.8_6	η^5(N121)-Sm(1)-η^5(N141)	166.7_5

Table 2: Selected bond lengths (Å) and angles (°) for complexes **(20)** and **(21)**.

Variations between the two C-Sm-N angles of 109.4(2) and 126.5(2)° in complex **(21)** possibly arise from the steric effect between trimethylsilylmethyl ligand and the macrocyclic unit. The variation within the C(1)-Si-C angles of the trimethylsilylmethyl ligand at 109.1(6), 113.7(5) and 113.9(4)° are possibly caused

by steric effects between the methyl groups and *N*-pyrrolide units giving the two larger angles while the third methyl group is directed towards a pyrrolide unit and is not subject to this steric effect. A weak γ-H agostic interaction with the samarium centre is also possible with the shortest associated distances involving C1102 of Sm⋯C and Sm⋯H of 4.38$_3$ and 4.00$_7$ Å, respectively.

The structures of the alkyl complexes (20) and (21) feature in common the absence of THF coordinated to the samarium centres, which was also found in the samarium(III) complex (XX)[10b]. This differs from the metallocene complexes [(η^5-C$_5$Me$_5$)$_2$Sm(Me)(THF)], (XXVII)[15], and [(η^5-C$_5$H$_5$)$_2$Lu(CH$_2$SiMe$_3$)(THF)], (XXVIII)[16].

The cross-cavity N⋯N distances in (21) between the two pyrrolide nitrogens N(111)⋯N(131), is 4.40$_3$ Å, which is slightly shorter than that of (20) (4.44$_8$ Å). The two *N*-methylpyrrole nitrogens N(121) and N(141) are separated by 4.71$_6$ Å, which is nearly the same as in (20), 4.71$_2$ Å. The tilt angles of the two *N*-methylpyrrole rings 79.0$_4$ and 79.4$_9$° are similar with those of (20), 80.5$_7$ and 78.8$_1$°, while the two pyrrolide rings have tilt angles of 48.4$_5$ and 47.0$_3$° which are flatter than those in (20), 50.15°. The cavity of (21), in terms of cross-cavity distances and tilt angles of the constituent rings, has a similar size to (20) and reveals again a closer interaction between the samarium centre and the macrocyclic unit compared with the samarium(II) complex (16).

5.2.3 Samarium(III) amide complexes of modified porphyrinogens

5.2.3.1 Syntheses of samarium(III) amide complexes of modified porphyrinogens

The samarium(III) amide complexes [(Et$_8$O$_2$N$_2$)SmN(SiMe$_3$)$_2$], (22), and [(Et$_8$N$_4$Me$_2$)SmN(SiMe$_3$)$_2$], (25), derived from *meso*-octaethyl-*trans*-dioxaporphyrinogen, (3), and *trans-N,N′*-dimethyl-*meso*-octaethylporphyrinogen, (6), were prepared from the metathetical exchange reactions of the samarium(III) halide complexes [(Et$_8$O$_2$N$_2$)SmI], (17), or [(Et$_8$N$_4$Me$_2$)SmCl], (18), with sodium bis(trimethylsilyl)amide in THF, as outlined in Scheme 2.

[(Et$_8$O$_2$N$_2$)SmI] **(17)**

or

[(Et$_8$N$_4$Me$_2$)SmCl] **(18)**

$\xrightarrow{\text{NaN(SiMe}_3)_2}$

(22) X = N, Y = O
(25) X = NMe, Y = N
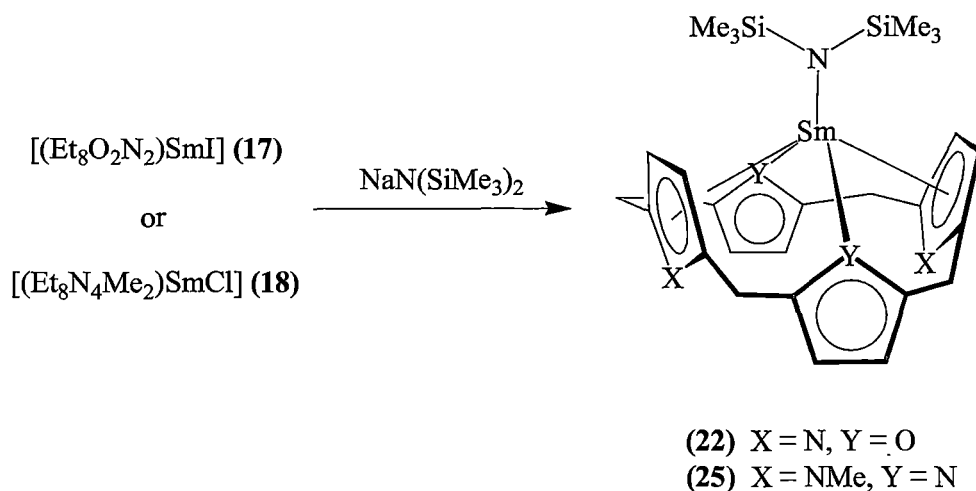
Scheme 2: Synthesis of [(Et$_8$O$_2$N$_2$)SmN(SiMe$_3$)$_2$], **(22)**, and [(Et$_8$N$_4$Me$_2$)SmN(SiMe$_3$)$_2$], **(25)**.

The samarium(III) halide complexes, prepared *in situ* from the oxidation of the divalent samarium(II) complexes **(15)** or **(16)** (see Section 5.2.1), were mixed in THF or THF/toluene with one equivalent of sodium bis(trimethylsilyl)amide and the mixture was stirred at ambient temperature. After three hours (for [(Et$_8$O$_2$N$_2$)SmN(SiMe$_3$)$_2$], **(22)**) or overnight (for [(Et$_8$N$_4$Me$_2$)SmN(SiMe$_3$)$_2$], **(25)**), the THF or THF/toluene was removed *in vacuo* and replaced by toluene. The only byproduct, presumably sodium iodide or sodium chloride, which is insoluble in toluene was separated by filtration. Complexes **(22)** and **(25)** were isolated by recrystallisation from toluene in 75% and 73% yield as yellow or orange crystals, respectively.

Exactly one molar equivalent of sodium bis(trimethylsilyl)amide should be used in the metathetical reactions to achieve the highest yields of complexes **(22)** and **(25)**. Extra sodium amide added in the reaction can result in metallation of the samarium amide products and subsequent samarium displacement can also occur (see Section 5.2.3.2). The rates of the two metathesis reactions varies notably, most likely due to the different solubility of the two samarium(III) halide complexes **(17)** and **(18)** in THF or THF/toluene. The homogeneous reaction, in the case of preparing **(22)**, occurs faster than the heterogeneous reaction in the case of **(25)**. The former reaction is complete in three hours, whereas the latter reaction requires overnight stirring to reach completion.

Both amide complexes **(22)** and **(25)** are soluble in THF and toluene, but are only slightly soluble in hexane. The good solubility of complexes **(22)** and **(25)** are expected due to the bulkiness of the ligand and the smaller Sm(III) centres residing deeper within the macrocyclic cavities.

Complexes **(22)** and **(25)** adopt monomeric structures without the presence of coordinated solvent molecules. In contrast to the structures of complexes of **(15)** and **(23)**, the macrocycle in complex **(22)** hosts only a single metal centre, leaving one vacant face of the dioxaporphyrinogen macrocyclic unit. Another two plausible structural alternatives for **(22)**, (a) and (b) possess similar features to that of complexes **(15)** and **(23)** (see Section 5.2.3.5), as shown in Figure 6. However, NMR spectroscopic studies of recrystallised samples of **(22)** show no differences in the presence of added NaI or NaN(SiMe$_3$)$_2$.

(a)

(b)
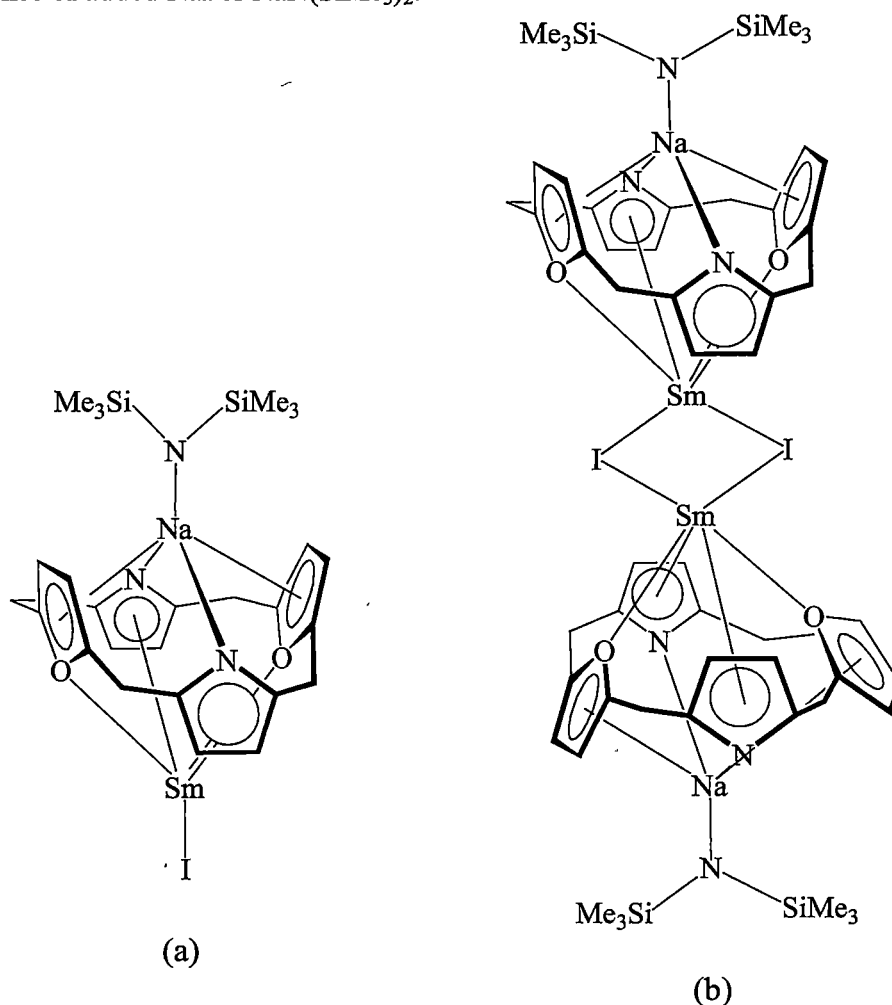
Figure 6: Plausible alternative structures for complex **(22)** which host two metal centres within the macrocyclic cavity.

Complexes **(22)** and **(25)** appear to be moderately sensitive to air and moisture. Both complexes have been characterised by IR, ^{1}H NMR and ^{13}C NMR spectroscopies, microanalysis and single crystal X-ray structure determinations.

5.2.3.2 Metallation and samarium displacement

The samarium(III) amide complex **(22)** of the dioxaporphyrinogen **(3)** reacts with excess sodium or potassium bis(trimethylsilyl)amide leading to deprotonation of a γ-methyl group of one trimethylsilyl group of the amide ligand affording complexes **(23)** and **(24)**. Samarium displacement by alkali metals results in the presence of a large excess of the alkali metal amide, as shown in Scheme 3.

(23) (M = Na), **(24)** (M = K), (L = THF)

M = Na **(10)**, K, L = THF
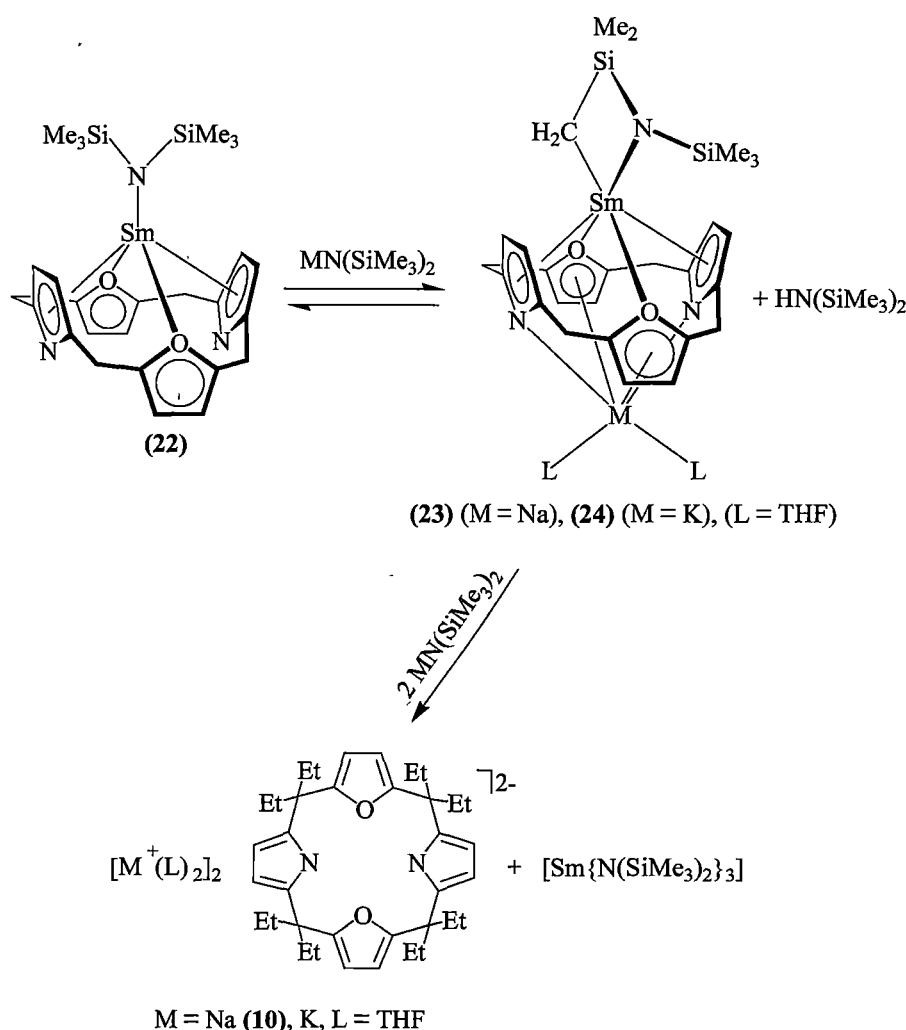
Scheme 3: Deprotonation and samarium displacement from [(Et$_8$O$_2$N$_2$)SmN(SiMe$_3$)$_2$], **(22)**, in the presence of alkali metal amides.

The reaction of complex (22) with one equivalent of sodium bis(trimethylsilyl)amide in THF at 55°C leads to a pale red solution after 3 hours (solutions of (22) are yellow). After the removal of all THF *in vacuo*, recrystallisation of the residue from toluene led to crystals of both the yellow reactant (22) and the red deprotonated complex (23) isolated in 20% yield as a toluene adduct (η^6-sodium complex). In consequence of the metallation of the γ-methyl group, an alkali metal cation with coordinating solvent resides in the macrocyclic cavity along with the samarium centre.

Complex (23) (toluene adduct), despite being crystallised from toluene, is no longer soluble in toluene, but is soluble in THF. Complex (23) presumably exists as a bis(THF) adduct in THF rather than as a toluene adduct, since the ^{1}H NMR of complex (23) is identical in THF solution with or without the presence of toluene (excepting the toluene proton resonances). The very long Na-η^6 (toluene) bond distance in the structure of (23) supports the suggestion of the toluene/THF exchange for (23) in THF solution.

Complex (23) (M = Na, toluene adduct) was characterised by ^{1}H NMR spectroscopy, microanalysis and X-ray single crystal structure determination. Characterisation of the potassium analogue was limited to *in situ* ^{1}H NMR studies of the metallation of (22) with potassium bis(trimethylsilyl)amide.

The γ-methyl deprotonation of the amide ligand of complex (22) is reversible, as shown in Equation 5. The equilibrium can be affected by a number of factors, *e.g.*, (i) the product (23) reverts back to (22) by reaction with Brønsted acids such as H_2O, and (ii) addition of sodium hydride removes byproduct bis(trimethysilyl)amine, which drives the reaction towards the formation of (23).

$$[(Et_8O_2N_2)SmN(SiMe_3)_2] \underset{H^+}{\overset{MN(SiMe_3)_2}{\rightleftharpoons}}$$

(22)

$$[(THF)_2M(Et_8O_2N_2)SmN(SiMe_3)Si(Me)_2CH_2] + HN(SiMe_3)_2$$

M = Na, (23), M = K, (24)
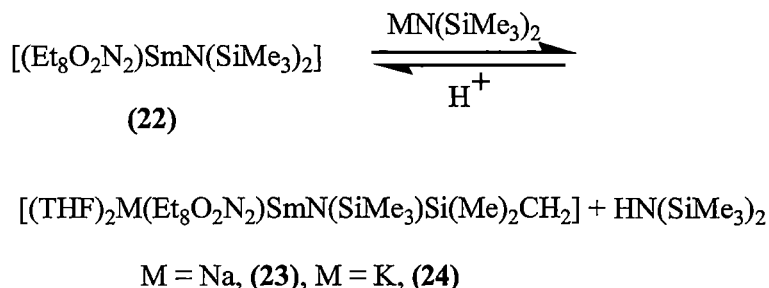
Equation 5

Compound (23) reacts with excess sodium bis(trimethylsilyl)amide leading to samarium exchange with the alkali metal. Thus the macrocyclic samarium complex

is transformed to the disodium complex $[(Et_8O_2N_2)Na_2(THF)_4]$, while the samarium centre is transformed to samarium tris(bis(trimethylsilyl)amide) in the metal exchange reaction.

The reaction of $[(Et_8O_2N_2)SmN(SiMe_3)_2]$, (22), with a large excess of potassium bis(trimethylsilyl)amide instead of sodium bis(trimethylsilyl)amide results in a more rapid deprotonation which is, again, followed by samarium displacement. Thus, when the yellow samarium amide complex $[(Et_8O_2N_2)SmN(SiMe_3)_2]$, (22), is reacted with a large excess of potassium bis(trimethylsilyl)amide at room temperature, the colour changed to light red in five minutes, which in turn changed to a colourless solution overnight in ambient temperature indicating that complete samarium exchange had occurred.

The samarium displacement reaction using either potassium or sodium bis(trimethylsilyl)amide appears to proceed *via* (23) or (24) to the disodium or dipotassium ((10), L = THF) complex of the dioxaporphyrinogen rather than (22) being transformed directly to sodium or potassium ((10), L = THF) complex. This mechanism has been confirmed by a kinetic study which will be described below. This reactivity suggests that it is unlikely to be able to prepare samarium(III) amide complexes of the dioxaporphyrinogen (3) through the following metal exchange reaction shown in Equation 6.

$$[(Et_8O_2N_2)K_2(THF)_4] + [Sm\{N(SiMe_3)_2\}_3]$$
$$\textbf{(10) (L = THF)}$$

$$\longrightarrow\!\!\!\times\!\!\!\longrightarrow \quad [(Et_8O_2N_2)SmN(SiMe_3)_2] + 2\ KN(SiMe_3)_2$$
$$\textbf{(22)}$$
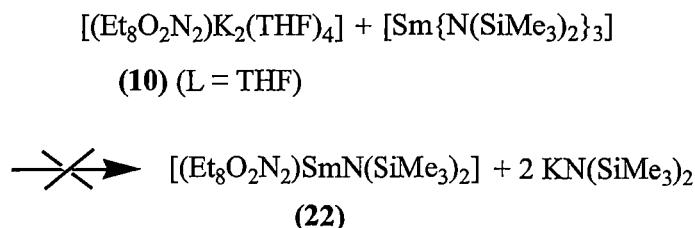
Equation 6

Kinetic studies of the deprotonation and subsequent samarium displacement of (22), based on ^1H NMR spectroscopy, were performed at 50°C and 55°C with an excess of sodium bis(trimethylsilyl)amide (ratio to (22) equals 3:2 (w/w) at 50°C (Figure 7 (a)) and 5:1 (w/w) at 55°C (Figure 7 (b)).

The ratio of the species involved in the deprotonation of (23) were based on the resonances of four aromatic protons of (22) at 14.94 ppm, four aromatic protons of (23) at 6.69 and 7.24 ppm and eight pyrrolide and furanyl protons at 5.95 and 6.15 ppm of the disodium or dipotassium ((10), L = THF) complexes of the

(a)

(b)
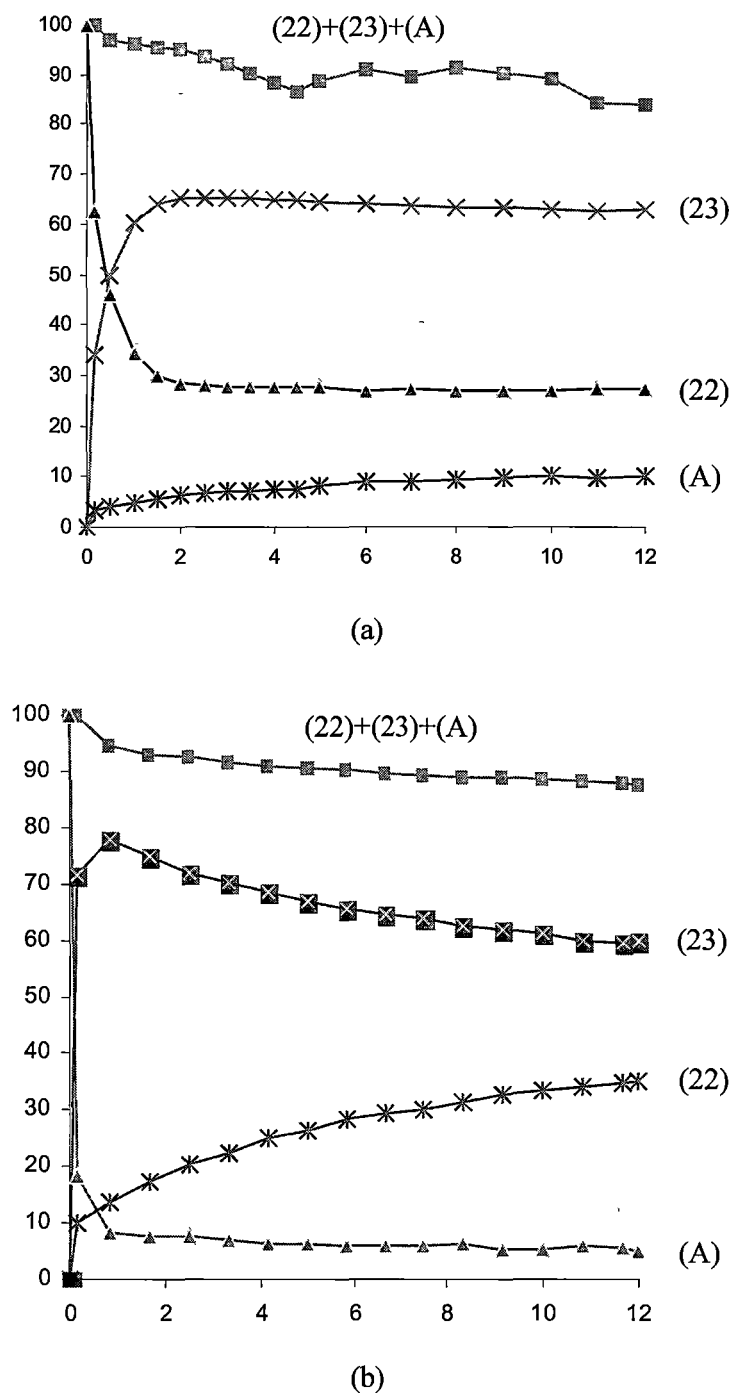
Figure 7: Metallation/samarium displacement of $[(Et_8O_2N_2)SmN(SiMe_3)_2]$, **(22)**, reacting with $NaN(SiMe_3)_2$ (A = $[(Et_8O_2N_2)Na_2(THF)_4]$, ^1H NMR, 399.694 MHz, THF-d^8 as solvent), (a) at 50°C [$NaN(SiMe_3)_2$:**(22)** = 3:2, (w/w)]; (b) at 55°C [$NaN(SiMe_3)_2$:**(22)** = 5:1, (w/w)].

dioxaporphyrinogen (3). The relative concentrations of each of the species were determined using the integration of each resonance (absolute integration mode). As the concentration summation of all three compounds decreased continuously from the initial value (scaled to 100%), a slow unknown decomposition reaction presumably occurs.

The deprotonation of (22) proceeds rapidly in both kinetic experiments, with the concentrations of compounds (22) and (23) dropping and climbing sharply, respectively, in the first hour. The former compound decreases to 37% (Figure 7 (a)) and to 8% (Figure 7 (b)) while the latter rises from 0% to 60% (Figure 7 (a)) and 77% (Figure 7 (b)) after only one hour.

In the first kinetic experiment, the concentration of compounds (22) and compound (23) decrease and increase, respectively, slowly in the second hour. After two hours, the concentration of (22) remained nearly unchanged and complex (23) decreased, by further reaction to form $[(Et_8O_2N_2)Na_2(THF)_4]$ slowly with the slight excess of $NaN(SiMe_3)_2$.

The second kinetic experiment shows that the concentration of compound (22) decreases slowly from 8% after the first hour to 5% (after 12 hours) and compound (23) decreased more rapidly from 77% (after the first hour) to 60% (after 12 hours). The more rapid decrease in the concentration of (23) is rationalised by the presence of a still larger excess of $NaN(SiMe_3)_2$ remaining after the deprotonation of (22) which is then implied in the samarium/sodium exchange to give $[(Et_8O_2N_2)Na_2(THF)_4]$ and $[Sm\{N(SiMe_3)_2\}_3]$.

In both experiments, the concentration of $[(Et_8O_2N_2)Na_2(THF)_4]$ increases gradually, but the second experiment sees a more rapid conversion to $[(Et_8O_2N_2)Na_2(THF)_4]$, 35% after 12 hours in the second experiment while it only formed in 8% after the same period in the former case.

$[(Et_8N_4Me_2)SmN(SiMe_3)_2]$, (25), has a greater stability towards γ-methyl deprotonation by the alkali metal amides compared with $[(Et_8O_2N_2)SmN(SiMe_3)_2]$, (22). When reacted with an excess (3:1; w/w) of sodium bis(trimethylsilyl)amide, deprotonation or subsequent samarium displacement of (25) is not observed. However, slow deprotonation accompanied with a very small extent of samarium displacement is observed using excess (3:1; w/w) of the stronger base potassium bis(trimethylsilyl)amide after three hours at 50°C.

The reactivity difference towards γ-methyl deprotonation of the two samarium amide complexes (22) and (25) reflects the different structural features of the macrocyclic units. The less sterically demanding dioxaporphyrinogen (3) enables an alkali metal to bind within the macrocyclic cavity along with the samarium centre, while the *trans*-N,N'-dimethylated porphyrinogen (6) prevents the alkali metal from binding within the macrocyclic cavity owing to the cavity-blocking position of the two N-methyl groups. The difference in steric demand of macrocycles manifests itself in major structural differences between (23) and the analogue derived from the potassium (or sodium) bis(trimethylsilyl)amide deprotonation of (25), as shown in Figure 8. The lack of suitable coordination options for the alkali metal within the macrocyclic cavity in the latter product (23A) make it less stable relative to (23). Further samarium displacement from (23) is advanced through the *endo*-cavity hosting of the alkali metal cation.

(23) (L = THF)   (23A) (L = THF)
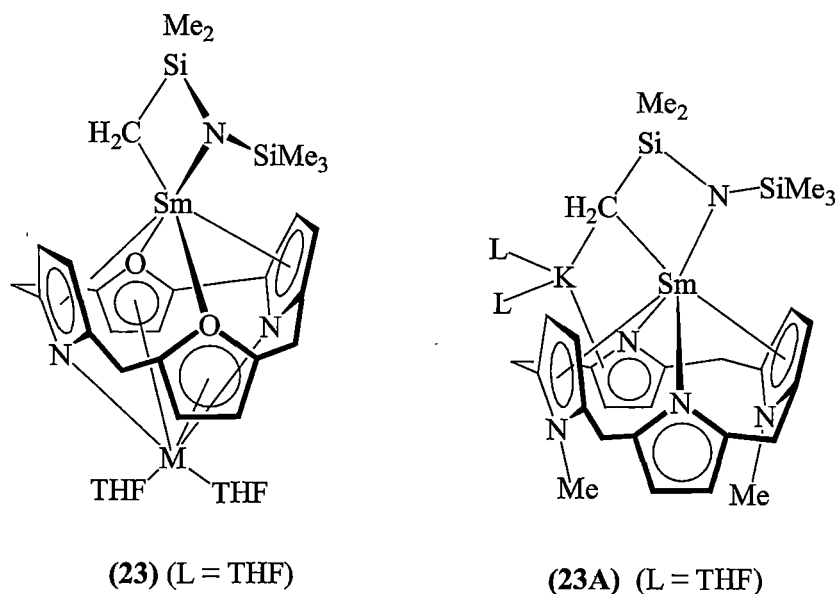
Figure 8: Comparison of the structure of (23) with the possible structure of the deprotonated product (23A) derived from (25).

5.2.3.3 ^{1}H and ^{13}C NMR spectroscopy of samarium(III) amide complexes of modified porphyrinogens

The paramagnetic samarium(III) centre ($4f^5$) has a fairly strong effect in both broadening and shifting the proton resonances in [(Et$_8$O$_2$N$_2$)SmN(SiMe$_3$)$_2$], (22). Thus, the protons resonance within a chemical shift range between δ = -6 ppm to 15 ppm in the ^{1}H NMR spectrum at 25°C in deuterated THF or benzene. Both gCOSY

and gHMBC spectra were obtained to help further assign resonances in both the ^{1}H NMR and ^{13}C NMR spectra of **(22)**.

In the ^{1}H NMR spectrum of [(Et$_8$O$_2$N$_2$)SmN(SiMe$_3$)$_2$], **(22)**, in C$_6$D$_6$, the macrocyclic unit has two chemically inequivalent of aromatic protons appearing as broadened and sharp resonances at δ = 15.14 and 4.48 ppm, respectively. There are four multiplet signals for the CH$_2$ protons of the *meso*-ethyl substituents far separated at δ = -5.89, 1.10, 1.77 and 4.67 ppm. Two chemically inequivalent CH$_3$ groups of the *meso*-ethyl groups appear at well separated chemical shifts of δ = -1.65 and 2.24 ppm, both as triplets with coupling constants of $^3J_{HH}$ = 6.0 and 6.8 Hz, respectively. The large upfield singlet observed at δ = -3.14 ppm is assigned to the trimethylsilyl protons of the amide ligand.

The ^{1}H NMR spectrum of [(Et$_8$O$_2$N$_2$)SmN(SiMe$_3$)$_2$], **(22)**, in THF-d^8 was also recorded. The spectrum is very similar to that decided above, though slight chemical shift changes are observed, most noticeably for the four arometic pyrrolide protons, δ = 4.48 in C$_6$D$_6$ and 4.94 ppm in THF-d^8, which reverse their relative position compared with a methylene resonance of a *meso*-ethyl substituent which remains largely unchanged (δ = 4.67 in C$_6$D$_6$ and 4.64 ppm in THF-d^8).

The ^{13}C NMR spectrum of [(Et$_8$O$_2$N$_2$)SmN(SiMe$_3$)$_2$], **(22)**, exhibits resonances for either the pyrrolide or furanyl ring at δ = 152.2 (=CR) and 126.8 (=CH), whilst the resonances of the other heterocycle appear at δ = 152.0 (=CR) and 120.8 (=CH). The quaternary *meso*-carbon resonance appears at δ = 47.0 ppm, while the adjacent *meso*-ethyl groups appear at δ = 5.2 and 9.1 ppm for CH$_3$, 21.3 and 26.5 ppm for CH$_2$. The upfield resonance at δ = 3.0 is assigned to the trimethylsilyl group of the amide ligand.

Both the ^{1}H NMR and ^{13}C NMR spectra of [(Et$_8$O$_2$N$_2$)SmN(SiMe$_3$)$_2$], **(22)**, with two singlet aromatic proton resonances assigned to the pyrrolide and furan rings and two inequivalent *meso*-ethyl groups suggest that the complex possesses the same molecular symmetry as the Group 1 metal complexes of the dioxaporphyrinogen **(3)** (see Section 3.2). This symmetry feature, and the singlet resonance of bis(trimethylsilyl)amide ligand suggest no long-lived γ-methyl agostic interaction with a single γ-methyl group on the NMR time scale.

Both   [(toluene)Na(Et$_8$O$_2$N$_2$)SmN(SiMe$_3$)Si(Me)$_2$CH$_2$],   (23),   and
[(THF)$_2$K(Et$_8$O$_2$N$_2$)SmN(SiMe$_3$)Si(Me)$_2$CH$_2$], (24), have very similar ^{1}H NMR
spectra, as shown in Table 3.

Compound number	Aromatic protons	CH$_2$Si	CH$_2$(Et)	CH$_3$(Et)	SiMe$_2$	SiMe$_3$
(23)	7.24, 6.69, 3.35, 3.07	5.56	0.44, 0.63, 0.93 (2×CH$_2$), 1.82, 1.96, 2.14, 2.46	0.10, 0.14, 0.31, 0.55	1.81	0.20
(24)	7.20, 6.64, 3.82, 3.47	5.68	0.41, 0.63, 0.95 (2×CH$_2$), 1.82, 1.96, 2.13, 2.49	0.11, 0.16, 0.30, 0.54	1.77	0.17

Table 3: ^{1}H NMR spectral data of [(toluene)Na(Et$_8$O$_2$N$_2$)SmN(SiMe$_3$)Si(Me)$_2$CH$_2$],
(23), and [(THF)$_2$K(Et$_8$O$_2$N$_2$)SmN(SiMe$_3$)Si(Me)$_2$CH$_2$], (24), (THF-d^8, 399.694
MHz, 298 K, ppm; toluene resonances are not listed).

The ^{1}H NMR spectra of both complexes (23) and (24) suggest that the
molecules are less symmetric than (22). There are four singlet proton resonances for .
the aromatic protons rather than two for (22). Four triplet resonances for the protons
CH$_3$ of the meso-ethyl groups are found in each complex (23) and (24) rather than
two in (22), and eight multiplets (overlap between two resonances) for the CH$_2$
protons of the ethyl groups for each resonance compared to four multiplets in (22).

Complexes (23) and (24) do not possess the mirror plane symmetry
containing the pyrrolide nitrogen centres and the samarium centre which is present in
complex (22). Complexes (23) and (24) still maintain the mirror plane symmetry
containing the two oxygen centres of the furan rings and the samarium centres. Four
triplet resonances for the methyl protons of the meso-ethyl groups suggest that the
molecules are still asymmetric with respect to the plane of macrocyclic cavity as was
the case of complex (22), as shown in Figure 9.
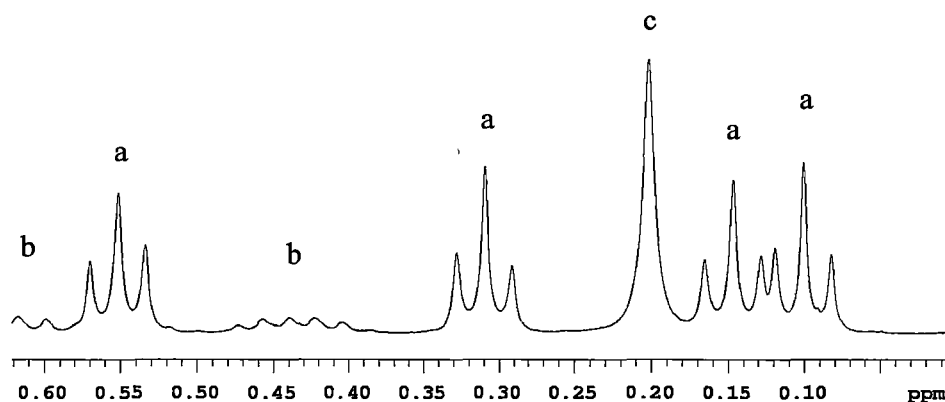
Figure 9: Methyl region of the ^{1}H NMR spectrum of [(toluene)Na(Et$_8$O$_2$N$_2$)SmN(SiMe$_3$)Si(Me)$_2$CH$_2$], **(23)**, (THF-d^8, 399.694 MHz, 298 K, ppm). The resonances of a, b, and c are from methyl, methylene and trimethylsilyl protons, respectively.

The ^{1}H NMR spectrum of the samarium amide [(Et$_8$N$_4$Me$_2$)SmN(SiMe$_3$)$_2$], **(25)**, derived from the *trans-N,N'*-dimethylated porphyrinogen **(6)** exhibits a narrowed chemical shift range for all resonances between -0.5 to 6.5 ppm compared with the analogous complex **(22)** derived from the dioxaporphyrinogen **(3)**. The aromatic proton resonances appear as two singlets at $\delta = 3.74$ and 6.10 ppm for the *N*-methyl pyrrole and pyrrolide rings, respectively. The other two singlet resonances of $\delta = 4.87$ and 1.08 ppm are for the *N*-methyl groups and the SiMe$_3$ moieties, respectively. The CH$_3$ groups of the *meso*-ethyl substituents again appear as two triplets at -0.17 and 0.75 ppm, while the four resonances of the CH$_2$ protons are seen at $\delta = 0.87$, 1.37 and 1.95 ppm (overlap between two resonances at 1.95 ppm).

The ^{13}C NMR spectrum of [(Et$_8$N$_4$Me$_2$)SmN(SiMe$_3$)$_2$], **(25)**, features the aromatic carbon resonances at $\delta = 103.5$ (β-C), 149.9 (α-C) for the pyrrolide units and 100.2 (β-C), 139.8 (α-C) ppm for *N*-methylpyrrole units. The *N*-methyl resonance appears at $\delta = 36.6$ ppm and the trimethylsilyl carbon resonance is seen at 7.9 ppm. Two inequivalent *meso*-ethyl groups appear at $\delta = 8.29$ (CH$_3$) and 23.1 (CH$_2$), 8.13 (CH$_3$) and 28.7 ppm (CH$_2$), respectively. The quaternary *meso*-carbon is seen at $\delta = 41.7$ ppm.

The average molecular symmetry of [(Et$_8$N$_4$Me$_2$)SmN(SiMe$_3$)$_2$], **(25)**, in solution is very similar to complex **(22)**. The molecule possesses mirror symmetry passing through the pyrrolide nitrogen centres, the samarium centre and the nitrogen centre of the amide ligand. Complex **(25)** also maintains the perpendicular mirror plane containing the two nitrogen centres of the *N*-methyl pyrrole units, the

samarium centre and the nitrogen centre of the amide ligand. However, complex (25) is again asymmetric with respect to the plane of macrocyclic cavity, thus, the two geminal *meso*-substituted ethyl groups are chemically inequivalent.

Full ^1H and ^{13}C assignment of the ^1H and ^{13}C NMR spectra of (25) has been achieved through gCOSY, gHMBC and gNOESY spectra. For example, the gCOSY spectrum of (25) shows correlations existing between CH_3 (-0.17 ppm) and CH_2 (1.95 ppm, 2× CH_2) and between CH_3 (0.75 ppm) and CH_2 (0.87 and 1.37 ppm), thus establishing the proton resonances of each *meso*-ethyl substituent, as shown in Figure 10. The gHMBC spectrum shows correlation between the N-CH_3 carbon (36.6 ppm in F1) and the N-CH_3 protons (4.87 ppm in F2) linked with the α-carbon of the N-methylpyrrole ring (139.8 ppm in F1), the β-protons (3.74 ppm in F2) and in turn the β-carbons (100.2 in F1). Similarly, correlations link the β-protons of the pyrrolide ring (6.10 ppm in F2) to both the α-carbons (149.9 ppm in F1) and the β-carbons (103.5 ppm in F2) to establish the assignment of the protons and carbons of the pyrrolide unit. Further correlations exist within the *meso*-carbon and *meso*-ethyl substituent region of the gHMBC spectrum, as shown in Figure 11.
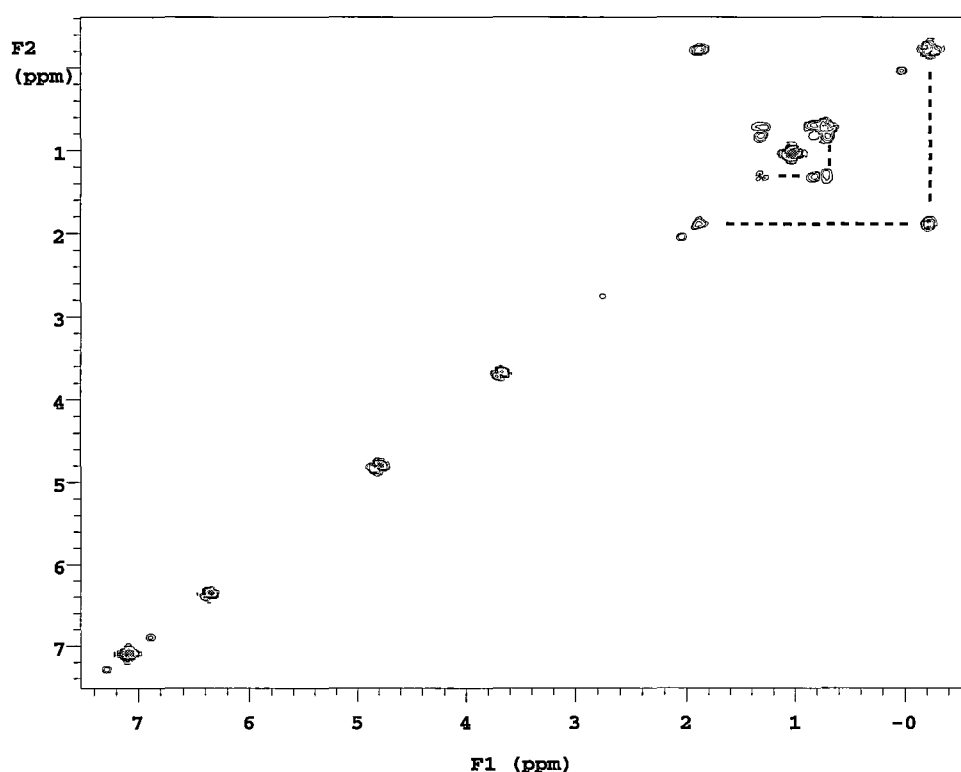
Figure 10: gCOSY spectrum of [(Et$_8$N$_4$Me$_2$)SmN(SiMe$_3$)$_2$], (25) (C$_6$D$_6$, 399.694 MHz, 298 K, ppm)
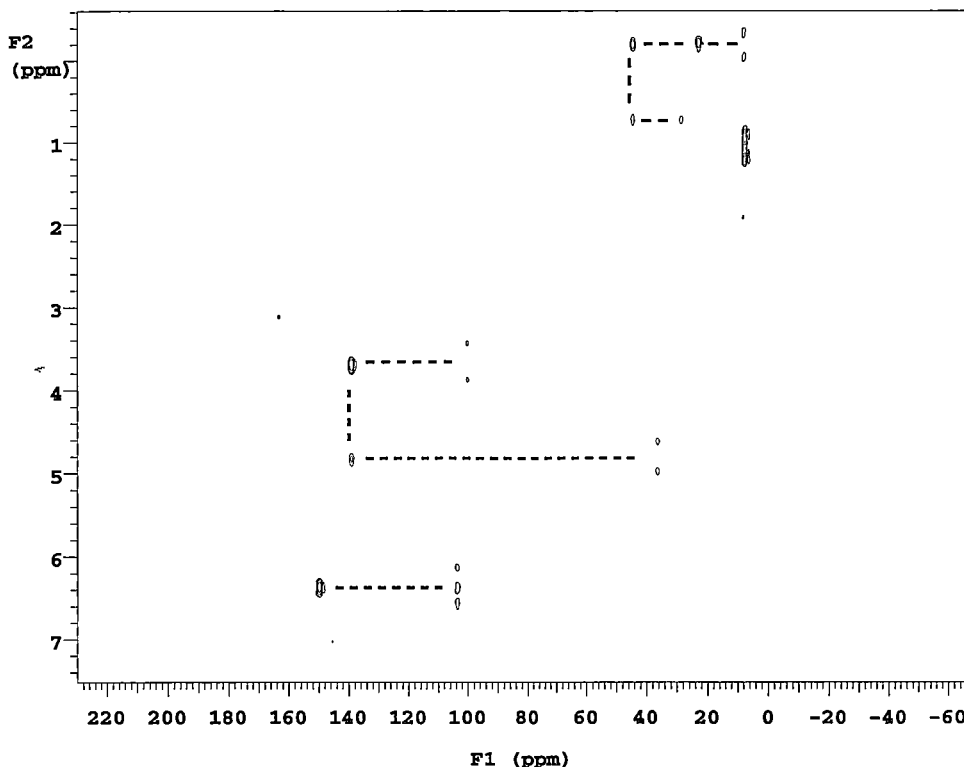
Figure 11: gHMBC spectrum of [(Et$_8$N$_4$Me$_2$)SmN(SiMe$_3$)$_2$], **(25)** (C$_6$D$_6$, 399.694 MHz for F2, 100.512 MHz for F1, J = 8.0-140 Hz, 298 K, ppm)

To explore the conformation of complex **(25)** in solution, gNOESY spectra were performed, as shown in Figure 12. NOE effects between the β-protons of the pyrrolide unit (6.10 ppm) and one of the *meso*-ethyl groups (0.75 ppm (CH$_3$), 0.87 ppm (CH$_2$)) are observed, as well as cross peaks linking the *N*-Me protons of the *N*-methyl pyrrole unit (4.87 ppm, (*N*-Me)) to the other *meso*-ethyl group (1.95 (2CH$_2$)). This is consistent with the macrocyclic conformation established for **(25)** in the solid state through crystal structure determination as the 1,3-alternate conformation places the *N*-Me substituents and the β-protons of the pyrrolide units in close contact distances of between 3.11-3.28 Å and 2.99-3.07 Å, respectively, allowing the NOE based stereochemical assignments shown in Figure 13(a). Thus through the combination of gCOSY, gHMBC and gNOESY spectra, full ^{1}H and ^{13}C assignment of **(25)** has been achieved, as shown in Figure 13(b).
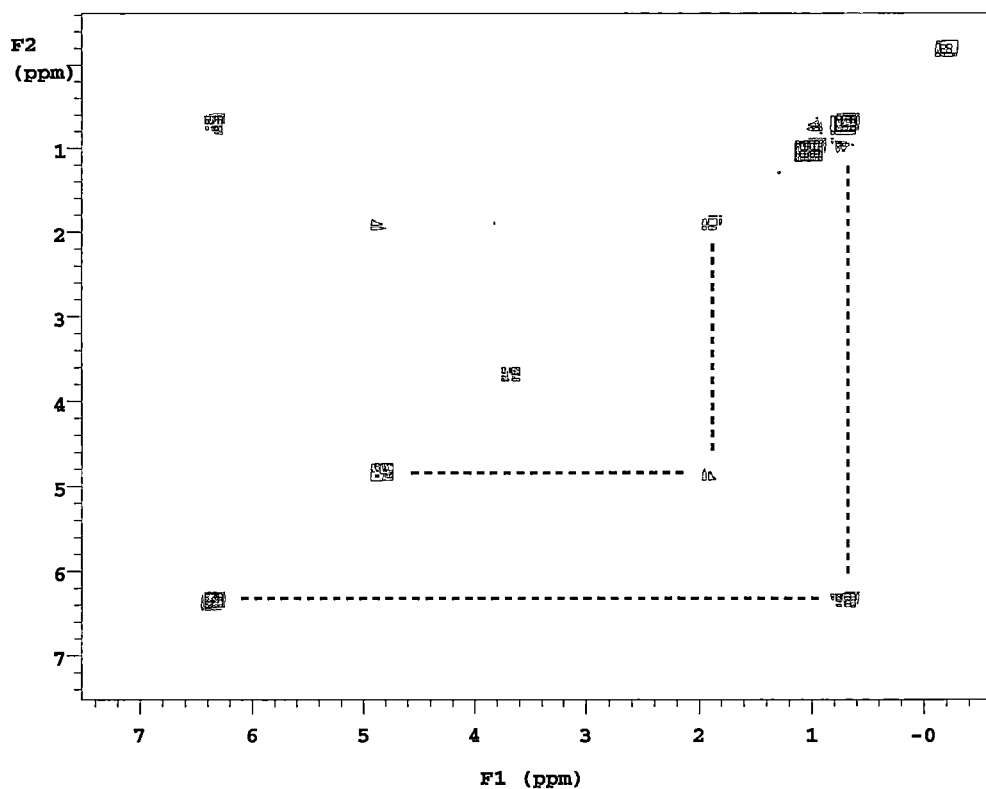
Figure 12: gNOESY spectrum of [(Et$_8$N$_4$Me$_2$)SmN(SiMe$_3$)$_2$], **(25)** (C$_6$D$_6$, 399.694 MHz, 298 K, ppm)

(a)   (b)
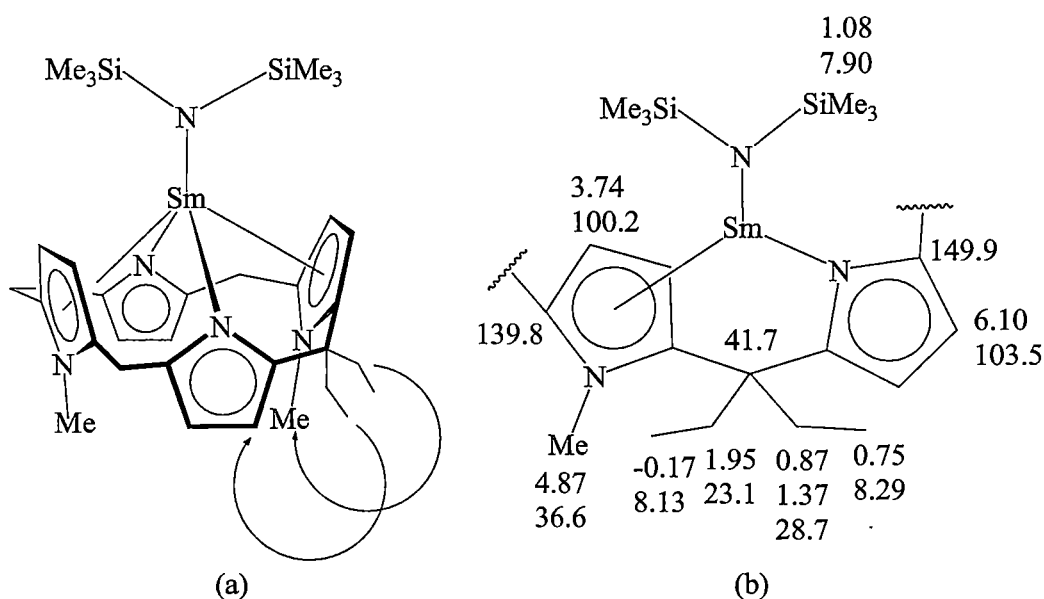
Figure 13: (a) NOE correlations for [(Et$_8$N$_4$Me$_2$)SmN(SiMe$_3$)$_2$], **(25)** (correlations are marked with arrows. (b) Full ^{1}H and ^{13}C NMR spectral assignment of **(25)**.

Variable temperature ^{1}H NMR spectroscopic studies for complex (25), summarised as an inverse absolute temperature plot between -50 to 50°C, is shown in Figure 14. Resonances of all protons vary linearly with 1/T following the Curie-Weiss law, which indicates a lack of any substantial changes or fluctionality in the molecular structure in the temperature range studied.

The chemical shifts of all the protons resonating upfield of 3 ppm have witnessed only very slight changes in the temperature range -50 to 50°C. Thus, six resonances vary less than 0.1 ppm in the temperature range. Each aromatic proton resonance has comparably larger chemical shift changes, where the β-protons of the N-methylpyrrole unit decrease in chemical shift from δ = 3.99 to 3.71 ppm and chemical shift for the protons of the pyrrolide unit increase from δ = 6.43 to 6.68 ppm. The largest chemical shift variation in the temperature range stems from the N-methyl protons, whose chemical shift varies 0.78 ppm from 5.10 to 4.32 ppm.
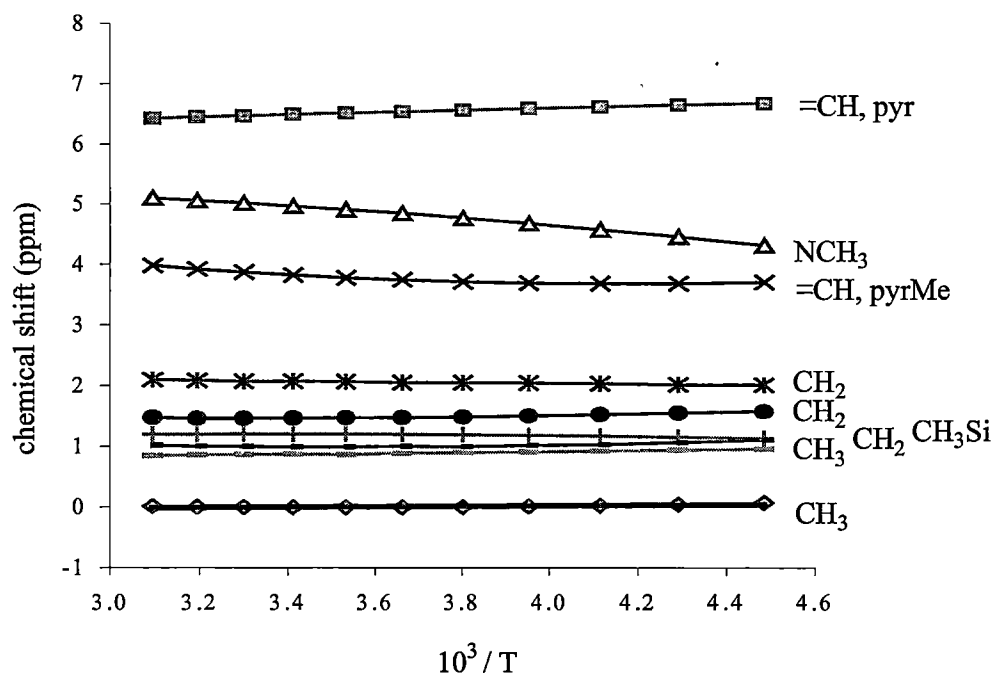
Figure 14: Variable temperature ^{1}H NMR spectral data for [(Et$_8$N$_4$Me$_2$)SmN(SiMe$_3$)$_2$], (25) (toluene-d^8, 399.694 MHz, ppm)

5.2.3.4 Molecular structure of [(Et$_8$O$_2$N$_2$)SmN(SiMe$_3$)$_2$], (22)

Yellow crystals of [(Et$_8$O$_2$N$_2$)SmN(SiMe$_3$)$_2$]; (22), suitable for X-ray crystal structure determination were grown from a hot saturated toluene solution that was

allowed to cool slowly to ambient temperature and stood overnight. The crystals belong to the monoclinic space group $P2_1/n$ (No. 14), $a = 12.1717(10)$, $b = 27.7942(3)$, $c = 13.62490(10)$ Å, $\beta = 113.1423(5)°$, with four molecules in the unit cell, the asymmetric unit consisting of one molecule of $[(Et_8O_2N_2)SmN(SiMe_3)_2]$, (22), as shown in Figure 15.
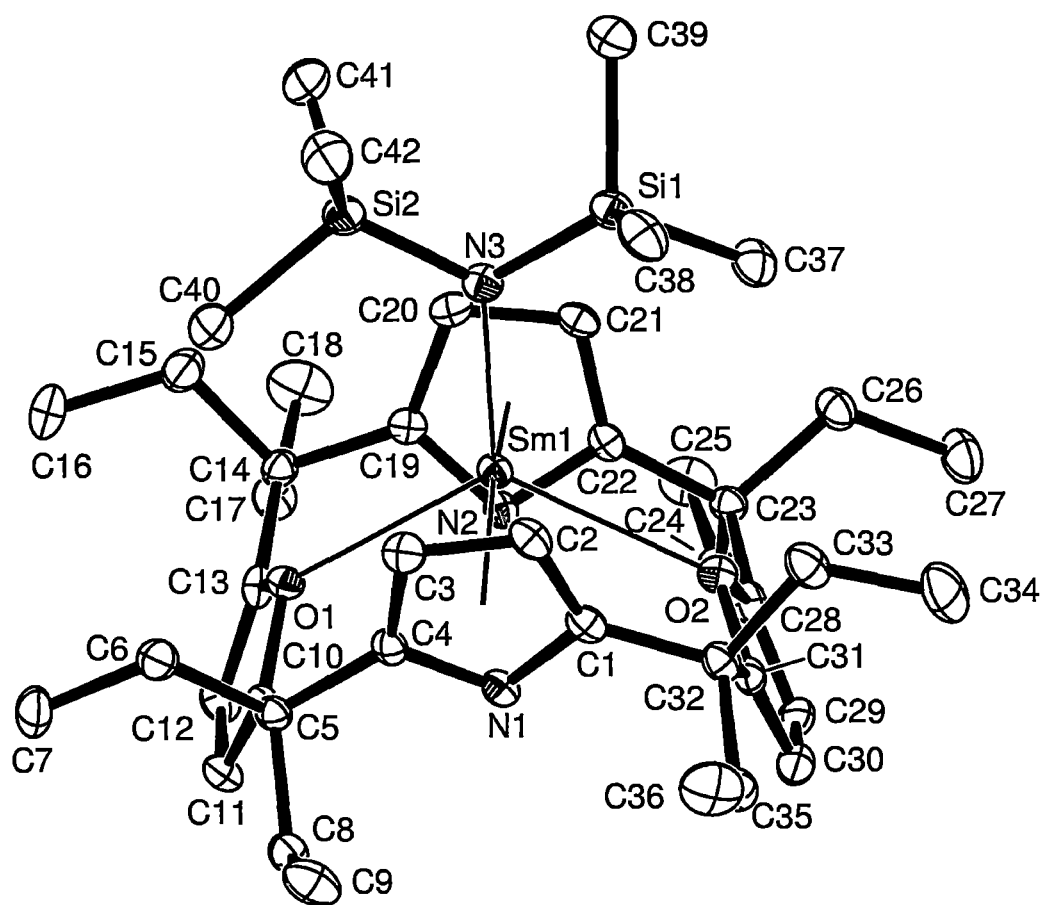
Figure 15: Molecular structure of $[(Et_8O_2N_2)SmN(SiMe_3)_2]$, (22), with thermal ellipsoids drawn at the level of 50% probability, protons have been removed for clarity.

Complex (22) adopts a monomeric structural form in the solid state. The samarium centre binds to the macrocycle by a $\eta^5{:}\eta^1{:}\eta^5{:}\eta^1$-bonding mode with the η^1-interactions through the two oxygen centres of the two opposite furanyl rings and η^5-interactions to the pyrrolide rings. The macrocycle features a 1,3-alternate conformation with oxygen atoms of the furan rings directed towards the upward face of the macrocyclic cavity (as depicted in Figure 15).

The samarium centre of complex **(22)** is η^1-bound to the two oxygen centres of furanyl rings at distances of 2.7181(16) and 2.7029(17) Å. The two η^5-interactions in **(22)** between the samarium centre and two opposite pyrrolide rings measure 2.52_6 and 2.52_9 Å (Sm-centroid distances). The samarium(III) centre in **(22)** displays closer interactions with the macrocyclic unit than that in samarium(II) complex **(15)**, which has longer Sm-O bond distances of 2.907(10) Å and longer Sm-centroid distances of 2.65_2 Å. Consistent with the closer interactions between the samarium centre and macrocycle in **(22)**, the samarium resides deeper in the macrocycle with a larger O(1)-Sm(1)-O(2) angle of 121.58(5)° than that in **(15)** (O-Sm-O = 110.1(4)°) and a larger metallocene bend angle (centroid-Sm-centroid) of 160.5_1° than that of **(15)** $(136.3_4$°). The metallocene bend angle in **(22)** is much larger than that in the related bis(pentamethylcyclopentadienyl)samarium(III) complex $[(\eta^5$-$C_5Me_5)_2SmN(SiMe_3)_2]$, **(XXVIII)**, which has a metallocene bend angle of 132.2°[17].

As shown in Figure 16, the top coordination hemisphere of the amide ligand in complex **(22)** experiences conformational restrictions arising from the bulky trimethylsilyl substituents, with the trimethylsilyl groups adopting a meshed orientation to avoid close contact with each other. A γ-methyl group in each trimethylsilyl substituent of the amide ligand is oriented towards the macrocycle and the C_2 symmetry of the amide ligand forces a C_2 twist of the macrocycle in turn to relieve interactions between the γ-methyl group of the amide and *meso*-ethyl substituents of the macrocycle.

(a)   (b)
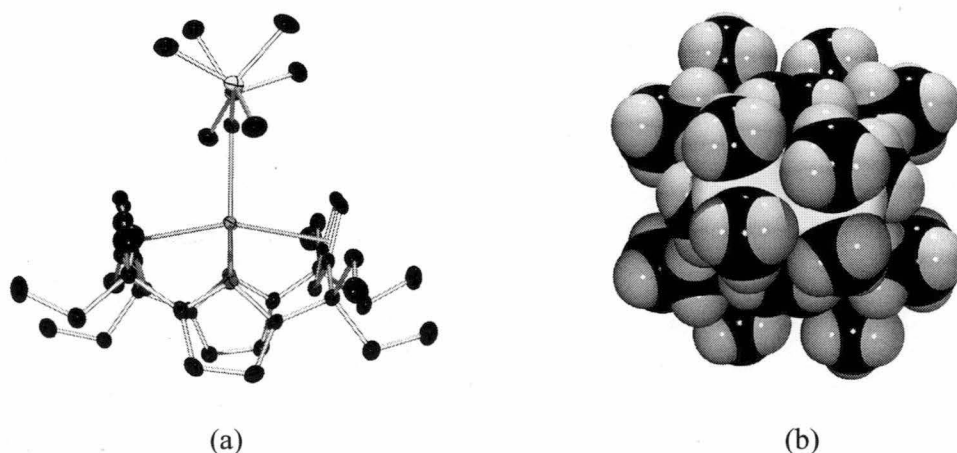
Figure 16: Molecular structure of $[(Et_8O_2N_2)SmN(SiMe_3)_2]$, **(22)**: (a) a side view; (b) space filling representation viewed from the amide ligand.

The Sm-N(3) bond distance of 2.314(2) Å in (22) is close to that of the bis(pentamethylcyclopentadienyl)samarium(III) complex [(η^5-$C_5Me_5)_2SmN(SiMe_3)_2$], (XXVIII), at 2.301(3) Å. The shortest Sm⋯C distances to the γ-methyl carbons of the amide ligand in (22) are 3.51_9 and 3.67_7 Å, which are longer than those in (XXVIII) at 3.21_6 and 3.28_2 Å and the closest Sm⋯H-CH$_2$-Si distances of 3.27_4, 3.42_5 Å are also longer than those in (XXVIII) at 2.9_7 and 3.03_1 Å. One proton attached to each of the γ-methyl groups closest to the samarium centre in (22) is orientated towards the samarium centre in the solid state, as shown in Figure 17, which indicates a possible weak γ-agostic interaction with the samarium centre (proton positions were located and refined in x, y, z). Relevant angles within the amide ligand are N-Si-C (37, 38 and 39, γ-carbon) = 111.47(11), 113.81(12) and 114.55(12)°, and N-Si-C (40, 41 and 42, γ-carbon) = 112.74(11), 114.03(12) and 113.42(13)°, displaying significant differences. Angles of Sm-N(3)-Si(1) = 120.95(11) and Sm-N(3)-Si(2) = 120.75(10)° angles have similar values, as expected owing to the presence of putative weak agostic interactions for each of the trimethylsilyl substituents. The Sm-N-Si angles in (22) are larger than those in (XXVIII) at 115.0_1 and 116.4_8°, which has much closer contact distances with the γ-methyl at Sm-C = 3.21_6 and 3.28_2 Å than (22).
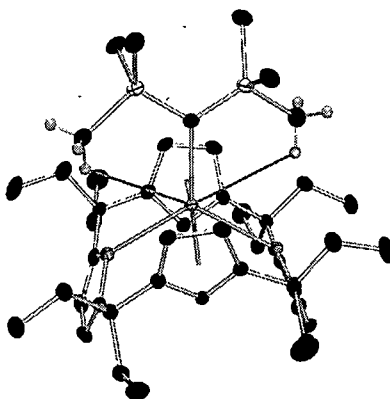
Figure 17: γ-methyl protons directed towards the samarium centre in [(Et$_8$O$_2$N$_2$)SmN(SiMe$_3$)$_2$], (22) (thermal ellipsoids drawn at the level of 50% probability), other protons omitted for clarity.

The macrocyclic cavity of (22) is quite similar to (15) in terms of cross-cavity O⋯O/N⋯N distances, with the O⋯O and N⋯N distances being 4.73_2 and 4.28_7 Å for (22) and 4.75_7 and 4.26_3 Å for (15), as shown in Table 4. The heterocycle ring tilt angles of (22) are 68.1_7 and 69.7_0° for the furanyl rings, and 73.8_1 and 74.3_7° for the pyrrolide rings, with the former rings lying flatter than those of (15) and the latter are steeper than those of (15). The similarity in the macrocyclic cavity size in (15) and

(22) differs from the Sm(II) and (III) complexes of *trans-N,N'*-dimethylated porphyrinogen (such as **(16)** and **(19)**, **(20)**, **(21)**), and can be assumed to be in response to the macrocycle in **(15)** hosting both samarium and potassium metal centres. In comparison with the macrocycle **(3)** itself, the cavity of **(22)** is much smaller, with the pyrrolide rings lying much steeper and the two opposite furanyl rings lying much flatter due to the interaction of samarium centre with the macrocycle and possibly also due to the bulky bis(trimethylsilyl)amide ligand introduced to the cavity (though comparative data on a less bulky samarium(III) amide or alkyl derivative is required to confirm this final point).

Compound number	Furanyl ring		Pyrrolide ring	
	Cross-cavity O⋯O distance (Å)	Ring tilt angles (°)	Cross-cavity N⋯N distance (Å)	Ring tilt angles (°)
(22)	4.73_2	68.1_7, 69.7_0	4.28_7	73.8_1, 74.3_7
(15)	4.75_7	70.3_9	4.26_3	70.2_8
(3)	4.85_7	79.0_3, 79.4_9	4.65_1	65.5_1, 67.1_1

Table 4: Cross-cavity O⋯O/N⋯N distances and heterocycle ring tilt angles for compounds **(22)**, **(15)** and **(3)**.

5.2.3.5 Molecular structure of [(toluene)Na(Et$_8$O$_2$N$_2$)SmN(SiMe$_3$)Si(Me)$_2$CH$_2$], (23)

Red crystals of [(toluene)Na(Et$_8$O$_2$N$_2$)SmN(SiMe$_3$)Si(Me)$_2$CH$_2$], **(23)**, suitable for X-ray crystal structure determination were grown from a hot saturated toluene solution that was allowed to cool slowly to ambient temperature and stood overnight. The crystals belong to the triclinic space group $P\bar{1}$ (No. 2), $a =$ 11.87350(10), $b = 12.41812(2)$, $c = 18.6506(2)$ Å, $\alpha = 88.0740(6)$, $\beta = 89.2062(6)$, $\gamma = 70.8546(4)°$, with two molecules of **(23)** and one noncoordinated toluene molecule in the unit cell, the asymmetric unit consists of one molecule of **(23)** and half of a toluene molecule disordered over an inversion centre, as shown in Figure 18.
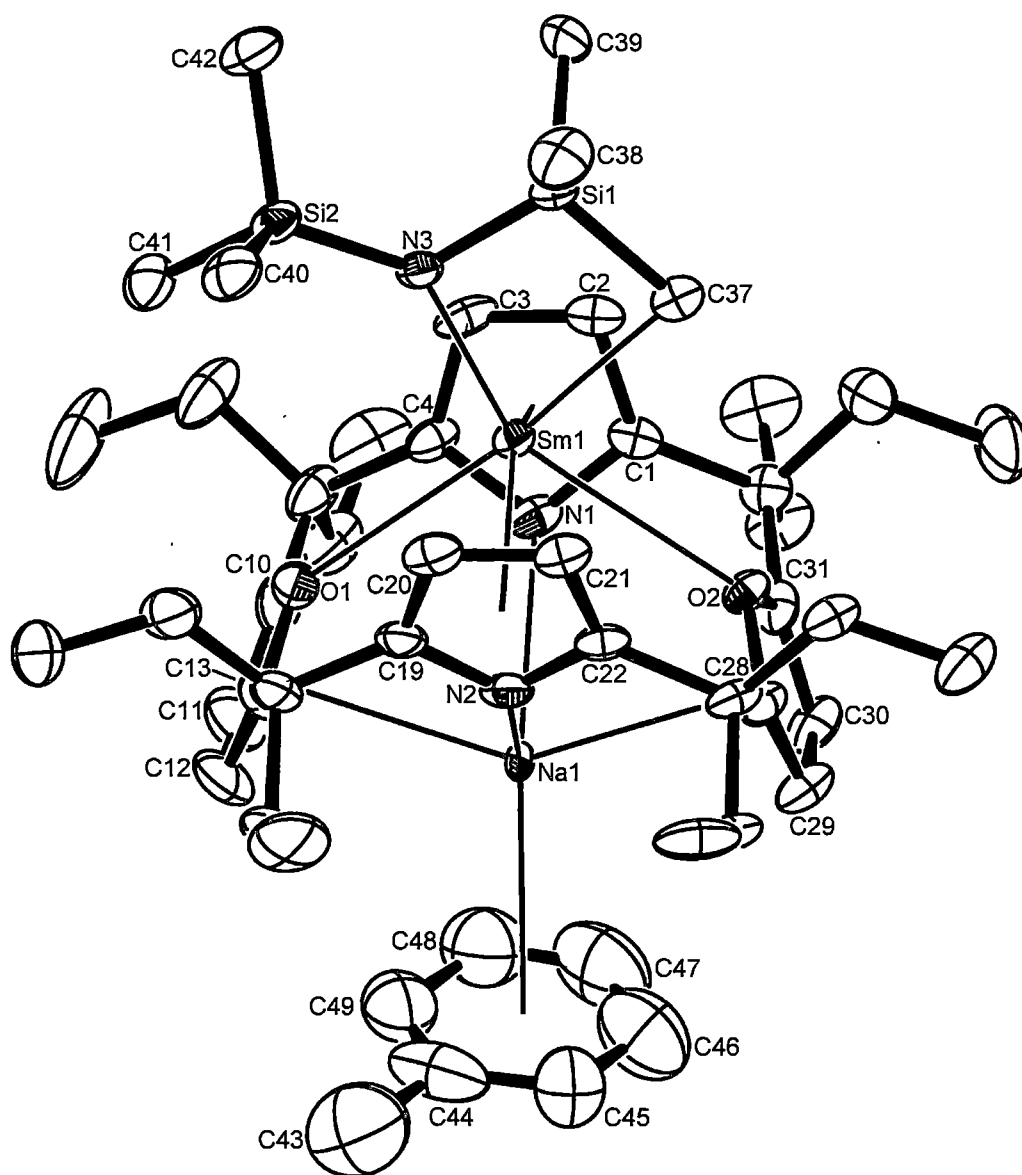
Figure 18: Molecular structure of [(toluene)Na(Et$_8$O$_2$N$_2$)SmN(SiMe$_3$)Si(Me)$_2$CH$_2$], **(23)**, with thermal ellipsoids drawn at the level of 50% probability, protons have been removed for clarity.

Complex **(23)** adopts a monomeric structure in the solid state. The macrocycle has a 1,3-alternate conformation with the two oxygen centres of the furanyl rings pointing towards one side of the macrocycle and the two nitrogen centres of the pyrrolide rings being orientated towards the other side. The macrocyclic cavity hosts both samarium and sodium centres, with each metal centre residing on either side of the average N$_2$O$_2$ plane. Both metals display η^5:η^1:η^5:η^1-bonding sequences, but adopt alternate bonding modes to the furanyl and pyrrolide

rings. Thus the samarium centre features η^5-binding to the nitrogen centres of both pyrrolide units, while the sodium centre σ-binds to these anionic heterocyclic units. Similarly, η^5-interactions of the furanyl rings are seen to the sodium cation, while these units bind in η^1-fashion with the samarium centre. The other coordination sites of samarium centre are occupied by the γ-deprotonated bis(trimethylsilyl)amide ligand which chelates the samarium centre through carbon and nitrogen centres, forming a planar four-membered SmNSiC metalla-heterocyclic ring. The remaining coordination sites of sodium centre are occupied by one toluene molecule through η^6-interactions.

The samarium centre in (23) is η^1-bound to two furanyl oxygen centres with Sm-O distances of 3.046(2) and 3.007(2) Å and the O-Sm-O angle is 107.06(8)°. The samarium centre is η^5-bound to two pyrrolide rings with Sm-centroid distances of 2.59_2 and 2.61_1 Å and the metallocene bend angle (centroid-Sm-centroid) is 141.4_3°. The samarium centre is bound to γ-deprotonated trimethylsilylamide ligand through a Sm-N bond distance of 2.292(2) Å and a Sm-C bond distance of 2.464(4) Å. Two significantly different Sm-N-Si angles of 96.43(11) and 139.41(16)° are observed, resulting from the formation of the strained four-membered ring. For the same reason, the N-Si-C angles of the deprotonated silyl group are markedly different with two being close at 111.12(17) and 111.82(17)°, for the methyl carbons, but much smaller for the methylene carbon 103.30(15)°. The Si-C-Sm angle is acute at 88.38(14)°, and the N-Sm-C ligand bite angle is 71.77(10)°. The sodium centre is η^1-bound to the two pyrrolide nitrogen centres with Na-N distances of 2.782(3) and 2.787(3) Å and the N-Na-N angle is 93.30(8)°. The sodium centre is η^5-bound to the two furanyl rings with Na-centroid distances of 2.97_3 and 2.99_4 Å and a metallocene bend angle (centroid-Na-centroid) of 141.4_9°. The sodium centre is η^6-bound to a toluene molecule with a long Na-centroid distance of 3.08_6 Å. Selected bond distance and angle data for complex (23) are listed in Table 5.

Sm(1)-N(3)	2.292(2)	N(3)-Si(1)-C(37)	103.30(15)
Sm(1)-C(37)	2.464(4)	N(3)-Si(1)-C(38)	111.12(17)
Sm(1)-O(1)	3.046(2)	N(3)-Si(1)-C(39)	111.82(17)
Sm(1)-O(2)	3.007(2)	N(3)-Sm(1)-C(37)	71.77(10)
Sm(1)-η^5(N1)	2.59$_2$	O(1)-Sm(1)-O(2)	107.06(8)
Sm(1)-η^5(N2)	2.61$_8$	η^5(N1)-Sm(1)-η^5(N2)	141.4$_3$
Na(1)-(N1)	2.782(3)	Sm(1)-N(3)-Si(1)	96.43(11)
Na(1)-(N2)	2.787(3)	Sm(1)-N(3)-Si(2)	139.41(16)
Na(1)-η^5(O1)	2.97$_3$	η^5(O1)-Na(1)-η^5(O2)	141.4$_9$
Na(1)-η^5(O2)	2.994$_2$		

Table 5: Selected bond lengths (Å) and angles (°) for [(toluene)Na(Et$_8$O$_2$N$_2$)SmN(SiMe$_3$)Si(Me)$_2$CH$_2$], **(23)**.

In comparison with the mononuclear samarium(III) complex **(22)**, **(23)** contains two metal centres within the cavity with the Sm-Na distance being 3.884$_1$ Å. The molecular structure is affected in consequence of this feature, for example, the samarium centre is 'pushed' out of the cavity compared with **(22)**. Thus η^1- and η^5-bond distances to samarium are longer than those of **(22)**. The related angles are also changed with the O-Sm-O and the metallocene bend angle involving the samarium centre being smaller in **(23)** than in **(22)**. The Sm-N bond distance to the amide ligand is slightly shorter in **(23)** in comparison to complex **(22)**, perhaps in response to decreased steric interactions of the amide ligand with the macrocycle arising from the samarium centre being forced out of the cavity somewhat due to the sodium cation. However, the chelate ring in the deprotonated amide ligand clearly impacts on this.

Related cyclometallated lanthanide complexes analogous to **(23)** are rare and there is no samarium complex available for comparison. Complex **(23)** features sodium centre stabilisation *via* coordination within the macrocyclic cavity and a toluene solvent molecule, while [Na(THF)$_3$Ln{N(SiMe$_3$)$_2$}$_2$N(SiMe$_3$)Si(Me)$_2$CH$_2$] (Ln = Sc, Yb and Lu)[18], **(XXIX)**, have their sodium centres poorly stabilised in

comparison to **(23)** through coordination to the methylene carbon and three THF solvent molecules.

The cross-cavity $O \cdots O/N \cdots N$ distances for **(23)** of 4.86_7 and 4.04_9 Å, respectively, compare with those of **(22)** (4.73_2 and 4.28_7 Å). The heterocycle ring tilt angles of **(23)** are 69.8_7 and $69.8_1°$ for two pyrrolide rings which are flatter than those of **(22)** (73.8_1 and $74.3_7°$). Two furanyl ring tilt angles measure 68.5_2 and $72.9_6°$, which are steeper than those of **(22)** (68.1_7 and $69.7_0°$).

5.2.3.6 Molecular structure of [(Et$_8$N$_4$Me$_2$)SmN(SiMe$_3$)$_2$], (25)

Orange crystals of [(Et$_8$N$_4$Me$_2$)SmN(SiMe$_3$)$_2$], **(25)**, suitable for X-ray crystal structure determination were grown from a hot saturated toluene solution that was allowed to cool slowly to ambient temperature and stood overnight. The crystals belong to the triclinic space group $P\bar{1}$ (No. 2), $a = 12.195(7)$, $b = 23.263(1)$, $c = 24.728(2)$ Å, $\alpha = 88.925(2)$, $\beta = 78.125(2)$, $\gamma = 75.229(2)°$, with six molecules in the unit cell, the asymmetric unit consisting of three molecules of [(Et$_8$N$_4$Me$_2$)SmN(SiMe$_3$)$_2$], **(25)**. The molecules have approximate symmetries ranging from C_{2v} to C_s with the variable tilting of the amide ligand seen in each of the three crystallographically independent molecules (ignoring the localised C_2 symmetry of the meshed bis(trimethylsilyl)amide ligand), as shown in Figure 19.

(1)
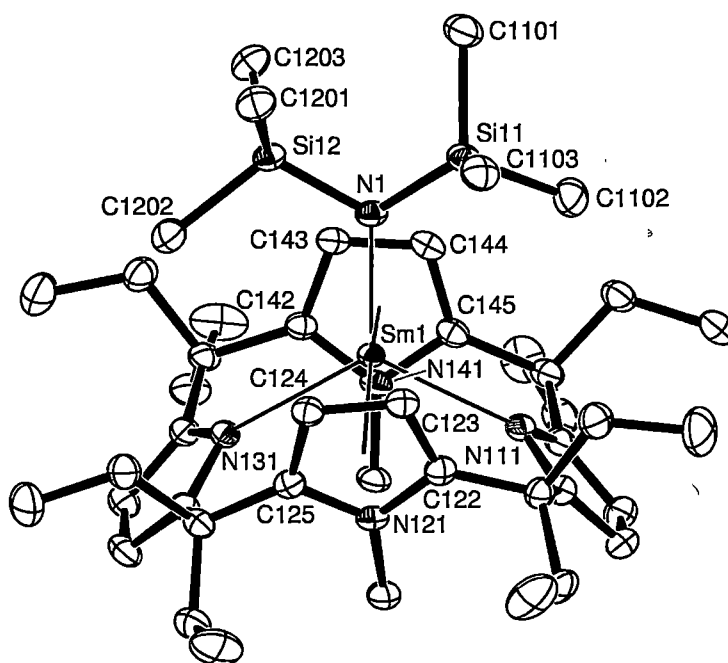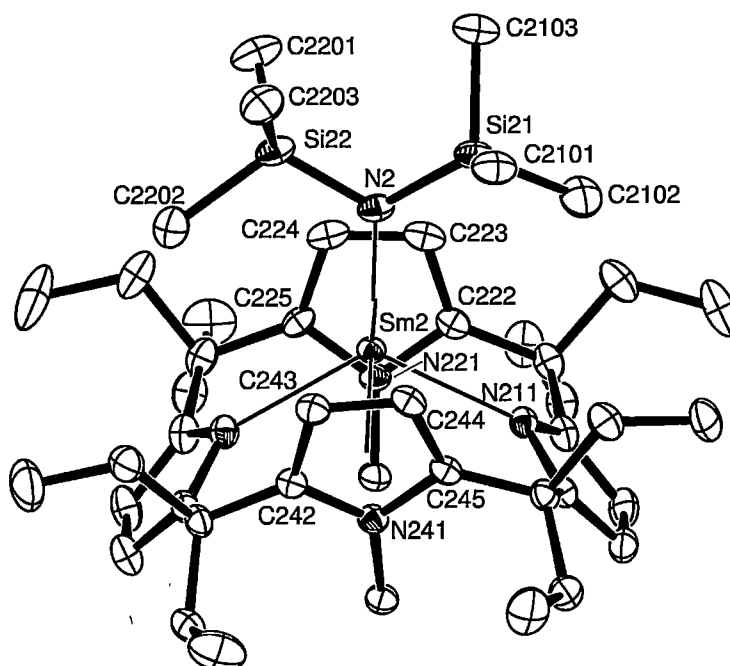
(2)
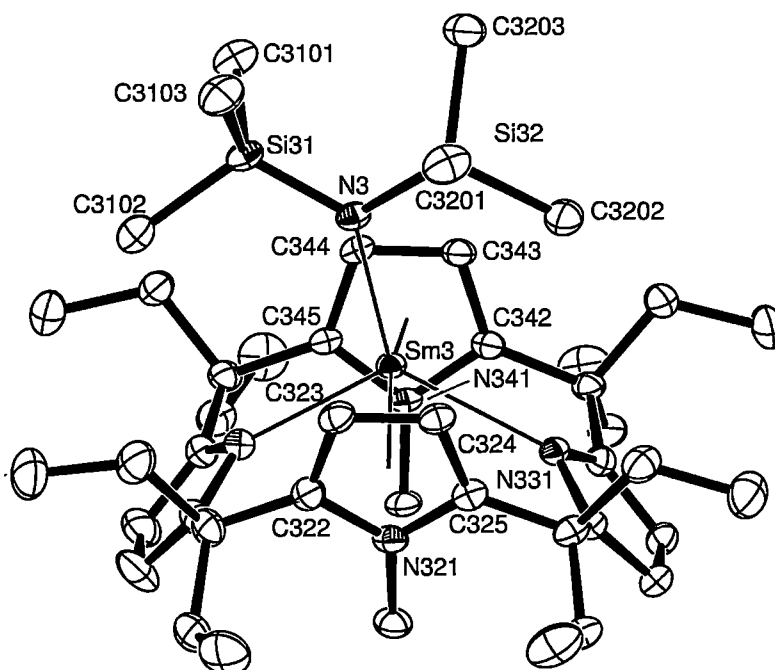
(3)

Figure 19: Molecular structure of [(Et₈N₄Me₂)SmN(SiMe₃)₂], **(25)**, with thermal ellipsoids drawn at the level of 50% probability, protons have been removed for clarity. All three crystallographically independent molecules of **(25)** are shown.

Complex **(25)** exists as a monomer in the solid state. The samarium centre in complex **(25)** is bound to the macrocycle through a $\eta^5{:}\eta^1{:}\eta^5{:}\eta^1$-bonding mode, adopting η^5-interactions to both *N*-methyl pyrrole rings and σ-bonding to both nitrogen centres of the pyrrolide rings, as noted in the cases of the Sm(II) complex **(16)**, the samarium(III) chloride **(19)** and the alkyl complexes **(20)** and **(21)** derived from the *trans-N,N'*-dimethylated porphyrinogen **(6)**. The bis(trimethylsilyl)amide ligand coordinates to the samarium centre from one face of the macrocyclic cavity, while the other side of the cavity features the two *N*-methyl groups preventing further coordination to the samarium centre or additional hosting of any further metal centres. The three independent molecules in the unit cell, as shown in Figure 19, display significant variations in their structures, mainly relating to the tilting of the amide ligands. This results in a closer contact between one γ-methyl group of a trimethylsilyl substituent of the amide ligand and the samarium centre, indicating a possible weak γ-H agostic interaction.

Selected quantitative structural data for molecule 1 of complex **(25)**, the most symmetrical of the three crystallographically independent molecules, are described below. In contrast to the analogous samarium(III) amide complex **(22)** based on the dioxaporphyrinogen **(3)**, the samarium centre in **(25)** is η^1-bound to the two anionic pyrrolide rings through nitrogen centres with greatly shorter Sm-N distances, 2.5169(17) and 2.5353(21) Å, than the two Sm-O bond distances in **(22)**, 2.7181(16) and 2.7129(17) Å, between samarium centre and the oxygen centres of neutral furanyl rings. However, the related N(111)-Sm(1)-N(131) angle of 121.02(7)° in **(25)** is similar to the corresponding O-Sm-O angle of 121.58(5)° in **(22)**. In turn, the two η^5-interactions between the samarium centre and the neutral *N*-methyl pyrrolide rings in **(25)**, with Sm-centroid distances of 2.65_0 and 2.65_6 Å, are longer than the two η^5-interactions of the samarium centre to the two anionic pyrrolide rings in **(22)** of 2.52_6 and 2.52_9 Å. The Sm-N bond distance to the amide ligand is slightly shorter in **(25)** at 2.3066(21) Å than in **(22)** at 2.314(2) Å. Selected bond distance and angle data for molecules 1-3 of complex **(25)** are listed in Table 6.

bonds or angles	Molecule 1	Molecule 2	Molecule 3
Sm(1)-N(1)	2.3066(21)	2.3097(22)	2.3139(22)
Sm(1)-N(111)	2.5169(17)	2.5134(17)	2.4703(18)
Sm(1)-N(131)	2.5353(21)	2.5432(22)	2.6036(21)
Sm(1)-η^5(N121)	2.65_0	2.66_7	2.66_8
Sm(1)-η^5(N141)	2.65_6	2.66_1	2.64_5
N(111)-Sm(1)-N(131)	121.02(7)	120.81(7)	120.78(7)
Sm(1)-N(1)-Si(1)	125.34(9)	124.95(9)	129.94(9)
Sm(1)-N(1)-Si(2)	118.78(11)	118.71(12)	113.30(11)
N(1)-Si(12)-C(1201)	113.67(11)	113.60(12)	114.40(12)
N(1)-Si(12)-C(1202)	112.48(12)	112.56(12)	109.54(11)
N(1)-Si(12)-C(1203)	112.97(11)	114.29(13)	115.43(13)
η^5(N121)-Sm(1)-η^5(N141)	160.9_2	160.8_2	160.0_8

Table 6: Selected bond lengths (Å) and angles (°) for molecules 1-3 of [(Et$_8$N$_4$Me$_2$)SmN(SiMe$_3$)$_2$], **(25)**. The corresponding atom numbers of molecules 2 and 3 are not shown for convenience.

The amide ligands tilt to a different degree in three crystallographically independent molecules of **(25)**. The Sm-N-Si angles represent the degree of tilting measuring 118.78(11) and 125.34(9)°, for molecule 1, 118.71(12) and 124.95(9)° for molecule 2, and 113.30(11) and 129.94(9)°, for molecule 3. The different geometries of the three independent molecules of **(25)** in the solid state arise either through crystal packing forces or the marginal energetic advantages of forming weak γ-H agostic interactions. This proposal is supported by the variation of N-Si-C angles of trimethylsilyl amide ligand, where significant differences are noted for molecule 3 with N-Si-C angles at 109.54(11), 114.40(12) and 115.43(13)°, indicating a possible interaction between the γ-methyl group and the samarium centre. The shortest distances found between the samarium centres and the relevant γ-carbons are 3.61_8 and 3.84_8 Å, for molecule 1, 3.60_8 and 3.85_4 Å, for molecule 2, and 3.33_7 and 4.05_9

Å, for molecule 3. These distances are longer than corresponding distances in $[(\eta^5\text{-}C_5Me_5)_2SmN(SiMe_3)_2]$, (XXVIII), at 3.21_6 and 3.28_2 Å, which has been claimed to exhibit no strong agostic interactions between the $Si(\beta)\text{-}C(\gamma)$ group and the samarium centre[17].

Complex (25)	N-Methylpyrrolide ring		Pyrrolide ring	
	Cross-cavity N⋯N distance (Å)	Ring tilt angles (°)	Cross-cavity N⋯N distance (Å)	Ring tilt angles (°)
Molecule 1	4.68_9	$77.5_1, 77.7_4$	4.39_8	$50.3_6, 45.4_5$
Molecule 2	4.70_9	$78.0_9, 76.9_9$	4.39_2	$50.8_5, 46.9_1$
Molecule 3	4.69_7	$78.1_0, 77.3_8$	4.41_2	$49.7_1, 49.0_9$

Table 7: Cross-cavity N⋯N distances and heterocycle ring tilt angles for $[(Et_8N_4Me_2)SmN(SiMe_3)_2]$, (25).

The cross-cavity N⋯N distances for the three independent molecules of (25) are of 4.86_7 and 4.39_8 Å, for molecule 1, 4.70_9 and 4.39_2 Å, for molecule 2, and 4.69_7 and 4.41_2 Å for molecule 3. The heterocycle ring tilt angles three molecules of (25) are 77.5_1, $77.7_4°$ for the N-methyl pyrrolide rings and 50.3_6, $45.4_5°$ for two pyrrolide rings in molecule 1, 78.0_9 and $76.9_9°$ for N-methyl pyrrolide rings and 50.8_5, $46.9_1°$ for the two pyrrolide rings in molecule 2 and 78.1_0, $77.3_8°$ for N-methyl pyrrolide rings and 49.7_1, $49.0_9°$ for two pyrrolide rings in molecule 3, as shown in Table 7.

5.3 Experimental

Synthesis of [(Et$_8$O$_2$N$_2$)SmI], (17)

To a solution of [{(THF)$_2$K(Et$_8$O$_2$N$_2$)Sm(μ-I)}$_2$], (15), (1.00 g, 0.50 mmol) in THF (100 mL), a solution of iodine (0.13 g, 0.50 mmol) in THF (40 mL) was added dropwise with stirring, during which time the colour of the solution changed from green to yellow. An insoluble white precipitate was filtered off and the yellow solution was concentrated *in vacuo* to 20 mL. The yellow solid product was collected by filtration and washed (2 x 20 mL) with toluene (0.77 g, 85%).

Anal. Calcd: C, 47.99; H, 5.37; N, 3.11. (C$_{36}$H$_{48}$N$_2$O$_2$Sm·1/2KI, FW 901).
Found: C, 47.72; H, 5.60; N, 2.71. (for Et$_8$O$_2$N$_2$)SmI+0.5KI).

Synthesis of [(Et$_8$N$_4$Me$_2$)SmCl], (18)

To a solution of [(Et$_8$N$_4$Me$_2$)Sm(THF)$_2$], (16), (0.86 g, 1.00 mmol) in toluene (50 mL), a solution of *tert*-butylchloride (0.093 g, 1.00 mmol) in THF (10 mL) was added dropwise over 5 minutes with stirring, during which time the colour of solution changed gradually from purple to light brown. The mixture was stirred continuously for 1 h and the pale brown solid product was collected by filtration and washed twice with toluene (0.68 g, 91%).

Anal. Calcd: C, 60.64; H, 7.23; N, 7.44. (C$_{38}$H$_{54}$ClN$_4$Sm, MW 752.68).
Found: C, 60.68; H, 7.18; N, 7.39.
MS (EI, m/z, %): 753 (M$^+$, 12%), 724 (M$^+$-Et, 46%), 568 (M$^+$-SmCl, 33%), 539 (M$^+$-SmCl-Et, 100%).

Synthesis of [{(Et$_8$N$_4$Me$_2$)Sm(μ-Cl)}$_2$], (19)

A: The pale brown compound (18) (0.75 g, 1.00 mmol) was stirred in toluene and heated gently to *ca.* 60°C for half an hour. The mixture was allowed to cool and stood at room temperature for three weeks and the red crystalline compound (19) was collected (0.23 g, 30%).

B: To a solution of [(Et$_8$N$_4$Me$_2$)Sm(THF)$_2$], (16), (0.086 g, 0.10 mmol) in toluene (10 mL), *tert*-BuCl (0.0093 g, 0.10 mmol) was allowed to vapour diffuse

slowly overnight. The red crystalline [{(Et$_8$N$_4$Me$_2$)Sm(μ-Cl)}$_2$], **(19)**, precipitated and was isolated by filtration (0.056 g, 75%).

Anal. Calcd: C, 60.64; H, 7.23; N, 7.44. (C$_{76}$H$_{108}$Cl$_2$N$_8$Sm$_2$, MW 1505.35).
Found: C, 60.79; H, 7.41; N, 7.38.

Synthesis of [(Et$_8$N$_4$Me$_2$)SmMe], **(20)**

To [(Et$_8$N$_4$Me$_2$)Sm(THF)$_2$], **(16)**, (0.86 g, 1.00 mmol) dissolved in toluene (80 mL), a solution of *tert*-butylchloride (0.093 g, 1.00 mmol) in THF (10 mL) was added dropwise with stirring, during which time the colour of the solution changed from purple to light brown. To the mixture, methyllithium (1.4 M solution in diethyl ether, 0.70 mL, 1.0 mmol) was added at -30°C and the solution stirred overnight at ambient temperature. An insoluble white solid was filtered off and the solvent was removed *in vacuo*. Recrystallisation from diethyl ether led to a pure crystalline orange product (0.40 g, 54%).

^{1}H NMR (C$_6$D$_6$, 399.694 MHz, 298 K, ppm): -0.56 (t, ^3J = 7.2 Hz, 12H, CH$_3$), 1.13 (m, 4H, CH$_2$), 1.44 (t, ^3J = 6.8 Hz, 12H, CH$_3$), 1.53 (m, 4H, CH$_2$), 1.95 (m, 4H, CH$_2$), 2.50 (m, 4H, CH$_2$), 2.98 (s, 4H, =CH, pyr), 3.69 (s, 6H, NMe), 6.76 (s, 4H, =CH, pyr), 8.94 (s, broad, 2H, CH$_2$).
Anal. Calcd: C, 63.97; H, 7.85; N, 7.65. (C$_{39}$H$_{57}$N$_4$Sm, MW 732.26).
Found: C, 64.01; H, 7.88; N, 7.51.

Synthesis of [(Et$_8$N$_4$Me$_2$)SmCH$_2$SiMe$_3$], **(21)**

To [(Et$_8$N$_4$Me$_2$)Sm(THF)$_2$], **(16)**, (0.86 g, 1.00 mmol) dissolved in toluene (80 mL), a solution of *tert*-butylchloride (0.093 g, 1.00 mmol) in THF (10 mL) was added dropwise with stirring, during which time the colour of solution changed from purple to light brown. To the mixture, trimethylsilylmethyllithium (1.0 M solution in pentane, 1.0 mL, 1.0 mmol) was added and the solution stirred overnight. The solvent was removed *in vacuo* and 40-60°C petroleum ether (60 mL) was added. An insoluble white solid was filtered off and the solution was concentrated *in vacuo* to *ca.* 20 mL. Recrystallisation from 40-60°C petroleum ether led to a pure crystalline orange product (0.50 g, 62%)

^{1}H NMR (C$_6$D$_6$, 399.694 MHz, 298 K, ppm): -0.53 (t, ^3J = 7.6 Hz, 12H, CH$_3$), 0.97 (s, 9H, CH$_3$), 1.18 (m, 4H, CH$_2$), 1.44 (t, ^3J = 6.8 Hz, 12H, CH$_3$),

1.51 (m, 4H, CH$_2$), 1.96 (m, 4H, CH$_2$), 2.75 (m, 4H, CH$_2$), 2.94 (s, 4H, =CH, pyr), 3.50 (s, 6H, NMe), 6.77 (s, 4H, =CH, pyr), 9.56 (s, broad, 2H, CH$_2$).

Anal. Calcd: C, 62.71; H, 8.14; N, 6.96 (C$_{42}$H$_{65}$N$_4$SiSm, MW 804.44).

Found: C, 62.59; H, 8.14; N, 6.84.

Synthesis of [(Et$_8$O$_2$N$_2$)SmN(SiMe$_3$)$_2$], **(22)**

To a solution of [{(THF)$_2$K(Et$_8$O$_2$N$_2$)Sm(μ-I)}$_2$], **(15)**, (1.00 g, 1.00 mmol) in THF (80 mL), a solution of iodine (0.13 g, 1.00 mmol) in THF (20 mL) was added dropwise with stirring, during which time the colour of the solution changed from green to yellow. To the mixture, sodium bis(trimethylsilyl)amide (1.0 M solution in THF, 1.0 mL, 1.0 mmol) was added and the solution stirred continuously overnight. The solvent was removed *in vacuo* and toluene (60 mL) was added. An insoluble white solid was filtered off and the solution was concentrated to *ca.* 20 mL. Recrystallisation from toluene led to a pure yellow prismatic crystalline product (0.64 g, 75%).

^{1}H NMR (C$_6$D$_6$, 399.694 MHz, 298 K, ppm): -5.89 (m, 4H, 2CH$_2$), -3.14 (s, 18H, 6CH$_3$), -1.65 (t, ^{3}J = 6.0 Hz, 12H, 4CH$_3$), 1.10 (m, 4H, 2CH$_2$), 1.77 (m, 4H, 2CH$_2$), 2.24 (t, ^{3}J = 6.8 Hz, 12H, 4CH$_3$), 4.48 (s, 4H, =CH), 4.67 (m, 4H, 2CH$_2$), 15.14 (s, 4H, =CH).

^{1}H NMR (THF-d^8, 399.694 MHz, 298 K, ppm): -5.55 (m, 4H, 2CH$_2$), -3.21 (s, 18H, 6CH$_3$), -1.32 (t, ^{3}J = 6.8 Hz, 12H, 4CH$_3$), 1.41 (m, 4H, 2CH$_2$), 2.11 (m, 4H, 2CH$_2$), 2.29 (t, ^{3}J = 6.8 Hz, 12H, 4CH$_3$), 4.64 (m, 4H, 2CH$_2$), 4.94 (s, 4H, =CH), 15.23 (s, 4H, =CH).

^{13}C NMR (THF-d^8, 100.512 MHz, 298 K, ppm): 3.0 (CH$_3$Si), 5.2 (CH$_3$), 9.1 (CH$_3$), 21.3 (CH$_2$), 26.5 (CH$_2$), 47.0 (CEt$_2$), 102.8 (=CH), 126.8 (=CR), 152.0 (=CR), 152.2 (=CR).

Anal. Calcd: C, 59.24; H, 7.81; N, 4.93. (C$_{42}$H$_{66}$N$_3$O$_2$Si$_2$Sm, MW 851.52).

Found: C, 59.30; H, 7.93; N, 5.01.

Synthesis of [(toluene)Na(Et$_8$O$_2$N$_2$)SmN(SiMe$_3$)Si(Me)$_2$CH$_2$], **(23)**

To a solution of [(Et$_8$O$_2$N$_2$)SmN(SiMe$_3$)$_2$], **(22)**, (0.50 g, 0.59 mmol) in THF (30 mL), sodium bis(trimethylsilyl)amide (1.0 M solution in THF, 0.60 mL, 0.60 mmol) was added and the mixture stirred for three hours at 55°C. THF was removed *in vacuo* and toluene (10 mL) was added. The mixture was heated for 5 minutes and

let stand for one week, after which time the red crystalline product precipitated and was collected (0.12 g, 20%).

> ^{1}**H NMR** (THF-d^8, 399.694 MHz, 298 K, ppm): 0.10 (t, ^{3}J = 7.6 Hz, 6H, 2CH$_3$), 0.14 (t, ^{3}J = 7.6 Hz, 6H, 2CH$_3$), 0.20 (s, 9H, SiMe$_3$), 0.31 (t, ^{3}J = 7.6 Hz, 6H, 2CH$_3$), 0.44 (m, 2H, CH$_2$), 0.55 (t, ^{3}J = 7.2 Hz, 6H, 2CH$_3$), 0.63 (m, 2H, CH$_2$), 0.93 (m, 4H, 2CH$_2$), 1.81 (s, 6H, Si(CH$_3$)$_2$), 1.82 (m, 2H, CH$_2$), 1.96 (m, 2H, CH$_2$), 2.14 (m, 2H, CH$_2$), 2.46 (m, 2H, CH$_2$), 3.07 (s, 2H, =CH, pyr or fur), 3.35 (s, 4H, =CH), 5.56 (s, 2H, SiCH$_2$), 6.69 (s, 2H, =CH), 7.24 (s, 4H, =CH, pyr or fur) (toluene was removed).
>
> **Anal.** Calcd: C, 62.33; H, 7.67; N, 4.15
>
> (23·1/2toluene, C$_{52.5}$H$_{77}$N$_6$NaO$_2$Si$_2$Sm, MW 1011.71).
>
> Found: C, 62.12; H, 7.69; N, 4.17.

Synthesis of [(THF)$_2$K(Et$_8$O$_2$N$_2$)SmN(SiMe$_3$)Si(Me)$_2$CH$_2$], **(24)**

To a solution of [(Et$_8$O$_2$N$_2$)SmN(SiMe$_3$)$_2$], **(22)**, (10 mg, 0.012 mmol) in THF-d^8 (0.8 mL), potassium bis(trimethylsilyl)amide (2.5 mg, 0.012 mmol) was added. The mixture was heated for three hours at 55 °C, during which time the colour of the solution changed gradually from yellow to red.

> ^{1}**H NMR** (THF-d^8, 399.694 MHz, 298 K, ppm): 0.11 (t, ^{3}J = 7.6 Hz, 6H, 2CH$_3$), -0.14 (t, ^{3}J = 7.6 Hz, 6H, 2CH$_3$), 0.17 (s, 9H, SiMe$_3$), 0.30 (t, ^{3}J = 7.6 Hz, 6H, 2CH$_3$), 0.41 (m, 2H, CH$_2$), 0.54 (t, ^{3}J = 7.6 Hz, 6H, 2CH$_3$), 0.63 (m, 2H, CH$_2$), 0.95 (m, 4H, 2CH$_2$), 1.77 (s, 6H, 2CH$_3$), 1.82 (m, 2H, CH$_2$), 1.96 (m, 2H, CH$_2$), 2.13 (m, 2H, CH$_2$), 2.49 (m, 2H, CH$_2$), 3.47 (s, 2H, =CH), 3.82 (s, 4H, =CH), 5.68 (s, 2H, SiCH$_2$), 6.64 (s, 2H, =CH), 7.20 (s, 4H, =CH).

Synthesis of [(Et$_8$N$_4$Me$_2$)SmN(SiMe$_3$)$_2$], **(25)**

To a solution of [(Et$_8$N$_4$Me$_2$)Sm(THF)$_2$], **(16)**, (0.86 g, 1.00 mmol) in toluene (50 mL), a solution of *tert*-butylchloride (0.093 g, 1.00 mmol) in THF (10 mL) was added dropwise with stirring, during which time the colour of solution changed from purple to light brown. To the mixture, sodium bis(trimethylsilyl)amide (1.0 M solution in THF, 1.0 mL, 1.0 mmol) was added and stirred overnight. An insoluble white solid was filtered off and the solution was concentrated *in vacuo* to *ca.* 15 mL. Recrystallisation from toluene led to a pure crystalline orange product (0.64 g, 73%)

^{1}**H NMR** (C_6D_6, 399.694 MHz, 298 K, ppm): -0.17 (t, ^3J = 7.60 Hz, 12H, 4CH$_3$), 0.75 (t, ^3J = 6.80 Hz, 12H, 4CH$_3$), 0.87 (m, 4H, 2CH$_2$), 1.08 (s, 18H, 2SiMe$_3$), 1.37 (m, 4H, 2CH$_2$), 1.95 (m, 8H, 4CH$_2$), 3.74 (s, 4H, =CH, pyrMe), 4.87 (s, 6H, NMe), 6.10 (s, 4H, =CH, pyr).

^{13}**C NMR** (C_6D_6, 100.512 MHz, 298 K, ppm): 7.9 (SiCH$_3$), 8.1 (CH$_3$), 8.3 (CH$_3$), 23.1 (CH$_2$), 28.7 (CH$_2$), 36.6 (NCH$_3$), 41.7 (CEt$_2$), 100.2 (=CH, pyrMe), 103.5 (=CH, pyr), 139.8 (=CR, pyrMe), 149.9 (=CR, pyr).

Anal. Calcd: C, 60.22; H, 8.27; N, 7.98 (C$_{44}$H$_{72}$N$_5$Si$_2$Sm, MW 877.61).

Found: C, 60.10; H, 8.36; N, 7.94.

5.4 References

[1]   **a.** H. Schumann, P.R. Lee, A. Dietrich, *Chem. Ber.,* 1990, **123**, 1331.
        b. S.W. Wang, Y.F. Yu, J.P. Hu, Z.W. Ye, G.C. Wei, Z.S. Jin, *Jiegou Huaxue (China), (J. Struct. Chem.),* 1994, **13**, 346.

[2]   H. Schumann, J. Winterfeld, H. Hemling, N. Kuhn, *Chem. Ber.,* 1993, **126**, 2657.

[3]   H. Schumann, E.C.E. Rosenthal, J. Winterfeld, G. Kociok-Kohn, *J. Organomet. Chem.,* 1995, **495**, 12.

[4]   H. Schumann, E.C.E. Rosenthal, J. Winterfeld, R. Weimann, J. Demtschuk, *J. Organomet. Chem.,* 1996, **507**, 287.

[5]   **a.** T. Dubé, S. Conoci, S. Gambarotta, G.P.A. Yap, G. Vasapollo, *Angew. Chem. Int. Ed.,* 1999, **38**, 3657.
        b. D.M.M. Freckmann, T. Dubé, C.D. Berube, S. Gambarotta, G.P.A. Yap, *Organometallics,* 2002, **21**, 1240.
        c. T. Dubé, S. Gambarotta, G.P.A. Yap, S. Conoci, *Organometallics,* 2000, **19**, 115.
        d. T. Dubé, S. Conoci, S. Gambarotta, G.P.A. Yap, *Organometallics,* 2000, **19**, 1182.

[6]   T. Dubé, M. Ganesan, S. Conoci, S. Gambarotta, G.P.A. Yap, *Organometallics,* 2000, **19**, 3716.

[7]   C.D. Berube, S. Gambarotta, G.P.A. Yap, *Organometallics,* 2003, **22**, 434.

[8]   **a.** J. Janczak, R. Kubiak, A. Jezierski, *Inorg. Chem.,* 1999, **38**, 2043.
        b. W.K. Wong, L.L. Zhang, W.T. Wong, F. Xue, T.C.W. Mak, *J. Chem. Soc., Dalton Trans.,* 1999, 615.
        c. H. Sugimoto, T. Higashi, A. Maeda, M. Mori, H. Masuda, T. Taga, *J. Chem. Soc., Chem. Commun.,* 1983, 1234.
        d. W.K. Wong, L.L Zhang, F. Xue, T.C.W. Mak, *J. Chem. Soc., Dalton Trans.,* 1999, 3053.
        e. M. Moussavi, A.D. Cian, J. Fischer, R. Weiss, *Inorg. Chem.,* 1986, **25**, 2107.

g. G.A. Spyroulias, C.P. Raptopoulou, D.D. Montauzon, A. Mari, R. Poilblanc, A. Terzis, A.G. Coutsolelos, *Inorg. Chem.*, 1999, **38**, 1683.

h. J.W. Buchler, A.D. Cian, J. Fischer, M. Kihn-Botulinski, R. Weiss, *Inorg. Chem.*, 1988, **27**, 339.

i. W.K. Wong, L.L. Zhang, F. Xue, T.C.W. Mak, *J. Chem. Soc., Dalton Trans.*, 2000, 2245.

j. M. Lachkar, A. Tabard, S. Brandes, R. Guilard, A. Atmani, A.D. Cian, J. Fischer, R. Weiss, *Inorg. Chem.*, 1997, **36**, 4141.

k. T.J. Foley, K.A. Abboud, J.M. Boncella, *Inorg. Chem.*, 2002, **41**, 1704.

l. J.W. Buchler, A.D. Cian, J. Fischer, M. Kihn-Botulinski, R. Weiss, *Inorg. Chem.*, 1988, **27**, 339.

m. C.J. Schaverien, A.G. Orpen, *Inorg. Chem.*, 1991, **30**, 4968.

n. J.Z. Jiang, L.L. Wei, P.L. Gao, Z.N. Gu, K.I. Machida, G.Y. Adachi, *J. Alloys and Compounds*, 1995, **225**, 363.

o. W.K. Wong, A.X. Hou, J.P. Guo, H.S. He, L.L. Zhang, W.Y. Wong, K.F. Li, K.W. Cheah, F. Xue, T.C.W. Mak, *J. Chem. Soc., Dalton Trans.*, 2001, 3092.

p. G.A. Spyroulias, A.G. Coutsolelos, C.P. Raptopoulou, A. Terzis, *Inorg. Chem.*, 1995, **34**, 2476.

[9]   E. Campazzi, E. Solari, R. Scopelliti, C. Floriani, *Inorg. Chem.*, 1999, **38**, 6240.

[10]   **a.** T. Dubé, S. Gambarotta, G.P.A. Yap, *Organometallics*, 2000, **19**, 817.

b. T. Dubé, S. Gambarotta, G. Yap, *Organometallics*, 2000, **19**, 121.

c. J.W. Guan, T. Dubé, S. Gambarotta, G.P.A. Yap, *Organometallics*, 2000, **19**, 4820.

[11]   W.J. Evans, J.W. Grate, I. Bloom, W.E. Hunter, J.L. Atwood, *J. Am. Chem. Soc.*, 1985, **107**, 405.

[12]   **a.** J. Jubb, S. Gambarotta, *J. Am. Chem. Soc.*, 1994, **116**, 4477.

b. E. Campazzi, E. Solari, C. Floriani, R. Scopelliti, *Chem. Commun.*, 1998, 2603.

c. E. Campazzi, E. Solari, R. Scopelliti, C. Floriani, *Chem. Commun.*, 1999, 1617.

[13]   **a.** W.J. Evans, G. Kociok-Köhn, J.W. Ziller, *Angew. Chem., Int. Ed. Engl.*, 1992, **31**, 1081.

b. W.J. Even, G. Kociok-Köhn, V.S. Leong, J.W. Ziller, *Inorg. Chem.*, 1992, **31**, 3592.

c. G.B. Deacon, Q. Shen, *J. Organomet. Chem.*, 1996, **511**, 1.

[14]   Z.W. Xie, K.L. Chui, Q.C. Yang, T.C.W. Mak, J. Sun, *Organometallics*, 1998, **17**, 3937.

[15   W.J. Evans, L.R. Chamberlain, T.A. Ulibarri, J.W. Ziller, *J. Am. Chem. Soc.*, 1988, **110**, 6423.

[16]   H. Schumann, W. Genthe, N. Bruncks, J. Pickardt, *Organometallics*, 1982, **9**, 1195.

[17]   W.J. Evans, R.A. Keyer, J.W. Ziller, *Organometallics*, 1993, **12**, 2618.

[18]   M. Karl, K. Harms, G. Seybert, W. Massa, S. Fau, G. Frenking, K. Dehnicke, *Z. Anorg. Allg. Chem.*, 1999, **625**, 2055.

CHAPTER 6

## INDOLIDE AND PYRROLIDE RELATED CHEMISTRY

6.1 INTRODUCTION

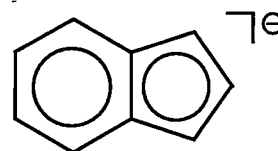#### 6.1.1 Indolide coordination chemistry

Indolide complexes feature the related benzoannelated *N*-heterocyclic anion bearing the five-membered pyrrolide ring as a substructure. Indolide anions should prefer σ-bonding coordination due to the readily available sp^2 hybridised lone pair of electrons of the nitrogen centre. The edge-fused six-membered ring of the indolide anion gives it additional π-bonding possibilities compared with related pyrrolide metal complexes. Indolide coordination chemistry has been poorly documented so far and π-bonding modes appear to be more difficult to obtain than for pyrrolides owing to inability to prepare complexes featuring bulky substituents in strategic positions analogous to 2,5-disubstituted pyrrolides. Currently, indolide based systems lack feasibility to act as competitive substitutes for the corresponding bicyclic aromatic (hydrocarbyl) indenide anion which typically act as η^5- or η^6- bound ligands.
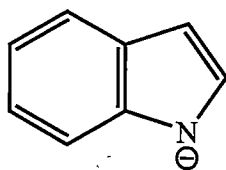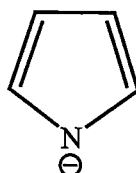
indolide anion   pyrrolide anion   indenide anion

The lithium indolide complexes (**I**)[1] and (**II**)[2] have been isolated as dimeric species in the solid state. Li_2N_2 four-membered rings comprise the core of the structures with the indolides bridging two lithium cations with coordinating THF or TMEDA molecules occupying the additional coordination sites. Complexes (**I**) and (**II**) display significant structural variations in the solid states. The Li_2N_2 ring is quite planar for (**I**) but not for (**II**) and the relative orientation of the indolide rings is towards the different sides of the Li_2N_2 ring in (**I**) (*i.e.*, *anti-*) but same side for (**II**) (*i.e.*, *syn-*). The N-Li bonds are all of similar length in (**I**) but two short and two long bonds occur in (**II**). The two indolide rings are almost parallel with each other in (**I**) but twist by an angle in (**II**). Moreover, the lithium cations are tetracoordinated in (**I**)

while lithium cations in **(II)** are pentacoordinated with the lithium centres interacting with the carbon centres in the 2-positions of the indolide.
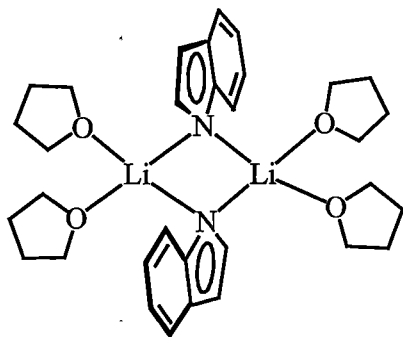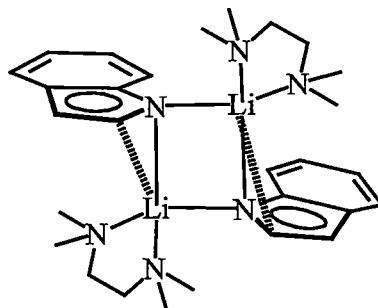
(I)   **(II)**

The sodium indolide complexes **(III)** and **(IV)** also have dimeric structures in the solid state[2]. Both complexes exhibit the same *anti*-orientations of the indolide rings with respect to the Na_2N_2 ring. Due to the different steric demand and coordination number arising from the Lewis bases, the structures vary slightly, *e.g.*, the sodium cations are six-coordinate in **(III)** but five-coordinate in **(IV)**, with an η^3- indolide interaction being described for the former complex. The two Na-N bond distances vary substantially for **(III)**, while they are identical in **(III)**.
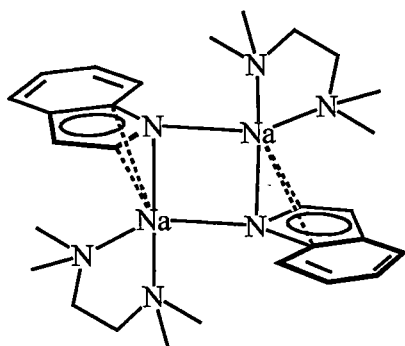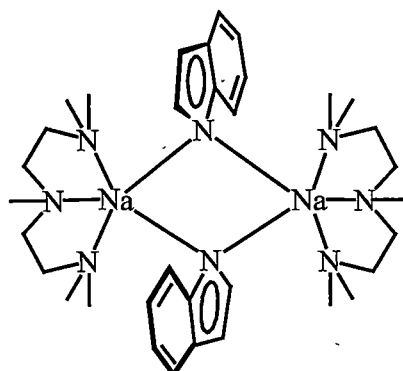
(III)   **(IV)**

Relatively few studies have been reported where an attempt has been made to alter the binding mode of indolides using ring substitution approaches. These substituted indolides have mainly given rise to σ-coordination modes with metals, however, the aggregation state of the complexes can be reduced compared to the corresponding nonsubstituted indolide complexes. The monomeric lithium indolide complex **(V)** was prepared using bulky substitution at the 2-position of the indolide[3]. The lithium cation is σ-bound to the indolide through the nitrogen centre.

Terminal σ-bonding modes of the indolide ligands have also been found in complexes of other metals[4], for example, iridium(I) complex (VI)[5].
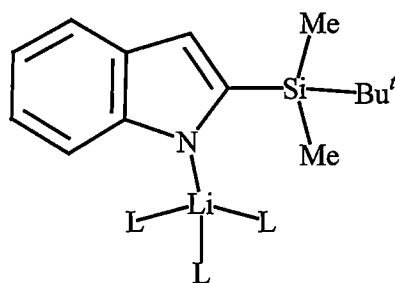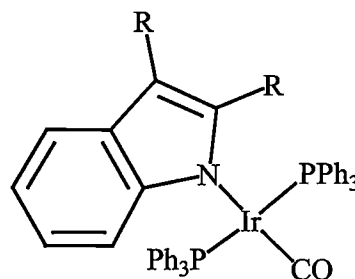
(V) (L = THF)   (VI)

The lanthanide indolide complexes featuring 2-phenyl substitution of the indolide, (VII), were reported by Deacon. Both monomeric [Yb(pin)₂(diglyme)(THF)] and dimeric [Yb(pin)₂(DME)]₂ (VIII) complexes have been prepared in the presence of different Lewis bases. Both Yb(II) complexes, feature σ-bonding of the 2-phenylindolide through nitrogen centres in both bridging and non-bridging fashion, even though the substituents at the neighbouring 2-position to the nitrogen centres are quite bulky[6]. Complex (VIII) is a rare example in which a five coordinate lanthanide centre is bridged solely by nitrogen atoms of a pyrrolide-based ligand.

pinH (VII)

(VIII)[6]
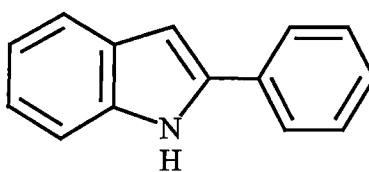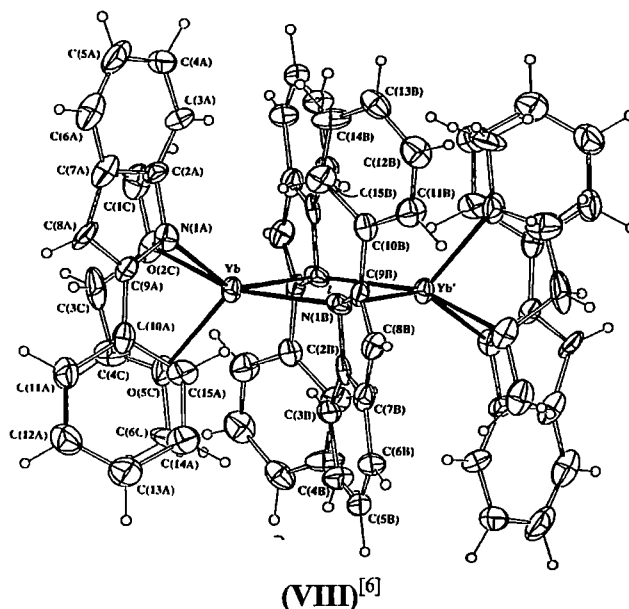
Only a few indolide complexes with η^5-bonding modes have been reported so far. Tricarbonyl-η^5-(2-methylindolyl)manganese, **(IX)**, was isolated in 16% yield by chromatography and sublimation of the mixture obtained from the reaction of potassium 2-methylindolide and bromopentacarbonylmanganese in benzene[7]. The Fe(II) indolide [(η^5-C_8NH_6)(η^5-C_5Me_5)Fe], **(X)**, was described and proposed to feature a η^5-bonding mode based on NMR spectroscopy and mass spectrometric characterisation, however the structural prediction lacks confirmation by X-ray crystal structure determination[8].

(IX)   **(X)**
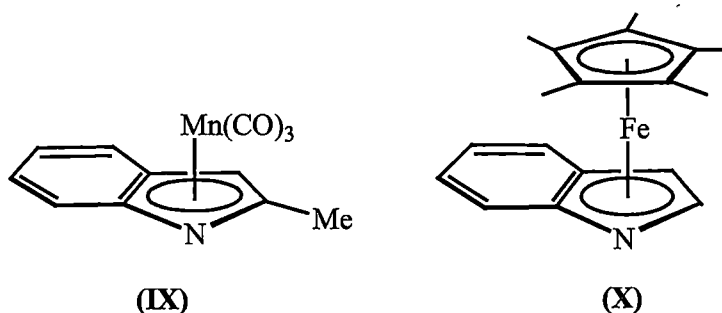
Recent studies of Group 1 metal 18-crown-6 complexes, such as **(XI)**, featuring pendant 3-indolyl substituents have shown η^5-bonding modes to be obtainable for complexes of highly electropositive metals, which is of biological relevance[9]. Further π-bonding alternatives have been shown for indolides by virtue of the extended aromatic system, for example, complexes **(XII)** feature the six-membered ring being involved in η^6-bonding to the ruthenium centres[10].

(R' = R" = H)
(XII) (R' = R" = Me)
(R' = Me; R" = H)

(XI)
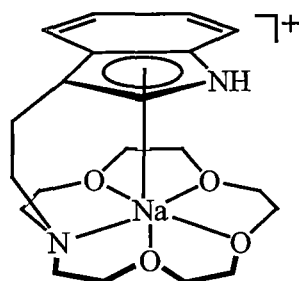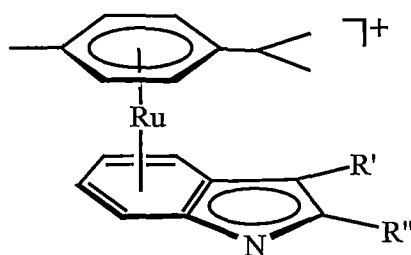
6.1.2 Indolide ligands with chelate ring strain

The approach of utilising more than one pyrrolide unit in a ligand to affect the bonding modes of pyrrolide anions has been studied recently. Metallo-porphyrinogen complexes represent important examples of the approach, where macrocyclic ring strain is influential in forcing η^5-binding modes upon the large radii metal centres bound within the macrocyclic cavity. Simpler systems, such as the linked bis(cyclopentadienyl) ligands (XIV)[11], (XV)[12] and di(2'-pyrrolyl)methanes (XVI) (see Section 4.1), have been studied, for which η^5-binding modes are frequently obtained for lanthanide metal complexes. The approach is unknown for diindolide ligands.
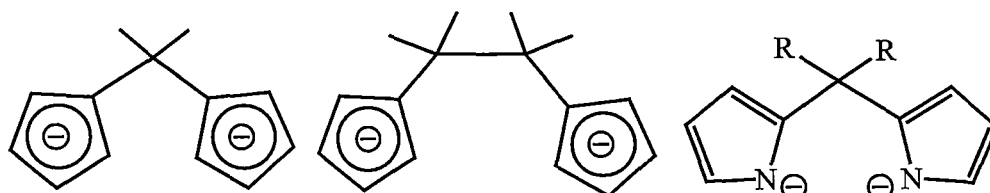
(XIV)   (XV)   (XVI)

6.2 RESULTS AND DISCUSSION

6.2.1 2,5-Bis{(3'-indolyl)diethylmethyl}furan, H₂(IOI) (26)

The synthesis of 2,5-bis{(3'-indolyl)diethylmethyl}furan, H_2(IOI) (26), was achieved in 71% yield through the condensation of the dialcohol (1) with two equivalents of indole in the presence of a catalytic amount of trifluoroacetic acid in ethanol, as shown in Equation 1.
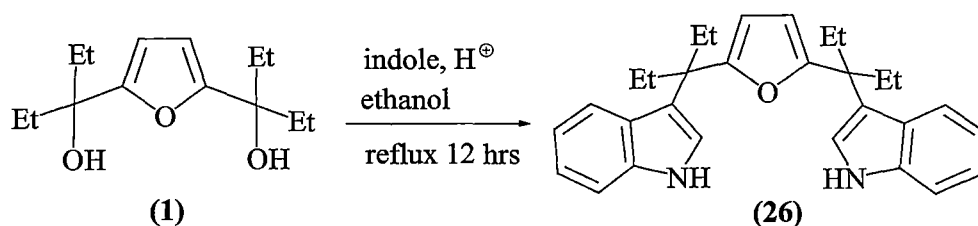
Equation 1

The diindole **(26)** features substitution in the 3-position of the indole units rather than the 2-position for pyrrole in the related condensation reaction with diol **(1)** in the synthesis of the dioxaporphyrinogen **(3)** (see Section 2.2.1.1). When the 3-position is substituted, for example in 3-methyl indole, the reaction in Equation 2 gave only a trace of the corresponding 2-substituted diindole product (3.3% yield, GC-MS).
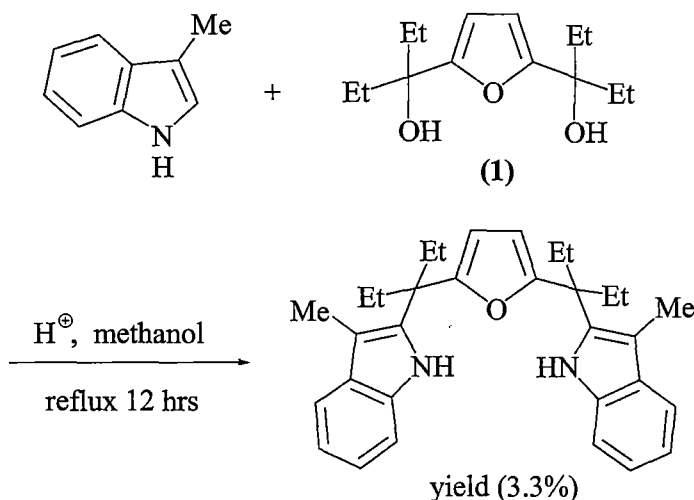
Equation 2

The diindole $H_2(IOI)$, **(26)**, is a colourless solid, soluble in diethyl ether, THF, benzene, less soluble in hexane, and insoluble in methanol and ethanol. The compound was characterised by ^1H, ^{13}C NMR and IR spectroscopies, microanalysis, mass spectrometry and single crystal X-ray structure determination.

The ^1H and ^{13}C NMR spectra of $H_2(IOI)$, **(26)**, confirm the formulation, in particular the resulting 3-indole substitution. The ethyl group proton resonances appear as triplets for the methyl protons at 0.63 ppm and multiplets for methylene protons at 2.00 ppm. The singlet protons at 6.12 ppm are from the aromatic protons of the furanyl ring. The two triplets at 6.87 and 7.05 ppm are assigned to the two aromatic protons at the 5- and 6-positions of the indolyl ring while the two doublets at 7.16 and 7.27 ppm are assigned to the two aromatic protons at the 4- and 7-

positions of the indolyl rings. The singlet at 7.25 ppm is assigned to the aromatic protons at the 2-position of the indolyl units (see Figure 1). The two NH protons appear as a broad resonance at 7.57 ppm. In the ^{13}C NMR spectrum of (26), the quaternary carbon resonance is at 43.8 ppm, the ethyl groups resonate at 8.4 ppm for the methyl carbons and 28.2 ppm for the methylene carbons. The aromatic carbons of the indolyl and furanyl rings appear as ten resonances between 106.0 and 159.0 ppm. The two ethyl groups which are borne on the quaternary carbons bridging the furan and indole rings appear chemically equivalent in solution by both ^{1}H and ^{13}C NMR spectroscopy. This is in contrast to the majority of the metallated macrocyclic compounds in this study and is an indication that molecules of (26) have non-restricted conformational freedom in solution at room temperature. Variable temperature NMR studies were not conducted to further study this phenomenon.
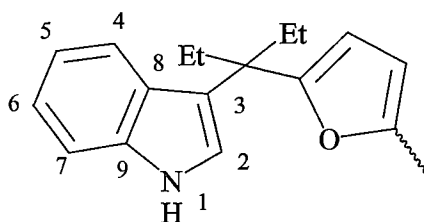
Figure 1: Numbering scheme for the NMR characterisation of H$_2$(IOI), (26)

Mass spectrometric studies of the diindole H$_2$(IOI), (26), shows the molecular ion at 438 (M$^+$, 8%). Other ions include 409 (M-Et, 100%) and 380 (M-2Et, 20%). The IR spectrum of (26) features the N-H stretching band at 3430 cm^{-1}. Compound (26) gave a satisfactory microanalysis result.

Crystals of the diindole H$_2$(IOI), (26), suitable for single crystal X-ray structure determination were grown from a saturated diethyl ether/hexane solvent mixture (1:1; v/v), which was stored at -30 °C for three days. The crystals belong to the triclinic space group $P\bar{1}$ (No. 2), a = 9.987(1), b = 14.117(2), c = 19.218(2) Å, α = 104.951(3), β = 96.440(4), γ = 105.405(3)°, with four molecules in the unit cell. The asymmetric unit contains two molecules with nearly identical geometries. Figure 2 shows the geometry of molecule 1.
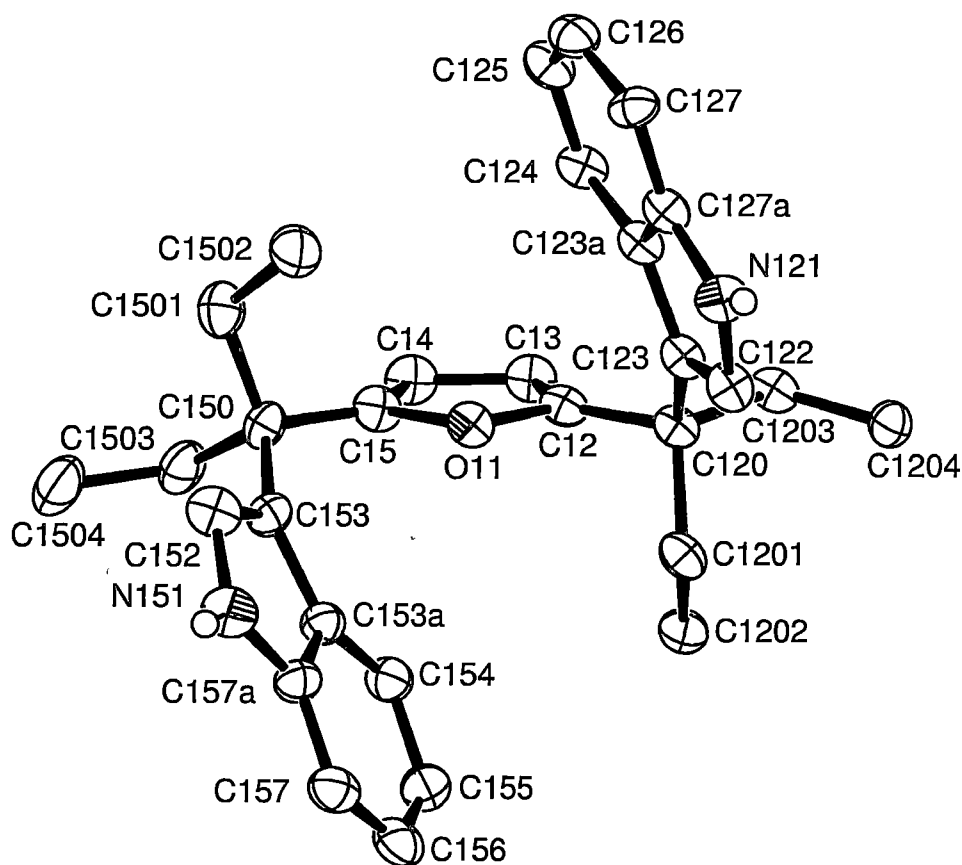
Figure 2: Molecular structure of H$_2$(IOI), **(26)**, with thermal ellipsoids drawn at the level of 50% probability, protons (except *N*-H protons) have been omitted for clarity.

The solid state conformation of **(26)** has the two indole units extending on either side of the plane of the furan unit in an *anti-* disposition. The oxygen centre of the furan functionality is directed inwards towards the void created by the two indole rings. The conformation of the diindole is preorganised for an unusual C_2 symmetric internally coordinated *ansa*-metallocene that could be envisaged upon dimetallation of the indole functionalities.

6.2.2 Group 1 metal complexes of 2,5-bis{(3'-indolyl)diethylmethyl}furan

6.2.2.1 Complex syntheses

A range of Group 1 metal complexes have been prepared from the dimetallation of the diindole **(26)** with Bu^{n}Li, NaH, and K in THF or toluene, as shown in Scheme 2.
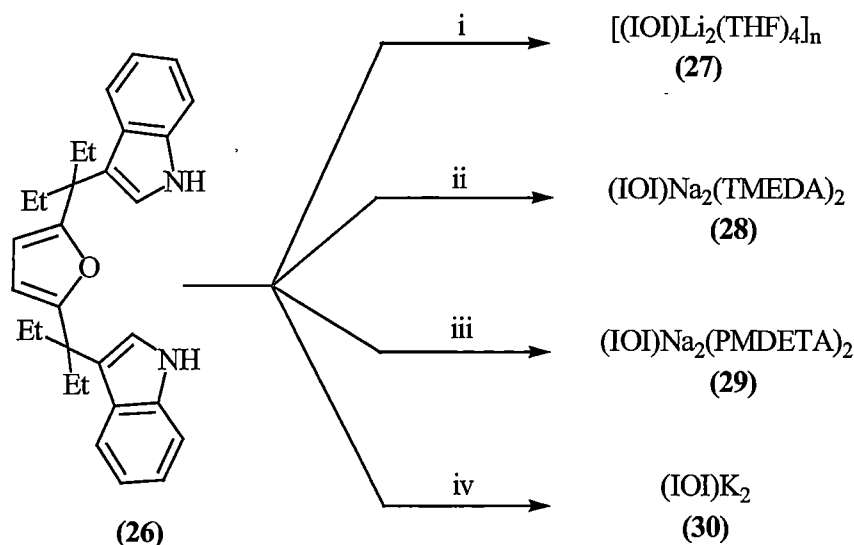
Scheme 2: Synthesis of Group 1 metal complexes of 2,5-bis{(3'-indolyl)diethylmethyl}furan, **(26)** (i. Bu^{n}Li, THF; ii. NaH, TMEDA, iii. NaH, PMDETA; iv. K or KH, THF).

The dilithium complex was isolated as the THF adduct, [(IOI)Li$_2$(THF)$_4$]$_n$, **(27)** and the disodium complex was isolated as TMEDA and PMDETA adducts, (IOI)Na$_2$(TMEDA)$_2$, **(28)**, and (IOI)Na$_2$(PMETA)$_2$, **(29)**, while the dipotassium complex was isolated in a solvent free form (IOI)K$_2$, **(30)**. The four complexes were isolated in good to excellent yields of 90% for **(27)**, 65% for **(28)**, 93% for **(29)** and 91% for **(30)**. The colourless complexes were characterised by ^{1}H, ^{13}C NMR and IR spectroscopies. A single crystal X-ray structure determination was performed in the case for **(27)**. All complexes gave satisfactory microanalyses, except **(30)** which gave a low carbon content.

The dilithium complex **(27)** is slightly soluble in THF and insoluble in toluene. Both the disodium and dipotassium complexes are moderately soluble in THF. The THF adduct of the disodium complex (isolated but not characterised) may lose coordinated THF during repeated recrystallisation or evaporation under vacuum, resulting in a white powder which is no longer soluble in THF. The solubility of corresponding unsolvated dipotassium complex remained unaffected by the same process. The dipotassium complex is considered to initially exist as THF adduct of undetermined stoichiometry when isolated from a THF solution, but completely loses the coordinated THF *in vacuo* (25°C, 10^{-2} mbar, 1 hr).

The ^{1}H NMR spectra of all complexes **(27)-(30)** exhibit all the expected proton resonances of the diindolide ligands and the solvent molecules contained, as listed in Table 2. The number scheme used for NMR discussion is shown in Figure 3.

Compound number.	CH$_3$	CH$_2$	=CH, (s), fur	=CH, (t), (5, 6)	=CH, (s) (2)	=CH, (d), (4, 7)
(26)	0.63	2.00	6.12	6.59, 6.86	7.06	7.16, 7.27
(27)	0.82	2.25	5.93	6.59, 6.71	7.31	7.34, 7.39
(28)	0.89	2.38	6.15	6.68, 6.86	7.32	7.48, 7.55
(29)	0.92	2.38	6.11	6.68, 6.86	7.35	7.48, 7.56
(30)	0.83	2.10, 2.26	6.46	6.56, 6.72	7.02	7.05, 7.10

Table 2: ^{1}H NMR spectroscopic data of complexes **(27)**, **(28)**, **(29)** and **(30)** (in THF-d^8, 399.694 MHz, 298 K, ppm, protons of TMEDA, PMDETA and toluene are not listed). The ^{1}H NMR spectroscopic data for H$_2$(IOI), **(26)** (CDCl$_3$, 399.694 MHz, 298 K, ppm) is included for comparison.
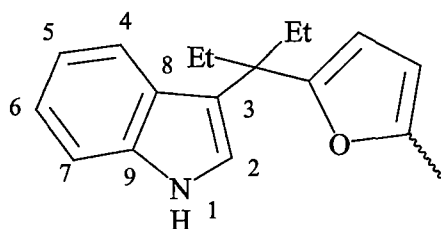
Figure 3: Numbering scheme for the NMR characterisation of **(26)-(30)**

Upon dimetallation of **(26)** with Group 1 metals, the methyl and methylene protons belonging to ethyl groups experience a downfield shift change of *ca.* 0.2-0.3 ppm. Only minor changes are apparent for the resonances of protons at the 5- and 6-positions of the indolide rings for all compounds listed. However, significant differences are found between the smaller sized lithium or sodium complexes and the potassium complex in terms of the proton resonances of the furanyl ring and 2-, 4- and 7-positions of the indolide rings. The lithium complex **(27)** and sodium complexes **(28)**, **(29)** display their singlet (2-indolide protons) and two doublets resonances (4- and 7-indolide protons) shifted downfield relative to **(26)** (0.2-0.3

ppm), but in the potassium complex (30) an upfield shift change of 0-0.2 ppm is observed for the same proton resonances. While the potassium complex (30) experiences a downfield chemical shift change of 0.34 ppm for singlet resonance of the aromatic protons of the furan ring relative to (26), all other complexes (27)-(29) show only slight changes for the same proton resonances relative to (26) (0.09, 0.03, 0.01 ppm for (27), (28) and (29), respectively.

The significant differences of the ^{1}H NMR spectral features among complexes (27)-(30) suggests that the different sized metals very likely have different bonding modes with the tricyclic dianion in solution. The proton resonances of the furanyl ring have been affected noticeably by potassium coordination but only slightly in the cases of other small sized metals. This indicates that potassium might coordinate to both indolyl and furanyl rings, while the other smaller sized metals most likely coordinate with the indolide rings only (as in the solid state structure of complex (27) in which lithium cations are σ-bound only to indolide rings through the nitrogen centres, see Section 6.2.2.2). This proposal is supported further by the chemical inequivalence of the methylene protons of the ethyl groups for (30), which indicate a conformational restriction resulting from the coordination of potassium with both indolide and furanyl rings that would be expected in such a chelating structure. In addition, differences in the mode of interaction of the various metals with the indolide units is likely, perhaps with potassium forming multihapto-interactions involving the five-membered ring of the indolide units as evident from the different chemical shifts of the protons in the 2-, 4- and 7-positions of the indolide unit in (30) compared to complexes (27)-(29).

The ^{13}C NMR spectra of complexes (27) – (30) display most of the resonances expected at typical chemical shifts and have not been assigned to individual aromatic carbons of the indolide or furan units. IR spectroscopy confirmed the dimetallation of diindole (26), with removal of both N-H protons in all complexes (27)-(30).

6.2.2.2 Molecular structure of [(IOI)Li₂(THF)₄]ₙ, (27)

Crystals of the lithium complex [(IOI)Li$_2$(THF)$_4$]$_n$, (27), suitable for single crystal X-ray structure determination were grown by the dropwise addition of a toluene solution of (27) into THF which was left to stand for three hours. The crystals belong to the monoclinic space group $P2_1/c$ (No. 14), $a = 15.0093(3)$, $b = 23.2614(6)$, $c = 16.6626(4)$ Å, $\beta = 111.6609(15)°$. The asymmetric unit consists of

one monomeric unit of (27) and several disordered solvent molecules partially modelled as THF molecules. Figure 3 shows a portion of the polymeric structure of (27).
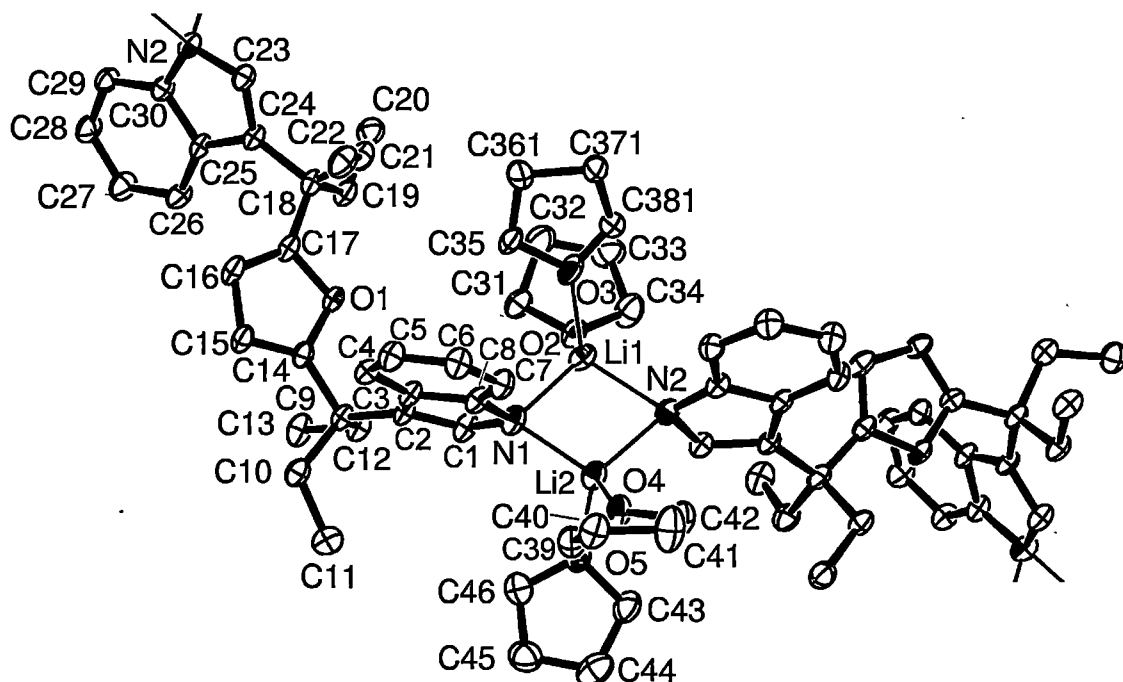
Figure 3: Molecular structure of $[(IOI)Li_2(THF)_4]_n$, (27), with thermal ellipsoids drawn at the level of 50% probability, protons have been removed for clarity.

The crystal structure reveals (27) to be a polymeric species in the solid state. Each diindolide unit coordinates with four lithium cations by μ_2-bridging through indolide units. Each lithium cation, with two coordinated THF molecules, σ-binds the indolide units through the bridging nitrogen centres. Two bridging lithium cations and two σ-bound indolide nitrogen centres comprise a four-membered Li_2N_2 ring core. Thus each diindolide unit participates in two Li_2N_2 cores with two other diindolide units and, in this way, the molecule extends to a polymeric form.

The Li_2N_2 ring in (27) is quite planar, which is similar to that seen in dimeric [{N-lithioindole(THF)$_2$}$_2$], (I)[1], but different from that in dimeric [{N-lithioindole(TMEDA)$_2$}$_2$], (II)[2], in which the shape of Li_2N_2 ring is obviously affected by the chelating TMEDA molecules. The tetracoordinated lithium cations in (27) is in common with dimeric [{N-lithioindole(THF)$_2$}$_2$], (I), but different from dimeric [{N-lithioindole(TMEDA)$_2$}$_2$], (II), in which the lithium cations are five coordinate, resulting again from the effect of the chelating TMEDA molecules. For

this reason, the Li-N bond distances in (27) are of similar lengths (2.065(9), 2.065(10), 2.032(9), 2.076(9) Å) to those in [{N-lithioindole(THF)$_2$}$_2$], (I), (2.067(6), 2.092(7) Å), rather than existing with two short and two long Li-N bonds as in [{N-lithioindole(TMEDA)$_2$}$_2$], (II), (2.004(7), 2.231(10) Å) arising from the distorted nature of the μ_2-N bridging indolide units which imply lesser and greater amounts of involvement of the π-orbitals and sp^2-hybridised atomic orbitals on the nitrogen centres of the indolide units. The N-Li-N and Li-N-Li angles related to Li$_2$N$_2$ ring for (27) (103.2(4) and 76.7(4)°) are also similar to those in (I) (103.6(3) and 76.4(2)°, respectively) but are different from those in (II) (96.6(3) and 82.5(3)°), further indicating the different bonding nature in the latter case.

The indolide rings in (27) are orientated a *syn*- disposition relative to the Li$_2$N$_2$ ring, as shown in Figure 4. This is different from [{N-lithioindole(THF)$_2$}$_2$], (I), in·which the rings are arranged in *anti*- dispositions despite the lithium cations also being solvated by THF molecules. A *syn*-arrangement is also noted for [{N-lithioindole(TMEDA)$_2$}$_2$], (II). Each indolide ring involved in the Li$_2$N$_2$ ring cores are not parallel with each other in (27), nor are they perpendicular to the plane of the Li$_2$N$_2$ ring, which differs from [{N-lithioindole(THF)$_2$}$_2$], (I). This twist is clearly the result of the substitution of diindolide ligand and the geometric restraints that this imposes on the formation of the polymeric complex, and perhaps interactions between the ¯*syn*- orientated six-membered rings of the indolide units in the Li$_2$N$_2$ ring cores.
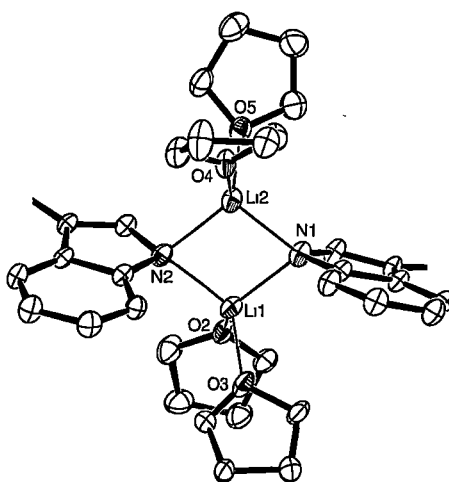
Figure 4: View of the Li$_2$N$_2$ core in the molecular structure of (27), with thermal ellipsoids drawn at the level of 50% probability, protons have been removed for clarity.

In contrast to the polymeric structure of **(27)**, featuring μ_2-bridging indolide anions, bulky 2-substituents have been shown to result in monomeric lithium indolides, such as **(V)**[3]. Clearly, the substitution of the indolide in the 3-position of **(27)** doesn't have such a drastic effect in bringing about this structural change.

6.2.3 Lithiation of N',N'',N'''-trimethyl-*meso*-octaethylporphyrinogen, [(Et$_8$N$_4$Me$_3$)Li(THF)$_2$] (31)

The reaction between N',N'',N'''-trimethyl-*meso*-octaethylporphyrinogen Et$_8$N$_4$Me$_3$H, **(7)**, and *n*-butyllithium leads to the formation of the monomeric lithium complex [(Et$_8$N$_4$Me$_3$)Li(THF)$_2$] **(31)**, as shown in Scheme 3.
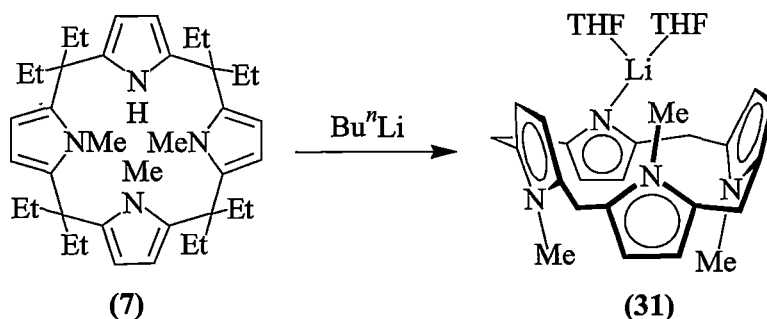
Scheme 3: Synthesis of [(Et$_8$N$_4$Me$_3$)Li(THF)$_2$], **(31)**.

The synthesis of **(31)** was performed in toluene in view of the good solubility of both the porphyrinogen **(7)** and *n*-butyllithium. The lithium complex [(Et$_8$N$_4$Me$_3$)Li(THF)$_2$], **(31)**, is not soluble in toluene and thus precipitated from the reaction after stirring for three hours at 50°C. The colourless solid product was collected and recrystallised from THF leding to a pure crystalline product in 69% yield. Complex **(31)** was characterised by ^{1}H NMR spectroscopy, microanalysis and an X-ray crystal structure determination.

The ^{1}H NMR spectrum of **(31)** in deuterated THF was largely unexceptional. The proton resonances of the *meso*-ethyl groups appear between 0.41-0.64 ppm, for CH$_3$, and 1.75-2.06 ppm, for CH$_2$ protons. Two of the three *N*-methyl groups are chemically equivalent identical and resonate as a singlet at 2.82 ppm, while the other *N*-methyl group appears as a singlet at 2.42 ppm. The pyrrolide or methylated pyrrole aromatic protons resonate at between 5.74 and 6.00 ppm. One THF molecule can be seen in the molecule, whose resonances appear at 1.77 and 3.58 ppm.

Microanalytical data on (31) are consistent with the ^{1}H NMR spectroscopic studies that show only one THF solvent molecule to be present. These results differ from the X-ray crystal structure which shows two bound THF moieties attached to lithium cation in the molecule. Apparently half of the THF is lost during NMR spectroscopic and microanalytical sample preparation involving vacuum transferral into the glove-box.

Colourless crystals of [(Et$_8$N$_4$Me$_3$)Li(THF)$_2$], (31), suitable for X-ray crystal structure determination were grown from a hot saturated THF solution which was stored at room temperature overnight. The crystals belong to the monoclinic space group $P2_1$ (No. 4), a = 10.290(2), b = 19.562(4), c = 10.788(2) Å, β = 100.024(4)°, with two molecules in the unit cell, the unit cell containing one molecule of (31). The structure of (31) is shown in Figure 5.
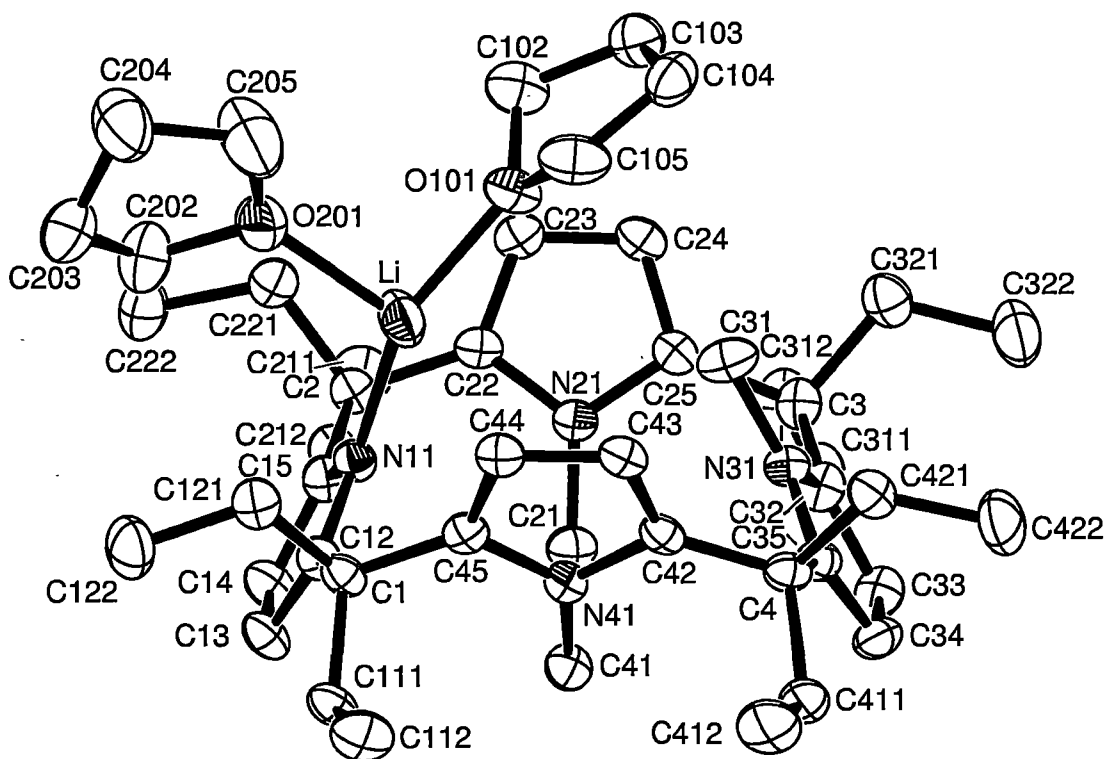
Figure 5: Molecular structure of [(Et$_8$N$_4$Me$_3$)Li(THF)$_2$], (31), with thermal ellipsoids drawn at the level of 50% probability, protons have been removed for clarity.

Complex (31) is monomeric in the solid state. The lithium centre has two coordinated THF molecules and binds to the macrocyclic unit through the nitrogen

centre for the pyrrolide ring in σ-fashion with the Li-N bond distance being
1.9661(78) Å, which is slightly longer than the related Li-N bond distance for
[(THF)$_2$Li{NC$_4$H$_2$(Bu$^t_2$-2,5)}$_2$] ((II), Section 3.1) of 1.926(4) Å[13]. The Li-N bond
distances is shorter than seen in most lithium complexes of porphyrinogens ((VI),
(VII), (VIII) and (IX), Section 3.1)[14]. Complex (31) adopts the 1,3-alternate
macrocyclic conformation, with the metal centre obviously displaying less much less
effect on the macrocyclic unit than in the parent porphyrinogen tetralithiated
complexes which adopt flattened or 'chaise longue' conformations. The two THF
molecules adopt a perpendicular orientation with respect to each other, with one
(O201) roughly parallel to two nearby ethyl groups and the other THF molecule
(O101) lying against the face of the macrocyclic cavity. The N11-Li-O101 angle of
153.05(35)° is much larger than N11-Li-O201 of 110.59(31)° and lithium cation is
0.41$_4$ Å out of the plane of the nonmethylated pyrrolide ring (away from the
macrocyclic cavity) indicating that the THF (O101) molecule encounters a steric
effect from the three N-methyl pyrrolyl rings and probably most significantly from
the N-methyl of the pyrrolyl ring which is directed towards the affected THF
molecule. The Li-O distances are close at 1.9983(74) and 2.0086(70) Å, giving no
indication of which THF molecule is lost when the complex is placed *in vacuo*.

The cross-cavity N···N distance of N(11)···N(31) = 4.96$_4$ Å involving lithiated
pyrrolide ring is longer than that (4.84$_5$ Å) of the protonated macrocycle (7). The
N···N distance of the other N-methylated pyrroles (N(21)···N(41) = 4.71$_1$ Å) is shorter
than the corresponding distance of 4.87$_4$ Å in (7). The heterocyclic ring tilt angles
with respect to the plane of the macrocyclic cavity are 62.1$_7$°, for the lithiated
pyrrolide ring, and 60.1$_1$° for the opposite N-methylpyrrole ring. The other N-
methylated pyrrole rings are steeper with tilt angles of 63.4$_5$° and 66.5$_4$°. These
cavity parameters are consistent with the structural features described above relating
to the steric interactions between the lithium coordinated THF molecule and the N-
methyl group which is *trans*- to the pyrrolide unit.

6.3 Experimental

Synthesis of $H_2(IOI)$, **(26)**

To a flask containing 2,5-bis(hydroxydiethylmethyl)furan, **(1)**, (4.8 g, 20.0 mmol) and indole (4.8 g, 41.0 mmol) in degassed absolute ethanol (80 mL), trifluoroacetic acid (0.32 mL, 0.47 g, 4.1 mmol) was added dropwise with stirring and the mixture refluxed overnight. The precipitated product was collected by filtration and washed with methanol (3 x 20 mL) three times to leave a colourless solid 6.2 g (71%, m.p. 173-176°C). Crystals suitable for X-ray crystal structure determination were obtained by recrystallisation from a hexane/diethyl ether solvent mixture (1:1; v/v).

^{1}H NMR (CDCl$_3$, 399.694 MHz, 298 K, ppm): 0.63 (t, 12H, CH$_3$), 2.00 (m, 8H, CH$_2$), 6.12 (s, 2H, =CH, fur), 6.59 (t, 2H, =CH, ind, 5 or 6), 6.86 (t, 2H, =CH, ind, 5 or 6), 7.06 (s, 2H, =CH, ind, 2), 7.16 (d, 2H, =CH, ind, 4 or 7), 7.27 (d, 2H, =CH, ind, 4 or 7), 7.57 (s, broad, 2H, NH, ind).

^{13}C NMR (CDCl$_3$, 100.512 MHz, 298 K, ppm): 8.4 (CH$_3$), 28.2 (CH$_2$), 43.8 (CEt$_2$), 106.1, 110.8, 118.6, 120.1, 121.0, 121.1, 122.3, 126.2, 136.5, 158.4 (=CH and =CR, fur and ind).

MS: 438 (M$^+$), 409 (M-Et, 100%), 380 (M-2Et), 365 (M-2Et-Me)

IR (υ (cm^{-1}), KBr): 485 (s), 584 (m), 737 (s), 963 (m), 1107 (m), 1242 (w), 1333 (m), 1422 (m), 1457 (s), 1545 (w), 1618 (w), 2873 (m), 2963 (s), 3430 (s).

Anal. Calcd.: C, 82.16; H, 7.81; N, 6.39 (C$_{30}$ H$_{34}$N$_2$O, MW 438.60).

  Found: C, 81.97; H, 8.01; N, 6.30

Synthesis of $[(IOI)Li_2(THF)_4]_n$, **(27)**

To a solution of $H_2(IOI)$, **(26)**, (1.32 g, 3.00 mmol) in toluene (40 mL), was added n-butyllithium (4.5 mL, 1.6 M in hexane, 7.2 mmol) with stirring at ambient temperature overnight. THF (20 mL) was added and the product precipitated as a colourless crystalline solid which was collected by filtration (2.00 g, 90%). Crystals suitable for X-ray crystal structure determination were obtained by crystallisation through the dropwise addition of a toluene solution of **(27)** to THF (1:10, v/v).

^{1}H NMR (THF-d^8, 399.694 MHz, 298 K, ppm): 0.82 (t, 12H, CH$_3$), 1.90 (m, 16H, THF), 2.25 (q, 8H, CH$_2$), 3.77 (m, 16H, THF), 5.93 (s, 2H, =CH, fur),

6.59 (t, 2H, =CH, ind, 5 or 6), 6.71 (t, 2H, =CH, ind, 5 or 6), 7.31 (s, 2H, =CH, ind, 2), 7.34 (d, 2H, =CH, ind, 4 or 7), 7.39 (d, 2H, =CH, ind, 4 or 7).

^{13}C NMR (THF-d^8, 100.512 MHz, 298 K, ppm): 10.4 (CH$_3$), 27.0 (THF), 31.7 (CH$_2$), 46.5 (CEt$_2$), 68.8 (THF), 107.2, 114.4, 116.3, 120.8, 130.5, 137.6, 150.2, 161.2 (=CH and =CR, fur and ind).

IR (υ (cm^{-1}), Nujol): 736 (s), 892 (s), 1012 (s), 1048 (s), 1104 (w), 1138 (s), 1162 (s), 1200 (m), 1230 (m), 1300 (s), 1334 (s), 1596 (w).

Anal. Calcd.: C, 74.77; H, 8.73; N, 3.79 (C$_{46}$H$_{64}$Li$_2$N$_2$O$_5$, MW 738.91).
        Found: C, 74.65; H, 8.48; N, 3.64.

Synthesis of (IOI)Na$_2$(TMEDA)$_2$·C$_7$H$_8$, (28)

To a solution of H$_2$(IOI), (26), (1.32 g, 3.00 mmol) in THF (40 mL), sodium hydride (0.17 g, 7.20 mmol) was added at ambient temperature with stirring. The mixture was allowed to stir overnight and the solution was filtered from any remaining solids. The volume of the solution was reduced (20 mL) and TMEDA (2.79 g, 3.62 mL, 24.0 mmol) was added, followed by toluene (10 mL). A colourless crystalline product appeared after storage for two weeks at ambient temperature which was collected (1.57 g, 65%).

^{1}H NMR (THF-d^8, 399.694 MHz, 298 K, ppm): 0.89 (t, 12H, CH$_3$), 2.31 (s, 24H, NCH$_3$), 2.38 (m, 8H, CH$_2$), 2.48 (s, 8H, NCH$_2$), 2.49 (s, 3H, CH$_3$Ph), 6.15 (s, 2H, =CH, fur), 6.68 (t, 2H, =CH, ind, 5 or 6), 6.86 (t, 2H, =CH, ind, 5 or 6), 7.26-7.38 (m, 7H, =CH(ind) + C$_6$H$_5$), 7.48 (d, 2H, =CH, ind, 4 or 7), 7.55 (d, 2H, =CH, ind, 4 or 7).

^{13}C NMR (THF-d^8, 100.512 MHz, 298 K, ppm): 10.2 (CH$_3$), 22.1 (CH$_3$Ph), 31.0 (CH$_2$), 46.3 (CEt$_2$), 46.8 (NCH$_3$), 59.5 (NCH$_2$), 106.6, 115.5, 116.4, 117.1, 117.1, 120.9, 126.6, 129.5, 130.3, 137.8, 138.7, 149.8, 161.2 (=CH and =CR, fur, ind and toluene).

IR (υ (cm^{-1}), Nujol): 734 (s), 942 (m), 1020 (m), 1170 (m), 1290 (s), 1334 (m).

Anal. Calcd.: C, 72.92; H, 8.99; N, 10.41 (C$_{49}$H$_{72}$N$_6$Na$_2$O, MW 807.11).
        Found: C, 72.68; H, 8.80; N, 9.61.

Synthesis of (IOI)Na$_2$(PMDETA)$_2$, (29)

To a solution of H$_2$(IOI), (26), (1.32 g, 3.00 mmol) in THF (40 mL), sodium hydride (0.17 g, 7.20 mmol) was added at ambient temperature with stirring. The

mixture was let stir overnight and the solution was filtered from any remaining solids. The solution was concentrated to 10 mL and PMDETA (4.16 g, 5.01 mL, 24.0 mmol) was added. Recrystallisation from THF gave a colourless crystalline product (2.26 g, 91%).

> ^{1}**H NMR** (THF-d^8, 399.694 MHz, 298 K, ppm): 0.92 (t, 12H, CH$_3$), 2.21 (d, 6H, NCH$_3$), 2.33 (d, 24H, NCH$_3$), 2.41-2.60 (m, 24H, NCH$_2$+CH$_2$), 6.11 (s, 2H, =CH, fur), 6.68 (t, 2H, =CH, ind, 5 or 6), 6.86 (t, 2H, =CH, ind, 5 or 6), 7.35 (s, 2H, =CH, ind, 2), 7.48 (d, 2H, =CH, ind, 4 or 7), 7.56 (d, 2H, =CH, ind, 4 or 7).
>
> **Anal.** Calcd.: C, 69.53; H, 9.48; N, 13.51. (C$_{48}$H$_{78}$N$_8$Na$_2$O, MW 829.17).
>
> Found: C, 69.44; H, 9.55; N, 13.68.

Synthesis of (IOI)K$_2$, (30)

To a solution of H$_2$(IOI), (26), (1.32 g, 3.00 mmol) in THF (40 mL), potassium (0.28 g, 7.20 mmol) was added with stirring and the mixture refluxed for 2 hours and let cool to room temperature. The solution was filtered from any remaining solids and concentrated to 20 mL. Recrystallisation from THF led to a colourless product which was isolated by filtration (1.43 g, 93%).

> ^{1}**H NMR** (THF-d^8, 399.694 MHz, 298 K, ppm): 0.83 (t, ^3J = 7.60 Hz, 12H, CH$_3$), 2.06-2.12 (m, 4H, CH$_2$), 2.30-2.22 (m, 4H, CH$_2$), 6.46 (s, 2H, =CH, fur), 6.56 (t, 2H, =CH, ind, 5 or 6), 6.72 (t, 2H, =CH, ind 5 or 6), 7.02 (s, 2H, =CH, ind, 2), 7.05 (d, 2H, =CH, ind, 4 or 7), 7.10 (d, 2H, =CH, ind, 4 or 7).
>
> ^{13}**C NMR** (THF-d^8, 100.512 MHz, 298 K, ppm): 9.3 (CH$_3$), 28.9 (CH$_2$), 45.1 (CEt$_2$), 106.4, 116.1, 116.4, 117.1, 117.8, 120.1, 128.9, 136.4, 161.8 (=CH and =CR, fur and ind).
>
> **IR:** 734 (s), 962 (m), 1028 (m), 1116 (w), 1144 (m), 1266 (s), 1278 (m), 1342 (m).
>
> **Anal.** Calcd.: C, 69.99; H, 6.27; N, 5.44 (C$_{30}$H$_{32}$K$_2$N$_2$O, MW 514.18).
>
> Found: C, 67.92; H, 6.41; N, 4.86.

Synthesis of [(Et$_8$N$_4$Me$_3$)Li(THF)$_2$], (31)

To a solution of N',N'',N'''-trimethyl-*meso*-octaethylporphyrinogen, Et$_8$N$_4$Me$_3$H (7), (1.17 g, 2.00 mmol) in toluene (40 mL), n-butyllithium (1.5 mL, 1.6 M in hexane, 2.4 mmol) was added with stirring and the mixture was let stir at 50°C

for 3 hours. The precipitated solid product was collected by filtration and the product was washed twice with toluene (20 mL). Recrystallisation from THF gave a pure crystalline sample of **(31)** (0.91 g, 69%).

^{1}H NMR (THF-d^8, 399.694 MHz, 298 K, ppm): 0.41-0.64 (m, 24H, 8CH$_3$), 1.75-2.06 (m, 20H, CH$_2$+THF), 2.42 (s, 3H, CH$_3$), 2.82 (s, 6H, 2CH$_3$), 3.61 (m, 4H, THF), 5.74-6.00 (m, 8H, pyrMe+pyr).

Anal. Calcd.: C, 78.14; H, 9.91; N, 8.48

(C$_{43}$H$_{65}$LiN$_4$O, for Et$_8$N$_4$Me$_3$)Li(THF), MW 660.94)

Found: C, 77.95; H, 10.04; N, 8.31.

6.4 References

[1]   A. Frenzel, R. Herbst-Irmer, U. Klingebiel, M. Noltemeyer, M. Schäfer, *Z. Naturforsch., Teil B*, 1995, **50**, 1658.

[2]   K. Gregory, M. Bremer, W. Bauer, P. von R. Schleyer, N.P. Lorenzen, J. Kopf, E. Weiss, *Organometallics*, 1990, **9**, 1485.

[3]   A. Frenzel, R. Herbst-Irmer, U. Klingebiel, M. Noltemeyer, S. Rudolph, *Main Group Chemistry*, 1996, **1**, 399.

[4]   **a.** M.-C. Corbeil, A.L. Beauchamp, *Can. J. Chem.*, 1988, **66**, 2458.
        b. C. Crotti, S. Cenini, B. Rindone, S. Tollari, F. Demartin, *J. Chem. Soc., Chem. Commun.*, 1986, 784.
        c. F.T. Ladipo, J.S. Merola, *Inorg. Chem.*, 1990, **29**, 4172.
        d. G.C. Hsu, W.P. Kosar, W.D. Jones, *Organometallics*, 1994, **13**, 385.
        e. O. Yamauchi, M. Takani, K. Toyada, H. Masuda, *Inorg. Chem.*, 1990, **29**, 1856.
        f. K.G. Parker, B. Noll, C.G. Pierpont, M.R. DuBois, *Inorg. Chem.*, 1996, **35**, 3228.
        g. K.I. Hardcastle, H. Minassian, A.J. Arce, Y. De Sanctis, A.J. Deeming, *J. Organomet. Chem.*, 1989, **368**, 119.
        h. S.F. Liu, Q.G. Wu, H.L. Schmider, H. Aziz, N.X. Hu, Z. Popovic, S.N. Wang, *J. Am. Chem. Soc.*, 2000, **122**, 3671.
        i. T.J. Johnson, A.M. Arif, J.A. Gladysz, *Organometallics*, 1994, **13**, 3182.

[5]   S. Chen, B.C. Noll, L. Peslherbe, M.R. DuBois, *Organometallics*, 1997, **16**, 1089.

[6]   C.T. Abrahams, G.B. Deacon, C.M. Forsyth, W.C. Patalinghug, B.W. Skelton, A.H. White, *Aust. J. Chem.*, 1995, **48**, 1933.

[7]   **a.** J.A.D. Jeffreys, C. Metters, *J. Chem. Soc., Dalton Trans.*, 1977, 1624.
        b. P.L. Pauson, A.R. Qazi, B.W. Rockett, *J. Organomet. Chem.*, 1967, **7**, 325.

[8]   M. Suginome, G. Fu, *Chirality*, 2000, **12**, 318.

[9]   J.X. Hu, L.J. Barbour, R. Ferdani, G.W. Gokel, *Chem. Commun.*, 2002, 1810.

[10]   S. Chen, V. Carperos, B.C. Noll, R.J. Swope, M.R. Dubois, *Organometallics*, 1995, **14**, 1221.

[11]   **a.** A.V. Khvostov, V.K. Belsky, B.M. Bulychev, A.I. Sizov, B.B. Ustinov, *J. Organomet. Chem.*, 1998, **571**, 243.
b. A.V. Khvostov, V.K. Belsky, A.I. Sizov, B.M. Bulychev, N.B. Ivchenko, *J. Organomet. Chem.*, 1998, **564**, 5.

[12]   **a.** P.F. Yan, N.H. Hu, Z.S. Jin, W.Q. Chen, *J. Organomet. Chem.*, 1990, **391**, 313.
b. C.D. Sun, Z.S. Jin, G.C. Wei, W.Q. Chen, *Chin. Chem. Lett.*, 1992, **3**, 941.
c. C.D. Sun, G.C. Wei, Z.S. Jin, W.Q. Chen, *J. Organomet. Chem.*, 1993, **453**, 61.
d. C.D Sun, G.C. Wei, Z.S. Jin, W.Q. Chen, *Polyhedron*, 1994, **13**, 1483.

[13]   M. Westerhausen, M. Wieneke, H. Nöth, T. Seifert, A. Pfitzner, W. Schwarz, O. Schwarz, J. Weidlein, *Eur. J. Inorg. Chem.*, 1998, 1175.

[14]   **a.** S. De Angelis, E. Solari, C. Floriani, A. Chiesi-Villa, C. Rizzoli, *J. Chem. Soc., Dalton Trans.*, 1994, 2467.
b. J. Guan, T. Dubé, S. Gambarotta, G.P.A. Yap, *Organometallics*, 2000, **19**, 4820.
c. J. Jubb, P. Berno, S. Hao, S. Gambarotta, *Inorg. Chem.*, 1995, **34**, 3563.
d. J. Jubb, S. Gambarotta, R. Duchateau, J.H. Teuben, *J. Chem. Soc., Chem. Commun.*, 1994, 2641.

CHAPTER 7

CONCLUSION

7.1 CONCLUDING REMARKS

The work described in this thesis focuses on the organolanthanide chemistry of dimetallated *meso*-octaethyl-*trans*-dioxaporphyrinogen, $Et_8O_2N_2H_2$ **(3)**, and *trans-N,N'*-dimethyl-*meso*-octaethylporphyrinogen, $Et_8N_4Me_2H_2$ **(6)**. The thesis also includes the synthesis and characterisation of related macrocycles and Group 1 metal derivatives that are accessed in the preparation of target samarium(II) and (III) complexes. The compounds prepared have been characterised in most cases by ^1H and ^{13}C NMR and IR spectroscopies, microanalyses and X-ray crystal structure determinations.
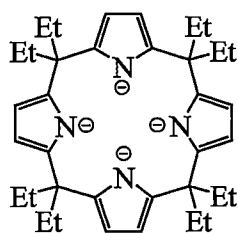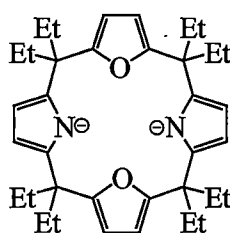
(4)-4H: $(Et_8N_4)^{4-}$ **(3)-2H: $(Et_8O_2N_2)^{2-}$**   **(6)-2H: $(Et_8N_4Me_2)^{2-}$**
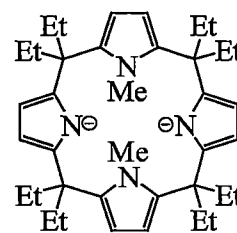
i) Synthesis

The dioxaporphyrinogen $Et_8O_2N_2H_2$, **(3)**, was prepared in a '3+1' approach from the condensation of 2,5-bis{(2'-pyrrolyl)diethylmethyl}furan, **(2)**, and 2,5-bis(hydroxydiethylmethyl)furan, **(1)**, in toluene in the presence of trifluoroacetic acid[1]. The *trans-N,N'*-dimethylated porphyrinogen $Et_8N_4Me_2H_2$, **(6)**, was prepared from the reaction of the tetrasodium complex of the parent porphyrinogen $Et_8N_4H_4$, **(4)**, with 2.5 molar equivalents of methyl iodide in the presence of 18-crown-6[2]. The *trans-N,N'*-dimethylated porphyrinogen **(6)** was isolated as the major product and other byproducts such as *N,N',N''*-trimethyl-*meso*-octaethylporphyrinogen, $Et_8N_4Me_3H$ **(7)**, and *N,N',N'',N'''*-tetramethyl-*meso*-octaethylporphyrinogen, $Et_8N_4Me_4$ **(8)**, were separated by chromatography. The nonmacrocyclic 2,5-bis{(3'-indolyl)diethylmethyl}furan, $H_2(IOI)$ **(26)**, was prepared from the condensation of 2,5-bis(hydroxydiethylmethyl)furan, **(1)**, with two equivalents of indole in the presence of a catalytic amount of trifluoroacetic acid.

The Group 1 metal complexes (lithium, sodium and potassium) (8) -. (11) featuring the dioxaporphyrinogen $Et_8O_2N_2H_2$, (3), (12) - (14) derived from the *trans-N,N'*-dimethylated porphyrinogen $Et_8N_4Me_2H_2$, (6), (27) - (30) featuring the diindolyl $H_2(IOI)$, (26), and [($Et_8N_4Me_3$)Li(THF)$_2$], (31), have been synthesised from the direct metallation of the pyrrole and indole based heterocycles (3), (6), (26) and (7) in THF or toluene using *n*-butyllithium, sodium hydride and potassium metal, respectively.

The samarium(II) complexes [{(THF)$_2$K($Et_8O_2N_2$)Sm(μ-I)}$_2$], (15), and [($Et_8N_4Me_2$)Sm(THF)$_2$], (16), derived from the modified porphyrinogens $Et_8O_2N_2H_2$, (3), and $Et_8N_4Me_2H_2$, (6), were prepared from the metathetical exchange reactions of the dipotassium complexes (10) and (14) (prepared *in situ*) with samarium(II) diiodide in THF. The samarium(III) iodide complex [($Et_8O_2N_2$)SmI], (17), and the samarium(III) chloride complex [($Et_8N_4Me_2$)SmCl], (18), or [{($Et_8N_4Me_2$)Sm(μ-Cl)}$_2$], (19), were prepared from the oxidation of the samarium(II) complexes (15) and (16) using iodine or *tert*-butyl chloride in THF or toluene. The alkyl complexes [($Et_8N_4Me_2$)SmR] ((20) R = Me, (21) R = CH_2SiMe_3), and amide complexes [($Et_8O_2N_2$)SmN(SiMe$_3$)$_2$], (22), and [($Et_8N_4Me_2$)SmN(SiMe$_3$)$_2$], (25), were synthesised from metathetical exchange reactions of the samarium(III) halides (17) or (18) and alkyl lithium reagents or sodium bis(trimethylsilyl)amide in THF. The γ-methyl deprotonation of (22) was serendipitously found to be a rapid reaction, forming [(toluene)Na($Et_8O_2N_2$)SmN(SiMe$_3$)Si(Me)$_2$CH$_2$], (23).

ii) Molecular structure

X-ray crystal structure determinations· have been performed for the heterocyclic compounds $Et_8O_2N_2H_2$, (3), $Et_8N_4Me_3H$, (7), $Et_8N_4Me_4$, (8), and $H_2(IOI)$, (26), the Group 1 metal complexes [($Et_8O_2N_2$)K$_2$(TMEDA)$_2$], (10), [($Et_8N_4Me_2$)K$_2$(THF)$_2$]$_n$, (14), [(IOI)Li$_2$(THF)$_4$]$_n$, (27) and [($Et_8N_4Me_3$)Li(THF)$_2$], (31), the samarium(II) complexes [{(THF)$_2$K($Et_8O_2N_2$)Sm(μ-I)}$_2$], (15), [($Et_8N_4Me_2$)Sm(THF)$_2$], (16), the samarium(III) chloride complex [{($Et_8N_4Me_2$)Sm(μ-Cl)}$_2$], (19), the alkyl complexes [($Et_8N_4Me_2$)SmMe], (20) and [($Et_8N_4Me_2$)Sm(CH$_2$SiMe$_3$)], (21), and the amide complexes [($Et_8O_2N_2$)SmN(SiMe$_3$)$_2$], (22), [(toluene)Na($Et_8O_2N_2$)SmN(SiMe$_3$)Si(Me)$_2$CH$_2$], (23), and [($Et_8N_4Me_2$)SmN(SiMe$_3$)$_2$], (25).

The majority of the samarium complexes prepared feature no retention of alkali metal cations, as compared with related tetrametallated complexes of parent porphyrinogen $Et_8N_4H_4$ which often incorporate alkali metal cations[3]. The lower charged dimetallated modified porphyrinogens effectively negate the requirement to include the alkali metal cations for reasons of charge balance alone, unless the availability of favourable alkali metal binding sites are at issue. Such was the case in a number of complexes featuring the less bulky dioxaporphyrinogen (3), which have sodium or potassium incorporation. In no cases have disamarium complexes been observed nor have macrocycle rearrangements been noted in even trace amounts in our studies thus far. This highlights the significant structure and reactivity control that we have demonstrated through the utilisation of modified porphyrinogens.

The structurally characterised complexes of the modified porphyrinogens (3) and (6) are monomeric species, with the exception of complexes (14) and (15). The macrocyclic unit in both the macrocycles themselves and the complexes derived from the modified porphyrinogens adopt 1,3-altenate conformations. The *endo*-cavity-bound metal centres coordinate with the macrocyclic units with $\eta^5:\eta^1:\eta^5:\eta^1$-bonding modes in all the potassium and samarium complexes. The samarium(III) complexes (22) and (23) of the dioxaporphyrinogen (3) feature η^5-bonding modes of the samarium centres to the pyrrolide units and η^1-bonding modes to the furanyl rings. The related samarium(II) complex (15) is presumed to have this same structure feature. The samarium(II) and (III) complexes of the *trans-N,N'*-dimethylated porphyrinogen (6) feature η^5-bonding of the samarium centres to the *N*-methylpyrrole units and η^1-bonding modes to the pyrrolide units through nitrogen centres. The two *endo*-cavity-bound potassium centres in the dipotassium complex (10) derived from the dioxaporphyrinogen (3) feature alternate $\eta^5:\eta^1:\eta^5:\eta^1$- and $\eta^1:\eta^5:\eta^1:\eta^5$-bonding modes, respectively, with the macrocyclic unit from each side of the cavity. The two potassium centres in the *trans-N,N'*-dimethylated porphyrinogen analogue (14) are divided into an *endo*-cavity-bound potassium centre, which binds to the macrocyclic unit with the same bonding modes as the samarium centres in related complexes, and an *exo*-cavity-bound potassium centre, which adopts η^5- and η^2-bonding modes to the outside faces of two pyrrolide rings of two adjacent macrocyclic units forming a polymeric structure.

The potassium, samarium(II) and samarium(III) complexes (10), (15) and (23) of the dioxaporphyrinogen $Et_8O_2N_2H_2$, (3), and the related complexes (14) and (16) of the *trans-N,N'*-dimethylated porphyrinogen $Et_8N_4Me_2H_2$, (6), have different structural features. Both complexes (10) and (15) feature divergent coordination of

potassium, sodium or samarium centres from each side of the macrocyclic cavities. However, the potassium and samarium centres in complexes **(14)**, **(16)**, **(19)**, **(20)**, **(21)** and **(25)** coordinate to the macrocyclic units in more controlled fashions with one side of the macrocyclic cavity being blocked by the two N-methyl substituents. The samarium(III) amide complex **(22)** derived from the dioxaporphyrinogen **(3)** features one open face of the macrocyclic cavity, rendering it prone to γ-methyl deprotonation of the amide ligand in the presence of base, which demonstrates the reduced coordination control that is achievable for the dioxaporphyrinogen **(3)** in comparison to the *trans-N,N'*-dimethylated porphyrinogen **(6)**.

The coordination numbers of the samarium centres in the structurally characterised complexes display some variations. The samarium(II) complexes **(15)** and **(16)** adopt samarium coordination numbers of 10, but a lowered coordination number of 9 in the samarium(III) alkyl complexes **(20)**, **(21)** and amide complexes **(21)**, **(25)** is observed. A coordination number of 10 is observed in the samarium(III) complexes **(18)** and **(23)**, where the longer Sm-Cl bond length allows dimerisation and the bidentate coordination mode of the N,C-dianion, respectively, permit this coordination number increase. The large coordination numbers in these complexes contrast with coordination numbers of upto only 8 typically seen for related bis(cyclopentadienyl)samarium(II) and (III) complexes[3].

The metallocene bend angles (centroid-Sm-centroid) in all the samarium(II) and (III) complexes reflect the ionic radii of samarium in these oxidation states. Thus the angles are larger for the closer bound samarium(III) centres than those in the samarium(II) complexes. Also monometallic complexes have larger bend angles than dimetallic (Sm/Na and Sm/K) complexes in response to metal - metal repulsion. The metallocene bend angles, listed in order of decreasing angles, are [(Et$_8$N$_4$Me$_2$)SmMe], **(20)**, 168.8$_6$°, [(Et$_8$N$_4$Me$_2$)SmCH$_2$SiMe$_3$], **(21)**, 166.7$_5$°, [{(Et$_8$N$_4$Me$_2$)Sm(μ-Cl)}$_2$], **(19)**, 162.3$_3$°, [(Et$_8$N$_4$Me$_2$)SmN(SiMe$_3$)$_2$], **(25)**, 160.9$_2$°, [(Et$_8$O$_2$N$_2$)SmN(SiMe$_3$)$_2$], **(22)**, 160.5$_1$°, [(Et$_8$N$_4$Me$_2$)Sm(THF)$_2$], **(16)**, 154.4$_4$°, [(toluene)Na(Et$_8$O$_2$N$_2$)SmN(SiMe$_3$)Si(Me)$_2$CH$_2$], **(23)**, 141.4$_3$°, [{(THF)$_2$K(Et$_8$O$_2$N$_2$)Sm(μ-I)}$_2$], **(15)**, 135.3$_4$°. The metallocene bend angles are similar to those of the related complexes of tetrametallated parent porphyrinogens[4], but much larger than typically observed for bis(cyclopentadienyl)samarium(II) and (III) complexes[3]. The size of the macrocyclic cavities in each structurally authenticated complex in this study also reflect the closeness of the interaction between the metal centres and the macrocyclic units. The size of the macrocycle cavity is measured through cross-cavity N···N distances (or O···O) and the

heterocycle ring tilt angles with respect to the average plane of the macrocycle defined by the four *meso*-carbon centres. Upon deprotonation and hosting of the metal centres, the macrocyclic cavity size is reduced compared to the macrocycles themselves. The samarium(III) complexes have smaller macrocyclic cavities than the related samarium(II) complexes, again indicating closer interactions between the samarium centres and the macrocyclic units for the trivalent samarium complexes compared with the divalent samarium complexes.

iii) NMR characterisation

The ^{1}H NMR spectra of the Group 1 metal complexes (8) - (11) and (12) - (14) of the modified porphyrinogens (3) and (6) display various diferences compared with the macrocycles themselves. The trends existing among the Group 1 metal complexes suggest different bonding modes of the different alkali metals coordinating with the dimetallated modified porphyrinogens. A similar phenomenon exists in the series of the Group 1 metal complexes (27) - (30) of the diindolide ligand system (26). The ^{1}H and ^{13}C NMR spectra of these complexes reflect the symmetry of all compounds in terms of the *mm*2 symmetry through the average plane of the molecules defined by the four *meso*-carbon centres, rendering asymmetry with respect to each side of the macrocyclic plane in the majority of compounds. Only compounds (3) and (9) display more symmetric structures as evidenced by their NMR spectra, with single resonances for the CH$_3$ and CH$_2$ resonances for all *meso*-ethyl groups indicating a rapid fluxional process within the molecules. The variable temperature ^{1}H NMR spectra of these complexes show that the macrocyclic conformations of all Group 1 metal complexes (12) - (14) of the *trans-N,N'*-dimethylated porphyrinogen (6) are rigid with no significant changes being noted, while changes were detected at high temperature for complex (10) of the less bulky dioxaporphyrinogen (3).

The ^{1}H and ^{13}C NMR spectra of the samarium complexes (15) - (25) are affected by the presence of the paramagnetic Sm(II) or (III) centres. The proton resonances of the complexes show variously broadened and shifted resonances, *e.g.,* (16) (δ = -21 to 43 ppm at room temperature). The molecular symmetry features of the samarium complexes derived from both the modified porphyrinogens resemble the majority of the related Group 1 metal complexes described above. The variable temperature ^{1}H NMR spectra of (15) and (25) show linear chemical shift variations with the inverse of temperature, indicating conformance to the Curie-Weiss law and the rigid macrocyclic conformations of the complexes in solution.

gCOSY, gHMQC, gHMBC and gNOESY spectra were performed to enable the full assignment of the ^{1}H and ^{13}C NMR spectra and to establish conformational assignments of many complexes in solution. However, the effect of the paramagnetic metal centre and/or poor solubility prevented such NMR spectroscopic characterisation and spectral assignments for complexes **(15)**, **(17)**, **(18)** and **(19)**.

iv) Reactivity studies

The samarium(III) amide complex **(22)** derived from the dioxaporphyrinogen **(3)** underwent deprotonation at the γ-methyl position of the amide ligand in the presence of alkali metal bases and a kinetic study of this process was performed. As the related samarium(III) complex **(25)** derived from the *trans-N,N'*-dimethylated porphyrinogen **(6)** shows no reaction under the same conditions, the driving force of the reaction is considered to be the residence of the alkali metal cation in the macrocyclic cavity of the less bulky dioxaporphyrinogen.

The reactivity of the majority of the new complexes presented in this thesis is further established through the synthetic reactions that have been discussed throughout the thesis. Many significant structural and reactivity differences have been noted between the two modified porphyrinogen systems under study, namely, the dioxaporphyrinogen system and the more steric demanding *trans-N,N'*-dimethylated porphyrinogen.

The initial catalytic reactivity of various the samarium(II) and (III) complexes in ethylene polymerisation (7 bar ethylene) has been performed. Complexes **(16)**, **(17)** and **(25)**, displayed no reactivity. Catalyst activation was attempted through THF removal by the addition of Lewis acidic tris(pentaflurophenyl)borane and methylaluminoxane (1000 equivalents). The samarium(III) methyl complex **(20)** is yet to be tested.

7.2 References

[1]   Y.S. Jang, H.J. Kim, P.H. Lee, C.H. Lee, *Tetrahedron Letters*, 2000, **41**, 2919.

[2]   Y. Furusho, H. Kawasaki, S. Nakanishi, T. Aida, T. Takata, *Tetrahedron Letters*, 1998, **39**, 3537.

[3]   **a.** W.J. Evans, J.W. Grate, H.W. Choi, I. Bloom, W.E. Hunter, J.L. Atwood, *J. Am. Chem. Soc.*, 1985, **107**, 941.

        b. W.J. Evans, I. Bloom, W.E. Hunter, J.L. Atwood, *J. Am. Chem. Soc.*, 1981, **103**, 6507.

        c. W.J. Evans, L.R. Chamberlain, T.A. Ulibarri, J.W. Ziller, *J. Am. Chem. Soc.*, 1988, **110**, 6423.

        d. H. Schumann, W. Genthe, N. Bruncks, J. Pickardt, *Organometallics*, 1982, **9**, 1195.

        e. W.J. Evans, R.A. Keyer, J.W. Ziller, *Organometallics*, 1993, **12**, 2618.

[4]   **a.** E. Campazzi, E. Solari, R. Scopelliti, C. Floriani, *Inorg. Chem.*, 1999, **38**, 6240.

        b. J. Jubb, S. Gambarotta, *J. Am. Chem. Soc.*, 1994, **116**, 4477.

        c. E. Campazzi, E. Solari, C. Floriani, R. Scopelliti, *Chem. Commun.*, 1998, 2603.

        d. E. Campazzi, E. Solari, R. Scopelliti, C. Floriani, *Chem. Commun.*, 1999, 1617.

        e. T. Dubé, S. Gambarotta, G.P.A. Yap, *Organometallics*, 2000, **19**, 817.

        f. T. Dubé, S. Gambarotta, G.P.A. Yap, *Organometallics*, 2000, **19**, 121.

        g. J.W. Guan, T. Dubé, S. Gambarotta, G.P.A. Yap, *Organometallics*, 2000, **19**, 4820.

APPENDIX

EXPERIMENTAL PROCEDURES

Unless otherwise stated all manipulations of complexes were carried out under an argon atmosphere (high purity) by using standard Schlenk techniques. Solvents for the preparation of complexes were dried over Na or Na/K. Storage of complexes and preparation of samples for various analyses required the use of a dry atmasphere glove box fitted with O_2 (CuO), H_2O (molecule sieve) and solvent (activated charcoal) removal columns, filled with a pre-dried, recirculating, atmosphere of high purity nitrogen. For the preparation of organic intermediates or ligands, solvents including methanol, ethanol, dichloromethane, toluene, 40-60°C or 60-80°C petroleum ether, diethyl ether were used as received or after degassing in some cases. All chemicals were obtained from Aldrich and used as received, except pyrrole and furan which were used in reactions after being freshly redistilled. 18-crown-6 was made according to the literature procedure[1].

NMR spectra were recorded in $CDCl_3$ or appropriately dried C_6D_6, THF-d^8, toluene-d^8 and pyridine-d^5 using Varian-Gemini 200 spectrometer operating at 199.975 (^{1}H) and 50.290 (^{13}C) MHz or a Varian-Unity-Inova 400 WB spectrometer operating at 399.694 (^{1}H) MHz and 100.512 (^{13}C) MHz. The ^{1}H NMR spectra were referenced to the residual ^{1}H resonances of $CDCl_3$ (7.26), C_6D_6 (7.15), toluene-d^8 (7.25), THF-d^8 (1.85 or 3.76) and pyridine-d^5 (8.62) and ^{13}C NMR were referenced to the ^{13}C resonances of $CDCl_3$ (77.0), C_6D_6 (128.0), THF-d^8 (68.0) and pyridine-d^5 (149.9). IR spectra were recorded in the range (400-4000 cm^{-1}) using Nujol mulls on KBr plates on a Bruker IFS-66 FTIR spectrometer. Melting points were determined on a Gallenkamp apparatus and are uncorrected. GC/MS spectra were performed using a HP5890 gas chromatograph equipped with an HP5790 Mass Selective Detector and a 25 m x 0.32 mm HPI column. Elemental analyses were performed by the Central Science Laboratory at the University of Tasmania. (Carlo Erba EA1108 Elemental Analyser) or the Chemical and Analytical Services Pty. Ltd., Melbourne. X-ray crystal structure determinations were carried out by Prof. Allan H. White and Dr. Brian W. Skelton of the University of Western Australia, Dr. Gary Fallon, Monash University and Dr. Michael G. Gardiner, using Bruker SMART and Nonius KappaCCD diffractometers.

[1]   G.W. Gokel, D.J. Cram, *J. Org. Chem.*,1974, **39**, 2445.

www.rsc.org/dalton

Dalton

Structural control of metalloporphyrinogens by macrocycle modification: steric blocking of the macrocyclic cavity through *trans-N,N'*-dimethylation

Jun Wang,[a] **Michael G. Gardiner,**[*a] **Evan J. Peacock,**[b] **Brian W. Skelton**[c] **and Allan H. White**[c]

[a] *School of Chemistry, University of Tasmania, Private Bag 75, Hobart, TAS, 7001, Australia.*
E-mail: Michael.Gardiner@utas.edu.au;

[b] *Central Science Laboratory, University of Tasmania, Private Bag 74, Hobart, TAS, 7001,*
Australia

[c] *Chemistry Department, University of Western Australia, Crawley, WA, 6009, Australia*

Reactions of potassium metal with *trans-N,N'*-dimethyl-*meso*-octaethylporphyrinogen or *meso*-octaethyldioxaporphyrinogen afford dipotassium complexes with one potassium cation excluded from the cavity on steric grounds in the former case, or both potassium cations bound inside the macrocyclic cavity in the latter case.

A decade of metalloporphyrinogen chemistry[1] has established the macrocyclic system as being capable of providing a flexible coordination framework for an extensive range of s-, d- and f-block metals.† Applications being pursued include nitrogen fixation, molecular batteries and their use as non-participative ligands for the stabilisation of novel chemistry. Control over the stoichiometry and/or structure of metalloporphyrinogen complexes has been an unsolved problem in some areas, where alkali metal inclusion and dinuclear complex formation are frequently observed. These features stem from the high anionic charge of the tetrametallated macrocycle and the ability of the macrocycles to bind more than one metal in the macrocyclic cavity. Whilst numerous modifications of porphyrinogens have been reported for supramolecular applications such as anion recognition,[2] the range of macrocycles studied in organometallic applications has been limited solely to variations *via* the *meso*-substituents which have had minimal structural influence on the derived complexes. Herein, we report the synthesis and structure of the first complex of a *N*-modified porphyrinogen (and a related analogue), whose structural features highlight the greatly improved reactivity control in metalloporphyrinogen chemistry that is possible through modification of the macrocycles, whilst achieving a desirable reduction in the anionic charge of the metallated macrocycles.

The reactions of potassium metal with macrocycles 1 and 2, respectively,[3,4] in thf (thf = tetrahydrofuran) reach completion after several hours reflux. Complex 3 precipitated as a crystalline polymeric thf adduct after adding toluene to a saturated thf solution. Complex 4 was obtained as a crystalline monomeric tmeda (tmeda = *N,N,N',N'*-tetramethylethylenediamine) adduct from a thf/petroleum ether (bp 40–60 °C) solution in the presence of 6 equivalents of tmeda, Scheme 1.‡ The products have been analysed by ¹H and ¹³C NMR spectroscopy,§ micro-

analysis and the solid state structures established by single crystal X-ray crystallography.¶

Complex 3 is polymeric in the solid state, Fig. 1 . One potassium cation is bound within the macrocyclic cavity and the other potassium cation necessarily binds outside of the cavity in consequence of the inhibition of access to the opposite opening of the cavity by the *N*-methyl substituents. The macrocycle adopts the 1,3-alternate conformation. The *endo*-cavity-bound potassium exhibits $\eta^5:\eta^1:\eta^5:\eta^1$ binding, with η^5-interactions to both *N*-methyl pyrrole rings and σ-bonding to both nitrogen centres of the pyrrolide rings. A thf molecule also coordinates to the *endo*-cavity-bound potassium. The *exo*-cavity-bound potassium bridges two porphyrinogen units by way of binding to two pyrrolide rings of adjacent macrocycles by η^5- and η^2-bonding modes (the latter to the β-carbons). In addition, the *exo*-cavity-bound potassium is coordinated by a thf molecule and has close contacts with two methyl groups of the adjacent *meso*-ethyl substituents of the macrocycle to which it is η^5-bound.

Complex 4 adopts a monomeric structure in the solid state, Fig. 2 . The macrocycle here also adopts a 1,3-alternate conformation. In contrast to complex 3, both potassium cations reside inside the macrocyclic cavity on either side of the average N_2O_2 plane, each displaying an $\eta^5:\eta^1:\eta^5:\eta^1$ bonding mode. Thus one potassium features η^5-binding to the nitrogen centres of both pyrrolide units and σ-binding to the oxygen centres of both furan units, and *vice versa* for the other potassium. Chelating tmeda molecules complete the coordination spheres of both potassium cations. The structure of 4 differs from the disodium complex of the *meso*-octamethyl analogue of 2.[5] The conformational change underlying the observed binding modes of the potassium cations in 4 is in response to providing a larger macrocyclic cavity to bind the larger cations. In the sodium complex, both nitrogen centres are involved in μ-bridges to the sodium cations through the macrocyclic cavity with the pyrrolide units flat with respect to the macrocyclic cavity. Each sodium is bound in η^5-fashion to a single furan ring and further coordinated by a 1,2-dimethoxyethane molecule, defining a partially flattened double cone conformation for the macrocycle. The same conformation exists for a cobalt(II)§ complex,[5] the only other structurally characterised metallodioxaporphyrinogen.

The qualitative structural features of complexes 3 and 4 are in consequence of the differences in the macrocycles 1 and 2. The two modifications that achieve reduction of the anionic charge of the metallated macrocycles, furan replacement or *N*-methyl substitution, drastically alter the accessibility of the macrocyclic cavities for metal binding. An extensive series of Group 1 metal complexes[1d] has established that unmodified porphyrinogens exclusively contain two metal cations bound in the macrocyclic cavity with various η^5- and η^1-interactions, which can thus be assumed to be the most favourable binding

[{K⁺(thf)}₂(1-2H)²⁻]ₙ
3

or

[{K⁺(tmeda)}₂(2-2H)²⁻]
4

1. X = NMe
2. X = O
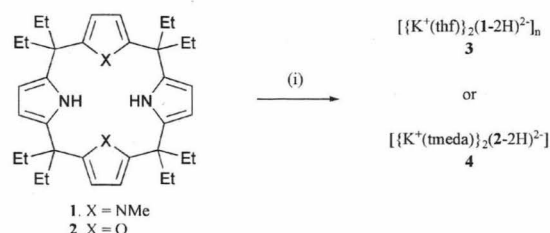
Scheme 1 Reagents and conditions: i, K, thf, then toluene (for **3**) or petroleum ether (bp 40–60 °C)/6 equivalents tmeda (for **4**).
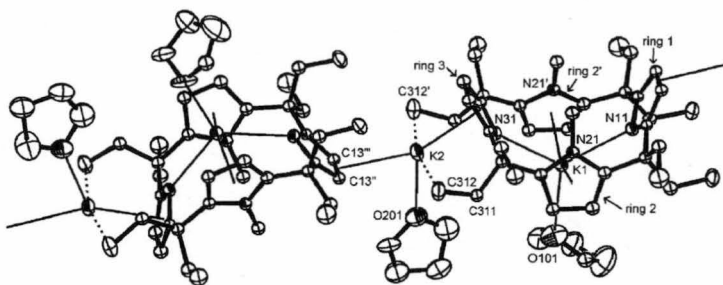
Fig. 1 Molecular structure of **3**. Selected distances (Å): K1–N11, N31 2.820(2), 2.815(2), K1–C2o 2.82₂, K1–O101 2.757(3), K2–C13 3.065(2), K2–C3o 2.77₈, K2–O201 2.678(2), K2–C312 3.143(2), K2–C311 3.371(2), K2–H312c, H312b 2.70(2), 3.15(2). ', " and ''' indicate transformations x, $\frac{1}{2} - y, z$; $x - \frac{1}{2}, \frac{1}{2} - y, \frac{3}{2} - z$ and $x - \frac{1}{2}, y, \frac{3}{2} - z$, respectively. "C*n*o" is the centroid of ring *n*.
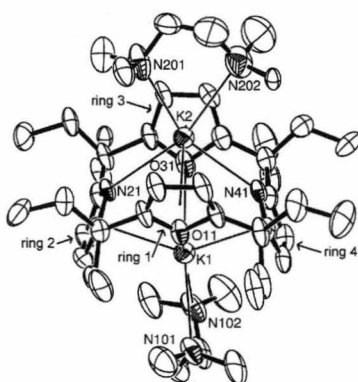

Fig. 2 Molecular structure of **4**. Selected distances (Å): K1–O11, O31 2.976(4), 2.972(4), K1–C2o, C4o 2.88₁, 2.93₁, K1–N101, N102 3.046(7), 3.080(7), K2–N21, N41 2.952(4), 2.898(4), K2–C1o, C3o 2.91₀, 2.92₃, K2–N201, N202 2.916(7), 3.076(8). "C*n*o" is the centroid of ring *n*.

mode for unmodified alkali metal porphyrinogen complexes. In these tetrametallated complexes the remaining two metal cations bind to outside faces of the pyrrolide rings leading to polymeric structures in the solid state. Thus, furan replacement in the porphyrinogen skeleton has maintained the *endo*-cavity metal binding characteristics of the macrocycle and, in contrast, *N*-methyl substitution has altered the *endo*-cavity metal binding characteristics of the porphyrinogen. In both **3** and **4**, the ubiquitous $\eta^5:\eta^1:\eta^5:\eta^1$ *endo*-cavity metal binding mode is observed, which is characteristic for large radii metals.

The structures of complexes **3** and **4** highlight the high level of control that can be attained by modification of the porphyrinogen skeleton. Reaction products from metathetical exchanges with **3** and **4** and metal halides are less likely to incorporate alkali metals owing to the reduced anionic charge of the macrocycles and, in the case of **3**, the sterically hindered cavity. This offers excellent promise that the structures of metalloporphyrinogen complexes can be greatly influenced by this approach. We are currently investigating the structure and reactivity of other modified metalloporphyrinogen complexes.

We thank the Australian Research Council for support.

Notes and references

† Porphyrinogens share many similarities to the well studied calixarene class of macrocycle and are also commonly referred to as calixpyrroles.
‡ Synthesis of **3**. Potassium metal (0.24 g, 6.0 mmol) was added to a solution of **1** (1.70 g, 3.0 mmol) in thf (100 mL) and refluxed for 6 hours. The thf was removed *in vacuo* and the solid washed twice with toluene. Drying *in vacuo* gave the product (2.25 g, 95%). Crystals of **3** suitable for X-ray analysis were obtained by the addition of an equal volume of toluene to a saturated thf solution. Anal. calc. for $C_{46}H_{70}K_2N_4O_2$: C, 70.00; H, 8.94; N, 7.10. Found: C, 67.64; H, 8.99; N, 6.85%. ^{1}H NMR (ppm): 0.69 (t, $^3J = 7.20$ Hz, 24H, CH₃), 1.91–2.15 (m, 24H, CH₂ and thf), 3.05 (s, 6H, NCH₃), 3.76–3.82 (m, 8H, thf), 5.75 (s, 4H, =CH, pyr), 5.89 (s, 4H, =CH, pyrMe). ^{13}C NMR (ppm): 9.6,

9.8 (CH₃), 26.0 (thf), 27.0, 31.8 (CH₂), 33.5 (NCH₃), 46.4 (CEt₂), 68.9 (thf), 101.1 (=CH, pyr), 104.6 (=CH, pyrMe), 142.5 (=CR, pyrMe), 144.5 (=CR, pyr).

Synthesis of **4**. Potassium metal (0.29 g, 7.2 mmol) was added to a solution of **2** (1.63 g, 3.0 mmol) in thf (60 mL) and refluxed for 3 h. The solution was filtered from the excess potassium and other undissolved species and concentrated to *ca.* 20 mL *in vacuo*. Addition of tmeda (2.10 g, 18 mmol), followed by petroleum ether (40 mL, bp 40–60 °C) and storage for one week at −4 °C yielded **4** as colourless crystals (2.25 g, 88%). Anal. calc. for $C_{48}H_{80}K_2N_6O_2$: C, 67.72; H, 9.47; N, 9.87. Found: C, 67.69; H, 9.51; N, 9.79%. ^{1}H NMR (ppm): 0.64 (t, $^3J = 7.20$ Hz, 12H, CH₃), 0.78 (t, $^3J = 7.20$ Hz, 12H, CH₃), 1.90–2.10 (m, 16H, CH₂), 2.48 (s, 8H, NCH₂), 2.32 (s, 24H, NCH₃), 5.89 (s, 4H, =CH, pyr), 6.18 (s, 4H, =CH, fur). ^{13}C NMR (ppm): 9.6, 8.7 (CH₃), 28.2, 30.7 (CH₂), 46.8 (NCH₃), 47.4 (CEt₂), 59.5 (NCH₂), 102.9 (=CH, pyr), 105.5 (=CH, fur), 145.0 (=CR, pyr), 164.5 (=CR, fur).
§ Spectra recorded in d_8-thf at 298 K on a Varian Inc. Unity Inova 400 MHz WB system (5 mm PFG inverse probe). Resonances assigned by interpretation of gCOSY, gHMQC, gHMBC and gNOESY spectra. The upfield ^{13}C NMR thf resonance was obscured by the resonance of d_8-thf.
¶ Crystals of both **3** and **4** were mounted in thin-walled glass capillaries. Intensity data were collected on a Bruker SMART system using Mo-Kα radiation ($\lambda = 0.71073$ Å). Anisotropic displacement parameters were refined for the non-hydrogen atoms and hydrogens were included at geometrically estimated positions. Both thf molecules in **3** were disordered across the mirror plane on $y = \frac{1}{4}$ and one tmeda molecule was disordered in **4** (both modelled with 50% disordered component occupancies). In Figs. 1 and 2, 50% probability displacement amplitude envelopes are shown for the non-hydrogen atoms and solvent disorder is omitted.
Crystal data for **3**: $C_{46}H_{70}K_2N_4O_2$, $M = 789.29$, orthorhombic, $a = 23.941(3)$, $b = 17.131(2)$, $c = 10.832(1)$ Å, $V = 4442.6(9)$ Å³, $T = ca.$ 153 K, space group P_{nma} (no. 62) $Z = 4$, $\mu = 0.25$ mm^{-1}, 43940 reflections measured, 5966 independent ($R_{int} = 0.034$), 4509 > 4$\sigma(F)$, conventional $R = 0.040$, $R_w = 0.047$, crystal dimensions 0.25 × 0.20 × 0.16 mm. CCDC reference number 196193.
For **4**: $C_{48}H_{80}K_2N_6O_2$, $M = 851.40$, triclinic, $a = 12.194(3)$, $b = 12.608(3)$, $c = 17.834(5)$ Å, $\alpha = 80.359(4)$, $\beta = 80.055(4)$, $\gamma = 68.724(4)°$, $V = 2500(1)$ Å³, $T = ca.$ 153 K, space group $P\bar{1}$ (no. 2), $Z = 2$, $\mu = 0.23$ mm^{-1}, 24183 reflections measured, 8738 independent ($R_{int} = 0.053$), 5825 > 4$\sigma(F)$, conventional $R = 0.086$, $R_w = 0.114$, crystal dimensions 0.35 × 0.31 × 0.27 mm. CCDC reference number 196192. See http://www.rsc.org/suppdata/dt/b2/b210600k/ for crystallographic data in CIF or other electronic format.

1 For papers dealing with a range of applications, see: (*a*) J. Jubb and S. Gambarotta, *J. Am. Chem. Soc.*, 1994, **116**, 4477–4478; (*b*) M. Rosi, A. Sgamellotti, F. Franceschi and C. Floriani, *Chem. Eur. J.*, 1999, **5**, 2914–2920; (*c*) T. Dubé, S. Gambarotta and G. P. A. Yap, *Angew. Chem., Int. Ed.*, 1999, **38**, 1432–1435; (*d*) L. Bonomo, E. Solari, R. Scopelliti and C. Floriani, *Chem. Eur. J.*, 2001, **7**, 1322–1332.
2 For reviews, see: (*a*) P. A. Gale, J. L. Sessler and V. Král, *Chem. Commun.*, 1998, 1–8; (*b*) P. A. Gale, P. Anzenbacher Jr. and J. L. Sessler, *Coord. Chem. Rev.*, 2001, **222**, 57–102.
3 Y.-S. Jang, H.-J. Kim, P.-H. Lee and C.-H. Lee, *Tetrahedron Lett.*, 2000, **41**, 2919–2923.
4 Y. Furusho, H. Kawasaki, S. Nakanishi, T. Aida and T. Takata, *Tetrahedron Lett.*, 1998, **39**, 3537–3541.
5 R. Crescenzi, E. Solari, C. Floriani, A. Chiesi-Villa and C. Rizzoli, *Inorg. Chem.*, 1996, **35**, 2413–2414.